SCHOLARLY PUBLICATIONS

A CURRENT AWARENESS BULLETIN
OF RESEARCH OUTPUT

@DTU

(31st Edition)

JULY 2015

BY: CENTRAL LIBRARY

DELHI TECHNOLOGICAL UNIVERSITY
(FORMERLY *DELHI COLLEGE OF ENGINEERING)*
GOVT. OF N.C.T. OF DELHI
SHAHBAD DAULATPUR, MAIN BAWANA ROAD
DELHI 110042

PREFACE

This is the **Thirty First** Issue of Current Awareness Bulletin started by Delhi Technological University, Central Library. The aim of the bulletin is to compile, preserve and disseminate information published by the faculty, students and alumni for mutual benefits. The bulletin also aims to propagate the intellectual contribution of Delhi Technological University (DTU) as a whole to the academia.

The bulletin contains information resources available in the internet in the form of articles, reports, presentations published in international journals, websites, etc. by the faculty and students of DTU. The publications of faculty and student which are not covered in this bulletin may be because of the reason that the full text either was not accessible or could not be searched by the search engine used by the library for this purpose.

The learned faculty and students are requested to provide their uncovered publications to the library either through email or in CD, etc to make the bulletin more comprehensive.

This issue contains the information published during **July 2015**. The arrangement of the contents is alphabetical. The full text of the article which is either subscribed by the university or available in the web is provided in this bulletin.

Central Library

CONTENTS

10. Enhancement of low Exposure Images via Recursive Histogram Equalization Algorithms, Kuldeep Singh, ***3.Rajiv Kapoor*** and Sanjeev Kr. Sinha, ECE, DTU

11. Finite Abelian Group Labeling, Pranjali, ***3.Mukti Acharya*** and Purnima Gupta, Applied Mathematics, DTU

12. Implementation Of Electromagnetic & RFID Technology IN Ambedkar Institute Of Technology, Delhi : A Study, ***3.Ramakant Shukla***, DTU

13. Improved tri-State buffer In MOS Current mode logic and its application, ***3.Neeta Pandey*** and ***3.Bharat Choudhary***, Electronics and Communication Engineering, DTU

14. Influence of Dopant lons on the Properties of Conducting Polycrylamide/Polyaniline Hydrogels, ***3.Reetu Prabhakar*** and ***3.D.Kumar***, Chemistry & Polymer Technology, DTU

15. Irreversibility Reduction in Vapour Compression Refrigeration Systems Using Al2O3 Nano Material Mixed in R718 as Secondary Fluid, ***3.R.S.Mishra***, Mechanical Engineering, DTU

16. Operational Transresistance Amplifier Based PID Controller, ***3.Rajeshwari Pandey***, ***3.Neeta Pandey***, ***3.Saurabh Chitranshi*** and Sajal K. Paul, ECE, DTU

17. Space Time Block Codes for MIMO SYSTEMS: History to Recent Develovpments, ***7.1.Himanshu Khanna***, Electronics and Communication Engineering, DTU

18. Thermal Evaporation and microstructure study of CdTe, ***3.Shailendra Kumar Gaur*** and ***3.R.S. Mishra***, Mechanical, Production & Industrial and Automobiles Engineering, DTU

19. Urban Canyon Modelling: A Need for the Design of Future Indian Cities, ***3.Kanakiya R.S.***, ***3.Singh S.K***. and Mehta P.M., Environmental Engineering Department, DTU

20. Adequacy Assessment Studies of Improved Circular Clarifier for Type - II Settling for Storm Water Treatment, ***8.Nandita Ahuja*** and Girish R. Pophali, Environmental Engineering, DTU

21. Zero Ring Labeling of Graphs, ***3.Mukti Acharya***, Pranjali and Purnima Gupta, Applied Mathematics, DTU

1. Vice Chancellor	***1.1. Ex Vice Chancellor***
2. Pro Vice Chancellor	***2.1. Ex Pro Vice Chancellor***
3. Faculty	***3.1. Ex Faculty***
4. Teaching-cum-Research Fellow	
5. Alumni	
6. Research Scholar	***6.1. Ex Research Scholar***
7. PG Scholar	***7.1. Ex PG Scholar***
8. Undergraduate Student	***8.1. Ex Undergraduate Student***

Wireless Pers Commun
DOI 10.1007/s11277-015-2863-7

A Novel Time-Domain Formulation of 3-D Dyadic Diffraction Coefficient for Arbitrary Polarized UWB Signals with Oblique Incidence

Bajrang Bansal[1] · **Sanjay Soni**[1]

Abstract In this paper, a new time-domain (TD) three-dimensional dyadic diffraction coefficient is proposed for ultra wideband (UWB) signals with arbitrary polarization and oblique incidence. Simulation results are presented for diffraction by a single wedge, double wedge and building scenario with consecutive diffractions. An excellent agreement of the proposed TD solution with the inverse fast Fourier transform (IFFT) of the corresponding exact frequency-domain (FD) solution proves the validity of the TD solution. Also it is observed that the TD solution is computationally more efficient than the IFFT–FD method. The presented TD solution can be used to analyze diffracted field for arbitrary polarized UWB signals with oblique incidence.

Keywords Radio propagation · Ultra wideband · Uniform theory of diffraction · Frequency-domain · Time-domain

1 Introduction

In recent years, ultra wideband (UWB) communication has gained much research interest in UWB propagation modeling and measurement [1–3]. This is because of the fundamental role of propagation characteristics in the design and implementation of the UWB systems [4]. This considerable attention to UWB propagation received a major boost by the 2002 decision of the US frequency regulator (Federal Communications Commission, FCC) to allow unlicensed UWB operation [5]. UWB technology communicates with sub nanosecond pulses and its large bandwidth possesses properties like accurate positioning and ranging [6], immunity to multipath fading [7], multiple access due to wide bandwidth

✉ Sanjay Soni
sanjoo.ksoni@gmail.com

[1] Department of Electronics and Communication Engineering, Delhi Technological University, Delhi 110042, India

Published online: 01 July 2015

[8], and high data rate [9]. However its unprecedented bandwidth introduces some problems that are not encountered in narrowband communication [10]. The spectrum of transmitted UWB signal occupying large bandwidth gets significantly changed during propagation because of the frequency-dependent propagation processes [4, 11, 12]. So the transmitted UWB pulse gets distorted in shape [13] and that distortion brings challenges in propagation modeling and receiver (Rx) design in UWB systems [14]. It is more appropriate to treat the impulse-like phenomena (implying large absolute bandwidth of UWB signals) in time-domain (TD) [15–17] rather than applying the inverse fast Fourier transform (IFFT) algorithms to convert the corresponding frequency-domain (FD) solutions into the TD. The TD analysis allows the simultaneous analysis of all the frequency components of transmitted UWB signal.

Diffraction of UWB signals plays a critical role in modeling of UWB indoor propagation channel [18]. A TD diffraction coefficient for a single straight perfectly conducting wedge and curved wedge was developed in [19] and [20] respectively. For double wedge obstruction, a TD solution based on slope uniform theory of diffraction (UTD) was presented in [21]. For general multiple-diffraction case, a TD solution was presented in [15] that incorporates the TD version of higher order diffraction coefficients and can predict diffracted field after an arbitrary number of objects. A different TD solution for the multiple building diffraction of plane or spherical waves was presented in [22, 23] that is a combination of UTD and physics optics (PO) approaches. UTD–PO model, based on recursion relation involves only single diffraction but has the limitation that objects should have uniform heights and spacing.

In a fully three-dimensional (3-D) scenario, the field is generally obliquely incident on the edge and can be polarized in any direction relative to the edge. Then it becomes necessary to use the 3-D dyadic diffraction coefficient [24–26] instead of normal two-dimensional (2-D) diffraction coefficient. A dyadic diffraction coefficient is the sum of dyads [25] that can be represented in matrix form, e.g. sum of four dyads that can be represented by 2×2 matrix with four non-vanishing elements. In [27], a high frequency solution for scattering from a 3-D dielectric slab was developed. Considering narrowband signals with arbitrary polarization, FD solution for 3-D dyadic diffraction coefficient was developed in [28]. But to the best of authors' knowledge, TD 3-D dyadic diffraction coefficient for UWB signals with arbitrary polarization has not yet been developed.

In this work, we propose a novel TD 3-D dyadic diffraction coefficient for UWB signals with arbitrary polarization that is based on its FD counterpart [28]. TD slope diffraction terms are considered for multiple-diffraction scenario. Propagation through lossy obstacles like wedge and building has been analyzed and it covers single diffraction, double diffraction and grazing incidence. An excellent agreement between the proposed TD and the corresponding IFFT–FD [29, 30] methods validates the proposed solution.

The paper is organized as follows. In Sect. 2, the propagation environments are discussed. Section 3 presents ray-fixed and edge-fixed coordinate systems with the relation in between them. In Sect. 4, following the FD formulations from technical literature, the proposed TD solution is presented for 3-D dyadic diffraction coefficient for arbitrarily polarized UWB signals. In Sect. 5, the accuracy of the proposed solution is confirmed by comparing the TD and the corresponding IFFT–FD results. Further the comparison of computational efficiency of the two approaches (IFFT–FD and TD) is performed to emphasize the significance of the TD solutions presented. Finally, Sect. 6 concludes the paper.

2 Propagation Environments

Figure 1 depicts the different 3-D propagation scenarios considered in this work. Figure 1a shows diffraction by a single wedge structure. The parameters h_t, h_r and h_w are the heights of the transmitter (Tx), Rx and wedge respectively with r_1 and r_2 as the propagation distances. Parameter a_i is the internal wedge angle with d_1 and d_2 as the distances of wedge from Tx and Rx respectively. Figure 1b shows diffraction by a double wedge structure and Fig. 1c shows diffraction by a building structure, a case of grazing incidence where incident angle at second wedge is $\phi_2' = 0°$.

In the next section, ray-fixed and edge-fixed coordinate systems are discussed with the relation in between them.

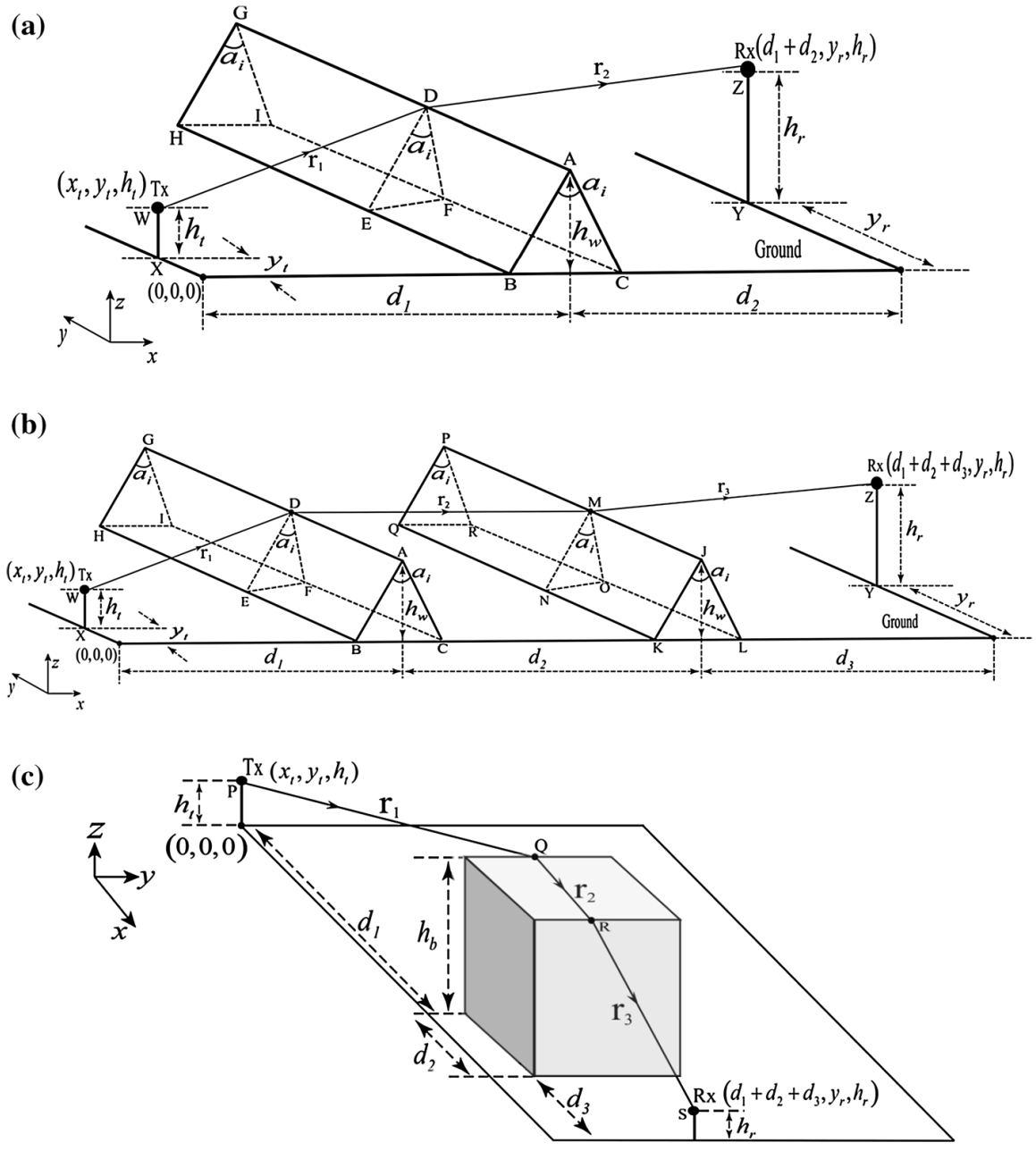

Fig. 1 **a** Diffraction by a 3-D single wedge structure. **b** Diffraction by a 3-D double wedge structure. **c** Diffraction by a 3-D building structure

3 Coordinate Systems for 3-D Diffraction

For 3-D modeling, it is necessary to express the field in certain coordinate systems where 2-D diffraction, reflection and transmission coefficients remain valid [27]. For reflection and transmission phenomena, ray-fixed coordinate system is used where the field is defined in terms of components parallel and perpendicular to the ordinary plane of incidence (POI) [31], the plane containing the incident ray and the normal to the reflecting surface. For incident ray, the unit vectors perpendicular and parallel to the plane of incidence are defined as [25–27]:

$$\hat{e}^i_\perp = \hat{n} \times \hat{I} / \left| \hat{n} \times \hat{I} \right| \tag{1}$$

$$\hat{e}^i_\parallel = \hat{I} \times \hat{e}^i_\perp \tag{2}$$

where $\hat{n}$ is the unit vector normal to the reflecting surface and $\hat{I}$ is the incident unit vector. Since the reflected ray lies in the plane of incidence, its unit vectors are $\hat{e}^r_\perp = \hat{e}^i_\perp$ and $\hat{e}^r_\parallel = \hat{R} \times \hat{e}^i_\perp$, where $\hat{R}$ is the reflection unit vector from the point of reflection to the observation point.

For diffraction, edge-fixed coordinate system [25] is used as shown in Fig. 2. Figure 2a, b illustrates the 3-D wedge geometry for oblique and normal incidence respectively. Parameters β'_o and β_o are the angles made by the edge with the incident and diffracted rays respectively, with $\beta_o = \beta'_o = 90^\circ$ for normal incidence (Fig. 2b). The angles ϕ' and ϕ are the same angles as used in 2-D diffraction case and are measured in a plane perpendicular to the edge. The plane of incidence for edge diffraction, called the edge-fixed plane of incidence (EFPOI) contains the incident unit vector $\hat{I}$, and the unit vector $\hat{e}$ that is tangential to the edge. Edge-fixed plane of diffraction (EFPOD) contains the unit vector $\hat{e}$ and the unit vector $\hat{D}$ that is in the direction of diffracted ray. The unit vectors perpendicular and parallel to the EFPOI are $\hat{\phi}'$ and $\hat{\beta}'_o$ which are defined as [25–27]:

$$\hat{\phi}' = -\hat{e} \times \hat{I} / \left| \hat{e} \times \hat{I} \right| \tag{3}$$

$$\hat{\beta}'_o = \hat{\phi}' \times \hat{I} \tag{4}$$

The unit vectors perpendicular and parallel to the EFPOD are:

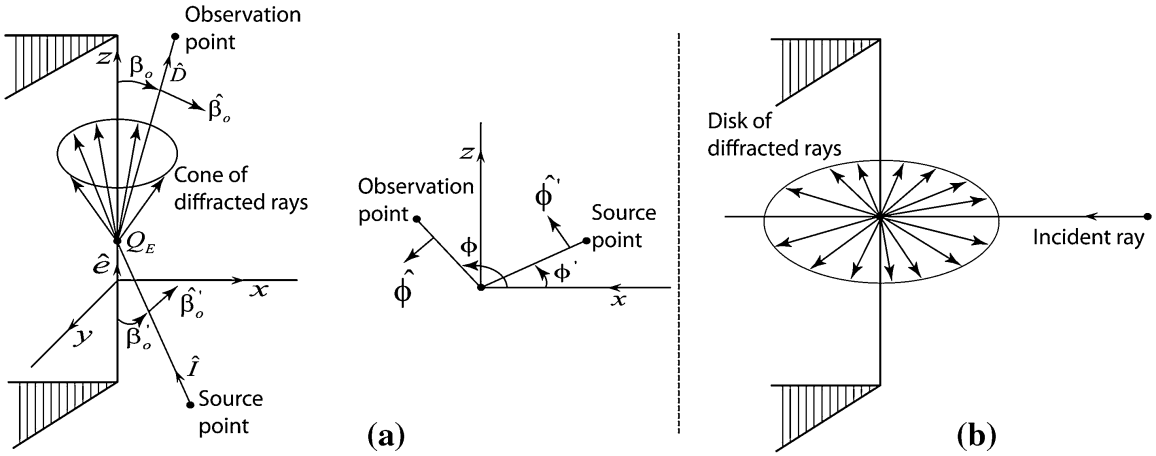

Fig. 2 Three-dimensional wedge geometry for oblique and normal incidence

$$\hat{\phi} = \hat{e} \times \hat{D} / \left| \hat{e} \times \hat{D} \right| \tag{5}$$

$$\hat{\beta}_o = \hat{\phi} \times \hat{D} \tag{6}$$

Figure 3 shows POI and EFPOI with α as the angle between them which can be defined as the acute angle between their respective normal vectors. For Fig. 3, the angle α is given as:

$$\alpha = \cos^{-1}\left(\frac{\overline{n_1} \cdot \overline{n_2}}{|\overline{n_1}||\overline{n_2}|} \right) \tag{7}$$

where $\overline{n_1}$ and $\overline{n_2}$ are normal vectors to POI and EFPOI respectively and are given as:

$$\overline{n_1} = (-(y_A - y)(h_t - h_w))\hat{i} + ((x_t - d_1)(y_A - y))\hat{k} \tag{8}$$

$$\overline{n_2} = (y_t - y)\hat{i} - (x_t - d_1)\hat{j} \tag{9}$$

where y_A is the y coordinate of the point A in Fig. 3. When the field is incident normal to the edge, the angle α reduces to 90°.

4 Theoretical Models

4.1 Frequency Domain Model

In the edge-fixed coordinate system, diffracted field at Rx for single diffraction (e.g. Figure 1a) can be expressed in the following manner [24, 28, 32]:

$$\begin{bmatrix} E^d_{\beta_o} \\ E^d_{\phi} \end{bmatrix} = \begin{bmatrix} D_{ss} & D_{sh} \\ D_{hs} & D_{hh} \end{bmatrix} \begin{bmatrix} E^i_{\beta'_o} \\ E^i_{\phi'} \end{bmatrix} \sqrt{\frac{r_1}{r_2(r_1 + r_2)}} \exp(-jkr_2) \tag{10}$$

where $E^d_{\beta_o}, E^d_{\phi}$ are the parallel and perpendicular components of the diffracted field at Rx with $E^i_{\beta'_o}, E^i_{\phi'}$ as the corresponding incident field components (incident field at point D in Fig. 1a).

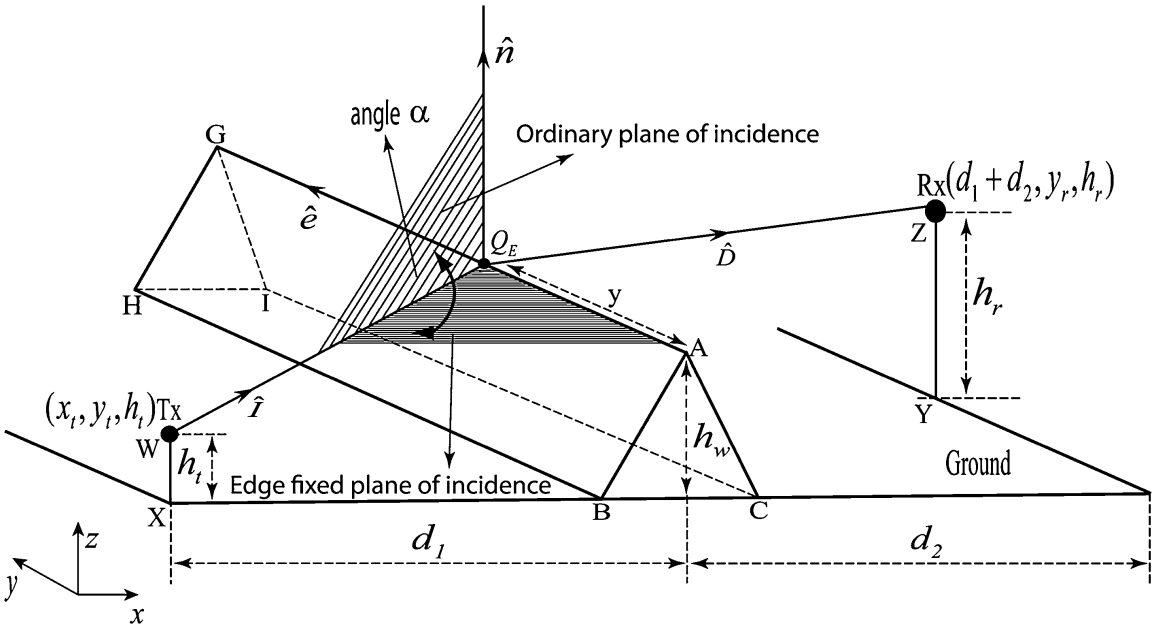

Fig. 3 Three-dimensional wedge geometry showing angle between POI and EFPOI

Parameter k is the wave number given by $k = \omega/c$, where ω is the angular frequency and c is the speed of light. The first matrix on right side in (10) is the 3-D dyadic diffraction coefficient matrix for wedge with each element having non-zero value for arbitrary polarized incident field. Subscripts s and h stand for soft (perpendicular) and hard (parallel) polarizations respectively. The parameters D_{ss}, D_{sh}, D_{hs}, and D_{hh} are derived on the basis of 2-D Holm's diffraction coefficient [15, 33] and each of these can be expressed as [24, 28, 32]:

$$D_{ss} = G_n^s R_\perp^0 R_\perp^n D_1 + G_0^s D_2 - \left[G_0^h R_\parallel^0 \cos^2\alpha - G_0^s R_\perp^0 \sin^2\alpha\right] D_3 - \left[G_n^h R_\parallel^n \cos^2\alpha - G_n^s R_\perp^n \sin^2\alpha\right] D_4 \tag{11}$$

$$D_{sh} = -\left[G_0^s R_\perp^0 + G_0^h R_\parallel^0\right] \sin\alpha\cos\alpha D_3 - \left[G_n^s R_\perp^n + G_n^h R_\parallel^n\right] \sin\alpha\cos\alpha D_4 \tag{12}$$

$$D_{hs} = \left[G_0^s R_\perp^0 + G_0^h R_\parallel^0\right] \sin\alpha\cos\alpha D_3 + \left[G_n^s R_\perp^n + G_n^h R_\parallel^n\right] \sin\alpha\cos\alpha D_4 \tag{13}$$

$$D_{hh} = G_n^h R_\parallel^0 R_\parallel^n D_1 + G_0^h D_2 + \left[G_0^h R_\parallel^0 \sin^2\alpha - G_0^s R_\perp^0 \cos^2\alpha\right] D_3 + \left[G_n^h R_\parallel^n \sin^2\alpha - G_n^s R_\perp^n \cos^2\alpha\right] D_4 \tag{14}$$

where superscripts *0* and *n* stand for 0-face and n-face of the wedge and subscripts $\parallel$ and $\perp$ refer to parallel and perpendicular polarizations respectively. The factor G signifies grazing incidence case where its value is ½ and otherwise its value is 1 for the used 2-D diffraction coefficient [33]. Parameters $R_\parallel(\psi)$ and $R_\perp(\psi)$ are the Fresnel reflection coefficients for parallel and perpendicular polarizations respectively [31]. The angle argument ψ is $\psi = \phi'$ for 0-face and $\psi = n\pi - \phi$ for n-face. The terms $D_i (i = 1, 2, 3, 4)$ have their usual meanings [15, 26, 33]. It can be seen that if $\alpha = 90°$, then the formulations presented in (11)–(14) gets converted to normal 2-D Holm's diffraction coefficient.

The double diffracted field at Rx (e.g. Fig. 1b) consists of amplitude diffracted and slope diffracted terms [28, 34]. For Fig. 1b, the parallel and perpendicular components of the amplitude diffracted field at Rx are expressed as:

$$\begin{bmatrix} E_{\beta_o}^{rad} \\ E_\phi^{rad} \end{bmatrix} = \begin{bmatrix} D_{ss2} & D_{sh2} \\ D_{hs2} & D_{hh2} \end{bmatrix} \begin{bmatrix} E_{\beta_o}^{d} \\ E_\phi^{d} \end{bmatrix} \sqrt{\frac{r_1 + r_2}{r_3(r_1 + r_2 + r_3)}} \exp(-jkr_3) \tag{15}$$

where the superscript *rad* denotes amplitude diffracted field at Rx and $E_{\beta_o}^d$, E_ϕ^d are the single diffracted field components at point M in Fig. 1b which can be computed following (10). Diffraction coefficient matrix in (15) is for second wedge and can be defined in the same manner as for the first wedge in (11)–(14). The angle arguments used in reflection coefficient are ϕ_1', $n\pi - \phi_1$ for first wedge and ϕ_2', $n\pi - \phi_2$ for second wedge. For the building structure (Fig. 1c), the angle argument for the n-face of first wedge is $n - \phi_1$ [34]. Also it can be seen in Fig. 1c for building structure that the incident angle at second wedge is $\phi_2' = 0°$, i.e. grazing incidence, so the elements of diffraction coefficient matrix in (15) gets multiplied by ½ [34].

The components of the slope diffracted field at Rx for Fig. 1b are given as [28, 34]:

$$\begin{bmatrix} E_{\beta_o}^{rsd} \\ E_\phi^{rsd} \end{bmatrix} = \frac{1}{jk} \begin{bmatrix} \frac{\partial D_{ss2}}{\partial \phi_2'} & \frac{\partial D_{sh2}}{\partial \phi_2'} \\ \frac{\partial D_{hs2}}{\partial \phi_2'} & \frac{\partial D_{hh2}}{\partial \phi_2'} \end{bmatrix} \begin{bmatrix} \frac{\partial E_{\beta_o}^d}{\partial n} \\ \frac{\partial E_\phi^d}{\partial n} \end{bmatrix} \sqrt{\frac{r_1 + r_2}{r_3(r_1 + r_2 + r_3)}} \exp(-jkr_3) \tag{16}$$

where the superscript *rsd* denotes slope diffracted field at Rx with $\frac{\partial E^d_{\beta_o}}{\partial n} = -\frac{1}{r_2}\frac{\partial E^d_{\beta_o}}{\partial \phi_1}$ and $\frac{\partial E^d_{\phi}}{\partial n} = -\frac{1}{r_2}\frac{\partial E^d_{\phi}}{\partial \phi_1}$ [15]. Again the term $\frac{1}{jk}$ in (16) gets multiplied by ½ for building structure. The term $\frac{\partial E^d_{\beta_o}}{\partial \phi_1}$ can be written using (10) and is given as:

$$\frac{\partial E^d_{\beta_o}}{\partial \phi_1} = \left[E^i_{\beta'_o}\frac{\partial D_{ss1}}{\partial \phi_1} + E^i_{\phi'}\frac{\partial D_{sh1}}{\partial \phi_1}\right]\sqrt{\frac{r_1}{r_2(r_1+r_2)}}\exp(-jkr_2) \tag{17}$$

Similarly $\frac{\partial E^d_{\phi}}{\partial \phi_1}$ can be obtained using (10). The terms $\frac{\partial D_{ss1}}{\partial \phi_1}$, $\frac{\partial D_{sh1}}{\partial \phi_1}$, $\frac{\partial D_{hs1}}{\partial \phi_1}$ and $\frac{\partial D_{hh1}}{\partial \phi_1}$ are given as:

$$\begin{aligned}\frac{\partial D_{ss1,hh1}}{\partial \phi_1} &= G^{s,h}_n R^0_{\perp,\parallel} R^n_{\perp,\parallel}\frac{\partial D_1}{\partial \phi_1} + G^{s,h}_n R^0_{\perp,\parallel} D_1\frac{\partial R^n_{\perp,\parallel}}{\partial \phi_1} + G^{s,h}_0\frac{\partial D_2}{\partial \phi_1}\\ &\quad - \left[G^{h,s}_0 R^0_{\parallel,\perp}\cos^2\alpha - G^{s,h}_0 R^0_{\perp,\parallel}\sin^2\alpha\right]\frac{\partial D_3}{\partial \phi_1}\\ &\quad - \left[G^{h,s}_n R^n_{\parallel,\perp}\cos^2\alpha - G^{s,h}_n R^n_{\perp,\parallel}\sin^2\alpha\right]\frac{\partial D_4}{\partial \phi_1}\\ &\quad - \left[G^{h,s}_n\frac{\partial R^n_{\parallel,\perp}}{\partial \phi_1}\cos^2\alpha - G^{s,h}_n\frac{\partial R^n_{\perp,\parallel}}{\partial \phi_1}\sin^2\alpha\right]D_4\end{aligned} \tag{18}$$

$$\begin{aligned}\frac{\partial D_{sh1,hs1}}{\partial \phi_1} &= \mp\left[G^s_0 R^0_{\perp} + G^h_0 R^0_{\parallel}\right]\sin\alpha\cos\alpha\frac{\partial D_3}{\partial \phi_1} \mp \left[G^s_n R^n_{\perp} + G^h_n R^n_{\parallel}\right]\sin\alpha\cos\alpha\frac{\partial D_4}{\partial \phi_1}\\ &\quad \mp\left[G^s_n\frac{\partial R^n_{\perp}}{\partial \phi_1} + G^h_n\frac{\partial R^n_{\parallel}}{\partial \phi_1}\right]\sin\alpha\cos\alpha D_4\end{aligned} \tag{19}$$

The terms $\frac{\partial D_{ss2}}{\partial \phi'_2}$, $\frac{\partial D_{sh2}}{\partial \phi'_2}$, $\frac{\partial D_{hs2}}{\partial \phi'_2}$, and $\frac{\partial D_{hh2}}{\partial \phi'_2}$ can be found out similar to (18) and (19).

4.2 Proposed Time Domain Model

In this section, our main objective is to derive the TD version of FD formulations presented in Sect. 4.1 to predict the received signals directly in the TD. The TD formulations for two components of the diffracted field in (10) are given as:

$$e^d_{\beta_o}(t) = \sqrt{\frac{r_1}{r_2(r_1+r_2)}}\left[\left(d_{ss}(t) * e^i_{\beta'_o}(t)\right) + \left(d_{sh}(t) * e^i_{\phi'}(t)\right)\right] * \delta\left(t - \frac{r_2}{c}\right) \tag{20}$$

$$e^d_{\phi}(t) = \sqrt{\frac{r_1}{r_2(r_1+r_2)}}\left[\left(d_{hs}(t) * e^i_{\beta'_o}(t)\right) + \left(d_{hh}(t) * e^i_{\phi'}(t)\right)\right] * \delta\left(t - \frac{r_2}{c}\right) \tag{21}$$

where $\delta(t)$ is the impulse function [35] and '*' is used for convolution operator. Based on their FD counterparts, the TD formulations of the elements of dyadic diffraction coefficient are given as:

$$\begin{aligned}d_{ss}(t) &= G^s_n\left(r^0_{\perp}(t) * r^n_{\perp}(t) * d_1(t)\right) + G^s_0 d_2(t) - \left[G^h_0 r^0_{\parallel}(t)\cos^2\alpha - G^s_0 r^0_{\perp}(t)\sin^2\alpha\right] * d_3(t)\\ &\quad - \left[G^h_n r^n_{\parallel}(t)\cos^2\alpha - G^s_n r^n_{\perp}(t)\sin^2\alpha\right] * d_4(t)\end{aligned} \tag{22}$$

$$d_{sh}(t) = -\sin\alpha\cos\alpha\left[G_0^s r_\perp^0(t) + G_0^h r_\parallel^0(t)\right] * d_3(t) - \sin\alpha\cos\alpha\left[G_n^s r_\perp^n(t) + G_n^h r_\parallel^n(t)\right] * d_4(t) \tag{23}$$

$$d_{hs}(t) = \sin\alpha\cos\alpha\left[G_0^s r_\perp^0(t) + G_0^h r_\parallel^0(t)\right] * d_3(t) + \sin\alpha\cos\alpha\left[G_n^s r_\perp^n(t) + G_n^h r_\parallel^n(t)\right] * d_4(t) \tag{24}$$

$$\begin{aligned} d_{hh}(t) = {} & G_n^h\left(r_\parallel^0(t) * r_\parallel^n(t) * d_1(t)\right) + G_0^h d_2(t) + \left[G_0^h r_\parallel^0(t)\sin^2\alpha - G_0^s r_\perp^0(t)\cos^2\alpha\right] * d_3(t) \\ & + \left[G_n^h r_\parallel^n(t)\sin^2\alpha - G_n^s r_\perp^n(t)\cos^2\alpha\right] * d_4(t) \end{aligned} \tag{25}$$

where $r_\parallel(t)$, $r_\perp(t)$ are the TD Fresnel reflection coefficients for parallel and perpendicular polarizations respectively [36] and the details of $d_i(t)(i = 1, 2, 3, 4)$ can be found out in [15].

Now the TD formulations corresponding to (15) are given as:

$$e_{\beta_o}^{rad}(t) = \sqrt{\frac{r_1 + r_2}{r_3(r_1 + r_2 + r_3)}}\left[\left(d_{ss2}(t) * e_{\beta_o}^d(t)\right) + \left(d_{sh2}(t) * e_\phi^d(t)\right)\right] * \delta\left(t - \frac{r_3}{c}\right) \tag{26}$$

$$e_\phi^{rad}(t) = \sqrt{\frac{r_1 + r_2}{r_3(r_1 + r_2 + r_3)}}\left[\left(d_{hs2}(t) * e_{\beta_o}^d(t)\right) + \left(d_{hh2}(t) * e_\phi^d(t)\right)\right] * \delta\left(t - \frac{r_3}{c}\right) \tag{27}$$

Expressions for $d_{ss2}(t)$, $d_{sh2}(t)$, $d_{hs2}(t)$, and $d_{hh2}(t)$ can be written similar to (22)–(25). The TD formulations corresponding to (16) are given as [15]:

$$\begin{aligned} e_{\beta_o}^{rsd}(t) = {} & -\frac{1}{r_2}A_1A_2\left[\begin{array}{l}\left(d_{ss2,der}(t;\phi') * \left\{\left(e_{\beta_o'}^i(t) * d_{ss1,der}(t;\phi)\right) + \left(e_{\phi'}^i(t) * d_{sh1,der}(t;\phi)\right)\right\}\right) + \\ \left(d_{sh2,der}(t;\phi') * \left\{\left(e_{\beta_o'}^i(t) * d_{hs1,der}(t;\phi)\right) + \left(e_{\phi'}^i(t) * d_{hh1,der}(t;\phi)\right)\right\}\right)\end{array}\right] \\ & * \delta\left(t - \frac{r_2 + r_3}{c}\right) \end{aligned} \tag{28}$$

$$\begin{aligned} e_\phi^{rsd}(t) = {} & -\frac{1}{r_2}A_1A_2\left[\begin{array}{l}\left(d_{hs2,der}(t;\phi') * \left\{\left(e_{\beta_o'}^i(t) * d_{ss1,der}(t;\phi)\right) + \left(e_{\phi'}^i(t) * d_{sh1,der}(t;\phi)\right)\right\}\right) + \\ \left(d_{hh2,der}(t;\phi') * \left\{\left(e_{\beta_o'}^i(t) * d_{hs1,der}(t;\phi)\right) + \left(e_{\phi'}^i(t) * d_{hh1,der}(t;\phi)\right)\right\}\right)\end{array}\right] \\ & * \delta\left(t - \frac{r_2 + r_3}{c}\right) \end{aligned} \tag{29}$$

where $A_1 = \sqrt{\frac{r_1}{r_2(r_1+r_2)}}$ and $A_2 = \sqrt{\frac{r_1+r_2}{r_3(r_1+r_2+r_3)}}$. The TD terms corresponding to (18) and (19) are given as:

$$\begin{aligned} d_{ss1,hh1,der}(t;\phi) = {} & G_n^{s,h}\left(r_{\perp,\parallel}^0(t) * r_{\perp,\parallel}^n(t) * d_{1,der}(t)\right) + G_n^{s,h}\left(r_{\perp,\parallel}^0(t) * d_1(t) * r_{\perp,\parallel,der}^n(t)\right) \\ & + G_0^{s,h} d_{2,der}(t) - \left[G_0^{h,s} r_{\parallel,\perp}^0(t)\cos^2\alpha - G_0^{s,h} r_{\perp,\parallel}^0(t)\sin^2\alpha\right] * d_{3,der}(t) \\ & - \left[G_n^{h,s} r_{\parallel,\perp}^n(t)\cos^2\alpha - G_n^{s,h} r_{\perp,\parallel}^n(t)\sin^2\alpha\right] * d_{4,der}(t) \\ & - \left[G_n^{h,s} r_{\parallel,\perp,der}^n(t)\cos^2\alpha - G_n^{s,h} r_{\perp,\parallel,der}^n(t)\sin^2\alpha\right] * d_4(t) \end{aligned} \tag{30}$$

$$
\begin{aligned}
d_{sh1,hs1,der}(t;\phi) = &\mp \sin\alpha\cos\alpha\left[G_0^s r_\perp^0(t) + G_0^h r_\parallel^0(t)\right] * d_{3,der}(t) \\
&\mp \sin\alpha\cos\alpha\left[G_n^s r_\perp^n(t) + G_n^h r_\parallel^n(t)\right] * d_{4,der}(t) \\
&\mp \sin\alpha\cos\alpha\left[G_n^s r_{\perp,der}^n(t) + G_n^h r_{\parallel,der}^n(t)\right] * d_4(t)
\end{aligned} \tag{31}
$$

where $r^n_{\perp,\parallel,der}(t)$ and $d_{i,der}(t)(i = 1, 2, 3, 4)$ can be found out in [15, 37]. TD expressions corresponding to $d_{ss2,hh2,der}(t;\phi')$ and $d_{sh2,hs2,der}(t;\phi')$ can be written similar to (30) and (31) respectively. Next in the result section, the accuracy of presented TD formulations is confirmed by comparing the TD results with corresponding exact IFFT–FD results.

5 Results and Discussion

In this section, the numerical simulation results are presented for the output field at Rx for all scenarios considered in this paper and the results are based on the aforementioned TD and FD solutions. The accuracy of the presented TD results is proved by comparison with the numerical IFFT of the corresponding exact FD results. Throughout our work the Gaussian doublet pulse is used as the excitation UWB signal [38].

First, diffraction by a single wedge structure (Fig. 1a) is shown in Figs. 4 and 5 for oblique and normal incidence of UWB pulse respectively. Dry concrete [16] is used as the lossy material for wedge. It can be seen here that for both parallel and perpendicular components, TD results exactly match with the corresponding IFFT–FD results thus confirming the accuracy of our formulations. Diffracted pulse shows distortion in shape and that is because of the frequency dependent diffraction coefficient [18]. Also it is observed that the magnitude of perpendicular polarized component is higher than that of parallel polarized component. Knowing the coordinates of Tx, Rx and wedge, the angle α between two planes (POI and EFPOI) can be computed using (7)–(9) and is calculated to be 60° for scenario presented in the inset of Fig. 4.

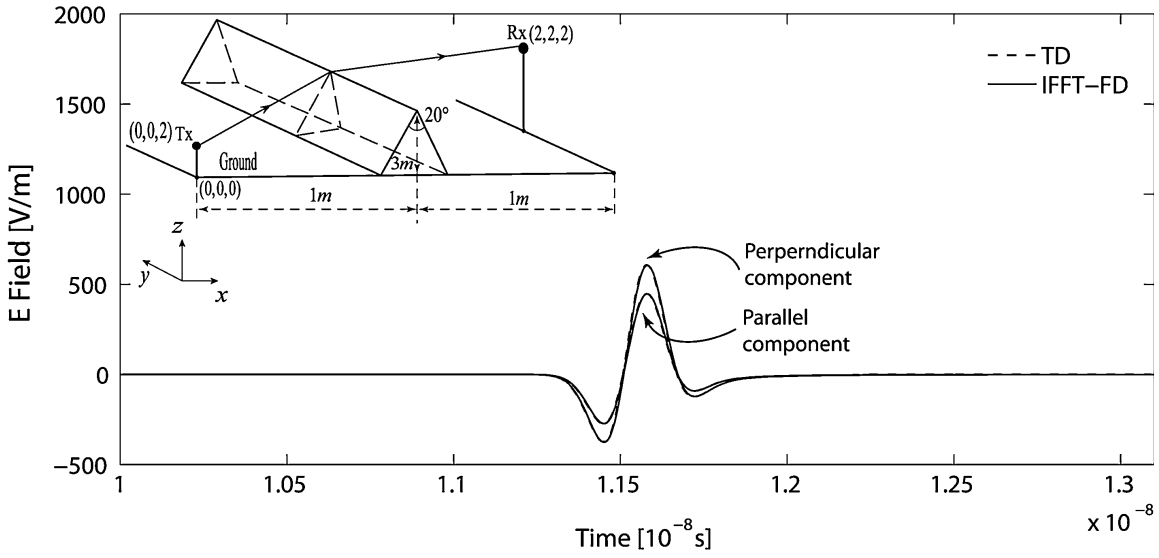

Fig. 4 Diffracted field for single wedge structure for oblique incidence ($\alpha = 60°$), with dry concrete [16]

Figure 6 shows single diffracted field for Fig. 1a, for different Rx positions. It is observed that with changing the Rx position along y direction, α decreases and the field strength gets slightly decreased. This small variation in field strength is because of the corresponding small variation in the magnitude of the transfer function (channel frequency response) with different Rx positions as shown in Fig. 7 for perpendicular polarization. It can also be observed from Fig. 7 that for diffraction, channel shows frequency selective behaviour which results in distortion of the incident UWB pulse.

Figures 8 and 9 shows double diffracted field at Rx for double wedge and building respectively. It is clearly observed that double diffracted field shows larger distortion in comparison to the single diffracted field. This is because of the stronger frequency dependent double diffraction propagation. As discussed in Sect. 2, for building structure, the incident angle at second wedge is $\phi_2' = 0°$, this results in a singularity in TD. This singularity is avoided by approximating $\phi_2' = 0°$ in TD computation by $\phi_2' = 0.01°$.

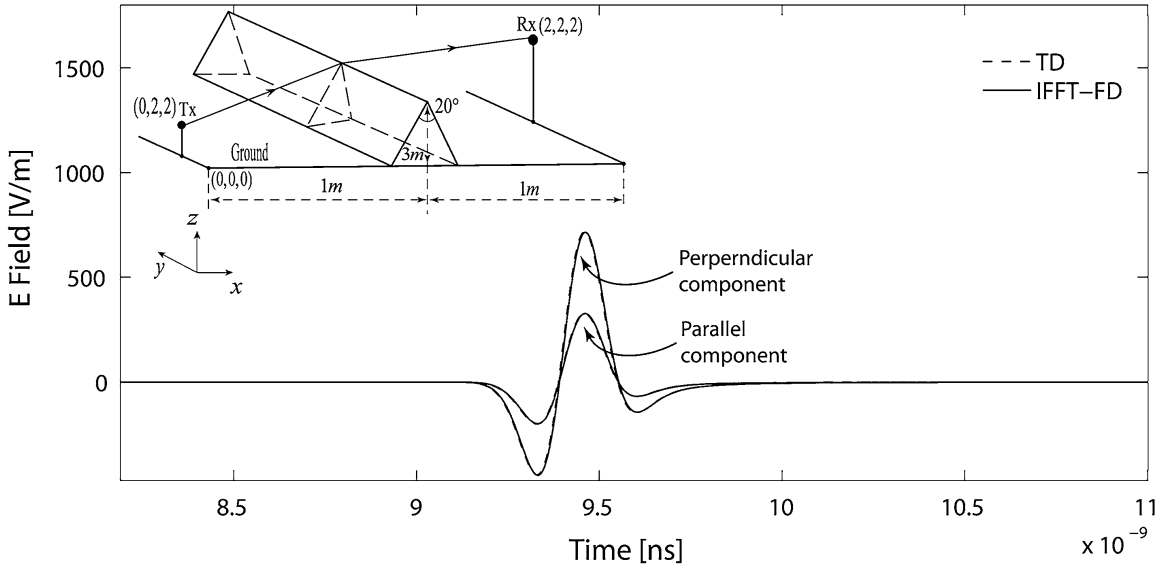

Fig. 5 Diffracted field for single wedge structure for normal incidence $(\alpha = 90°)$, with dry concrete [16]

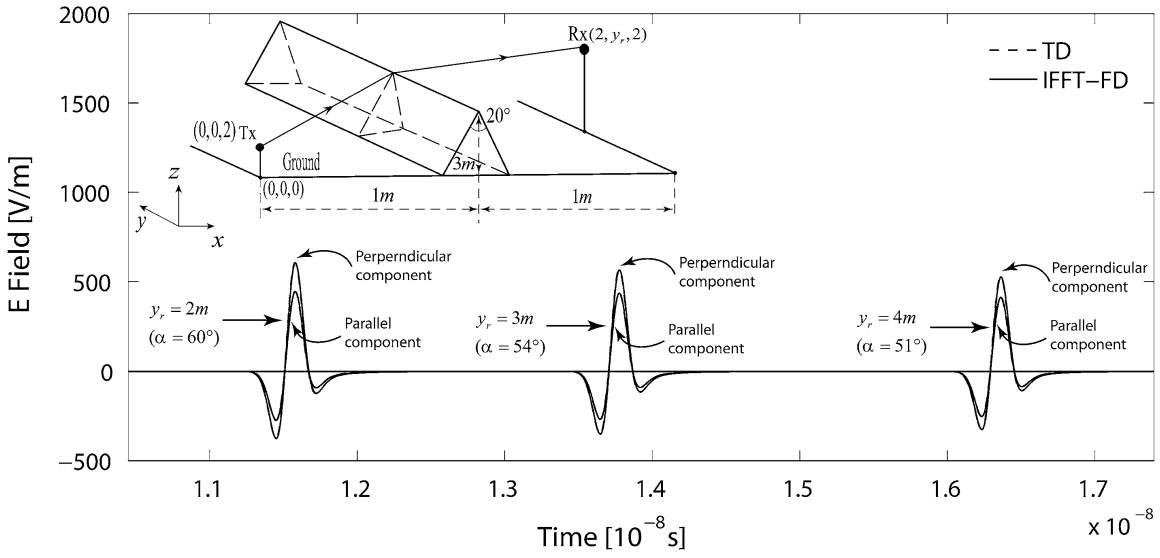

Fig. 6 Diffracted field for single wedge structure for different Rx positions along y direction

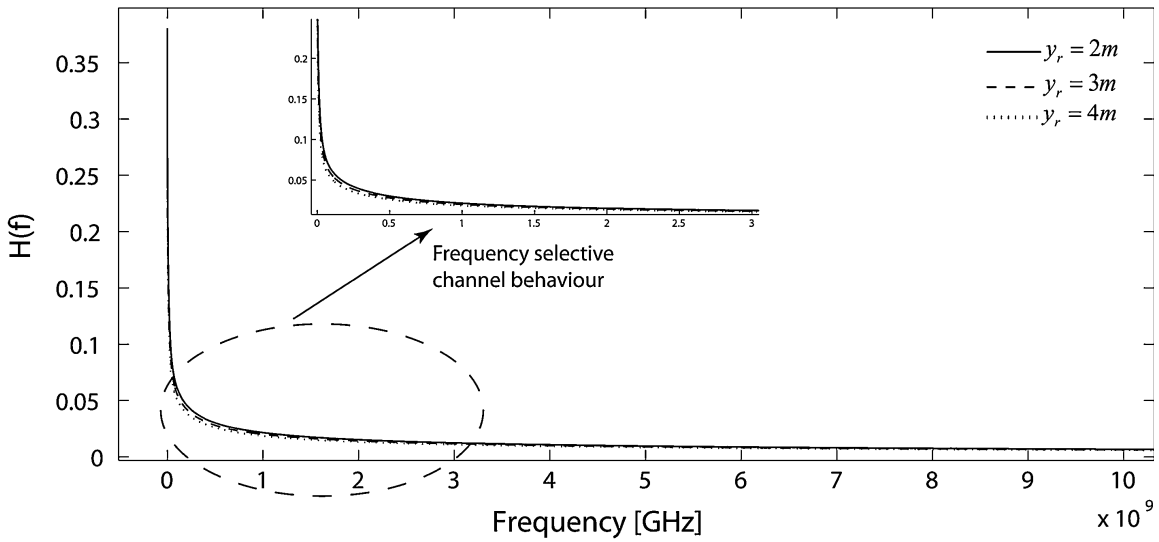

Fig. 7 Frequency response of channel for single wedge diffraction for different Rx positions along y direction

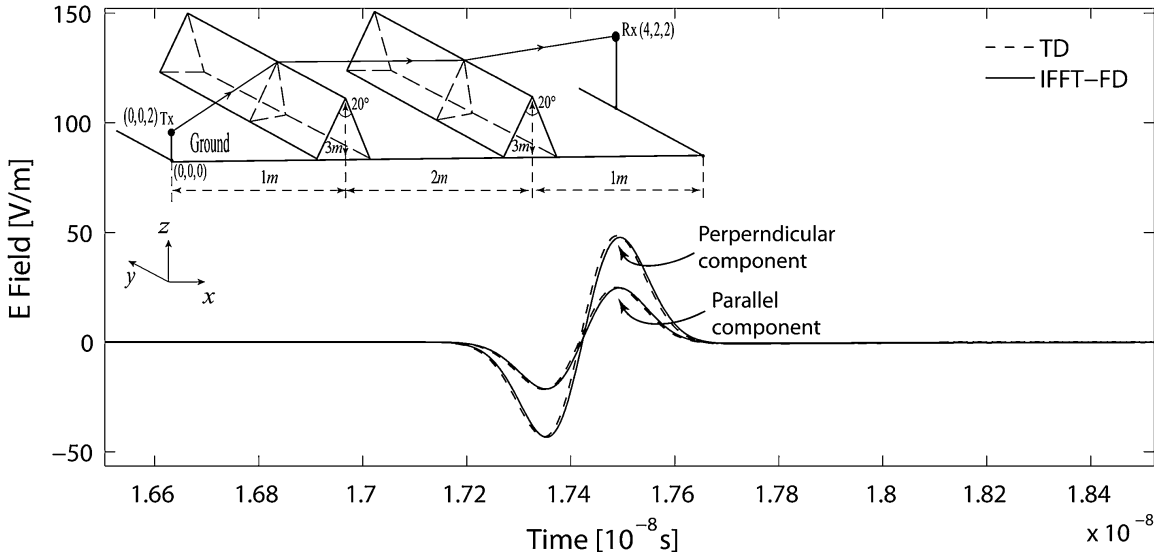

Fig. 8 Diffracted field for double wedge structure ($\alpha_1 = 69.06^\circ, \alpha_2 = 90^\circ$), with dry concrete [16]

Further the accuracy of this approximation is confirmed by comparing the corresponding IFFT–FD results for both values of incident angle ϕ_2', i.e. 0° and 0.01° which come to be exactly same. The good agreement between TD and IFFT–FD results confirms the accuracy of our proposed TD solution.

A comparison between the computation times of the IFFT–FD method and the proposed TD solution for different scenarios discussed here is presented in Table 1 (for parallel polarized components) which establishes that the proposed TD analysis is computationally more efficient in comparison to the IFFT–FD solution.

The main reason for such a significant reduction in the computational time in TD is the efficient convolution technique (Section 10.1, Fig. 10.1 and 10.2 in [29]) due to which few number of time samples suffice to provide accurate results.

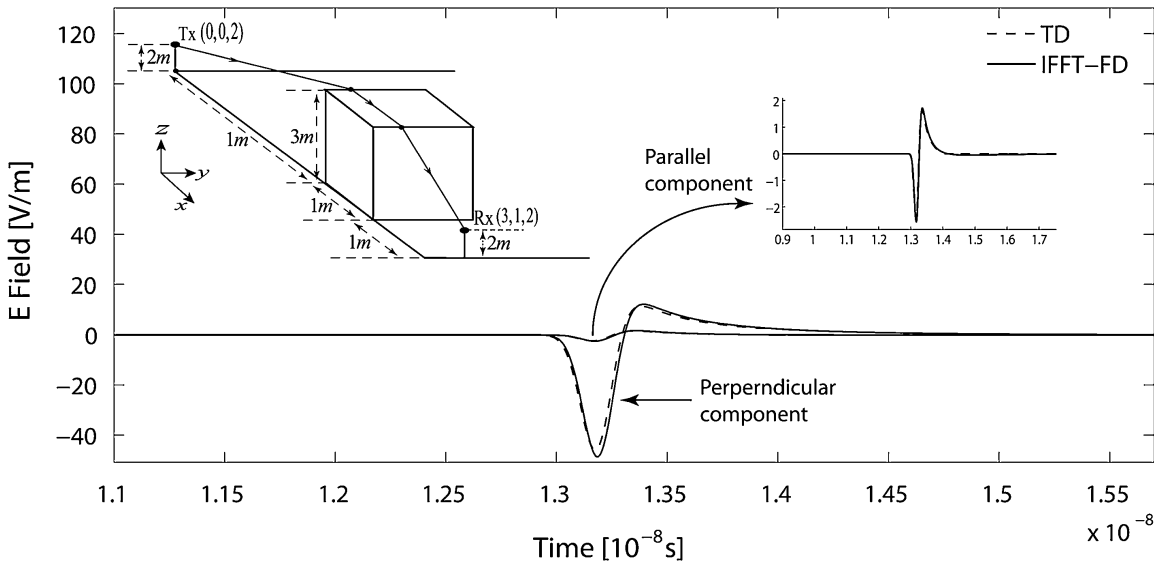

Fig. 9 Diffracted field for building structure $(\alpha_1 = 75.82^\circ, \alpha_2 = 90^\circ)$, with dry concrete [16]

Table 1 Average ratios of the computation time of the two methods

Propagation profile	$T_{IFFT-FD}/T_{TD}$
Single wedge 3-D propagation (Fig. 4)	~35.25
Single wedge 2-D propagation (Fig. 5)	~32.86
Double wedge 3-D propagation (Fig. 8)	~13.41
Single building 3-D propagation (Fig. 9)	~15.51

Considering the excellent agreement between proposed TD and corresponding IFFT–FD solutions for different lossy structures, it can be said that the presented TD solution is useful in computing the diffracted field for oblique incidence of UWB signals with arbitrary polarization.

6 Conclusion

A Novel TD solution of 3-D dyadic diffraction coefficient is presented for arbitrary polarized UWB signals with oblique and normal incidence. TD formulations are presented for amplitude diffraction and higher order slope diffraction terms. The excellent agreement between the proposed TD and corresponding IFFT–FD results validates the accuracy of our presented TD solution. The diffracted field shows attenuation and also distortion in shape due to frequency selective nature of the channel. Further the TD solution has been found computationally more efficient than IFFT–FD method. Considering the advantages of TD method, the presented TD solution proves significant in predicting the diffracted field for arbitrary polarized UWB signals.

References

1. Molisch, A. F. (2009). Ultra-wide-band propagation channels. *Proceedings of the IEEE, 97*(2), 353–371.

2. Santos, T., Karedal, J., Almers, P., Tufvesson, F., & Molisch, A. F. (2010). Modeling the ultra-wideband outdoor channel: Measurements and parameter extraction method. *IEEE Transactions on Wireless Communications, 9*(1), 282–290.
3. Haneda, K., Richter, A., & Molisch, A. F. (2012). Modeling the frequency dependence of ultra-wideband spatio-temporal indoor radio channels. *IEEE Transactions on Antennas and Propagation, 60*(6), 2940–2950.
4. Qiu, R. C. (2004). A generalized time domain multipath channel and its application in ultra-wideband (UWB) wireless optimal receiver design—part II: Physics-based system analysis. *IEEE Transactions on Wireless Communications, 3*(6), 2312–2324.
5. FCC first report and order: In the matter of revision of part 15 of the comparison's rules regarding ultra-wideband transmission system, FCC 02-48, April 2002.
6. Gezici, S., Tian, Z., Giannakis, G. B., Kobayashi, H., Molisch, A. F., Poor, H. V., et al. (2005). Localization via ultra-wideband radios. *IEEE Signal Processing Magazine, 22*(4), 70–84.
7. Win, M. Z., & Scholtz, R. A. (1998). On the energy capture of ultrawide bandwidth signals in dense multipath environments. *IEEE Communications Letters, 2*(9), 245–247.
8. Mireles, F. R. (2001). Performance of ultrawideband SSMA using time hopping and M-ary PPM. *IEEE Journal on Selected Areas in Communications, 19*(6), 1186–1196.
9. Batra, A., et al. (2003). *Multi-band OFDM physical layer proposal*. Document IEEE 802.15-03/267r2.
10. Gorniak, P., & Bandurski, W. (2008). Direct time domain analysis of an UWB pulse distortion by convex objects with the slope diffraction included. *IEEE Transactions on Antennas and Propagation, 56*(9), 3036–3044.
11. Qiu, R. C. (2002). A study of the ultra-wideband wireless propagation channel and optimum UWB receiver design. *IEEE Journal on Selected Areas in Communications, 20*(9), 1628–1637.
12. Qiu, R. C. (2006). A generalized time domain multipath channel and its application in ultra-wideband (UWB) wireless optimal receiver design—Part III: System performance analysis. *IEEE Transactions on Wireless Communications, 5*(10), 2685–2695.
13. Qiu, R. C., Zhou, C., & Liu, Q. (2005). Physics-based pulse distortion for ultra-wideband signals. *IEEE Transactions on Vehicular Technology, 54*(5), 1546–1555.
14. Molisch, A. F. (2005). Ultrawideband propagation channels-theory, measurement, and modelling. *IEEE Transactions on Vehicular Technology, 54*(5), 1528–1545.
15. Karousos, A., & Tzaras, C. (2008). Multiple time-domain diffraction for UWB signals. *IEEE Transactions on Antennas and Propagation, 56*(5), 1420–1427.
16. Bansal, B., & Soni, S. (2014). A new time-domain solution to transmission through a multilayer low-loss dielectric wall structure for UWB signals. *Wireless Personal Communications, 79*, 581–598.
17. Tewari, P., Soni, S., & Bansal, B. (2014). Time-domain solution for transmitted field through low-loss dielectric obstacles in a microcellular and indoor scenario for UWB signals. *IEEE Transactions on Vehicular Technology, 64*(2), 541–552.
18. Yang, W., Qinyu, Z., Jie, Z., & Naitong, Z. (2007). Analysis of UWB pulsed field diffracted by a perfectly conducting wedge. In *Proceedings of the second IEEE conference on industrial electronics and applications (ICIEA 2007)* (pp. 1539–1542), Harbin.
19. Veruttipong, T. W. (1990). Time domain version of the uniform GTD. *IEEE Transactions on Antennas and Propagation, 38*(11), 1757–1764.
20. Rousseau, P. R., & Pathak, P. H. (1995). Time-domain uniform geometrical theory of diffraction for a curved wedge. *IEEE Transactions on Antennas and Propagation, 43*(12), 1375–1382.
21. Karousos, A., & Tzaras, C. (2007). Time-domain diffraction for a double wedge obstruction. In *IEEE antennas and propagation society international symposium* (pp. 4581–4584), Honolulu, HI.
22. Liu, P., & Long, Y. (2009). Time domain UTD-PO solution for multiple building diffraction for UWB signals. *IEEE Electronics Letters, 45*(18), 924–926.
23. Han, T., & Long, Y. (2010). Time-domain UTD-PO analysis of a UWB pulse distortion by multiple-building diffraction. *IEEE Antennas and Wireless Propagation Letters, 9*, 795–798.
24. Remcom. (2008). Wireless insite, *Site-specific radio propagation prediction software user's manual version 2.3*.
25. Kouyoumjian, R. G., & Pathak, P. H. (1974). *The dyadic diffraction coefficient for a curved edge*. Nasa Contractor Report (NASA CR-2401), Washington.
26. Kouyoumjian, R. G., & Pathak, P. H. (1974). A uniform geometrical theory of diffraction for an edge in a perfectly conducting surface. *Proceedings of the IEEE, 62*(11), 1448–1461.
27. Burnside, W. D., & Burgener, K. W. (1983). High frequency scattering by a thin lossless dielectric slab. *IEEE Transactions on Antennas and Propagation, AP-31*(1), 104–110.
28. Soni, S., & Bhattacharya, A. (2010). Novel three-dimensional dyadic diffraction coefficient for wireless channel. *Microwave and Optical Technology Letters, 52*(9), 2132–2136.

29. Brigham, E. O. (1988). *The fast fourier transform and its applications*. Englewood Cliffs, NJ: Prentice Hall.
30. Sevgi, L. (2007). Numerical Fourier transforms: DFT and FFT. *IEEE Antennas and Propagation Magazine, 49*(3), 238–243.
31. Balanis, C. A. (1989). *Advanced engineering electromagnetic*. New York: Wiley.
32. Vandamme, J., Baranowski, S., & Mariage, P. (1995). High frequency diffraction by a dielectric wedge three dimensional study. In *Proceedings of the sixth IEEE international symposium on personal, indoor and mobile radio communications (PIMRC'95)* (pp. 125–129), Toronto.
33. Holm, P. D. (2000). A new heuristic UTD diffraction coefficient for nonperfectly conducting wedges. *IEEE Transactions on Antennas and Propagation, 48*(8), 1211–1219.
34. Luebbers, R. J. (1989). A heuristic UTD slope diffraction coefficient for rough lossy wedges. *IEEE Transactions on Antennas and Propagation, 37*(2), 206–211.
35. Ghavami, M., Michael, L. B., & Kohno, R. (2004). *Ultra wideband signals and systems in communication engineering*. Chichester: Wiley.
36. Barnes, P. R., & Tesche, F. M. (1991). On the direct calculation of a transient plane wave reflected from a finitely conducting half space. *IEEE Transactions on Electromagnetic Compatibility, 33*(2), 90–96.
37. Liu, P., Wang, J., & Long, Y. (2009). Time-domain double diffraction for UWB signals. In *PIERS proceedings* (pp. 848–852), Beijing, China.
38. Liu, P., Tan, J., & Long, Y. (2011). Time domain UTD-PO solution for the multiple diffraction of spherical waves for UWB signals. *IEEE Transactions on Antennas and Propagation, 59*(4), 1420–1424.

Bajrang Bansal was born in Haryana, India. He received his B.E. degree in Electronics and Communication from Institute of Technology and Management, Gurgaon, India in 2005 and the M.Tech. degree in VLSI Design and CAD from the Thapar University, Punjab, India in 2008. Currently he is working toward the Ph.D. degree at Delhi Technological University, Delhi, India. His research interests include wireless channel modeling and UWB technology.

Sanjay Soni was born in UP, India. He received his Bachelor of Engineering in Electronics Engineering from Madan Mohan Malviya Engineering College, Gorakhpur in 1997, the M.Tech. degree in communication engineering from IIT Kanpur in 2004, and Ph.D. in Wireless Communication Engineering from IIT Kharagpur in 2011. From 1998 to 2007 he was Assistant Professor in the Department of Electronics and Communication Engineering, G. B. Pant Engineering College, Pauri. From 2007 he joined IIT Kharagpur as a Research Scholar to pursue his Ph.D. In 2010 he joined back to the same institute at the post of Associate Professor. At present, He is an Associate Professor in the department of Electronics and Communication Engineering in G. B. Pant Engineering College, Pauri Garhwal, Uttarakhand, India. Currently, he is involved in teaching and research in the area of wireless communication. His research interest includes propagation modeling and characterization of wireless channel, time-domain analysis of propagation channel for UWB signals.

International Journal of Research (IJR)
e-ISSN: 2348-6848, p- ISSN: 2348-795X Volume 2, Issue 07, July 2015
Available at http://internationaljournalofresearch.org

An Experimental Investigation of an Inclined Solar Distillation and Domestic Water Heating System in Cogeneration

Jigmet Lodoe[a*]; Raghavendra Gautam[b]; SantoshKumar[c]& SandeepSudheer[d]

[a*]Research Scholar (M.TECH), Department of Mechanical Engineering ,Delhi Technological University,Delhi-India
[b]Assistant Professor, Department of Mechanical Engineering ,Delhi Technological University, Delhi-India
[c] Research Scholar(M.TECH), Department of Mechanical Engineering ,Delhi Technological University,Delhi-India
[d] Research Scholar(M.TECH), Department of Mechanical Engineering ,Delhi Technological University,Delhi-India
(jigmech10@gmail.com, raghvendrag80@yahoo.com,santee.me@gmail.com,sandeesudheerkallur@gmail.com)

[a*]Corresponding author,JigmetLodoe,Delhi Technological University,CVRHostel,room no:213,Bawana Road,delhi-110042,India,Tel No. +91-9910488350,email id: jigmech10@gmail.com

Abstract

Solar distillation system works on the simple principle of evaporation and condensation process .Unlike other types of distillation system which works either by consuming electrical energy or by burning fossil fuels; it works simply on thermal energy provided by the sun which is free in nature. The hot waste brackish water is cogenerated. It takes brackish or impure water as an input to the system and clean wateras well as hot brackish water as an output. The simplicity of the system makes it ideal for disaster situations mainly flood, where the water is plenty but unsafe to drink .Test run on the performance of the system on daily day basis in the month of April,2015 location : National Institute of Solar Energy (Latitude: $28^0 25' N$,Longitude:$77^0 9' E$) ,GwalPahari Haryana(India) by taking reading of daily clean water production corresponding to variation of temperature ,wind speed,solar radiation and ambient temperature during daytime for every 10 minutes from hour:min. (9.3a.m. to 5.00 p.m.)

Keywords : Brackish and saline water; Solar Distillation; Solar energy; Distilled Water; Low cost; Humidfication-Dehumidification process

1. Introduction

In the developing countries, unsafe drinking water, poor sanitary environment, malnutrition, and poverty are largely responsible for epidemic and deadly diseases. Half of the World's hospital beds are occupied by people suffering from water borne diseases.

In India, water-borne diseases alone are said to claim 73 million workdays every year. The cost in terms of medical treatment and lost of production is around Rs. 24,000 million (US $ 600 million) per year. More than 70 percent of Indian population lives in rural and sub-rural areas. India has nearly 559,553 villages out of which about 28% are reported to have unsafe drinking water due to chemical or biological contamination as reported by World Health Organisation(WHO).

International Journal of Research (IJR)
e-ISSN: 2348-6848, p- ISSN: 2348-795X Volume 2, Issue 07, July 2015
Available at http://internationaljournalofresearch.org

Now apart from consuming water intelligentily and spreading awareness of shortages of fresh water supply,there are various solution proposed like the Desalination Plants to produce fresh water andthere are nearly 15000 Desalination Plants worldwide so far but the drawback with this kind of technologies : powered by fossil fuels, high cost if backed by Solar Photovoltaic System and thirdly hot Brine released into the river.

Still the Desalination Plants are widely popular in the developed world but most of the people who are suffering from unsafe drinking water are living in rural areas or underdeveloped countries having a bright sunshine day where we can provide this kind of low cost design of Solar Distillation System solely work on thermal energy, i.e. Solar Energy as there is limited scope of electricity and shortages of investment in rural areas.

Xing li et al.(2014) have performed the solar humidification and dehumidification using a new sort of solar air heater with evacuated tubes and optimization by mathematical design method and found that higher outlet air temperature and relative humidity effectively increased fresh water production under same air temperature and cooling condition.CihanYildirim and Ismail Solmus (2014) have given the mathematical analysis by using the fourth order Ranga- Kutta method for humidification and dehumidification desalination system.J. Orfi et al.(2007) discussed dependency on the ratio between the salt water and the air mass flow rates and shown that, if ratio put to optimum level, it is possible to produce more than 40 L of fresh water daily per square meter of solar collector surface on a typical July day in Tunisia. ShaoboHou et al. (2005) have used the pinch technology which focussed on the ratio of mass flow rate of water to the dry air at a different spraying water temperature for performance optimization of solar humidification and dehumidification desalination system.Hikmet S. Aybar et al.(2005) have tested with variants : bare plate, black cloth-wick and black fleece wick and found that the fresh water production rate was increased two to three times when wick were used instead of bare plate. Margarita Castillo-Tellez et al.(2015) performed experiment on a forced convective double slope solar still and found that the thermal efficiency and production increment when the air velocity increases up to the value limit around 5.5 m/s and it then decreases at higher velocities and the velocity of 3.5 m/s is considered to be the optimum.Ahmad Ghazy (2002) showed the influence of environmental and design parameters. He also explains that the flow rate of feed water is insignificant on solar desalination system.

2. System description

Solar water distillation system (SWDS)consist of a galvanized steel absorber plate which is painted black and is covered with Teflon sheet formed a box of length ,breath and height are 0.5m,0.5m,and0.1m respectively.A black cloth is laid on the absorber plate to flow the water evenly on the plate and to increase the exposure time to solar radiation. The system is inclined to an angle of 45 degree in order to run the water down effectively and easily.

International Journal of Research (IJR)
e-ISSN: 2348-6848, p- ISSN: 2348-795X Volume 2, Issue 07, July 2015
Available at http://internationaljournalofresearch.org

fig.1. SWDS with black cloth and without Teflon sheet cover

2.1 Working : Feed water flow at the rate of (7.317ml per min) from a separate tank of brackish water through a pipe which is connected to distribution pipe on the top of absorber plate and its inlet is shown on the top right side fig.1. Now the water falls through the distribution pipe onto black cloth and can see the layer of water spreaded all over the absorber plate. Solarradiation warms the absorber plate and water on plate starts evaporating and finally condenses when it touches the cool Teflon sheet. The condensate water is collected at bottom in separate channel and the remaining hot water which is brackish in nature is also collected in separate channel and can used for heating purpose.

2.2 Instruments and its Specification

Solar irradiation measurement :Pyranometer

Manufacturer : the Eppley laboratory Inc. USA

Impedence : 650 ohm approx.

Receiver : Circular 1 cm^2, coated with Parson's black optical lacquer.

Temperature Dependence : ±1 % over ambient temperature -20 to 40 degree centigrade

Linearity : ±0.5 % from 0 to 2800 W/m^2

Response time : 1s

Anemometer

- Combined wind speed and direction sensor with 10 meter cable.
- ABS cups with retainer nut.
- Wiring details & test report copy.

Thermocouple

To measure the temperature of water and air inside the box (in degree centigrade) during the day.

3. Results of tests and discussions

The experiment was conducted during daytime between the hours of 10:15 am and 4:55 pm through the(21th of April ,2015 to 21th of May,2015) to study the performance of the system. In the test, amount of fresh water produced every 10 minutes during day and measured in measuring cylinder glass of 0.02m diameter corresponding to parameters like air temperature, solar radiation and wind speed.

In this paper ,the performance of the data taken for a day of the month(i.e. 22nd ,April) from hour:min 10:15am to 4:45pm when experienced maximum production of fresh or distilled water.

International Journal of Research (IJR)
e-ISSN: 2348-6848, p- ISSN: 2348-795X Volume 2, Issue 07, July 2015
Available at http://internationaljournalofresearch.org

3.1 From the table 1, the maximum rate of production of water increases in the time interval hour (11:25am to 1:55pm)

Table 1. Experimental data performed during day hours :

TIME	HEIGHT (m)	RADIUS (m)	VOLUME (m^3)
10.15	0	0	0
10.25	0.038	0.01	0.000011932
10.35	0.043	0.01	0.000013502
10.45	0.048	0.01	0.000015072
10.55	0.041	0.01	0.000012874
11.05	0.035	0.01	0.00001099
11.15	0.043	0.01	0.000013502
11.25	0.073	0.01	0.000022922
11.35	0.094	0.01	0.000029516
11.45	0.098	0.01	0.000030772
11.55	0.098	0.01	0.000030772
12.05	0.097	0.01	0.000030458
12.15	0.091	0.01	0.000028574
12.25	0.089	0.01	0.000027946
12.35	0.087	0.01	0.000027318
12.45	0.082	0.01	0.000025748
12.55	0.089	0.01	0.000027946
1.05	0.077	0.01	0.000024178
1.15	0.065	0.01	0.00002041
1.25	0.085	0.01	0.00002669
1.35	0.082	0.01	0.000025748
1.45	0.076	0.01	0.000023864
1.55	0.072	0.01	0.000022608
2.05	0.058	0.01	0.000018212
2.15	0.081	0.01	0.000025434
2.25	0.071	0.01	0.000022294
2.35	0.055	0.01	0.00001727
2.45	0.055	0.01	0.00001727
2.55	0.073	0.01	0.000022922
3.05	0.051	0.01	0.000016014
3.15	0.058	0.01	0.000018212
3.25	0.053	0.01	0.000016642
3.35	0.064	0.01	0.000020096
3.45	0.045	0.01	0.00001413
3.55	0.065	0.01	0.00002041
4.05	0.059	0.01	0.000018526
4.15	0.046	0.01	0.000014444

International Journal of Research (IJR)
e-ISSN: 2348-6848, p- ISSN: 2348-795X Volume 2, Issue 07, July 2015
Available at http://internationaljournalofresearch.org

4.25	0.06	0.01	0.00001884
4.35	0.058	0.01	0.000018212
4.45	0.075	0.01	0.00002355
4.55	0.05	0.01	0.0000157
total volume calculated			0.00084152

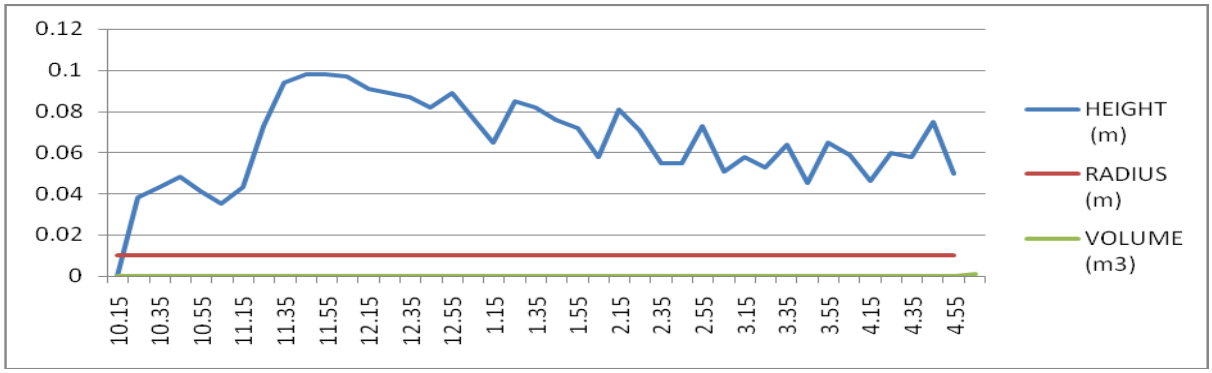

Fig.2. Distilled water production w.r.t time

From fig.2, the maximum production of fresh water (i.e 30.772ml) correspond to hr:min is 11:55 am. In order to analyse this, from Table 2.,the meteorological parameters has been recorded : Air temperature, pyrometer reading ,wind speed, wind direction and solar collector box inlet temperature(T5). The fresh water production is maximum corresponding inlet solar collector temperature is 66.354 ^{0}C,wind speed 3.9m/s ,air temperature 34.7106 ^{0}C and solar radiation 921.054 W/m^2.

3.2 Table 2: Meteorological data recorded from Data Logger :

time	temp1 (degC)	Temp2 (degC)	AIR TEMP (degC)	PYRO METER (W/m2)	WS (m/s)	WD (Degree)	T3 (degC)	T4 (degC)	T5 (degC)
10:15	33.78861	33.8882	29.8927	541.14594	1.88313	118.1248	30.0144	30.48	35.54249
10:25	33.9341	34.0004	29.96057	545.03229	2.15729	97.60529	30.05725	30.85	35.61501
10:35	34.90558	35.0084	30.61044	589.52234	1.95883	116.003	30.85876	31.667	36.50262
10:45	36.00957	36.0162	31.0697	643.61914	1.95172	154.2658	31.4642	32.185	37.03705
10:55	36.86571	37.0077	31.42282	694.56989	1.84056	89.50345	32.14376	32.54	37.75714
11:05	38.08306	38.0138	31.69995	741.89789	1.36393	117.6334	32.71545	32.722	38.94351
11:15	38.95967	39.009	32.23706	781.91296	1.85249	110.4459	33.61333	33.809	41.23521
11:25	40.60209	40.0161	33.29367	831.13922	1.83428	100.7608	34.25116	34.643	65.61723
11:35	41.63382	41.0042	33.79935	883.70862	1.65898	101.7789	34.77362	35.574	69.20994
11:45	42.55773	42.0204	34.392	893.20911	0.50497	162.9566	36.39042	36.48	71.51034
11:55	43.50193	43.0016	34.7106	921.05444	1.00125	73.80317	35.22845	36.282	70.35488
12:05	44.47609	44.0093	34.91736	909.86108	0.6694	21.11337	34.95366	36.955	66.9752
12:15	45.32588	45.0009	35.46741	912.48956	1.25101	92.90931	34.78605	37.045	68.42149
12:25	46.37498	46.0081	35.53302	932.89685	1.41436	95.51188	35.41653	36.831	68.59917
12:35	47.35219	47.0023	35.90735	943.24719	2.6885	104.1674	36.44224	37.893	68.60278

International Journal of Research
International Journal of Research (IJR)
e-ISSN: 2348-6848, p- ISSN: 2348-795X Volume 2, Issue 07, July 2015
Available at http://internationaljournalofresearch.org

12:45	48.35826	48.0092	36.04449	958.48962	2.20258	121.3044	36.12099	37.793	65.73474
12:55	49.57172	49.0052	36.20966	955.29773	2.86037	136.6818	36.50063	37.796	66.08283
01:05	50.29916	50.0255	36.34119	936.83911	4.66657	124.4062	37.58397	37.697	61.32798
01:15	51.38716	51.0032	36.49152	919.15845	2.92175	82.54091	39.224	37.371	67.1693
01:25	52.41565	52.0033	36.86224	913.48065	1.3644	122.8205	40.41548	38.33	72.41452
01:35	53.38478	53.0023	37.06778	908.12927	3.85273	88.72533	40.33407	38.248	68.41525
01:45	54.42944	54.0349	37.22272	904.24567	3.6735	143.4742	40.58913	38.364	66.13335
01:55	55.35653	55.008	37.39844	869.04797	2.77114	131.5803	40.62518	38.474	66.70116
02:05	56.29489	56.002	37.74207	822.99017	2.14046	80.10082	41.16352	38.675	69.61749
02:15	57.36283	57.0047	37.9613	779.71265	2.67609	97.51392	41.51331	39.22	67.95692
02:25	58.51859	58.0358	37.87704	745.0238	3.38106	111.0911	40.89417	38.899	68.16682
02:35	59.31875	59.0232	37.90701	724.5542	1.89685	106.8765	40.85691	38.776	70.05106
02:45	59.97492	60.0294	38.05267	658.28625	1.98353	105.3899	41.35727	38.908	70.35123
02:55	61.22981	61.0093	37.94922	568.77582	3.16288	108.8289	40.19754	38.71	67.6013
03:05	62.63996	62.0447	38.06628	555.69757	5.01703	57.3861	40.22823	39.947	67.5098
03:15	62.6053	63.0239	38.25403	461.75482	2.50974	113.1402	39.38255	40.135	67.5126
03:25	63.71277	64.0187	38.16672	330.62814	1.33304	122.4717	38.73515	40.462	60.24274
03:35	64.46634	65.0065	37.61102	179.88354	4.55981	124.3973	37.54161	39.315	56.26941

Fig. 3 shows the trend of meteorological data recorded every 10 sec .on 22nd April by Data Logger :

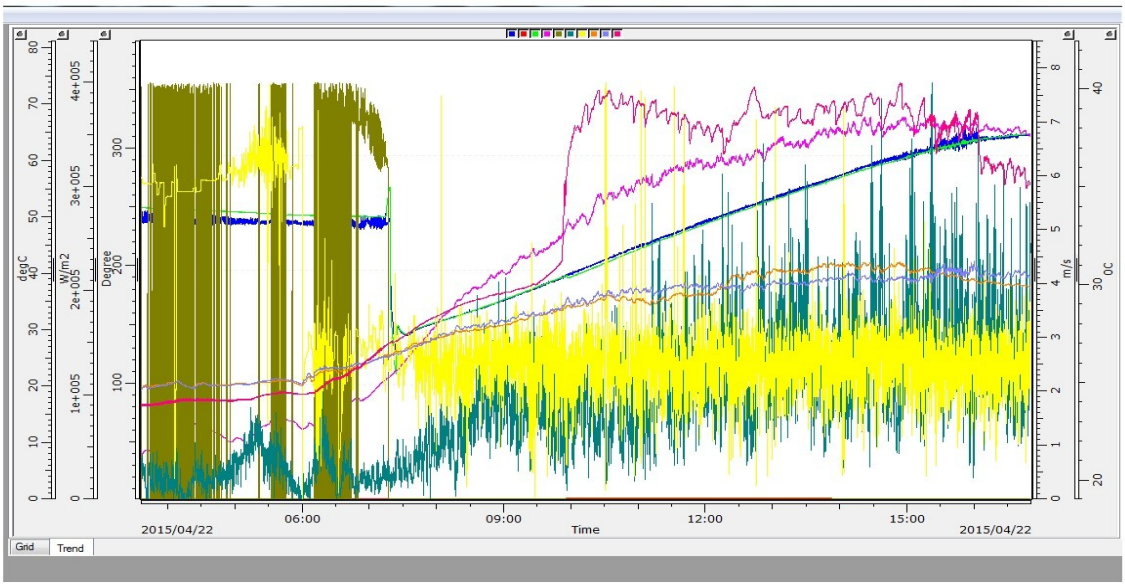

Fig3. The trend graph of the meterological data recorded

4. Conclusion

The production of the fresh water is maximum during a day in the month of22nd April, corresponding to Average air temperature(35.398^{0}C),Average wind speed (i.e. 2.333m/s),Average Solar Radiation (756.281W/m2) and Average solar collector box temperature (60.944^{0}C).The average maximum production of fresh water during the whole month is available at daytime hour (i.e.11.05 am to 2.55pm) of a day. Wind

speed plays a major role in the production of fresh water as it reaches to maximum value i.e30.772ml corresponding parameters (inlet solar collector temperature is 66.354 0C,wind speed 3.9m/s ,air temperature 34.7106 0C and solar radiation 921.054 W/m2) from Table 1 and Table 2. Now during the same daytime, at hour:min12:55 pm corresponding values of parameters (system inlet temperature 66.08280C, air temperature 36 .209 0C and solar radiation 955.297 W/m and wind speed 1.860 m/s) is higher though except wind speed yet produce less amount of fresh water i.e27.94 ml. Therefore wind speed accelerates the rate of evaporation and condensation process inside the system and hence produced more fresh water. Solar Water Distillation system(SWDS) is simple ,require less maintenance and low installation cost makes it ideal for the larger rural population safe drinking water as other options of Desalination Technologies is not feasible because of high cost and no electrification in rural areas.

Acknowledgements

The authors would like to thank and acknowledge the National Institute of Solar Energy (NISE) for giving permission to perform the experiments and grateful to UmakantaSahoo, Solar Thermal Testing Lab.(NISE) for his valuable guidance throughout the work.

References

[1]CihanYildirim and Ismail Solmus(2014), "a parametric study on a HDH desalination unit powered by solar air and water heaters", Energy Conversion and Management,vol.86,pp.568-575.

[2]G.N.Tiwari and N.K.Dhiman,(1991) "performance study high temperature solar distillation system" ,Energy Convers.&Mgmt,vol.32,pp.283-291.

[3]GN Tiwari and Hriday Narayan Singh, "Solar Energy Conversion and Photoenergy Systems-Solar Distillation-Vol.II

[4]Hikmet S. Aybar,FautEgelioglu,U.Atikol(2005), "an experimental study on an inclined solar water distillation system", Desalination,vol. 180,pp.285-289.

[5]Hassan ES Fath,AhmadGhazy(2002), "solar desalination using humidification – dehumidificationtechnology",Desalination142,pp.119-133.

[6]IDSA. (2010). Water Security for India: External dynamics. IDSA Task Force Report.

[7]J.Orfi,N.Galanis,M.Laplante(2007),"Air humidification–dehumidification for a water desalination system using solar energy",Desalination,vol.203,pp.471-481.

[8]Margarita Castillo-ellez,Issac Pilatowsky-Figuera,Aaron SanchezJuarez,Luiz Fernandez-Zayas(2015), "experimental study on the air velocity effect on the efficiency and fresh water production in a forced convective double slope solar still",Applied Thermal Engineering-vol.75,pp.1192-1200.

[9]ShaoboHou,ShengquamYe,Hefei Zhang(2005), "performance optimization of solar HDH desalination process using Pinch technology",Desalination183,pp.143-149.

[10]Rosegrant, M.W., Cai, X. and Clire, S.A. (2002). Global water outlook to 2025: Averting an impending crisis. Food Policy Report, IWMI. 36 pp.

[11]XingLi,GuofengYuan,ZhifangWang,HongyongLi, ZhibinXu(2014) , "experimental study on humidification and dehumidification desalination system of solar air heater with evacuated tubes",Desalination ,Vol .351,pp. 1-8

International Journal of u- and e- Service, Science and Technology
Vol.8, No. 6 (2015), pp.45-54
http://dx.doi.org/10.14257/ijunesst.2015.8.6.05

An Implementation of Intelligent Searching and Curating Technique on Blog Web 2.0 Tool

Harsh Khatter[1], Munesh C. Trivedi[2] and Brij Mohan Kalra[3]

Department of Computer Science
[1,2]ABES Engineering College, Ghaziabad, India
[3]Ajay Kumar Garg Engineering College, Ghaziabad, India
harsh.khatter@abes.ac.in, munesh.trivedi@abes.ac.in, brijkalra@yahoo.com

Abstract

There are numbers of web tools available to spread and explore information on internet. With the increasing use of Blogging sites, people are able to share their opinions, interests, experiences, and their views with others. However, it is not so easy to fetch required information from various Blogs in available time, which normally is very short. From last few years our major concern is on web searching and web mining. In this paper, a searching and curating model is discussed which introduces an approach of fetching the relevant information automatically from various Blog sites and fetches the personalized required information. That exactly is the need of the hour.

Keywords*: Web tools, Blogs, Web searching, Web mining, Curation, Internet, personalize search*

1. Introduction

Blogs are one of the major components of Web 2.0 also known as a Read-Write Web. Blogs are online diaries created by individuals, which provide excellent information on any topic all over the world. In this paper, a searching and curating model is discussed, which introduces a new approach of fetching the relevant information automatically from various Blog sites.

In this paper, a new Blog model is proposed to search the required information. The proposed model includes search module, login and personalization module, content curation module and rating module. Search module aggregates data from various blog sites. Curation module selects the relevant blog information from the searched data. Curation means to select the relevant information and removes the irrelevant data from the searched data. The content curation module automatically curates the blog posts from other blog sites. This proposed model performs searching and then curation on the Blog posts based on user's interest *i.e.,* proposed model is mining blog posts based on user's interest. That is why the model is named as "Blogminer".

This proposed Blog also works as a blog search engine, which gives blog post results from other blog sites available on World Wide Web. This new method of fetching relevant blog posts automatically called content curation, and this will improve the knowledge experience of a user and reduces the content search time, and utilization of system resources. In this paper, the gaps in current blog posts searching techniques are discussed. Further, the proposed solution with implementation is given. Hope this model will surely improve the searching and blogging experience of the user.

2. Literature Review and Gaps

Singh, *et al.,* (2010) mention that it is easy and simple to create blog posts, which has attracted people and companies across disciplines to exploit it for varied purposes. The

ISSN: 2005-4246 IJUNESST

valuable data contained in posts from a large number of users across the world provide a rich data source. Nasr and Ariffin (2008) also said that Blogging can also be seen as a means of Knowledge Sharing. They stated that the research delves into the use of blogging as a fast, up-and-coming means of knowledge and quality content sharing amongst communities of bloggers with similar interests. Dolinska (2010) discussed a simple blog searching framework and stated that Knowledge gathered on blogs can be used in personal e-Learning. It is a more informal and personal way of learning than the one is offered by traditional e-Learning courses. The framework consists of four modules: BL search tool, SNA analyzer, Network Visualizer, K-Blogs List as shown in Figure 1.

Singh and Joshi (2010) discussed that because of the increasing number of blogs and their unique characteristic, blogs have received much attention from researchers and various studies have been conducted. In addition, optimization of the mechanism is required to obtain the best results from the blogs.

If we discuss about the normal web content searching, over the past decades, various searching techniques are come into existence with the growth of World Wide Web. From the starting of the Web era, various searching methods, techniques and searching algorithms are introduced and as per searching requirement, they come in usage or implemented. There are lots of searching methods in which search can be done on keywords, on queries, on topics, on phrases, on pages, etc. The query based and topic based search is used in forums, whereas the page search or phrase search is used in search engines where the exact finding is required. Rest of all websites use keyword based searching. Keyword based searching provides an easier way to search the contents on internet. In the same way, maximum number of websites use keyword based searching.

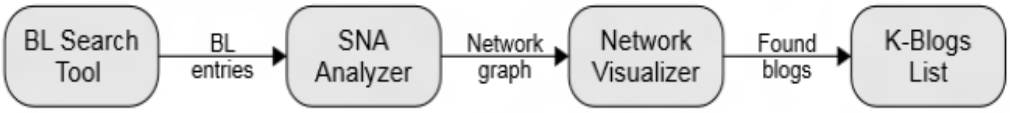

Figure 1. Simple Blog Searching Framework Scheme

Fu and Anyanwu (2011) discuss an effectively interpreting keyword queries on databases. Before this method, heuristics was used for interpreting the keyword queries. Keyword search queries might be in structured, unstructured or semi structured form. On Web, mostly the available data is in unstructured or semi structured form. Guoliang Li, *et al.,* (2008) suggested an efficient 3-in-1 keyword search method which works for all types of data. Zhou (2010) proposed an algorithm of personalized blog information retrieval based on user's interest model. He discussed the system architecture of representation and the algorithm flow of blog document similarity based on the vector space model.

Some major blog related works are discussed above. This is an evolutionary field. Therefore, everyday a new approach, framework, or model is introduced. Might be some other ensuing algorithm or approach will come with some better idea and great functionalities.

A. Gaps observed:

After the literature survey, various gaps are observed in the current systems.

- There is a large list of available blog search engines but they all are related to specific field only, *i.e.,* they do not cover the entire variety of blog topics.
- To search a relevant post, user has to search it manually on each individual blog site, which itself will consumes lot of time, effort and a large number of clicks. Moreover, the clicks introduce unnecessary traffic due to advertisements in each page, which consumes important system resources unnecessarily.
- At present, there is no method available, which automatically traverses other websites using their URLs and fetches the required information. The important factor is

"What exactly the user wants". That exactly is the need of the hour. There is a need to add some more functionality and service to the blogs.

In terms of blog and blog post searching, numbers of methodologies are already designed and published. After studying the work done in the past in the field of Blogs, Blog architecture, model, framework, its implementation, Blog posts searching, tagging, clustering, ranking, rating, and Blog personalization, it is concluded there is a time to club all in a simplified form. The goal of this paper is to find out the measures to provide user with reliable and accurate blog information conveniently.

3. Proposed Solution

Based on the gaps of current available systems, there is a need for a new approach, which will improve user's searching and knowledge experience with the blogs. The main objective is to create a blog, which will curate the content from various blogs as per the user requirements, and displayed to the user via a blog site named BlogMiner, (Khatter and Kalra, 2012).

As per the requirement, a new method, called Curation has been proposed. Curation means to select the relevant information from the aggregated data, which is aggregated from various other blog sites. The proposed model follows two main steps: searching and then curating. In searching, data from various blog sites is searched and aggregated. The aggregated data is stored into a temporary database. Curation method filters out irrelevant data and fetches the relevant information from the searched data based on user's interest. This data is displayed to the user through a web interface after searching, aggregation and curation.

The proposed model is named BlogMiner and provides following facilities:

- Allows a user to start its own blog.
- Allows a user to perform a local search *i.e.*, search within the blogs of BlogMiner.
- Allows a user to perform a global search *i.e.*, search for blog posts on WWW.

Therefore, the BlogMiner combines the blogging and searching together at one place, which is not available in the present system. (Khatter and Kalra, 2012).

A. Working of curation module:

The curator performs the following steps:

Step 1. Checks for the blog URLs from the database, which is inserted by a user.

Step 2. Traverses each URL and uses wget utilities to retrieve the required blog posts.

Step 3. Fetches all blog posts and hyperlinks on that page and temporarily stored in a database.

Step 4. Selects top rated blog posts from the temporary database within the specified period of blog creation.

Step 5. Stores the selected blog posts into the blog post database and rest of the contents is dropped.

Step 6. Relevant blog posts are displayed to the user through Curator's Interface.

The proposed system works in the manner as discussed below and shown in Figure 2:

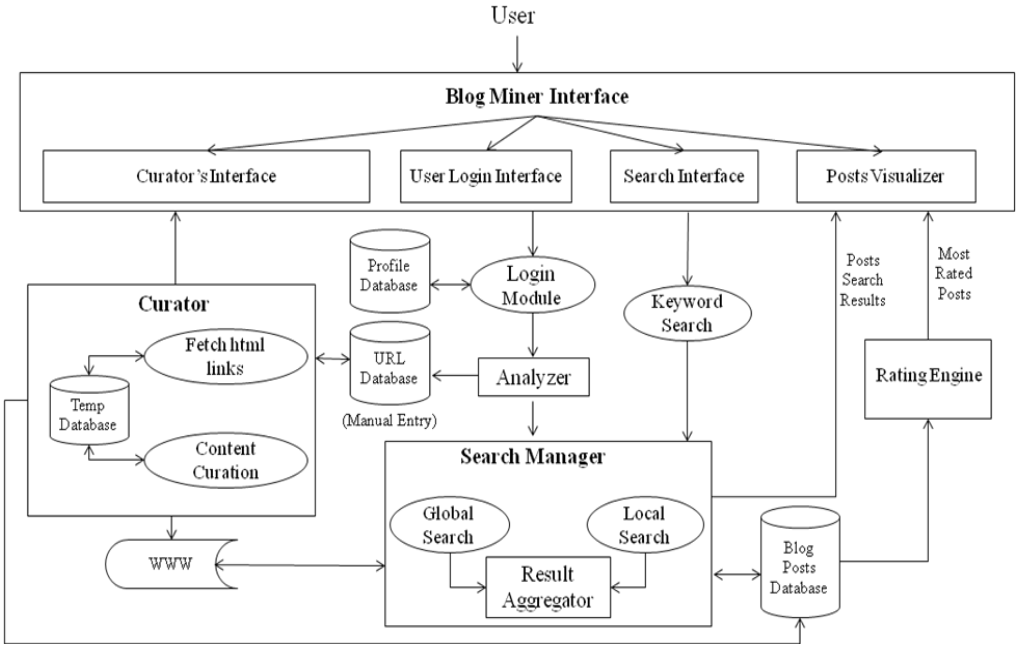

Figure 2. Model of BlogMiner

User will be presented with an opening page in which following facilities are available. User interacts with BlogMiner Interface to retrieve relevant blog posts. User enters a keyword in search bar, *i.e.*, local search bar or global search bar, to fetch the relevant blog posts. The working for local and global search is discussed separately in tabular form in Table 1.

Table 1. Working for Local/Global Search

For Local Search	For Global Search
1. Enters the keyword in local search bar for local blog posts search. **2.** Searches local blog posts for the input keywords (searches within local blog site for the relevant blog posts). **3.** Search is applied to the local blog posts database. **4.** Relevant blog posts are retrieved and presented to the user through BlogMiner Interface. **5.** Now user can read, comment, share and rate the blog posts.	**1.** Enters the keyword in global search bar to search for blog posts in blogosphere. **2.** Searches blog posts for the input keywords (Blogosphere search with the help of Google blog search). **3.** Google blog search results are presented to the user through BlogMiner Interface. **4.** When user clicks on any of the blog post of blogosphere post result, the user is redirected to the webpage of clicked blog post. **5.** User can read that blog post and share, but cannot comment and rate it.

When a user logs in, he/she is presented with blog posts of his interest only. Search Manger searches for the blog posts of user's interest from the blog posts database based on his/her specific interests. Login is of two types: Login for existing users and login for new users. For exiting users, users have to give their login id and password to perform sharing, rating, commenting, or creation of blog posts. For new users, users have to choose their username, password, and field of interests. Based on these, the registration of new users will be completed.

Curator curates the blog posts automatically. It takes the URLs from the URL Database. Periodically, Curator fetches all blog posts from to those URLs. Only the selected blog posts are stored into the blog post database and rest of the content is dropped.

User is permitted to rate the local blog posts by stars and the rating is displayed publicly to all the users in the form of stars. All the blog posts are displayed in reverse chronological order, and user can comment, rate, add and share the post information.

4. Implementation and Results

There are various parameters, which distinguish existing systems to proposed system, BlogMiner. Table 2 highlights the parameters in which existing and proposed system is same whereas Table 3 shows the parameters in which these models are different.

Table 2. Similarities between Existing and Proposed Model

Parameters	Existing system	Proposed system
Blog post search	Yes	Yes
Search engine	Yes	Yes
Top Rated	Yes	Yes
Latest Search/ Updates	Yes	Yes

Table 3. Differences between Existing and Proposed Model

Parameters	Existing system	Proposed system
Combined Search Approach (Blog + Blog Search Engine)	No	Yes
Automatic Content Curation	No	Yes
Personalization	No	Yes
Spams/Advertisement	Yes	No
Resource Consumption	More	Less

A. Testing

Some major blog search engines and blogging sites results are compared with the result of proposed model, BlogMiner. The blog search engines/blogging sites taken are **Google blog search (Earlier, it was blogspot.com), Technorati, Icerocket, and Regator.**

Individually, the resultant posts of these blog post sources are compared with BlogMiner post result on different keywords (*i.e.*, user's interest) as **Olympics, Apple, cricket, conferences, and tablet**. This comparison or test is performed only on the top 20 posts results. While fetching the blog posts results from blog sources, not all results may be blog posts or relevant to the keyword. Therefore, only the relevant blog posts are carried out.

1) Scenario 1 - Google blog search and BlogMiner

Table 4 shows the relevant and irrelevant posts results on education, web, cricket, conferences, and technology keywords of this scenario. Here, irrelevancy shows not all results are posts; some are images, videos, or a news article. Figure 3 shows the graphical representation of Scenario 1.

Table 4. Scenario 1 - Google Blog Search and Blogminer

Keywords	Google blog search		BlogMiner	
	Relevant Posts	Irrelevant Posts	Relevant Posts	Irrelevant Posts
Olympics	18	2	20	0
Special Issue	9	11	20	0
Apple	18	2	19	1
Tablet	16	4	19	1
Cricket	18	2	18	2

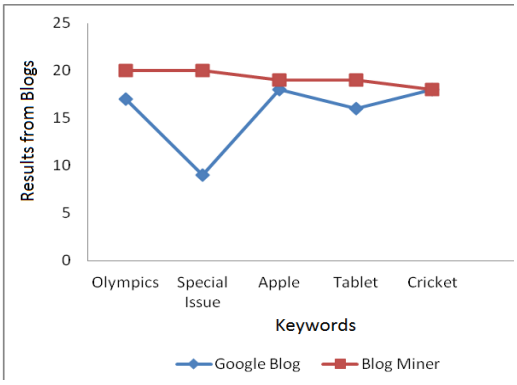

Figure 3. Scenario1 - Google blog search and BlogMiner

2) Scenario 2 - Technorati and BlogMiner

Table 5 shows the relevant and irrelevant posts results on education, web, cricket, conferences, and technology keywords of this scenario. Here, irrelevancy shows the semantically different posts. Figure 4 shows the graphical representation of Scenario 2.

Table 5. Scenario 2 - Technorati and Blogminer

Keywords	Technorati		BlogMiner	
	Relevant Posts	Irrelevant Posts	Relevant Posts	Irrelevant Posts
Olympics	20	0	20	0
Special Issue	1	19	20	0
Apple	18	2	19	1
Tablet	17	3	19	1
Cricket	18	2	18	2

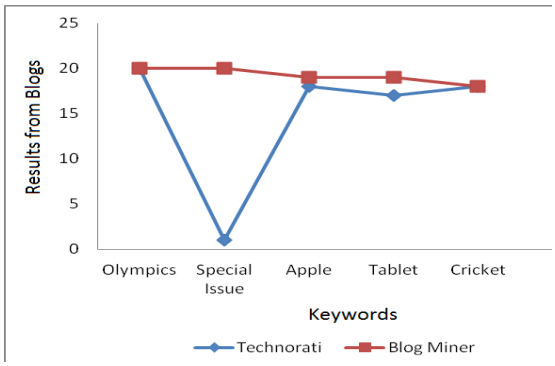

Figure 4. Scenario 2 - Technorati and Blogminer

3) Scenario 3 - Regator and BlogMiner

Table 6 shows the relevant and irrelevant posts results on education, web, cricket, conferences, and technology keywords of this scenario. Here, irrelevancy shows the semantically different posts and ambiguity. Figure 5 shows the graphical representation of Scenario 3.

Table 6. Scenario 3 - Regator and Blogminer

Keywords	Regator		BlogMiner	
	Relevant Posts	Irrelevant Posts	Relevant Posts	Irrelevant Posts
Olympics	16	4	20	0
Special Issue	2	18	20	0
Apple	14	6	19	1
Tablet	9	11	19	1
Cricket	14	6	18	2

4) Scenario 4 - Icerocket and BlogMiner

Table 7 shows the relevant and irrelevant posts results on Olympics, web, cricket, conferences, and technology keywords of this scenario. Here, irrelevancy shows the semantically different posts and language problem (translator must be required). Figure 6 shows the graphical representation of Scenario 4.

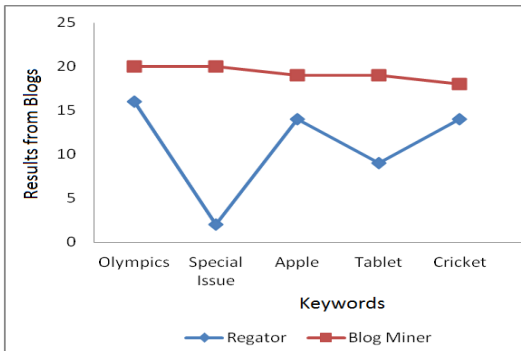

Figure 5. Scenario 3 - Regator and Blogminer

Table 7. Scenario 4 - Icerocket and Blogminer

Keywords	Icerocket		BlogMiner	
	Relevant Posts	Irrelevant Posts	Relevant Posts	Irrelevant Posts
Olympics	13	7	20	0
Special Issue	6	14	20	0
Apple	14	6	19	1
Tablet	8	12	19	1
Cricket	7	13	18	2

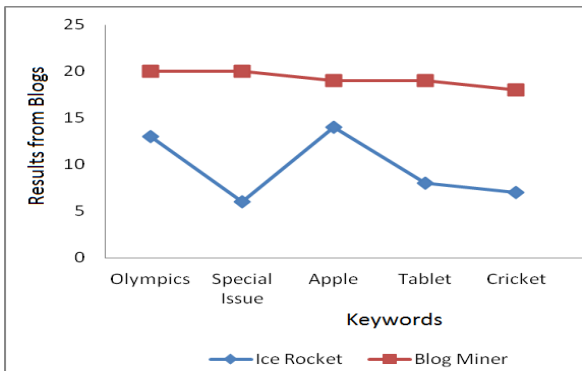

Figure 6. Scenario 4 - Icerocket and BlogMiner

B. Analysis

After observing the results, it is analysed that the proposed model, BlogMiner, is improving the searching experience of user by improving the relevant results. In compare to other blogging sites and blog search engines, results of BlogMiner are much better. An analytical table, Table 8 is shown below.

Table 8. Results Of Average Improvement In Relevant Blog Posts Search

Blog Posts Source	Average % of relevant blog posts
Google Blog Search	79%
Technorati	74%
Regator	55%
Icerocket	48%
BlogMiner	**96%**

In Table, the average percentage is calculated based on the relevant blog posts. In Google Blog Search, not all search results are blogs. Some of the results are the video, images, and other content like articles. After analysis, it is found that only 79% of the results are blog posts, or say, a relevant posts. In technorati, based on the sematics, the difference is easily examined between the relevant and irrelevant posts. The average blog posts search results are 74%. In Regator, 55% of the posts are relevant and rest of the posts are irrelevant due to the semantic difference and ambiguity. Icerocket gives 48% of relevant blog posts. BlogMiner curates only the relevant blog posts. Therefore, while searching the keywords only the relevant blog post results are displayed to the user and its average percentage of relevant posts is 96%.

5. Conclusion

BlogMiner is a combination of both, a blog search engine and a blog site. In addition, user can customize their search results based on his interest. To search a relevant post, user does not require wasting his valuable time on clicking here and there for getting the required information. Moreover, with this functionally user will get what exactly he/she wants. This proposed work is an innovative idea in the field of information retrieval from blogs and will surely improve the information searching and the knowledge experience of users.

References

[1] I. Dolinska, "Simple Blog Searching framework based on Social Network Analysis", Proceedings of the International Multi-conference on Computer Science and Information Technology, Poland, October 18-20, **(2010)**, pp. 611–617.

[2] H. Fu and K. Anyanwu, "Effectively interpreting keyword queries on RDF databases with a rear view", Proceedings of the 10th international conference on The semantic web – Germany, vol. Part I, **(2011)** October 23-27, pp. 193-208.
[3] G. Li, B. C. Ooi, J. Feng, J. Wang and L. Zhou, "EASE: an effective 3-in-1 keyword search method for unstructured, semi-structured and structured data", Proceedings of the International conference on Management of data ACM SIGMOD, Canada, **(2008)** June 09-12, pp. 903-914.
[4] N. A. Ahmad and M. A. Mazeyanti, "Blogging as a means of knowledge sharing: Blog communities and informal learning in the blogosphere", Proceedings of the International Symposium on Information Technology, Kuala Lumpur, Malaysia, **(2008)** August 26-28, pp. 1-5.
[5] A. K. Singh and R. C. Joshi, "Semantic tagging and classification of blogs", Proceedings of the International Conference on Computer and Communication Technology (ICCCT), Allahabad, India, **(2010)** September 17-19, pp. 455-459.
[6] V. K. Singh, D. Mahata and R. Adhikari, "Mining the Blogosphere from a Socio-political Perspective", Proceedings of the International Conference on Computer Information Systems and Industrial Management Applications (CISIM), Poland, **(2010)** October 8-10, pp. 365 - 370.
[7] Z. Ping, "Research on Personalized Blog Information Retrieval", Proceedings of the International Conference on Web Information Systems and Mining (WISM), China, **(2010)** October 23-24, pp. 289-292.
[8] K. Harsh and K. B. Mohan, "A New Appraoch to Blog Information Searching and Curating", Proceedings of the CSI 6th International Conference on Software Engineering (CONSEG), IEEE, Indore, **(2012)** September 5-7, pp. 372-377.

Authors

Harsh Khatter, he is working as assistant professor in ABES Engineering College, Ghaziabad, India. He has done Btech and M.tech in Computer Science stream. He is working on Web 2.0 tools, Blogs. His research interests include Web service, Data Mining and Databases, Fuzzy logics. He is a member of IEEE Society, CSI India.

Munesh Chandra Trivedi, he has completed post-graduation and doctorate in Computer Science. He has rich experience in teaching the undergraduate and postgraduate classes. He has published 20 text books and 50 research papers. **IEEE computer society has Sponsored (**Technically & financially) him for organizing IEEE international conference. He has also worked as Member of organizing committee in several IEEE international conferences in India and abroad. He is on the review panel of IEEE Computer Society, International Journal of Network Security, Pattern Recognition letter and Computer & Education (Elsevier's Journal). He is active member of IEEE Computer Society, International Association of Computer Science and Information Technology, Computer Society of India, International Association of Engineers, and life member of ISTE.

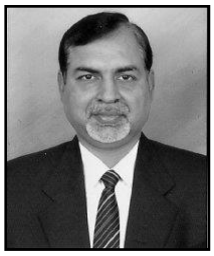

Mohan Kalra, he is currently working as a Professor and Head in the Department of Computer Science and Engineering at Ajay Kumar Garg Engineering College, Ghaziabad, India. He has done his B. Tech from Delhi College of Engineering, Delhi in 1977 and completed his M. Tech from IIT, Delhi in 1991. He has vast experience of 35 years of academia and industry in CSE and IT fields. His research interests include eLearning, Computer Networks, and Digital Logic Design. He is also a member of several professional bodies: IEEE, CSI, and IET.

IOSR Journal of Environmental Science, Toxicology and Food Technology (IOSR-JESTFT)
e-ISSN: 2319-2402,p- ISSN: 2319-2399.Volume 9, Issue 6 Ver. III (Jun. 2015), PP 48-53
www.iosrjournals.org

Assessing the Environmental Impacts Associated Withthe Life Cycle of Electronic Equipment

Ashwin Mehta[1], Deepak Chauhan[2], Sunil Kumar[3] and Anunay Gour[4]
(Department of Environmental Engineering, Delhi Technological University, Main Bawana Road, New Delhi, Delhi – 110042, INDIA)

Abstract: *Electronics is increasingly becoming a part of many aspects of life. This has led to a fast growing demand for electronic. The production of electronics requires various materials, energy, man-force and other resources. The various stages of production have their share of impact on the environment. Discarding these electronics poses another, rapidly increasing, danger on the environment. This is the issue of e-waste or electronic waste. A lot is being done to reduce the problems being caused by the electronic industry, but with optimization even more environment-friendly and economical solutions are possible. Environmental planning involves production in a sustainable manner with consideration given to the natural environment, social, political and economic factors. This paper broadly talks about the impacts, of the current practices of the electronics industry, on the environment and suggests ways to reduce those impacts. The main study is divided into sections discussing the environmental aspects, of the industry, related to raw materials, the manufacturing process, the packaging stage and discarding the equipment, i.e., generation of e-waste.*
Keywords *-Electronic Equipment, Environmental Impacts, E-waste, Packaging.*

I. Introduction

Technological advancement has been a major driver of progress and development. A rapid evolving and growing electronics industry is a necessity for continual improvement. The word 'electronics' refers to various types of equipment which involve but are not limited to computers, telephones, television, audio equipment and digital cameras.For the manufacture of electronics, the environment is exploited and after use, most of the constituents are returned to the environment, either directly or after applying certain treatment. Hence, e-waste is a growing problem.The sections of the paper help to understand the environmental impacts of the life cycle of electronics.

II. Literature Review

1.1 Raw Materials

Rapid changes in technology, coupled with falling prices and planned obsolescence, has led to rapidly growing demand for electrical and electronic devices.

The components which constitute the electronic devices are made up of certain processed raw materials. These components, such as capacitors, use metals like copper, aluminium, silver etc. andpetroleum based products, the most common being plastic. Metals are preferred for their conductivity and plastic for its heat resisting properties. Other materials used include ceramics, silicon and cobalt.

Mining for minerals can have adverse effects on the environment. These include erosion, loss of biodiversity, and contamination of water resources, soil. At times, mining is accompanied with additional forest logging in the vicinity.

Mineral exploration optimization is an important aspect for environment protection."The optimization of selection of ore deposit types and regions of search, the first task of an exploration planner, is based upon univariate stochastic models of the economic, geometric and occurrence characteristics of deposits supplemented by statistical testing requiring MANOVA and ANOVA models, ...The optimization of mineral exploration is carried out through the use of quantitative models which aim at representing the various stages of the mineral exploration sequence as faithfully as possible,but in a simplified manner..... "[1]

1.2 Manufacturing Process

Evaluating the environmental impacts of processes involved in production of electronic devices/ components is often difficult due to diverse inputs and outputs involved. Hence to form a better understanding we will be taking the example of semiconductors, a widely recognized and used constituent of most electrical and electronic devices. The same manufacturing issues are associated with most of the other constituents of electrical and electronic devices.[2]

2.2.1Environmental impacts included in the manufacturing of these constituents include:

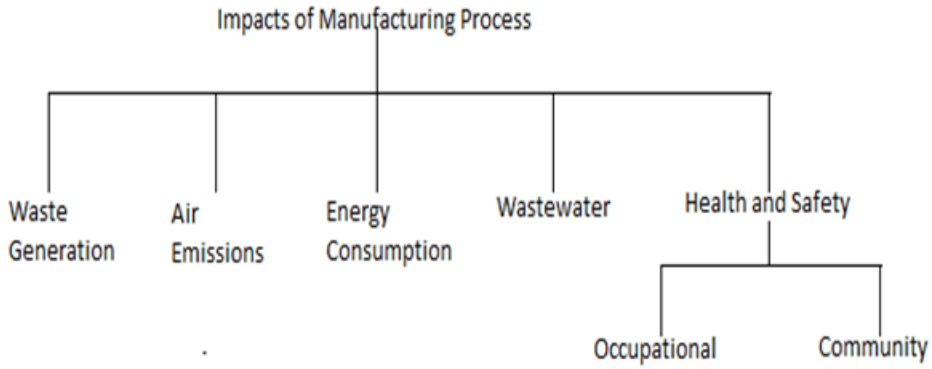

Fig.1 Impacts of Manufacturing Process

(a) Waste generation: Almost all steps involved in manufacturing lead to generation of waste, like spent epoxy material, which is generated in the manufacturing of semiconductors and PCBs. The environmental impacts can be prevented by techniques such as: process modification, raw material substitution, waste segregation and substance recovery. Also proper method and equipment is to be put in place for waste handling and disposal.

(b)Air Emissions: Substances such as volatile organic compounds (VOCs), acid fumes etc., which are toxic and corrosive in nature are to be given special attention. Greenhouse gases are also a nuisance. Diffusion and cleaning processes are the major contributors off all these emissions at the manufacturing stage. Scrubbers are preferable for tackling this issue. In some cases, equipment that can handle high flow rates might be required. Greenhouse gases can be controlled by enhancing energy efficiency, promoting forestry, carbon capture technologies, increasing use of renewable forms of energy, etc. There is always scope for emission-specific solutions. For example, VOC emissions can be controlled by installing regenerative thermal oxidizers as an add-on controlling device.

(c)Energy Consumption: With highly mechanized processes involved energy consumption is bound to be high for manufacturing semiconductor and related devices. Hence, optimal energy consumption becomes a necessity. This can be achieved while reducing the impact on the environment, caused due to other reasons, as stated above. What this means is that reduced energy consumption can be achieved in collaboration with advanced abatement efficiency.

(d) Wastewater: Wastewater may contain organic as well as inorganic substances. These include metals, cyanides, suspended solids, etc. Reuse is important to conserve the resource and reduce potential discharge impacts.For treatment of the wastewater, from the manufacturing process, source segregation and pre-treatment need to be considered as important. Further, units need to be involved for purposes like, reduction in heavy metal, chemical oxidation, dewatering and disposal of residuals. But these units need to be installed keeping in mind the processes involved in the manufacture. In some cases, additional control techniques, for example membrane filtration, activated carbon, etc., might be required.

Before moving on to occupational health and safety, PCBs also require some attention. A printed circuit board (PCB) is used in an electronic device to connect electronic components. This connection is made using conductive tracks, pads and various other features.

Many methods have been developed to reduce the environmental impact of PCB production. This includes improvements in the manufacturing process, like for cleaning and preparation of the surface, non-chelating cleaners can be used and the reuse of cleaners can be done. Also for etching, use differential plating and pattern versus panel plating. And ion exchange technologies can help in metal recovery.

(e) Occupational Health and Safety: The occupational health and safety hazards included in the manufacturing process include exposure to hazardous chemicals (such as acids, bases, metal powder, etc.) and materials released by substrates. To protect workers from the effects of exposure, substitution of hazardous materials can be considered. Also, gas detectors and other detection& alarm systems should be installed. Material specific protection should be looked into, which can involve isolated, automated systems and also engineering controls (such as ventilation systems).Precautions like periodically cleaning clothes and preferring wet processes, to avoid the dust nuisance, are also necessary.

Community Health and Safety: Community health and safety is also to be taken into consideration by the organization and the entities undertaking the manufacturing process, as this may have impact beyond the life of the project. Water quality, fire safety, traffic safety, disease prevention and emergency preparedness are some of the issues which fall in this category and vary according to the manufacturing process. [3,4]

2.2.2 Power saving and Eco-labels

In1992, the U.S.EPA introduced the Energy Star symbol. Energy Star power management features help in order to reduce the amount of energy consumed by various computer systems. Buyers must ensure that this symbol is present, when they buy the device. Apart from lower energy consumption, the Energy Star symbol ensures the use of technology which increases efficiency and hence the life of the device. The devices which have these systems, that are Energy Star qualified, are not expensive when compared to the devices without these systems. [5]

Eco-labels are for environmental performance certificates. In contrast to self-claimed performances, these labels are provided by an impartial third party. Eco-labels generally represent more than simple power saving technologies. Eco-labels are issued based on overall performance efficiency and proven environmental preference. [6]

1.3 Packaging

An important but often overlooked aspect of the electronics industry, which can have an impact on the environment, is the packaging. The disposal issue with packaging material is well understandable. Paper and plastic are the most used materials for packaging.Over the years, with changing shapes & sizes of devices, and for enhancing the appeal of the device, organizations, manufacturing these devices, have constantly being changing the way they pack these devices. The material used, at times, is non-biodegradable and toxic in nature.But with growing concern for the environment around the globe and organizations understanding their role, there have been many innovations, which without overlooking the safety and appeal factor for the device, are minimising the impact of the organization on the environment and also promoting environment conservation.

The properties which make a packaging material environment-friendly include biodegradability, recyclability and reusability. Also, the manufacturing process of the packaging material helps determine its overall environmental impact. The packaging can be optimized by designs which require less material.

An innovative methodology used by the company Dell,is the application of bamboo as a packaging solution. They use it for cushioning some lightweight products. Dell bamboo packaging is certified as compostable which also implies its biodegradability. Other advantages of bamboo are good strength, good durability and recyclability. Also, it is easy to grow bamboo and growing bamboopromotes health soil by preventing soil erosion. [7]

Another lightweight and odourless packaging solution, which is biodegradable, is thermocol. Thermocol, a packaging solution having customized finishes, has a cushioning property that avoids damages. Also, it is insulated and resistant against fungus.

Recycled paper and cardboard boxes should be promoted, as paper products are generally considered not to be environment friendly. The inks, used for decoration, should also be environment friendly.

1.4 E-waste

E-waste can be defined as electrical and electronic equipment, which includes all components that are part of the product at the time of discarding. [8]

1.4.1 Constituents of e-waste

Electronic devices that can be hazardous include televisions, CRT computer monitors, LCD screens. But the list is not limited to this.

Though electrical and electronic equipment contains components that are hazardous, they do not pose a threat to the environment until it reaches the stage of discarding, after which it is considered e-waste and what follows is processing and disposal. For example, one can consider the cathode ray tubes (CRTs) of computer monitors. These contain heavy metals such as lead, cadmium and barium. These heavy metals can be very harmful to the health (human respiratory and nervous system) and environment if they enter the waste stream. [9] Apart from this, e-waste also contains non-hazardous substances such as tin, copper, aluminium etc.In addition to these, electronic items containvaluable materials. This includes, for example, gold and silver. Gold is used with respect to connector plating, primarily in computer equipment. [10]

1.4.2 Quantity of e-waste

An important thing to note is that a large number of equipment labelled e-waste is not waste in the true sense. But it is rather equipment or components that can be reused or recycled, which can lead to material recovery. 50 million metric tons of e-waste is estimated to reach dumps every year.The US-EPA has estimated an increase in the quantity of e-waste generated globally. Something more surprising and a cause of concern is only around 13% of this current quantity is recycled. Also it is estimated that amount of e-waste generated globally will reach 65m tonnes by 2017.[11]

Also international trade of waste helps developed countries to dump e-waste in developing countries for disposal and treatment. Though many regulations have been formulated to avoid developed countries from dumping toxic waste (by first screening the waste) into developing countries, but it is still considered easy for them to dump the toxic waste, to save money, in the name of recycling.In India, e-waste handling and recycling is mostly done by the informal sector. Being informal, they do not have proper techniques and knowledge to handle the e-waste. Hence, processing occurs at a very rudimentary level. This leads to risk of harm to human health and environment. Fair trade involving cooperation can lead to creation of sustainable jobs. This can also bring affordable technology to countries, with high repair and reuse activities. [12,13]

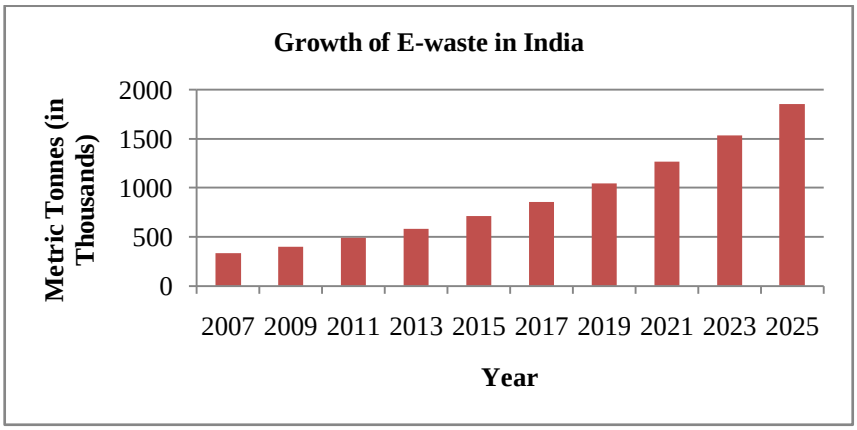

Fig.2 Growth of E-waste in India [14]

1.4.3 E-waste management

Optimizing e-waste management can help in conserving natural resources and money, a lot of which goes into manufacturing of the equipment. According to a UN study, to manufacture one computer and a screen, it requires at least 22 kg of chemicals, 240 kg of fossil fuels and 1.5 tonnes of water (Kuehr and Williams, 2003). Also, according to the EPA, recycling 1 million cell phones can recover about 24 kg (50 lb) of gold, 250 kg (550 lb) of silver, 9 kg (20 lb) of palladium, and more than 9,000 kg (20,000 lb) of copper. [15]

(a) Incineration: Incineration involves burning to destroy the waste. In the case of e-waste, which contains toxic substances, incineration can lead to dispersion of these substances into the environment. Toxicity is not limited to the gases released but also the residue ash is harmful to the health and environment. When flame retardants are incinerated, dioxin formation is catalysed by copper, present in PCBs and cables. Inhalation of emissions released from incineration of e-waste (with no prior treatment) can lead to acute respiratory problems and also chronic health related issues. For example, the burning of PVC, which releases hydrogen chloride. On mixing with water in the lungs it forms hydrochloric acid. This formation can lead to many respiratory complications and corrosion of lung tissues.

Many valuable elements, which could have been recovered, are lost due to incineration with no prior treatment. Prior treatment is important. Particle size, temperature and availability of sufficient oxygen help in optimizing the incineration process. Flue gas purification is also considered helpful in addition to prior treatment.

The incineration process can be optimized by certain measures:

i. Consider other rapid oxidation options where nutrient recovery is viable.
ii. Segregation prior to incineration.
iii. Capturing usable energy which is produced.
iv. Reuse possibility of ash.
v. Flexible scalability to avoid unnecessary demand-side growth. [16]

(b) Landfills: Though landfills are widely used, they are prone to leakage. This is true for even the best ones, in the long run. The leachate which contains toxic materials can easily pollute the ground and water resources. Uncontrolled dumping also poses the threat of hazardous emissions. When circuit breakers are destroyed, mercury may leach. Landfills are also prone to uncontrolled fires.To optimize landfilling separating toxic materials and those which have possibilities of recycling, is helpful. Good quality landfills which follow standards of environment safety should be used.

(c)Recycling: Columnist Steve Lohr, in April 1993, published the first major report on the recycling of electronic waste. Recycling involves sorting, dismantling and recovery. Recovery refers to the recovery of valuable materials. For example, the printed circuit boards contain precious metals (like gold, silver, etc.) and base metals (like copper, iron, etc.). One way of recovery involves melting the circuit boards, burning cable sheathing for recovering the copper wire and the open pit acid leaching for separating valuable metals. The conventional method of mechanical shredding and separation has low recycling efficiency. Alternative methods for recycling of PCBs are being studied. One such method is cryogenic decomposition.

Consumers can play their part by sending devices back to the manufacturers or to a recycler. Corporate recycling involves companies being responsible for compliance with regulations. In America, under the Resource Conservation and Recovery Act, this practice is to be followed even if the recycling process is outsourced. Information security is considered an important aspect in these cases.

There are companies that not only take care of data protection and security but also follow green disposal procedures and help improve the environment. Many of these companies have been started by amateur recyclers, facing the issue of unemployment. They help in stripping, components of electronics, of their most valuable components, leading to recovery of metals like aluminium, gold, palladium, etc. As an economic incentive, the processing charge for old devices should be, if possible, included in the sale price of the new device.

Optimized recycling can be considered comprising of these steps:

(i) Removal of critical components: This is done to avoid contamination later. An example of critical component can be CFC gases from refrigerators
(ii) Mechanical processing: This step generally would involve use of crushers, shredders, magnetic- and air-separators. This type of processing is done to recover recyclable material and remove remaining fractions of hazardous substances.
(iii) Refining: This is important before final disposal or for recovery of substances which can be used as secondary raw materials. Glass and plastics are given importance at this stage. [17]

The gas emissions are also to be filtered.

Recycling can be beneficial to a larger extent with responsible methods. These methods consider health, safety and environmental aspects.

(d) Reuse: Reuse is an alternative to recycling. Reuse extends the lifespan of a device. Though eventual recycling is needed but reuse helps postpone recycling.There are environmental as well as social benefits connected with reuse, such as diminished use of landfills, diminished demand for raw material and new devices etc. The option for sale and donating electronics is available for the consumers. Though information security is an issue, some organizations are working which not only help in pick up but also wipe the data clean and give estimates of the devices` value. Another way is through online auctions.

Manufacturers can offer free replacement and pickup services to customers wanting to purchase a new device. There also exist organizations which work in purchasing and recycling old and broken devices from individuals and corporations.

2.4.4 Issues and Regulations

Though there exist regulations and increased concern over environmental harm, but still unscreened e-waste still gets exported from mature economies to developed countries. 'The Basel Convention on the Control of Trans boundary Movements of Hazardous Wastes and Their Disposal' is a treaty which was designed as a way of reducing transfer of hazardous wastefrom developed to developing economies.Guiyu, in China, is sometimes referred to as the e-waste capital of the world. It is a huge e-waste processing area, which has over 150,000 e-waste workers. The work they do involve activities such as snipping cables, dipping circuit boards in acid baths, etc. They cause problems like ground water contamination and air pollution due to activities such as uncontrolled burning, disassembly and disposal. Such activities also lead to occupational safety and health issues. Another important issue to be understood is that even in ecology-responsible regions of the world, there is a widening gap between the equipment sold and the e-waste collected.[18,19]

'The Restriction of Hazardous Substances Directive 2002/95/EC, RoHS, short for Directive on the restriction of the use of certain hazardous substances in electrical and electronic equipment, was adopted in February 2003 by the European Union.' The directive is designed for the removal of six hazardous materials (lead, mercury, cadmium, hexavalent chromium, poly-brominated biphenyls and poly-brominated di-phenyl ether) in the manufacture process of electronic and electrical equipment.

Another notable directive is the WEEE Directive. 'The Waste Electrical and Electronic Equipment Directive (WEEE Directive) is the European Community directive 2002/96/EC on waste electrical and electronic equipment (WEEE) which, together with the RoHS Directive 2002/95/EC, became European Law in February 2003. The WEEE Directive set collection, recycling and recovery targets for all types of electrical goods, with a minimum rate of 4 kilograms per head of population per annum recovered for recycling by 2009.' It made the manufacturers focus on the material content of new equipment that they were putting forward for the customer, in the market.

"E-Cycling" is an initiative for management of e-waste. It refers to reuse, shredding and general collection of used devices/electronics. This concept has been introduced by the United States Environmental Protection Agency. It also involves the process of disassembling, repairing and recycling of whole or components of the e-waste. E-cycling facilities have been gaining attention. This can be attributed to technology's rapid rate of obsolescence and opportunities for manufacturers to influence the market of used products.There have been supports as well as criticism towards the e-cycling concept. One opposition to this concept is that many dangerous problems are associated with the disassembly process, apart from it being costly.[20]

III. Conclusion

Due to the nature of production of electronics and disposal of e-waste, it can be said that the problem is of global concern. The tendency of electronics and waste being hazardous in nature poses a threat to humans and the environment. Unregulated treatment procedures have low efficiency, due to focus on few valuable substances, and harmful for the environment. Apart from new and improved techniques, which promote resource efficiency at the manufacturing as well as disposal stage, what is required is public, corporate and government cooperation. With already limited resources being used up and huge amounts of e-waste getting dumped every year, the world needs measures for continued production in a sustainable manner and safe disposal of the waste. The annual e-Day initiative by Computer Access New Zealand (CANZ) can be considered one such step towards sustainability. The initiative is about raising awareness about e-waste and promoting environment friendly disposal.

References

[1]. J.G. De Geoffroy, Statistical Models for Optimizing Mineral Exploration (Plenum, 1987)
[2]. T.E. Norgate*, S. Jahanshahi, W.J. Rankin, Assessing the environmental impact of metal production processes, Journal of Cleaner Production 15 (8-9), 2007, 838-848
[3]. World Bank group, IFC, Environmental, Health, and Safety General Guidelines, 2007.
[4]. World Bank group, IFC, Environmental, Health, and Safety Guidelines for Semiconductors & Other Electronics manufacturing, 2007.
[5]. Melanie Adamson, Robert Hamilton, Kathryn Hutchison, Kaitlin Kazmierowski, Joming Lau, DeighMadejski, and Nicole MacDonald, Environmental Impact of Computer Information Technology in an Institutional Setting ,University of Guelph,2005.
[6]. Retrieved from http://www.globalecolabelling.net/what_is_ecolabelling/index.htm, last accessed on June 6, 2015.
[7]. Retrieved from http://www.dell.com/learn/us/en/uscorp1/corp-comm/bamboo-packaging, last Accessed on 19 April 2015.
[8]. G. Gaidajis, K. Angelakoglou and D. Aktsoglou, E-waste: Environmental Problems and Current Management, 3(1), 2010, 193-199
[9]. RYAN JOHN L. DE LARA ,E- Wastes & Radiation, Nueva Ecija University of Science and Technology Cabanatuan City, 2014.
[10]. Retrieved from http://www.step-initiative.org/Initiative_WhatIsEwaste.html?page_a5=5 , last accessed on April 14, 2015.
[11]. Retrieved from http://www.theguardian.com/sustainable-business/50m-tonnes-ewaste-designers-manufacturers-recyclers-electronic-junk ,last Accessed on 19 April 2015.
[12]. Vijay N.Bhoi and Trupti Shah, E-Waste: A New Environmental Challenge, International Journal of Advanced Research in Computer Science and Software Engineering, Volume 4, Issue 2, February 2014, 442-447
[13]. Technology focus, E-waste Management In India,2009http://www.globalewastemanagement.com/contents/article/E-waste-India.pdf
[14]. Ravinder Pal Singh, Seth Sushil Kumar, India: A Matter of Electronic Waste; the Government Initiatives, Journal of Business Management & Social Sciences Research, Volume 2, No.4, April 2013, 15-20
[15]. Retrieved from http://www.step-initiative.org/news.php?id=0000000163, last accessed on 18 April 2015.
[16]. Retrieved from http://catalystreview.net/2011/03/transiting-from-waste-to-energy-to-an-integrated-strategy-for-materials-management-towards-.beneficial-incineration/, last accessed on April 15, 2015.
[17]. Retrieved from http://ewasteguide.info/state-art-recycling-, last Accessed April 19, 2015.
[18]. Retrieved from http://www.basel.int/TheConvention/Overview/tabid/1271/Default.aspx , last accessed April 19, 2015.
[19]. Retrieved from http://www.salon.com/2006/04/10/ewaste/ , last Accessed April 14, 2015
[20]. Eric Williams and RuedigerKuehr, Computers and the Environment: Understanding and managing their Impacts (Kluwer academic, 2003).

ASSESSMENT OF DEGRADATION CAUSED TO THE ENVIRONMENT DURING CONSTRUCTIONS AND THE EXTENT OF ITS REPLENISHMENT

CONFERENCE PAPER · MAY 2013

3 AUTHORS, INCLUDING:

Shishir Bansal
Delhi Technological University
14 PUBLICATIONS **2** CITATIONS
SEE PROFILE

S. K. Singh
Delhi Technological University
66 PUBLICATIONS **52** CITATIONS
SEE PROFILE

Program & Papers / Abstracts

ICCS13
TOKYO

First International Conference on Concrete Sustainability

27-29 May 2013

Toshi Center Hotel, Tokyo, Japan

Organized by Japan Concrete Institute (JCI)

Co-organized by
International Federation for Structural Concrete
American Concrete Institute
International Union of Laboratories and Experts in Construction Materials, Systems and Structures

ASSESSMENT OF DEGRADATION CAUSED TO THE ENVIRONMENT DURING CONSTRUCTIONS AND THE EXTENT OF ITS REPLENISHMENT

Shishir BANSAL
Research Scholar, Delhi Technological University, Delhi, India

Jose KURIAN
President, Indian Concrete Institute, India

Santosh K. SINGH
Head, Environmental Engineering Department, Delhi Technological University, Delhi, India

ABSTRACT:
Civil constructions in urban areas are essential for the benefits of the community. But, while enjoying its outcomes, the slow damage caused to the environment due to construction activities over a period of time cannot be ignored. It is essential that every such activity should be environment friendly as the Environment too has a right to remain protected from any kind of damages. The need of the hour is to have a focus on sustainable development in the best interest of environment and community at large. To assess the amount of the degradation and required mitigation measures, it is essential to understand the environmental characteristics of the area in which structure is taking birth.
Keywords: construction activities, sustainable construction, environmental characteristics, impacts, mitigation

1. INTRODUCTION

For the last several billion years, nature has nurtured the planet evolving complex Eco-systems (the biosphere) that conserve and recycle energy and materials. Climate change is the most visible result – storms, droughts, floods and the like are rising in frequency and severity and the consensus is that we are to blame. Civil constructions in urban areas are essential for overall development and benefits of the community. It is essential that every such activity should be environment friendly as the Environment too has a right to remain protected from any kind of damages. We are, however, the agents of our own eventual doom. We are choking and poisoning ourselves – slowly.

Degradation caused to the environment during construction of series of flyovers, Underpasses, River Bridges and other infrastructure projects taken up in the new millennium in New Delhi has been discussed in this paper. The assessment of degradation and the extent of replenishment will be discussed specifically in case of Mukarba Grade separator and Barapulla elevated road projects.

In India, the importance of Environmental Impact Assessment for sustainable development was recognized in the early nineteen eighties. However, it was only by mid-eighties that Environmental Impact Assessment was introduced as a necessary step for the clearance of various developmental activities under the Environmental Protection Act 1986.

To assess the amount of the degradation caused, it is essential to understand the environmental characteristics of the area in which structure is taking birth. Once a sincere assessment is done, then it is the core part of ethics of any Engineering to mitigate the degradation.

2. ENVIRONMENTAL CHARACTERISTICS OF NEW DELHI

Delhi being the capital city is the center of socio-economic, cultural and political activities of the country. The city has become an important center of trade and commerce and for international events, (Commonwealth games 2010), thus desiring a continued and sustained effort to maintain the transport system most effective, direct and fast at internationally acceptable standards. The city also acts as a major center of trade and commerce and is the nodal point for five national highways and intercity rail corridors, carrying large volumes of heterogeneous passenger and goods traffic.

2.1 Geographical features

National capital territory, Delhi is located in northern India between the latitudes of 28°-24’-17” and 28°-53’-00” North and longitudes of 76°-50’-24” and 77°-20’-37” East. It has an area of 1,483 square kilometers. It shares borders with the States of Uttar Pradesh and Haryana. The Yamuna River and terminal part of the Aravalli hill range are the two main geographical features of the city.
Situated on the banks of river Yamuna, Delhi is considered to be a part of the Aravalli Range, major

part of Delhi is a plain area or Bhangar which is very fertile. The plains can be divided into Delhi, New Delhi and Delhi Cantonment. The other regions of Delhi namely the Yamuna plains are flood-prone while the ridge which is the most dominating feature in this region is surrounded by the Aravallis. Yamuna is an important river in Delhi which fertilizes the alluvial soil.

Owing to its location, and good connectivity with the neighboring states, it is being used as a corridor for a large volume of the vehicular traffic travelling within these two states and beyond them also to Punjab, Rajasthan etc. etc. Thus the amount of traffic moving in Delhi has generated many folds.

2.2 Traffic Scenario

Delhi has the most extensive road network in India - 21% of its geographical area is just motorways. Yet, there is not enough space for the traffic.

Delhi had just five flyovers at the end of Asian Games it hosted in 1982. Today, the number has increased to 74. In last three decades, Delhi's vehicle stock has increased 51 times. 10% of the country's vehicles are registered in Delhi. 17% of country's all private vehicles run on Delhi's roads.

The number of vehicles is growing at 10% every year. According to a Centre for Science and Environment projection, the daily trips are expected to explode from 15 million today to 25 million in 2020. The road spaces have been increased to decongest the existing traffic. But new roads end up attracting more traffic which is explained as the "induced traffic" phenomenon. The studies on traffic concluded that half of the increased roadway capacity is consumed by added traffic in about five years, 80 % of increased capacity is eventually consumed by induced traffic.

In fact in many cities in the West and also in US, dismantling of flyovers and expressways is taking place. Delhi may not need to take such extreme steps yet, but soon it will be impossible to keep adding to infrastructure beyond its physical limits.

3. ENVIRONMENTAL IMPACTS

Since the start of new millennium, the city has seen mega construction projects especially due to the commonwealth games organized in this city in 2010. The construction industry is a major source of pollution, responsible for around 4% of particulate emissions, more water pollution incidents than any other industry, and thousands of noise complaints every year. Although construction activities also pollute the soil, the main areas of concern are air, water, land and noise Pollution.

Construction and operation are the two major activities in which the project interacts physically with the environment and as a result of which the environmental deterioration occur. In assessing the effects of these processes therefore, all potential impacts of the project should be identified, and attempt to replenish is taken to mitigate the adverse impacts.

Following sections evaluate the impact of the Infrastructure Projects completed in large numbers in this millennium.

3.1 Air Pollution

Construction activities that contribute to air pollution include land clearing, operation of diesel engines, demolition, burning and toxic materials.

(1) Earthwork excavation, refilling, handling and transportation of construction materials (like sand and aggregate), and construction of earthen ramps produce large volumes of dust if it is not done properly. This dust can carry for large distances over a long period of time. Construction dust is classified as PM10 - particulate matter less than 10 microns in diameter, invisible to the naked eye. Research has shown that PM10 penetrate deeply into the lungs and cause a wide range of health problems including respiratory illness, asthma, bronchitis and even cancer.

(2) Another major source of PM10 on construction sites comes from the diesel engine exhausts of vehicles and heavy equipment. This is known as diesel particulate matter (DPM) and consists of sulphate and silicates, all of which readily combine with other toxins in the atmosphere, increasing the health risks of particle inhalation. Diesel is also responsible for emissions of carbon monoxide, hydrocarbons, nitrogen oxides and carbon dioxide. Noxious vapors from oils, glues, thinners, paints, treated woods, plastics, cleaners and other hazardous chemicals that are widely used on construction sites, also contribute to air pollution.

(3) Because of sheer volume, cement concrete is the major contributor to embodied energy in most structures, hence contributes most to carbon emission in in the initial stages

3.2 Water Pollution

Sources of water pollution on building sites include diesel/ oil, paints, solvents, cleaners, other harmful chemicals and construction debris/dirt. When land is cleared, it causes soil erosion that leads bearing run-off and sediment pollution.

(1) Silt and soil that runs into natural waterways turns them turbid and when runs into city drainage system cause silting of drains.

(2) Surface water run-off carries pollutants from the site, such as diesel and oil, toxic chemicals, and building materials like cement. When these substances get into waterways they cause water pollution.

(3) Pollutants on construction sites can also soak into the groundwater, a source of human drinking water. Once contaminated, groundwater is much more difficult

to treat than surface water.

3.3 Land Pollution

Construction activities that contribute to land pollution include uprooting of trees, excavation of foundations, land clearing.

(1) Invariably any construction activity of a grade separator requires uprooting of number of trees thus disturbing the ecological balance in the project environment. It is observed that for a project comprising of 10000 sqm area, around 200 trees are removed from the construction site.

(2) Excavation produces large quantity of waste soil, which needs proper disposal. This however is utilized in construction earthen ramps, so that the surplus soil that requires proper disposal is minimal.

(3) During deep excavation for pile foundation, water gets collected in the void, needing disposal. Indiscriminate disposal of this silt – laden water may choke drains, lead to water accumulation etc. Also, existing drains in the ROW gets disturbed.

(4) Excavation has a potential of causing damage to the existing infrastructure/utilities. There is always number of various utilities like electric poles, transformers, water lines, drainage lines, Telephone cables, Gas lines etc. within the ROW, which needs to be relocated.

3.4 Noise Pollution

Construction sites produce a lot of vibration and noise, mainly from vehicles, heavy equipment and machinery, excavation for casting piles, braking up pile heads, road surface but also from people shouting and radios turned up too loud. Excessive noise is not only annoying and distracting, but also lead to sleep disturbance and extreme stress. Even during the operation stage, lot of noise is produced by the fast moving vehicles on flyovers, which is an area of concern in urban environment.

3.5 Social Factors

In Urban Environment, the disturbance caused to the public residing in vicinity is to given due regard and the inconvenience of any kind or sudden disturbance on their life style due to taking up of any project in their vicinity is an area of concern.

(1) Generally there exists a commercial area including road side vendors along the roads, shops and other business loose income due to impeding of costumer's access.

(2) Large scale disturbance to moving traffic is caused due to construction activities at site as well as off side in casting yard like carrying of RMC or precast segments in case of segmental constructions etc. Even there is a general increase in traffic due to trucks carrying construction material and heavy equipment to site.

(3) Workers and public at construction site as well as the public at large passing nearby the construction sites in Urban Environment are always subjected to a risk of accidents or life from accidents on site

4. MITIGATION MEASURES ADOPTED IN DELHI

Good construction site practice can help to control and prevent pollution. The first step is to prepare environmental risk assessments for all construction activities and materials likely to cause pollution. Environment Agency and other government bodies are putting increasing pressure on construction companies to reduce pollution and conform to environmental regulations. In the past the pollution fines have been low and environmental regulations slack, and it could have been perceived as cheaper to pollute than to prevent pollution. This situation is now changing, and enforcement of environmental regulations is not only very expensive but can be irreversibly damaging to the reputation of a firm. Measures to reduce and control pollution are relatively inexpensive and cost-effective, and the construction industry needs to incorporate these into an environmental management strategy. By employing these practices, the construction industry is well positioned to clean up its act. Measures can then be taken to mitigate these risks.

4.1 Erosion of soil and run-off

(1) Land disturbance is minimized and maximum vegetation cover is left. Dust is controlled through fine water sprays to dampen down the site and the surface of the developing ramps any soil stockpiled on site by spraying with water, when necessary during dry weather. Trucks loaded with loose construction materials are covered using tarpaulins. Materials are brought as and when required. While unloading the material, particularly aggregate, at the site dust generated is controlled by sprinkling water and ensuring the unloading in a barricaded area. Water is sprinkled in truck after downloading material or covered with tarpaulin to avoid dust raging from the truck while it is moving.

(2) Piles of building materials like cement, sand and other powders are well covered and regularly inspected for spillage. These are located where they will not be washed into waterways or drainage areas. Toxic substances are segregated, tightly covered and monitored to prevent spills and possible site contamination.

4.2 Disposal of surplus soil

Surplus soil is utilized for beneficial purposes such as in construction activities elsewhere and filling up low lying areas.

4.3 Uprooting of trees

Whenever trees are removed to make the site clear for

taking up the construction activities, it is ensured that 10 times the trees removed are planted as compensatory plantation measures according to the Afforestation Policy under Forest Conservation Act-1980. While trees are uprooted, best efforts are made to keep the bulb of roots intact and replant the same at other location. It is experienced that 60% of the trees replanted continue to survive.

4.4 Drains contamination

All drains in the construction site are covered up properly and protected from all possible contamination. Any wastewater generated from site activities like Bentonite from the piling activity are collected in settlement tanks, screened and re-circulated or disposed off according to environmental regulations.

4.5 Shifting of infrastructure/utilities

Location of underground infrastructure/utilities is done before start of work by physically excavating the earth and by collecting the required information from all the utilities owing departments. Proper planning is done to shift these utilities in safe corridors either through the utilities owners or by construction agency itself. Sometimes shutdown is required in case of essential services like water lines or electric lines. In such a situation, prior public information is provided about the likely disruption of services. It is ensured that alternate arrangements like water tankers are provided during the relocation period.

4.6 Social aspects

(1) Resident Welfare Associations (RWAs), public in general and business establishments in particular are taken into the confidence by consultation with them and informing them of the nature, duration and likely effects of the construction work and the mitigation measures in place

(2) At the work site, public information/caution boards are provided with information of project name, cost and schedule executing agency and contract details, nature and schedule of work, traffic diversion details, if any, entry restriction information, competent official's name and contact information for public complaints.

(3) Alternative traffic arrangement/detours are provided so that traffic can be distributed and move on different roads and it is ensured that public is informed about such traffic diversions through media – daily newspapers and local cable television (TV). Service roads and pedestrian walks are maintained in good condition to allow smooth traffic movement. Necessary personnel /Marshalls are provided to guide and control the traffic.

4.7 Safety Measures for workers and public

(1) Standard and safe construction practices are followed. Entire construction area that may come under influence in case of accidents is barricaded properly. This is particularly critical during fixing of pre-cast girders or segments using heavy duty cranes. These activities are generally conducted during lean traffic periods and if required traffic is also stopped. Accidental entry of traffic (pedestrian / vehicular) into site is avoided. Warning boards/ sign boards and post security guards are provided throughout the day and night.

(2) It is ensured that all workers are provided with and use appropriate Personal Protective Equipment like helmet, hand gloves, boots, masks, safety hoists when working at height or in foul conditions, etc.

(3) Standard practices of safety checks as prescribed are followed before use of equipment such as cranes, hoists, etc. Environmental, Health and Safety (EHS) Expert is employed at site. Health and Safety Training for all site personnel is provided at site. Any accident that happen at site is reported to the authorities promptly and records maintained.

4.8 Noise Pollution

Noise pollution is reduced through careful handling of materials, use of modern, quiet power tools, equipment and silent generators. High noise and vibration generating activities like rock blasting are not permitted involved in the project taken up in Urban Environment and manual methods are only deployed, wherever required. Noise generating activities are avoided in the night and work programme is planned properly so that any particularly noisy activities can be scheduled to avoid sensitive times. Modern vehicles and machinery are utilized with the requisite adaptations to limit noise and exhaust emissions and ensuring that these are maintained to manufacturers' specifications at all times.

5. MUKARBA CHOWK GRADE SEPERATOR

5.1 Location

Mukarba Chowk is located in North Delhi at the junction of Rohini-ISBT axis & NH 1- Azadpur axis. NH1 is part of the Grand Trunk Road. It is amongst the most heavily trafficked junctions in the country. Traffic types is a mixed cocktail of Pedestrians, Two wheelers, Three wheelers, Motor cars, Buses (interstate and local), Trucks etc. etc. Traffic Intensity, based on traffic studies in 2000 at this intersection is 3,30,000 pcu/day.

The intersection was to be made signal free with provision of full clover leaves, dedicated cycle track both along outer ring road and GT Karnal road, Bus bays at flyover level and road level, Ramps for the safe movement of physically challenged persons from subway to flyover level along with the provisions of lift, escalator and a Subway for crossing of both pedestrian and cyclist

5.2 Challenges with the project

Apart from traffic challenges, other challenges were the essential protection of Archaeological (heritage) structure (see Plate 1), Graveyard (burial ground), Sanitary landfill and garbage dump of the Municipal Corporation of the city, major Electrical sub-station of 33 and 11 KV existing structures/features at this

intersection.

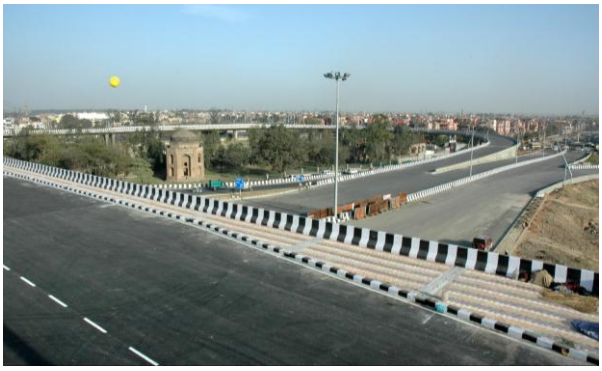

Plate 1 : Archeological monument in the scheme

The project was conceived in a manner that all the above could be incorporated into the interchange without demolition or causing any damage to them.

5.3 Sustainability Considerations and Green concepts in Project

(1) The Project has been conceived with concrete as main structural material and concrete-steel composite sections for the plate girders supporting the deck slab. It was planned with more embankments and less structure to reduce carbon footprint. For preparation of the concrete, use of blended cement was another important consideration to reduce carbon footprint. Blast furnace slag was added in concrete design to increase the service life of the structure. Furthermore, slim structures and geo-grids were used for retaining walls of the embankment so as to reduce the use of concrete and thus reducing the material consumption

(2) It was essentially required to retain essential cultural and social characteristics of the present environment. Existing structures, utilities, monument, city garbage dump have been made a part of the overall design concept. Simultaneously the aesthetics of structures along with well-planned landscaping all around the Project area have been given due importance for people to "own" the project. Evolving structural shapes that would be aesthetic and enhance the quality of the environment.

(3) The design and construction technologies were planned in a manner to reduce construction period and minimize works on site

(4) Total signal-free movement of traffic in all directions was provided to avoid atmospheric pollution from stationary vehicles.

(5) The space occupied by the city's landfill and garbage dump (see Plate 2) has been suitably utilized for socially relevant purposes. Nallahs (drains) have been used as an asset and making them part of the overall landscaping (see Plate 3).

Plate 2 : Excavation in the landfill area

Plate 3 : Landfill converted to green belt

(6) Public transport system in preference to personal motorized vehicles has been given due importance and due provisions have been made along with the safe and convenient movement of pedestrians and cyclists. Safety of road users was a paramount consideration during construction period.

6. BARAPULLA ELEVATED ROAD PROJECT

Govt. of India had a commitment to common Wealth Federation for connectivity from Games Village to Main Stadium (Jawaharlal Nehru Stadium). Around 10000 Sport Persons had to have unhindered access to Stadium from games village through this corridor.

In spite of many Flyovers Built over Ring Road some sections of Ring Road namely, Maharani Bagh, Ashram, Lajpat Nagar & South Extension were still choked in Peak hour. Ring Road Caters 165000 PCU/Day (Capacity constrained). As per NCRPB report, the projected Traffic is estimated to be 400,000 by 2021. Bhairon Marg had also experienced choking during peak hour which was required to be decongested.

6.1 Location

The Proposed Barapulla Nala Corridor (see Plate 4) was conceived as an East-west corridor as an alternative route to congested section of Ring Road between Sarai Kale Khan and AIIMS that facilitates the immediate need of Commonwealth Games and in long run for the movement of freight, goods, people, and utilities. The alignment which is along Barapula Nala

drain collects the discharges of other internal, peripheral and trunk drains to further discharge its contents-1,25,000 Kld of domestic sewage into the Yamuna. Barapula Nala in its east west orientation starts from Ring Road to INA.

6.2 Challenges with the project

(1) The feasibility study of alignment connecting Ring Road at Barapula Nala and INA near Dilli Haat demands most direct, economical, aesthetic, traffic worthy intersections and interchanges and its speedy constructability.

Plate 4 : A view of Barapulla Nallah

(2) The project must enhance the visual quality of the urban space. Interventions adjacent to historic monuments should be sensitive.

Plate 5 : Planning of Khan-e-Khana's tomb

(3) The alignment of the road with reference to Khan-e-Khana's Tomb should be as far as possible, even more than 100 meters boundary away from the notified monuments designated as Prohibited Area within which no construction is permitted. Archeological Survey of India (ASI) suggested engaging a heritage consultant for Khan-e-Khana's Tomb and Barapulla Bridge (see Plate 5). It was found that the earlier preferred alignment option is contrary to the stipulations of the Ancient Monuments and Archeological Sites and Remains Act 1958. Alignment was shifted towards east to provide 107 mts distance between the Monument and structure soffit level was raised from 5.5 mts to 12 mts above Mathura Road Level.

(4) The work was to be executed without disrupting the traffic by careful planning the sequence of operations so that the traffic moves unhindered at all times.

(5) Noise barriers were to be provided at all sensitive receivers. Removal of bottlenecks and relieving congestion in constricted sections through improved design was aimed at. A proper mix of indigenous species comprising of broad-leaved evergreen and deciduous species will be planted along roadside. The deciduous species to be planted on slopes. The inhabited locations shall be bypassed as far as possible such that the road does not pass through any critical areas.

6.3 Sustainability Considerations and Green concepts in Project

(1) The Archaeological Beauty of the area has been restored by landscaping the area. Edge Alignment is 107m away from Khan-e-Khana Mirza Abdur Rahims khan Tomb (Protected Monument) with vertical Clearance of 12 m from Mathura road to ensure visibility of Khan-e-khana Tomb. Elevated Road provides unhindered visibility to Old Barapulla Bridge compiling with ASI observations.

Plate 6 : No disturbance to road traffic

The Barapulla Bridge is aesthetically visible while driving from Sarai kale khan to INA on new Elevated Corridor.

(2) In order to safeguard the disturbance to road and rail traffic, segmental construction was planned and the sequence of operation were such that the road as well as rail traffic moved uninterrupted at all times of construction (see Plates 6 and 7).

Plate 7 : No disturbance to Rail Traffic

(3) Turfing has been done on embankment Slopes as per the recommended practice for treatment of embankment slopes for erosion control. Trees have been planted on both sides of the road and in the island formed near rotary species.

(4) No disturbance has been caused to the existing drainage pattern. Side drains have been provided with its connectivity to main outfall drain. Sections of the corridor have been modified suitably along with the cross drainage structures.

(5) Safety of workers during construction was ensured by providing helmets, masks, safety goggles, etc. Adequate signage, barriers and persons with flags to control traffic had been provided during construction. Adequate drainage, sanitation, and waste disposal facilities were provided at work places. Proper drainage was ensured around the sites to avoid water logging leading to disease. At every workplace, potable and sufficient drinking and washing water supply is maintained to avoid water-related diseases and to secure the health of workers.

7. CONCLUSIONS

(1) It is true that civil constructions in urban areas are essential for overall development and benefits of the community, but same is successful only if equal importance is given to the environment and it is given due care for a sustainable development.

(2) It is essential that every construction activity should be environment friendly as the Environment too has a right to remain protected. Engineering solutions to minimize the Environment impacts and for adopting the mitigation measures are available.

(3) Many times it happens that planning a Project requires disturbance to heritage structures existing in the vicinity of the scheme. In such a situation, it requires the consultation with heritage experts. Solutions are available under such circumstances, but these may be more challenging for Engineers to plan and construction besides the cost factors. But importance of heritage structures, their restoration is essential and has to be given due importance.

(4) Adoption of standard and safe construction practices is very much essential particularly in urban environment. It must be ensured in all times that all workers adopt best safety protections in their own interest. Protection of Health, Safety and Environment should always be kept as the prime goal.

(5) The right of respectful living of the residents residing around the construction sites should not be jeopardized. It should be given due consideration without compromising on their comforts, safe movements and safe livelihood.

ACKNOWLEDGEMENT

The authors would like to express their sincere thanks to Dr. Prabhakant, Ph.D.in Energy Sciences, Dr. Aditya Tyagi, Ph.D. in Water Resource Engineering and Prof. Mahesh Tandon, Managing Director, Tandon Consultants Pvt. Ltd. for providing the required data of Environment related issues required for concluding this paper

REFERENCES

1. Report on Impact Assessment of Bridges and Barrages on River Yamuna (Wazirabad – Okhla section) by Environics trust, New Delhi & Peace Institute Charitable Trust, Delhi.
2. Initial Examination Environment DPR for flyover at Mohan Nagar Junction at Ghaziabad by Wilbur Smith Associates.
3. Feasibility Report for Barapulla Nallah May 2008by M/S VKS Infratech Management Pvt. Ltd. Consulting Engineers Planners & Managers H.No.-181, Pratap Nagar Lane No. - 18, Pocket IV, Mayur Vihar Phase-I, Delhi-110 091.
4. Presentation on "Sustainable construction in Urban transportation structures "during a Seminar on green technologies for sustainable concrete construction presented by Prof. Mahesh Tandon, Managing Director, Tandon consultants Pvt. Ltd. and distinguished visiting Professor IIT Kanpur and IIT Roorkee on 13th – 14th April 2012.
5. Environmental Assessment of Infrastructure Projects of Water Sector in Baghdad, Iraq by Allaa M. Aenab, S. K. Singh, Journal of Environmental Protection, 2012, 3, 1-10 doi:10.4236/jep.2012.31001 Published Online January 2012
6. NR2C (New Road Construction Concepts) towards reliable, green, safe & smart and human infrastructure in Europe
7. Environment impact assessment process in India and the drawbacks Prepared by – Environment conservation team (Aruna Murthy, Himansu Sekhar Patra) September 2005, Vasundhara, 15, Sahid Nagar, Bhubaneshwar – 751 007.

Available Online at www.ijcsmc.com

International Journal of Computer Science and Mobile Computing

A Monthly Journal of Computer Science and Information Technology

ISSN 2320–088X

IJCSMC, Vol. 4, Issue. 6, June 2015, pg.966 – 974

RESEARCH ARTICLE

Association Rule Mining for Structured Data in Big Data Using Parallel RDB-Miner Algorithm

Tererai Tinashe Maposa[1], Manoj Sethi[2]

[1]Department of Computer Engineering & Delhi Technological University, India

[2]Department of Computer Engineering & Delhi Technological University, India

[1] tereraimaposa@gmail.com; [2] manojsethi@dce.ac.in

Abstract— In recent years data volumes have astronomically skyrocketed. Almost all data is now regarded as big data and is now measured in the magnitudes of Yotabytes and Petabytes. This has been catalyzed by the rapid development of the Internet and the central role it has claimed in our daily lives. Data has become the most valuable asset for most organizations as it allows them to glean some business intelligence from it. Commercial organizations now gather as much data about their clients as possible. Governments have also invested heavily in data gathering and analytics. This has resulted in an enormous sea of data of all formats and structures. However there has been a misconception that all big data is unstructured or semi-structured and do not have a defined structure. This has resulted in a bias towards research areas. Lately most technologies and techniques that have been developed are intended for unstructured and semi-structured big data. This paper aims to parallelize an association rule mining algorithm for relational data called RDB-Miner Algorithm and implement it on structured big data in a HadoopDB multi-cluster environment.

Keywords— Big Data, RDB-Miner algorithm, HadoopDB, SQL-on-Hadoop, association rule mining

I. INTRODUCTION

The role that the Internet has taken in our daily lives has birthed the era of big data. This has been aided by technological advancements in hardware; hardware capacities (storage and processor power) have been ever increasing whilst its cost has been plummeting. This has afforded the scientific and commercial communities the luxury of collecting any data they deem necessary. Data from sensor networks, meteorological departments, genomics, medical data (such as X-ray images), posts on social networks (such as photos and comments on Facebook and Twitter), advertisements, stock exchanges, retail transactions, online video and audio conferencing, and so on is now being stored with relative ease[1, 2]. This obsessive collection of data has resulted in a massive sea of "meaningless" data. Consequently, it has become a cumbersome task to mine/extract and discover any business intelligence, patterns or associations from this large pool called BIG DATA [3]. Many technologies and techniques have been developed in order to aid in the data mining process. However, most projects have been aimed at unstructured and semi-structured data. A blind eye has been turned on the structured big data. This project aims to enhance the RDB-Miner algorithm which is an association rule mining algorithm for relational data model (structured data). The project intends to make it applicable and adoptable to structured big data. The project aims to parallelize the algorithm and implement it in a multi-cluster HadoopDB environment.

II. STRUCTURED DATA IN BIG DATA

Structured data is data that has a defined, predictable and repeating layout. It is data that can be easily put into rows and columns or that can take up the relational data model. As the world's view of data transitions from just data to big data, there is a false impression that all big data is unstructured or semi-structured. There is a notion that only unstructured data is increasing and only it requires new handling techniques. The heat map by the McKinsey Global Institute et al [1] below shows that all sectors still produce more text or numbers (which is in most cases structured) than any other types of data (audio, video and images which are unstructured data). The heat map is in terms of the number of units and not size of data.

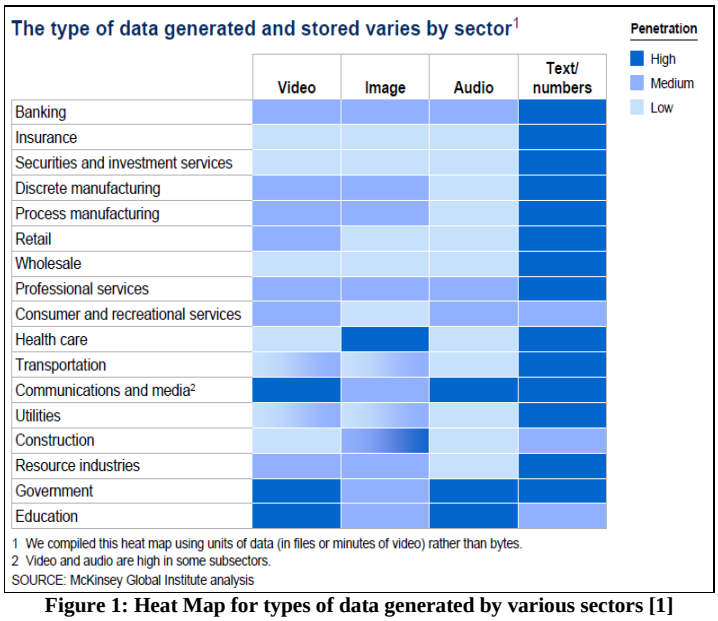

Figure 1: Heat Map for types of data generated by various sectors [1]

According to an article on IBM Data Magazine by Cristian Molaro et al [5], structured data still constitutes approximately 10% of the overall volume of big data. He also claims that this 10% is the one that matters the most because most of the 90% of the unstructured data are "cutie selfies" which in most cases have no business value. Most organizations, decision makers, and business analysts and other information consumers, can derive better business intelligence from big data–derived information when it is organized in a defined and structured manner rather than an unstructured one. This proves that as much as most of the big data (in terms of size) is unstructured, we cannot afford to ignore the structured data in big data. This 10% of big data requires new techniques and technologies because it is too big for traditional methods. There is therefore need for new platforms that can efficiently manage the enormous volumes of structured data being generated. Most algorithms that are currently in existence are mainly intended to handle unstructured data and may not be as efficient in handling structured data.

III. EXISTING TECHNOLOGIES FOR STRUCTURED DATA IN BIG DATA

Hadoop is synonymous to big data; it is difficult to talk about one and leave the other. However due to the steep learning curve involved in Hadoop and its inability to properly handle structured data; some hybrid technologies that combine the desired features of databases and Hadoop are being developed. These technologies are called SQL-on-Hadoop and they include, among others:

1) ***HadoopDB*** was developed at Yale in 2009. The thrust behind HadoopDB is to connect multiple single-node database systems using Hadoop as the task coordinator and network communication layer [6, 7]. Queries are parallelized across nodes using the MapReduce framework. HadoopDB runs on a shared-nothing architecture using commodity hardware. Any Open Database Connectivity (ODBC) compliant database can be used for example MySQL or PostgreSQL.
2) ***HAWQ*** (Hadoop With Query) is a commercial product developed by Pivotal HD which enables enterprises to benefit from tried and tested Massively Parallel Processing (MPP) based analytic features and its query performance while harnessing the power of the Apache Hadoop stack [8].
3) ***Spark SQL:*** Apache's Spark project is for real-time, in-memory, parallelized processing of Hadoop data. Spark SQL builds on top of it to allow SQL queries to be written against data.

Other tools that help support SQL-on-Hadoop include BigSQL, Apache Drill, Hadapt, H-SQL, Cloudera's Impala, JethroData, Polybase, Presto, Shark (Hive on Spark), Splice Machine, Stinger, and Tez (Hive on Tez).

IV. RDB-MINER ALGORITHM

Association Rule Mining (ARM) is one of the most prominent fields of data mining. It seeks to discover data items that frequently occur and their relationship. ARM has two steps involved: discovery of frequent itemsets and the establishment of association rules [9]. The classic algorithm for association rule mining, the Apriori algorithm, was first developed in 1994 [9]. The Apriori algorithm uses the layer search method to produce (k + l) itemsets from the k itemsets [9]. Many enhancements of the Apriori algorithm have been introduced; these include among others, Count Distribution [10], Data Distribution [10] and Candidate Distribution [10]. Most of them work on the market basket data format which is represented as a set of rows where each row consists of a unique identifier called transaction ID and a set of items purchased in the transaction. Market basket data violets the relational data model which does not allow multi-valued attributes.

Abdallah Alashqur in [11] introduced the RDB-Miner algorithm which directly mine association rules from a relational dataset. According to [11] RDB-MINER can be viewed as an algorithm that performs inter-attribute frequent itemset mining.

Algorithm *RDB-MINER [11]*

Input

R: a database relation
exclude_set: a subset of the attributes of R
0 Begin
1 ***Varchar*** *SQL_str (512)*
2 Compute_N (N, R, exclude_set)
3 Compute_PowerSet (P (A) , R, exclude_set) *;*
4 ***For*** *c = 1 to N* ***do***
5 Extract_Ec (Ec , P (A) *);*
/ Ec ⊂* P (A) *and each ISI ∈ Ec has a cardinality of c. */*
6 ***For*** *each itemset intension ISI ∈ Ec* ***do***
7 Generate_SQL (SQL_Str, ISI, Relation_Name);
8 Execute SQL_Str;
9 SQL_str = "";
10 End

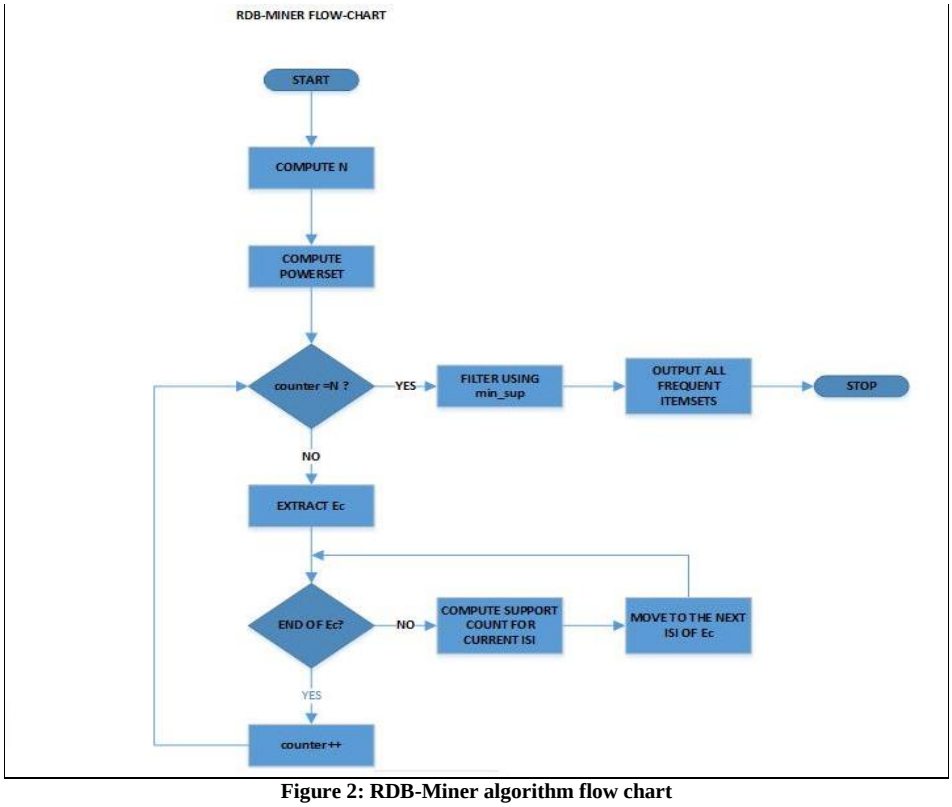

Figure 2: RDB-Miner algorithm flow chart

V. PARALLELIZATION STRATEGY

To parallelize the RDB-Miner algorithm we followed the logic outlined in [12]. However the proposed algorithm will not broadcast the consolidated global frequent itemsets to all nodes in the cluster; instead each node will transmit its local frequent itemsets to the coordinator which in turn consolidates the local findings of each node to construct the global frequent itemsets. The coordinator will filter for frequent itemsets using the supplied min_sup. This strategy seeks to reduce node communication hence making the algorithm more efficient as outlined in [13, 14, 15]. Nodes will only have to communicate with the coordinator node.

The transaction data is horizontally divided into N data subsets which are sent to N number of nodes. We modified the second **for** loop of the RDB-Miner algorithm; such that before it moves to ***k-itemsets*** it has to consolidate the ***(k-1)-itemsets*** from all the nodes. The logic is as follows:

1. Each node scans its data subset to generate the set of candidate itemset ***C p*** (candidate ***k-itemset***);
2. ***N*** nodes respectively accumulate the support count of the same itemset to produce the local support, and determine the set of frequent itemset ***Lp*** in the partition. At this point the nodes will not use the min_sup parameter to filter the frequent itemsets.
3. Each node then sends its computations to the coordinator for aggregation/consolidation.
4. The coordinator merges the output of the N nodes and filters the merged result using the set min_sup to generate the set of global frequent itemset ***Lp***.
5. Do the same for ***(k+1) –itemsets*** until c=N (number of attributes in the relation).

The algorithm enforces the Apriori property which states that any subset of frequent itemset must be frequent [16]. It achieves this by ignoring all the infrequent itemsets in the preceding iteration (N-1) when it is executing iteration N. This technique not only reduces the average transaction length but also reduces the data set size significantly. The number of items in the data set might be large, but only a few will satisfy the support threshold [15].

1) Pseudo Code for the proposed PRDB-Miner Algorithm

Input at each node
R: a partition of database relation
exclude_set: a subset of the attributes of R
min_sup: user specifies the min support to be used by the coordinator node

```
0  Begin
1  Varchar SQL_str (512)
2  Compute_N (N, R, exclude_set)
3  Compute_PowerSet ( P (A) , R, exclude_set) ;
4 c = 1
5        While c < (N+1) do
6        Extract_Ec (Ec , P (A) );
7        For each itemset intension ISI ∈  Ec do
8        Generate_SQL(SQL_Str,ISI,Relation_Name);
9                Execute SQL_Str = Cp;
10               Send_Results(Cp);
11               End For

12 If CheckNodeCount() = TRUE then ConsolidateResults();
13           c ++
14           GOTO 5
15       End While
```

The improvements were put on lines 4 through 12. The explanations are as follows:

- Lines 1 to 3 remain the same but they are executed at the master/coordinator node,
- Line 4: a counter, c is initialized to 1,
- The commands in line 5 to line 10 are executed at the slave nodes,
- Line 5: the **while** loop checks to see if the counter c which counts the number of attributes in the relation/table has reached the total number of the attributes in the relation. If it true then it exits the loop and goes to line 16 and lets the master display the results,

- Lines 6 to 9 are the same as in the original algorithm,
- Line 10: ***SendResults()*** is a function that sends node results to the coordinator node. Its argument is the result generated by the ***Execute_SQL*** function in line 9.
- Line 12: ***CheckNodeCount*** function is executed by the coordinator only to check if all slave nodes have sent their results to it. It returns TRUE if all nodes have sent else it returns FALSE.
- Line 12: ***ConsolidateResults*** function is also used by the coordinator only to combine the results from all nodes and filters for frequent itemsets using minSup
- Line 13 increments the counter c
- Line 14 triggers the agent at each node to execute the mining function at each node. It passes the incremented counter c as an argument.

Below is the flow chart of the proposed Parallel RDB-Miner.

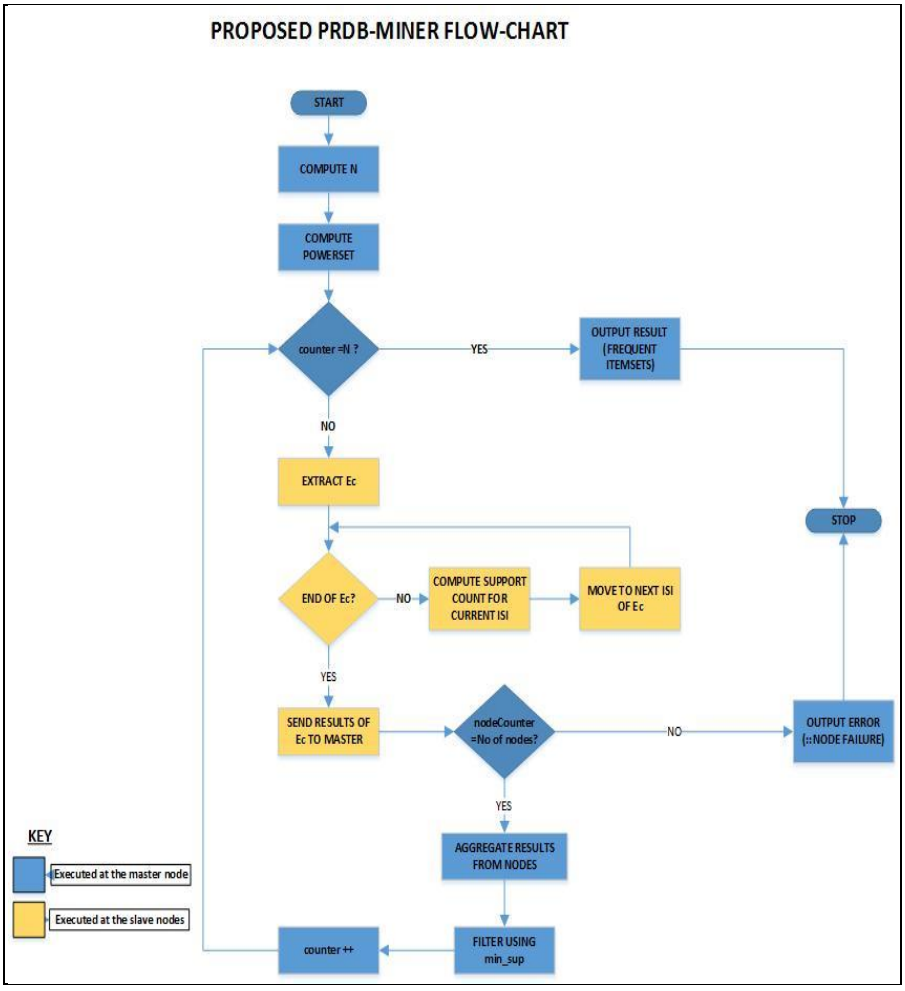

Figure 3: Parallel RDB-Miner flow chart

VI. IMPLEMENTATION OF THE PARALLEL RDB-MINER ALGORITHM

We implemented the algorithm on a four node HadoopDB cluster. One of the nodes acted as the coordinator. The coordinator was responsible for aggregating node findings, filtering for frequent itemsets and displaying the final results. The coordinator was also the point of entry for the query where the user triggers the application. The coordinator also acted as the master node which hosted the NameNode and JobTracker; important components for the Hadoop framework. A simple recommender application was developed. The application used the PRDB-Miner algorithm to find product association based on customer reviews. The data used was formatted into three columns {userID, prodID, rating}. The application would find users who highly rated product X and also likes product Y. If the number of these users is high then product X and Y are highly associated to each other and that number of users is the support count for the rule X=>Y. The user interface for the application is web page designed using PHP. The user will be able to specify the minimum support from the

proposed user interface. The relational database used on top of Hadoop is MySQL because it is ODBC compliant and also open source.

VII. EXPERIMENTAL RESULTS

In this paper we observed **Execution time** as a performance indicator. Execution time denotes the time taken (in seconds) by the application to produce all association rules with the desired support. The execution time was displayed and observed on the master node of the cluster. Three variables were altered as the performance was being observed. The variables that were altered are ***minSup***, ***number of cluster nodes*** and ***volume of data*** being worked on.

A. Results for varying minSup

This experiment was carried out with 1.7 million records horizontally partitioned and uploaded into three cluster nodes. The minSup variable used is the absolute count. The graphical results are shown below.

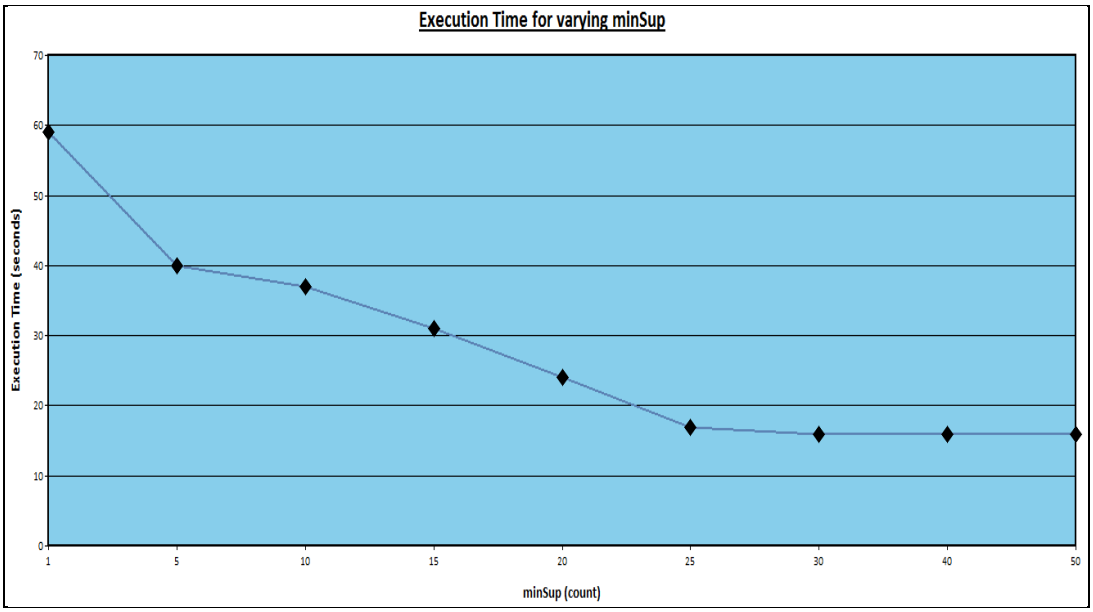

Figure4: Results for varying minSup for PRDB-Miner

Observation

The execution time gradually declined as the minSup increased. The execution time had a steady decent from minSup of 0 to 25 but it eventually became constant as the minSup continued to increase.

Explanation

Low minSup value means that the algorithm will have to deal with a lot of data hence the longer execution times. The master node is responsible for filtering for frequent itemsets using the minSup value; if the value is low it means a lot of itemsets will qualify as frequent itemsets. If the number of records remains high for most cycles of the algorithm, it results in longer execution time. However as the minSup increases, it means that the algorithm filters out most of the records and disqualifies them as infrequent itemsets. As the algorithm continues to scan the node databases it will be left with just a few records to deal with hence it becomes faster to generate the rules.

As the minSup continues to increase, the execution time becomes constant because the effects of all big minSup values will be the same. For example if there is no frequent itemset with a support of 30 in the whole cluster, if we put a minSup of 31 and if we put 50, the results will the same because no frequent itemset will be found in both scenarios.

B. Results for varying data volumes

The algorithm was also tested for varying volumes of data. This experiment was carried out using three nodes. Each node was allocated an equal potion of the whole data. The records in each partition were equally increased by 1 000 000 records during each experiment. The total number of records used in the five experiments was, 1.2, 1.5, 1.8, 2.1 and 2.4 million respectively. The minSup was set to default 5 during the whole experiment. Below is the graph for the execution time.

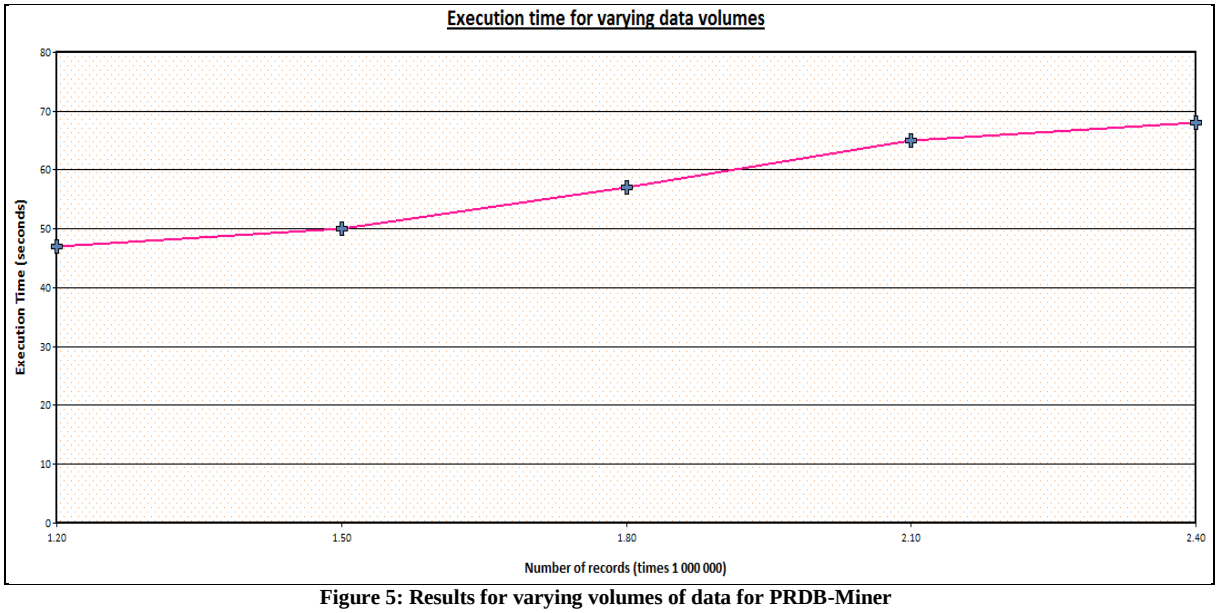

Figure 5: Results for varying volumes of data for PRDB-Miner

Observation

The execution time gradually increased as the volumes of data increased. However the increase was not very significant; an average of 2 to 3 seconds between experiments was observed.

Explanation

As the volume of data increases it means more data items and consequently more frequent itemsets. The more data there is the higher the execution time because the number of records remains high for most cycles of the algorithm. More records imply that large volumes of data will be exchanged between slave nodes and the master node resulting in some overheads. Also there will be strain on the master node as it will be having more data to filter and aggregate.

C. Results for varying number of cluster nodes

The algorithm was also tested on varying number of nodes in the cluster. The maximum number of nodes we could use was four. The number of records and minSup remained constant in this experiment. 1.7 million records and minSup of 5 was used in this experiment. Below is the graph of results observed:

Observation

The execution time gradually decreased as the number of nodes increased.

Explanation

The steady and gradual decrease of the execution time is as a result of increased "division of labor". Since the number of records remained constant as the number of nodes increased; it means each node received a smaller portion of the data than in the preceding run. Consequently this resulted in a shorter processing time for each node.

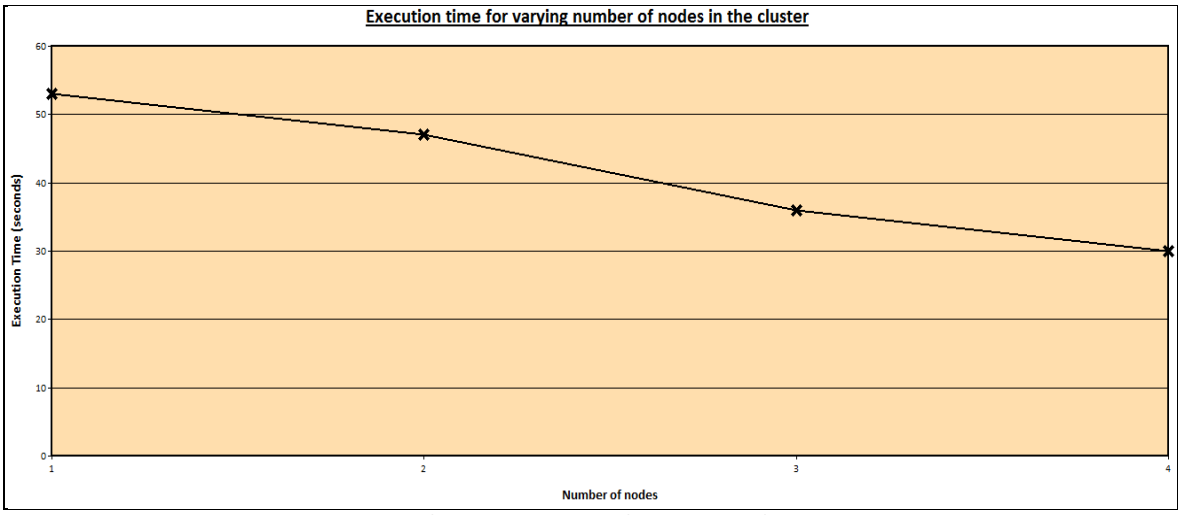

Figure 6: Results for varying number of cluster nodes for PRDB-Miner

VIII. OPTIMUM NUMBER OF NODES

It is our hope that there exist an optimum number of nodes for the algorithm. The optimum point is where we can get the best performance of the algorithm. As the number of nodes continues to increase after reaching this point, it is most likely that the performance of the algorithm will start to fall because the data will be continually partitioned into smaller and smaller chunks such that each node will have very few records. Each node will have very little to do. The major task will be that of filtration and aggregation which are undertaken by the master node. This will result in a bottleneck at the master node since it will be faced with a lot of records to deal with. In such cases parallelization will be of no effect as one node (the master node) will be left with much of the work. The optimum number of nodes is dependent on the number of records being acted upon. For fewer records the optimum number will be smaller.

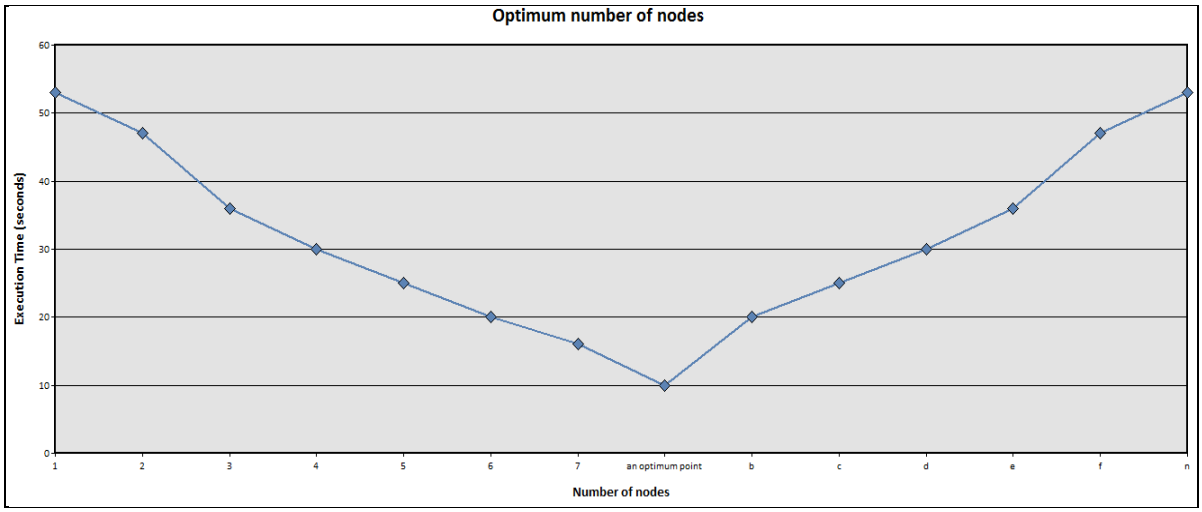

Figure 7: Optimum number of nodes

IX. CONCLUSION

The proposed algorithm, Parallel RDB-Miner performed remarkably. We also concluded that Parallel RDB-miner works well for relations that have a few number of attributes but have a large number of records. A high number of attributes results in a higher number of iterations thereby resulting in poor performance.

In future we hope to find a formula that calculates the optimum number of cluster nodes given the number of records. We also desire to further enhance the algorithm such that it becomes more resilient to node failure since this is a reality we cannot afford to ignore. Also we intend to test the algorithm on other open source SQL-on-Hadoop tools.

REFERENCES

[1] Marko Grobelnik, Jozef Stefan Institute, Ljubljana, Slovenia, *"Big Data Tutorial",* May 2012.

[2] Andrew Pavlo, Erik Paulson, Alexander Rasin, *"A comparison of approaches to large-scale data analysis,"* in Proc. SIGMOD'09, 2009, p. 165.

[3] Daniel J. Abadi, *"Data management in the cloud: limitations and opportunities,"* Bulletin of the IEEE Computer Society Technical Committee on Data Engineering.

[4] Xindong Wu, Fellow, IEEE, Xingquan Zhu, Senior Member, IEEE, Gong-Qing Wu, and Wei Ding, Senior Member, IEEE, *"Data Mining with Big Data",* 2014.

[5] *http://ibmdatamag.com/.*

[6] Azza Abouzeid1, Kamil BajdaPawlikowski, Daniel Abadi1, Avi Silberschatz1, Alexander Rasin2, *"HadoopDB: An Architectural Hybrid of MapReduce and DBMS Technologies for Analytical Workloads",* Yale University, Brown University.

[7] HadoopDB Project. Web page.*db.cs.yale.edu/hadoopdb/hadoopdb.html*.

[8] http://blog.*pivotal.io/big-data-pivotal/products/why-mpp-based-analytical-databases-are-still-key-for-enterprises.*

[9] R. Agrawal and R. Srikant, *"Fast Algorithms for Mining Association Rules,"* Proceedings of the International Conf. on Very Large Databases (VLDB'94), 1994, pages 487-499, Santiago, Chile.

[10] Jianwei Li, Northwestern University; Ying Liu, DTKE Center and Grad. Univ. of CAS; Wei-keng Liao, *"Parallel Data Mining Algorithms for Association Rules and Clustering",* Northwestern University; Alok Choudhary, Northwestern University.

[11] Abdallah Alashqur *"RDB-MINER: A SQL-Based Algorithm for Mining True Relational Databases"* Faculty of Information Technology Applied Science University Amman, JORDAN.

[12] Lingjuan Li, Min Zhang, *"The Strategy of Mining Association Rule Based on Cloud Computing",* College of Computer Science, Nanjing University of Posts and Telecommunications, Nanjing, China.

[13] Dr (Mrs). Sujni Paul, *"Parallel and Distributed Data Mining",* Karunya University, Coimbatore, India.

[14] Dr (Mrs).Sujni Paul, Associate Professor, Department of Computer Applications, *"An optimized distributed association rule mining algorithm in parallel and distributed data mining with XML data for improved response time",* Karunya University, Coimbatore, Tamil Nadu, India.

[15] Mafruz Zaman Ashrafi, Monash University, David Taniar, Monash University, Kate Smith, Monash University, *"ODAM: An Optimized Distributed Association Rule Mining Algorithm",* IEEE Computer Society Vol. 5, No. 3; March 2004.

[16] Jaiwei Han and Micheline Kamber, *"Data Mining Concepts and Techniques, Third Edition"* page 298.

Carboxymethyl guar gum–silver nanocomposite film: Preparation and antimicrobial activity

2 AUTHORS, INCLUDING:

DEVENDRA KUMAR VERMA
Delhi Technological University
6 PUBLICATIONS **1** CITATION

SEE PROFILE

Carboxymethyl guar gum–silver nanocomposite film: Preparation and antimicrobial activity

DEVENDRA KUMAR VERMA* and ANEK PAL GUPTA

Department of Applied Chemistry and Polymer Technology, Delhi Technological University (Formerly Delhi College of Engineering), Shahabad, Daulatpur, Bawana Road, Delhi -110042, India

ABSTRACT

Silver nanoparticles have been utilized in various applications because of its highly conductive and antimicrobial properties. A new method for the synthesis of silver nanoparticles has been used by reduction process to prepare carboxymethyl guar gum- silver (CMGG/Ag) nanocomposite as an antimicrobial film for food packaging applications. The nanoparticles and composites are tested by XRD, FTIR, SEM, TEM, EDX, UV and UTM. Antimicrobial property is tested by using gram positive and gram negative bacteria.

***K**ey **W**ords: Carboxymethyl guar gum, silver nanoparticles, nanocomposite film, antimicrobial activity, food packaging*

INTRODUCTION

A huge commercial demand of nanoparticles is for wide applicability in various areas such as electronics, catalysis, chemistry, energy, and medicine[1]. Especially silver nanoparticles (Ag NPs) are being interested among scientists because of their different antibacterial, catalytic and specific physical and optical properties[2]. There have been a lot of reports for synthesis of Ag NPs, for example, electrochemical techniques[3], photochemical reactions in reverse micelles[4], chemical reduction[5] and green synthesis[6]. The reliable, easy, fast, and eco-friendly method is till awaited for preparation of highly pure Ag NPs. In this article glycerol as green reducing agent and sodium hydroxide as catalyst has been used for preparation Ag NPs.

In recent years, antimicrobial packaging has been found one of the most reliable and promising tool for the next generation of 'active' packaging[7]. It is well known that silver ions and silver-based compounds are highly toxic to microorganisms showing strong biocidal effects on as many as 16 species of bacteria including *E. coli* . Silver, as an antibacterial component, have been used in the formulation of dental resin composites, ion exchange fibres and in coatings of medical devices[8]. Undoubtedly, the most prominent area of research and development is food packaging. The biggest benefit of silver as antimicrobials is that silver can be easily mixed into different materials such as plastics and textiles for desirable uses, where as traditional antimicrobials would be impractical.

Ag NPs make nanocomposites very comfortably with nonbiodegradable plastic or synthetic polymers. But this is also fact that these synthetic non biodegradable polymers have created a tough situation for the living being for a healthy life[9]. This scenario prompted us to change the direction of our research from non-biodegradable to the biodegradable polymeric products. In this article we have introduced carboxymethyl guar gum (CMGG) as a matrix for CMGG/Ag nanocomposite. Guar and its derivatives are all biodegradable and have been used in many applications including food, drug-delivery and health care products because of their natural abundance and their low cost and other desirable functionalities[10]. CMGG is an anionic semi-synthetic guar gum derivative[11,12]. CMGG is a cheap and easily water soluble commercial polysaccharide because it covers a wide range of industrial applications, and has a good film forming property[13]. In this communication, we have reported the synthesis and characterization of Ag NPs by a reduction process and then preparation of CCMG/Ag nanocomposites by *ex-situ* method to study the antibacterial activity for food packaging applications.

EXPERIMENTAL

Materials

CMGG powder has been obtained from Hariom gum industry, Gujarat, India and used without further purification. Sodium hydroxide, silver nitrate ($AgNO_3$) and glycerol have been purchased from Merck, Germany. All aqueous solutions were made using ultrahigh de-ionized (DI) water.

Preparations of Ag nanoparticles (Ag NPs)

Ag NPs were synthesized by reduction process by using glycerol as a reducing agent and sodium hydroxide as a catalyst. Many researchers have used the glycerol as reducing agent[14,15]. The importance thing of this process was the quick synthesis of Ag NPs and no wastage of chemicals. Glycerol is very eco-friendly and sodium

Asian Chitin J., **11(1)**, 11-16 (2015)

*Corresponding author: E-mail: vermadev148@gmail.com

hydroxide can be reused. For the synthesis of Ag NPs, a stock solution of 0.2 M $AgNO_3$ was prepared in DI water. The solution has been mixed with 2 mL glycerol solution followed by addition of sodium hydroxide (0.5 M) drop wise at room temperature with continuous stirring. Immediately it formed yellowish black colloidal solution indicating the formation of Ag NPs. The solution was centrifuged and dried at 20 ^{0}C and stored in the desiccator until further use.

Preparation of carboxymethyl guar gum-silver nanoparticle (CMGG/Ag) nanocomposite film

CMGG/Ag nanocomposites have been synthesised in one step by *ex-situ* method. First of all 1% w/v CMGG solution have been made using DI water. For this 1 gm of CMGG powder was mixed in 100 mL of DI water in 250 mL beaker with constant stirring for 30 min, requisite amount of Ag NPs (1% w/w of CMGG) have been mixed with this solution with constant stirring for 4-5 h until we get clear viscous solution of CMGG/Ag. Then CMGG/Ag nanocomposite film was prepared by solution casting method. This nanocomposite film was dried in room temperature for overnight at room temperature.

Characterization of synthesized AgNPs and CMGG/Ag nanocomposite film

The size, morphology and composition of the nanoparticles and nanocomposites have been tested by of scanning electron microscope (SEM) (HITACHI-S-3700), transmission electron microscopy (TEM), energy dispersive X-ray analysis (EDX) (BRUKER D8-ADVANCE, Fourier Transform infrared spectroscopy (FTIR) (Thermo scientific Nicolet 380) and ultraviolet-visible spectrophotometer (UV- Vis, Parkin Elmer Lambda -750). The tensile strength of the films was tested with UTM (Universal Testing Machine) and compared with standard biodegradable corn packaging films. CMGG/Ag nanocomposite films have also been tested against antimicrobial activity against gram positive (*S. Bacillus*) and gram negative (*E. coli*) bacteria, for different Ag NPs concentration with variation of CMGG. Antimicrobial testing was analysed by Kirby – Bauer method by using Luria Broth as a bacteria growing media.

RESULTS AND DISCUSSION

UV–Vis, SEM and TEM analysis of Ag NPs

The prepared Ag NPs shows an intensive UV–vis absorbance band around 411 nm. In general, the Ag NPs often shows an intense SPR band[16] from 350 to 450 nm (Szunerits & Boukherroub, 2006). According to the reported literature, the position of UV-absorption of Ag NPs depends on their size and shape as well as their surrounding medium[17]. Thus it clarifies that the particles are not homogeneous in size, but there is of great change in size.

The morphologies of the prepared Ag NPs and CMGG/Ag nanocomposite film are done by using SEM and TEM (Fig. 1(a), (b), (c), (d), (e) and (f)). From the SEM images (Fig.1a and 1b), it is cleared that nanoparticles have been formed in a spherical shape. Further the TEM images of the nanoparticles (Fig.1c and 1d) shows clear formation of Ag NPs in range 20 nm to 70 nm in agglomeration form. The average particle size was found ~ 40 nm. From Fig. 1e and 1f it can be seen clearly that Ag NPs are well dispersed in the CMGG matrix. This confirms the formation of CMGG/Ag nanocomposite film.

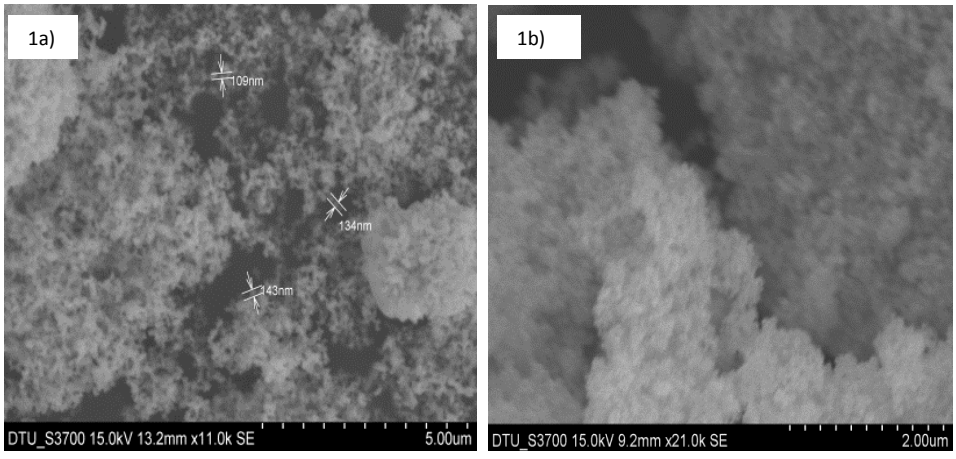

Asian Chitin J., **11(1)**, 11-16 (2015)

*Corresponding author: E-mail: vermadev148@gmail.com

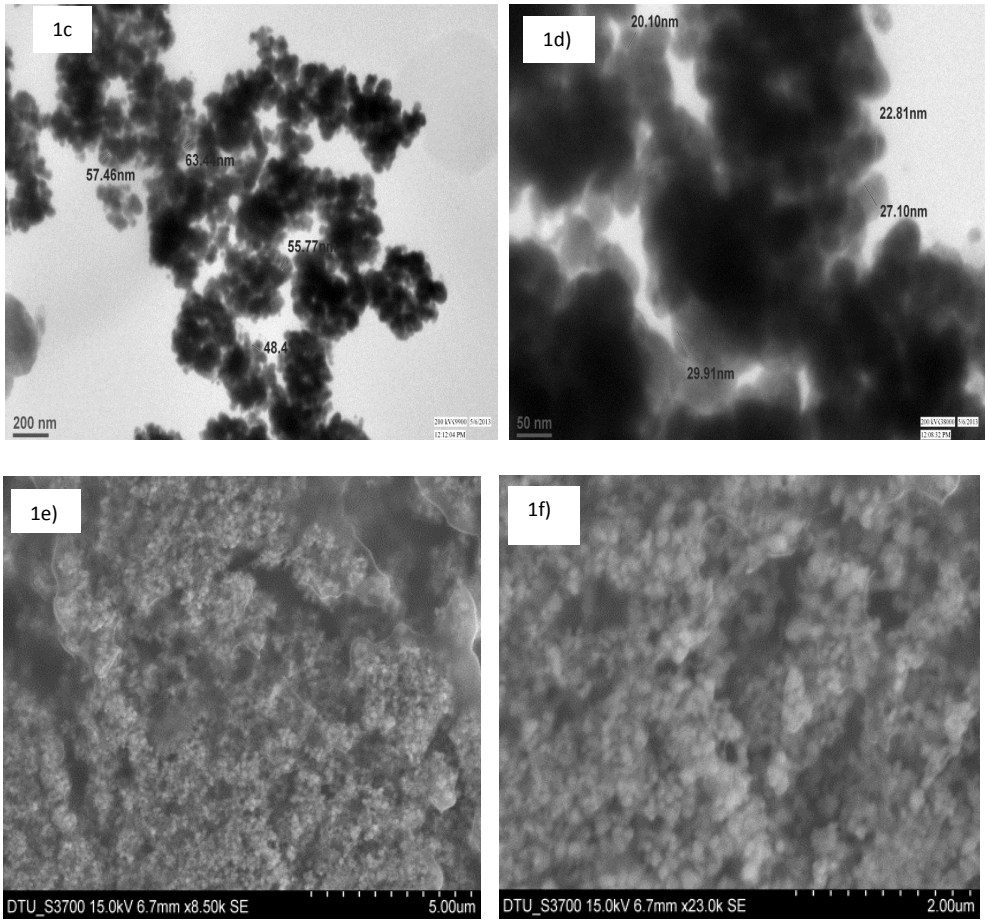

Fig.1. (a) and (b) SEM images of spherical silver nanopariticles, (c) and (d) TEM images of Spherical silver nanoparticles showing different sizes of spherical nanoparticles, (e) and (f) SEM images of CMGG/Ag nanocomposite films.

Fourier Transform Infrared Spectroscopy (FTIR) and EDX analysis

The infrared spectra of silver nanoparticles, CMGG and CMGG/Ag nanocomposite film are shown in Fig. 2 (a), (b), (c). No peak was obtained in Ag NPs FTIR spectrum, it shows that silver nanoparticles were pure and, no chemical bond was attached to Ag metal during the synthesis of Ag NPs. Formation of silver nanoparticle was also proved by EDX analysis (Fig. 2d). The characteristic broad band for O-H group of CMGG appeared at 3438 cm^{-1}. A peak around 2928 cm^{-1} was attributed to an asymmetrically stretching vibration of C-H band in alkanes. The asymmetrical and symmetrical vibrations due to moiety were assigned to 1604 cm^{-1} and 1422 cm^{-1} which may be attributed to carboxymethyl groups into guar gum molecule. Several absorption bands between (814-1030) cm^{-1} were attributed to the contribution of various functional groups, such as C-O and C-O-C bondings. All these peaks were found in pure CMGG powder[18]. The spectral band for CMGG/Ag nanocomposite film (Fig. 2c) appears with slide shifting of peaks for O-H group, 2928 cm^{-1} to 2918 cm^{-1} for asymmetrically stretching vibration of C-H band in alkanes, 1604 cm^{-1} and 1422 to 1637 cm^{-1} and 1430 cm^{-1} for carboxymethyl groups in to guar gum molecule. This shows that the there was no covalent formation between Ag NPs and CMGG.

Asian Chitin J., **11(1)**, 11-16 (2015)

*Corresponding author: E-mail: vermadev148@gmail.com

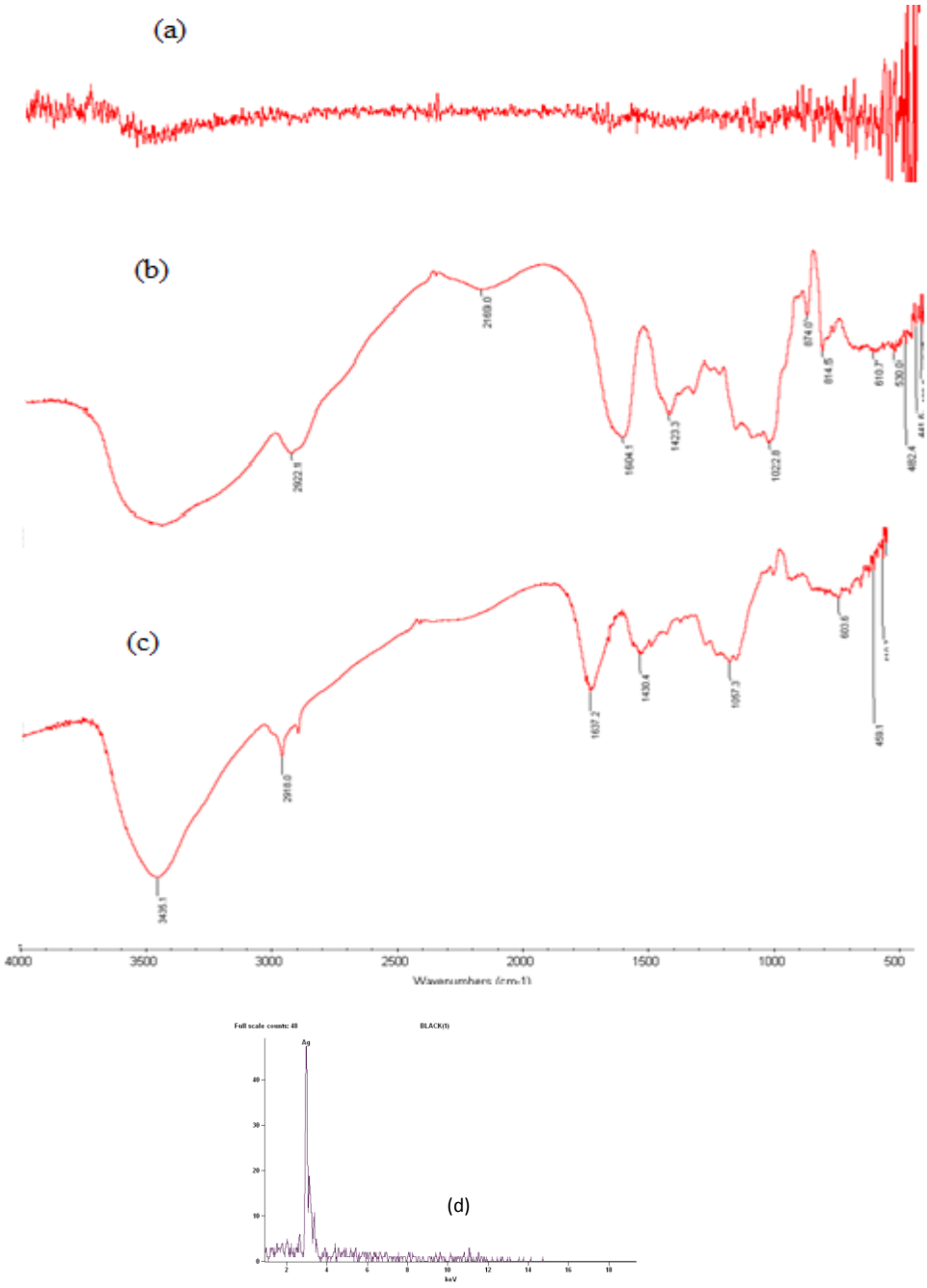

Fig.2. FTIR spectrum of silver nanoparticles synthesized by reduction process (a), FTIR pattern of CMGG powder (b),FTIR spectrum of CMGG/Ag nanocomposite synthesized by exsitu method (c) and EDX patter of the silver nanoparticles (d).

XRD analysis

The nature of the silver nanoparticles synthesized by such process has been evaluated in free stage as well as in CMGG/Ag nanocomposite by XRD method. The XRD of CMGG and Ag NPs was compared. XRD of CMGG shows amorphous nature (Fig. 3b), while the XRD profile of Ag nanoparticles in free state, as well as in composite state, presented in Fig. 3.(a) and (c) exhibit characteristic peaks at scattering angle (2θ) 38.12, 44.46, 64.5, 77.54 (Fig. 3a) and 38.14, 44.36, 64.56, 77.52 (Fig. 3c), corresponding with scattering from the (111), (200), (220), and (311) planes, respectively. These diffraction peaks firmly represent a face centred cubic structure of crystalline silver nanoparticles[19,20]. This also represents a high purity of synthesized silver crystal.

*Corresponding author: E-mail: vermadev148@gmail.com

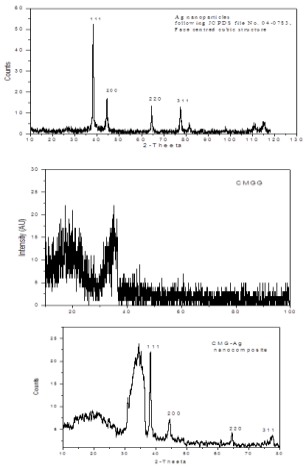

Fig.3. XRD pattern of silver nanoparticles(face centred cubic lattice)synthesized by green synthesis(a), XRD spe ctrum of CMGG powder(b), XRD spectrum of CMGG/Ag nanocomposite film prepared by solution casting method(c).

Antimicrobial activity

The antimicrobial susceptibility of CMGG/Ag nanocomposite film is evaluated by using the disc diffusion of Kirby-Bauer method. This method has been recommended by the national committee for clinical laboratory standards (NCCLS)(NCCLS,03). CMGG/Ag nanocomposite films of different concentration (A1C = 0.5 wt %, A2C =0.75 wt %, A3C =1.0 wt %, A4C =1.25 wt %, C= 0 wt % of Ag NPs of CMGG powder) were cut in the circular shape with same size and put in the inoculated plates and stored for 24 h at 37^{o}C in incubator. After 24 h, incubation zones of inhibition were measured. It was found that CMGG/Ag nanocomposite at a certain level inhibited bacterial growth by more than 90%. The diameters of inhibition zones (in mm) around the different CMGG- Ag nanocomposite films are shown in Table 1.

Table 1 CMGG/Ag nanocomposite films with variable amount of silver nanoparticles (wt %) and respective inhibition zones

Bacterial	Variable amount of silver nanoparticles in CMGG/Ag nanocomposite (wt %) and respective inhibition zones in mm.				
	A1C film	A2C film	A3C film	A4C film	Pure CMGG film (C)
Gram positive	14	18	20	24	Biodegradable
Gram negative	25	27	30	34	

Tensile strength

Tensile strength of the CMGG/Ag nanocomposite films are determined by using Universal Testing Machine (UTM). Comparison study of the tensile strength is done for different concentrations of CMGG/Ag nanocomposites films with standard corn natural polymer film available in the market. For the testing of CMGG/Ag nanocomposite films, CMGG film and corn film, all the films were cut in the fine strips as mentioned in standard of UTM. Length, weight and thickness of all the strips were measured by using electronic vernier calliper by two times and their average value was used.
Tensile strength of CMGG-Ag nanocomposites films of different concentrations (A1C=0.5%, A2C=0.75%, A3C=1.0 %, A4C=1.25 %,) were found respectively 23.737 MPa, 29.488 MPa, 44.092 MPa and 28.340 MPa. Tensile strength of CMGG film and corn film were found 24.346 MPa and 5.922 MPa respectively. Thus from tensile results it was found that as the concentration of the silver was increased from 0.5 wt% to 1.25 wt% the tensile strength also increased, which was good agreement with literature reports[21,22]. The tensile strength of nanocomposites was found greater than pure CMGG film and corn films. This result explains that prepared CMGG/Ag nanocomposite film may be used as antimicrobial films for food packaging applications.

CONCLUSIONS

Ag NPs were synthesized successfully via reduction process using green reducing agent (glycerol). Silver nanoparticles were found of spherical shape of average size 20-70 nm. Silver nanoparicles were pure and in crystalline form. Bulk amount of silver nanoparticles in a very less time can be synthesized by this method. This method was found very fast, easy and reliable with no wastage of chemicals. The CMGG/Ag nanocomposite

*Corresponding author: E-mail: vermadev148@gmail.com

film was successfully prepared by solution casting method. A little amount of nanocomposite film was found sufficient for antimicrobial activity for both types of bacteria. Tensile strength of the nanocomposite films were also found very good and greater than of corn film and pure CMGG films. It was concluded that in future with slight improvement, CMGG/Ag nanocomposite films can be used in food packaging.

REFERENCES

1. Geethalakshmi R and Sarada D V L, International Journal of Engineering Science and Technology, **2(5),** 970 (2010).
2. Król-Gracz A, Nowak P, Michalak E and Dyonizy A, Proceedings of the International Congress on Advances in Applied Physics and Materials Science, Antalya Acta Physica Polonica, A **121 (**2011).
3. Rodriguez-Sanchez L, Blanco M C and Lopez-Quintela M A, J. Phys. Chem., **104 (41),** 9683 (2000).
4. Tamura S, Takeuchi K, Mao G, Csencsits R, Fan L, Otomo T, Saboungi M-L, Journal of Electroanalytical Chemistry, **559** 103 (2003).
5. Tripathi R N, Saxena A, Gupta N, Kapoor H and Singh R P, Digest Journal of Nanomaterials and Biostrucutres, **5,** 2 (2010).
6. Singh C, Sharma V, Naika P K, Khandelwal V and Singh H, Digest Journal of Nanomaterials and Biostructures, **6,** 535 (2011).
7. Tripathi S, Mehotra G K and Dutta P K, Bull. Mater. Sci., **34(1),** 29 (2011).
8. Timothy V. Duncan, Journal of Colloid and Interface Science, **363,** 1 (2011).
9. Gupta A P and Verma D K, International Journal Of Biological Macromolecule, **68**, 247 (2014).
10. Sreenivasan Soumyaa R, kumar Ghoshb S, Abrahama E T, International Journal of Biological Macromolecules, **46,** 267 (2010).
11. Gong H, Liu M, Chen J, Fei Han, Gao C and Zhang B, Carbohydrate Polymers, **88(3),** 1015 (2012).
12. Gupta A P and Verma D K, International Journal of Advanced Research, **2 (1)**, 680 (2014).
13. Garg P, Studies on Hydrogels Based on Polyacrylamide and Guar Gum Derivatives, A Major-II Dissertation Submitted to Delhi Technological University India, 2013.
14. Alba E. Díaz-Álvarez and Victorio Cadierno, Appl. Sci., **3**, 55 (2013).
15. Sinha A and Sharma B P, Bull. Mater. Sci., **28(3),** 213 (2005).
16. Szunerits S and Boukherroub R, Langmuir, 22, 1660 (2006).
17. Prasad B L V, Stoeva S I, Sorensen C M, Zaikovski V, Klabunde K J, J Am Chem Soc 125, 10488 (2003).
18. Dodi G, Hitcu D and Popa M I, Cellulose Chemistry and Technology, **45(3-4),** 171 (2011).
19. Kirubaharan C J, Kalpana D, Lee Y S, Kim A R, Yoo D J, Nahm K S and Kumar G G, Industrial and Engineering Chemistry Research, **51,** 7441 (2012).
20. Wen X, Xie Y T, Mak M W C, Cheung K Y, Li X Y, Renneberg R and Yang S, Langmuir, **22,** 4836 (2006).
21. Islam Md S, Masoodi R and Rostami H 2013 Hindawi Publishing Corporation, Journal of Nanoscience, 275037, 10 (2013).
22. Perumalraj R, ISRN Chemical Engineering, 842021, 4 (2012)

Received: 30 January 2015
Accepted: 10 March 2015

*Corresponding author: E-mail: vermadev148@gmail.com

International Journal of Science and Research (IJSR)
ISSN (Online): 2319-7064
Index Copernicus Value (2013): 6.14 | Impact Factor (2013): 4.438

Comparison of Fuzzy Algorithms on Images

Vikrant Dabas[1], Sachin Nandal[2], Prakhar Dogra[3]

[1]Department of Computer Engineering , Delhi Technological University, New Delhi, India

[2]Department of Information Technology, MaharajaSurajmal Institute of Technology, New Delhi, India

[3]Department of Computer Engineering, Delhi Technological University, New Delhi, India

Abstract: ***Image segmentation is a process by which an image is partitioned into regions with similar features. Many approaches have been proposed for image segmentation, but generally we use Fuzzy C-Means method, because it gives better results for large class of images. However, using this method is not suitable for images with noise and it is a lengthy process in terms of duration when compared with other method. For this reason, many other methods have been proposed to improve the shortcomings of image segmentation using fuzzy C-Means. Techniques like Credibilistic Fuzzy C-Means overcomes the problem of noise persisted using FCM. Intuitionistic Fuzzy C-Means introduces the concept of non-membership for a cluster. Krishnapuram and Keller [1] suggested usage of Possibilistic C-Means clustering which relaxes the column constraint of FCM so that membership matrix better reflects the typicality of particular data point in a cluster and noise could be avoided. We perform a comparison of these clustering algorithms on the basis of execution time and validity function for each algorithm applied on different kind of images taken in consideration.***

Keywords: clustering, segmentation, C-Means, fuzzy, images

1. Introduction

Clustering is a process for classifying objects or patterns in such a way that samples of the same group are closer than samples belonging to different groups. Differentstrategies for clustering have been used, broadly the hard clustering and the fuzzy clustering scheme, which are different to each other in a characteristic way. The conventional hard clustering method restricts each point of the data set to exclusively just one cluster. As a result, having such approach the segmentation results are often very crisp, i.e., each pixel of the image gets clustered to exactly one class. However, in the original situations, for images, problems like poor contrast,limited spatial resolution, noise, overlapping intensities, and intensity in homogeneities variation make this hard (crisp) segmentation a difficult task. Thanks to the fuzzy set theory [4], which produced the idea of partial membership of belonging described by a membership function. Among the fuzzy clustering methods, fuzzy c-means (FCM) algorithm [5] is the most popular method used in image segmentation because it has robust characteristics for ambiguity and can retain much more information than hard segmentation methods [6].

Various properties of clustering techniques are: clustering techniques must assign lower memberships to all the outliers for all the clusters[7], centroids generated by Clustering Techniques on noisy images should not deviate significantly from those generated for the corresponding noiseless images, obtained by removing the outliers, clustering techniques must be independent of any number of clusters i.e. able to identify outliers by changing the number of clusters for the same images, they should be independent of any amount of outliers i.e. Centroids generated by these techniques should not deviate by increasing the number of outliers[8].

Image segmentation is an important, challenging problem and a pre-requisite for image analysis as well as for interpretation of high-level image. Understanding highly detailed imaging produced by robotic vision, medical imaging etc. are few of the application of image segmentation. Main function of image segmentation is partition of an image into a set of disjoint regions with uniform and homogeneous attributes such as intensity, colour, tone or texture, etc. Many different segmentation techniques have been developed and detailed surveys can be found in references [2–3].

Synthetic-aperture radar (SAR) is a form of radar imaging which is used to create images of large objects, such as a landscape – these images can be 2Dimensional or 3Dimensional representations of the landscape or piece of land taken for consideration. “SAR creates high resolution images with comparatively small physical antennas”. [9]. In this document we compare the use of fuzzy based classification techniques over SAR and Hestain images and conclude which algorithm gives better results.

2. Theoretical Background for clustering

a. Fuzzy C-Means (FCM)

Fuzzy clustering in fuzzy logic deals with the degree ofbelonging of each point to a cluster, rather than belongingcompletely to just one cluster. It was first developed by Dunn[10] and improved by Bezdek [11] which proved to be base of all fuzzy clustering algorithm is specified in terms of membership matrix. There have been several clustering criteria proposed for identifying optimal fuzzy c-partitions. Out of all those, the most appropriate method is:

$$J_{FCM}(X:U,V)=\sum_{j=1}^{c}\sum_{i=1}^{N}(u_{ij})^{m}\left\|x_i-v_j\right\|^2, 1<m<\infty \quad (1)$$

Here J is an objective function and where $\|x_i - v_j\|^2$ is a chosen distance measure between a data point x_i and the cluster centre v_j, is an indicator of the distance of the *n* data points from their respective cluster centres and here distance measure is Euclidean distance. Fuzzy partitioning is carried out through an iterative optimization of the objective function shown in the equation above, with the updating of membership u_{ij} and the cluster centres v_j by:

$$u_{ij} = \frac{1}{\sum_{k=1}^{c}\left(\frac{d_{ik}}{d_{jk}}\right)^{2/(m-1)}} \quad (2)$$

$$v_j = \frac{\sum_{i=1}^{N} u_{ij}^m x_k}{\sum_{i=1}^{N} u_{ij}^m}, \forall j = 1,.....c \quad (3)$$

This iteration will stop when $\max_{ij}\left(u_{ij}^{k+1} - u_{ij}^{k}\right) < \in$, where $\in$ is a termination criterion between 0 and 1, whereas *k* is the number of iteration steps. This procedure converges to a local minimum or a saddle point of J_m using Lagrange's multiplier theorem these values have been calculated. In this clustering algorithm, centre of cluster defined is assumed, m is a degree of fuzziness and value of m > 1 in fuzzy clustering algorithms. The fuzzy clustering technique using alternatingly equation (2) and (3) is called Fuzzy C Means.

b. Possibilistic C-Means (PCM)

Krishnapuram and Keller [1] suggest relaxing the column constraint of FCM so that membership matrix better reflects the typicality of particular data point in a cluster and noise could be avoided. Here they have calculated typicality matrix as T.

$$T = [t_{ik}]_{cxn}$$

Here T represents possibility of an object belongs to particular matrix with the associated weight, the value of the weight function is estimated from the data and the membership values can be interpreted as degrees of possibility of the points belonging to the clusters implies the compatibilities of the points with the class prototypes. The Primary aim of possibilistic clustering was to overcome the problems and limitations of fuzzy clustering methods. Krishnapuram and keller proposed a possiblistic approach by minimizing the objective function as

$$J_{PCM}(U,V) = \sum_{i=1}^{c}\sum_{k=1}^{N} t_{ik}^m d_{ik}^2 + \sum_{i=1}^{c}\gamma_i \sum_{k=1}^{N}(1-t_{ik})^m$$

Where U is the membership function, V is the centre matrix of clusters, γ_i gives the weight associated with all clusters which is user defined and $\gamma_i > 0$. In the above equation the first term tries to reduce the distance from data points to centroids as low as possible and second term forces t_{ik} to be as large as possible.

c. Credibilistic Fuzzy C-Means(CFCM)

To reduce the effect of outliers Krishna K. Chintalapudi [7] proposed credibilistic fuzzy c means (CFCM) and introduced a new variable i.e. credibility. CFCM defines Credibility as:

$$\Psi_k = 1 - \frac{(1-\Theta)\alpha}{max_{j=1.n}(\alpha j)}, 0 \le \beta \le 1$$

Where $\alpha_k = i = 1, \dots . c^{min}(d_{ik})$

Setting ɵ=1 reduces the scheme to FCM while ɵ=0 assigns zero membership to the most noisy vector. If ɵ is set to 1 then there is no noisy vector that is present in the dataset, thus we choose ɵ=0 in all our implementations. CFCM partitions X by minimizing (the objective function of FCM):

$j_{cfcm} = \sum_{i=1}^{i=c}\sum_{k=1}^{k=n} u_{ik}^m \|x_k - v_i\|^2$,

Subject to constraints,

$$\sum_{i=1}^{i=c} u_{ik} = \Psi_k ; k = 1, \dots ., n.$$

The conditions for local minima are,

$$u_{ik} = \frac{\Psi_k}{\sum_{j=1}^{j=c}\left(\frac{d_{ik}}{d_{jk}}\right)^{\frac{2}{m-1}}} \forall\, i,k$$

Memberships generated by CFCM for outliers are lower than those generated by FCM because for outliers credibility is very small. Main advantageous function of CFCM is reducing the effect of outliers on regular clusters.

d. Intuitionistic fuzzy c-means (IFCM)

Intuitionistic fuzzy c-means work on generalized fuzzy sets in which elements are characterized by both characteristics of membership, and non-membership value. Degree of belongingness is indicated by membership value, whereas the degree of non-belongingness of an element tothat set is indicated by non-membership values. Atanassov introduced a parameter called hesitation degree, $\pi_A(x)$, which explains lack of knowledge in defining the membership degree of all elements x in the set A. It is calculated as:

$\pi_A(x) = 1 - \mu_A(x) - v_A(x)$

The objective function for intuitionistic fuzzy c-means [12] include modified objective function of FCM and intuitionistic fuzzy entropy.

$$J_{IFCM} = \sum_{i=1}^{c}\sum_{k=1}^{n} u_{ik}^{*m} d_{ik}^2 + \sum_{i=1}^{c} \pi_i^* e^{1-\pi_i^*}$$

$u_{ik}^* = u_{ik} + \pi_{ik}$, in which u_{ik}^* denotes the intuitionisticfuzzy membership

u_{ik} gives the normal fuzzy membership of the k^{th} data in i^{th} class.

From the above equation,π_{ik} denotes the hesitation degree, which is:

$\pi_{ik} = 1 - u_{ik} - (1 - u_{ik}^{\alpha})^{1/\alpha}$, $\alpha > 0$

Yager gave an intuitionistic fuzzy complement which is used to calculate above defined constant:

$N(x) = (1-x^{\alpha})^{1/\alpha}$, $\alpha > 0$

Intuitionistic fuzzy entropy (IFE), is the second term of objective function for IFCM.Zadeh introduced fuzzy entropy, which is the measure of fuzziness in a fuzzy set. Mathematically IFE is derived as:

$$IFE\ (A) = \sum_{i=1}^{n} \pi_A\ (x_i) e^{[1-\pi_A(x_i)]}$$

Where $\mu_A\ (x_i)$ is the membership degree

$v_A(x_i)$is the non-membership degree

$\pi_A(x_i)$is the hesitation degree

As Euclidian distance measure is used in IFCM, hence only hyper-spherical clusters can be detected in the data[13]. Non-linearly separable data can't be worked upon by IFCM.

3. Results

Performance evaluation of the algorithms have been done over certain parameters which distinguishes there potential to be used for image segmentation. To find the most suitable method of image segmentation using fuzzy clustering techniques we used two images which are generally used for image analysis.We can see the results on images after using different clustering techniques.

A. Westconcordaerial.png [14]

Westconcordorthophoto.png, the Mass GIS georegisteredorthophoto. It is a panchromatic (grayscale) image, supplied by the Massachusetts Geographic Information System (MassGIS) that has been orthorectified to remove camera, perspective, and relief distortions (via a specialized image transformation process). The orthophoto is also georegistered (and geocoded) — the columns and rows of the digital orthophoto image are aligned to the axes of the Massachusetts State Plane coordinate system. In the orthophoto, each pixel center corresponds to a definite geographic location, and every pixel is 1 meter square in map units.

SAR IMAGE

FCM for n=3

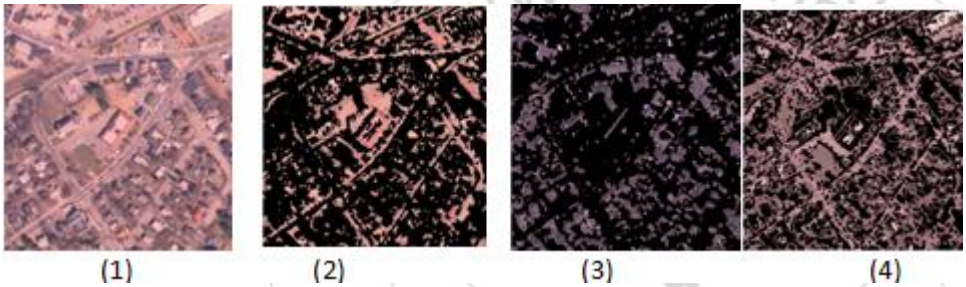

IFCM for n=2

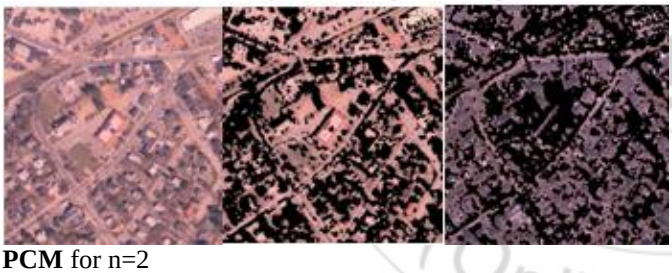

PCM for n=2

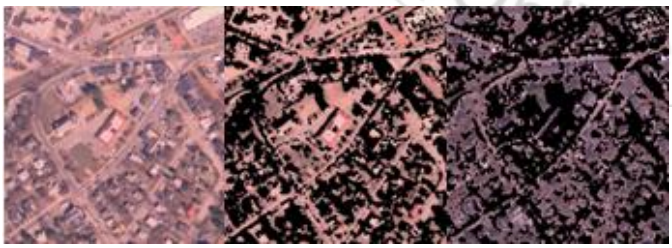

CFCM for n=2

B. Hestain.png[15]

It is an image of tissue stained with hemotoxylin and eosin (H&E). This staining method helps pathologists distinguish different tissue types.

HESTAIN image

a. FCM for n=3

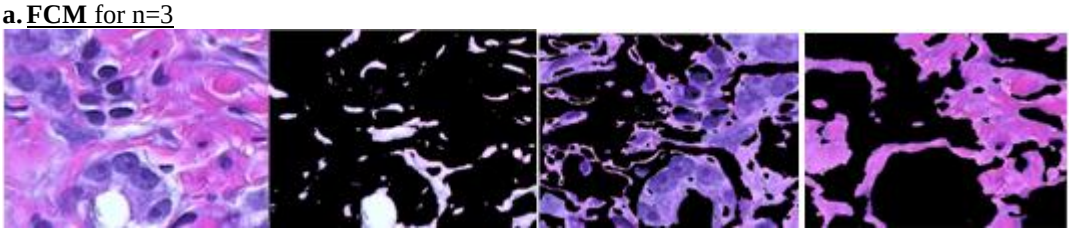

b. IFCM for n=2

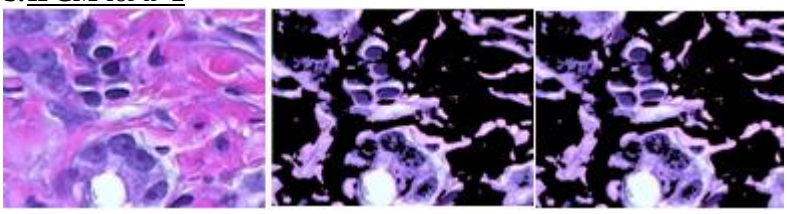

PCM for n=4

c. CFCM for n=2

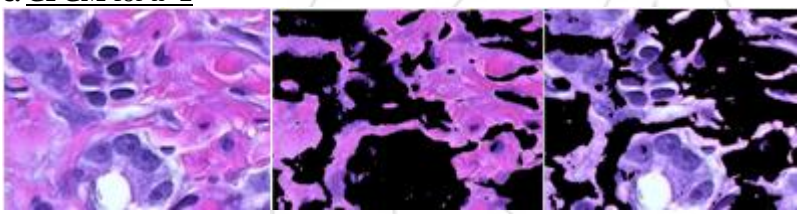

C. Performance Evaluation

a. Execution Time

We have used Tic Toc function of MATLAB to calculate the time taken for an algorithm in analysing the image. The function records the internal time at execution of the tic command. Display the elapsed time with the toc function. It is observed that in case of SAR Image, FCM technique has least execution time but the convergence rate of IFCM algorithm is best. Whereas in case of Synthetic image, PCM technique has least execution time but the convergence rate of IFCM algorithm is best.

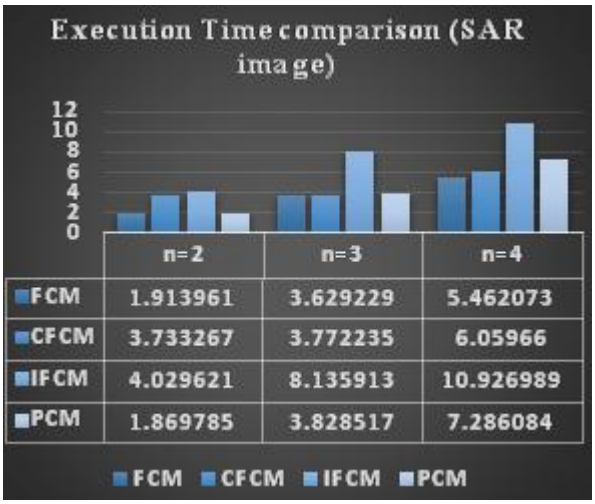

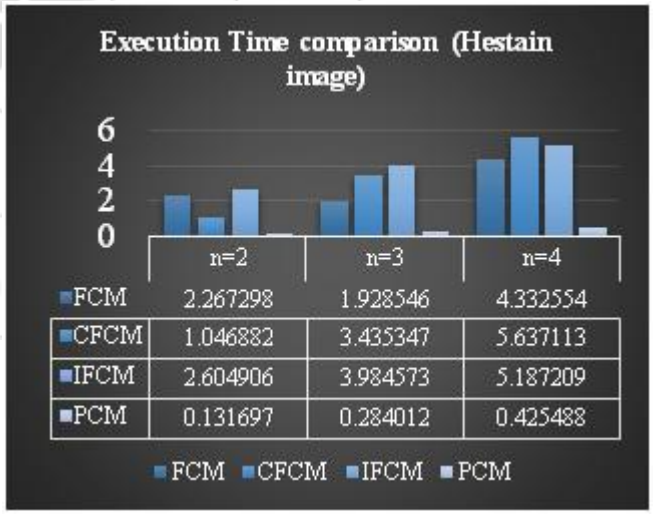

b. Validity Function

The qualitative evaluation of the performance of segmentation is done using two types of cluster validity functions: the feature structure and the fuzzy partition. The functions that represents the fuzzy partition are partition entropy [16] and partition coefficient [17]. They are defined as:

$V_{pc}(u) = \sum_{i=1}^{n} \sum_{k=1}^{c} {u_{ki}}^2$

$V_{pe}(u) = -\frac{1}{n} \{\sum_{i=1}^{n} \sum_{k=1}^{c} [u_{ki} log u_{ki}]\}$

Best clustering results are achieved when $v_{pc}$is maximum or $v_{pe}$is minimum. Disadvantage of v_{pc} and v_{pe} are that they measure only the fuzzy partition and do not specify featuring property.

4. Conclusion

Digital images generally contain unknown noise and consider able uncertainty. Traditionally, FCM is a popular segmentation method for digital images. However, it is an intensity-based clustering algorithm which is not robust against noisy images. In this paper, we have compared Fuzzy C-Means (FCM), Intuitionistic Fuzzy C-Means(IFCM), Possibilistic C-Means(PCM), and Credibilistic Fuzzy C-Means(CFCM) methods under different environments. We observed the results of these four algorithms on two different types of images – Hestain.png which is a synthetic image, and Westconcordaerial.png which is a SAR image. We compared the experimental results of PCM, CFCM, FCM, IFCM on both the images. Quantitative and qualitative analysis of the results showed that the algorithm is more efficient compared to two others.

Table: Comparison of Fuzzy Algorithms on basis of Execution Time, and Validity Functions.

IMAGE	METHOD	Clusters	Execution Time	Vpc	Vpe
SAR	FCM	2	1.913961	1.0935e +05	-5.7167e +04
		3	3.629229	9.3171e + 04	-9.1313e + 04
		4	5.462073	8.1837 e + 04	-1.1828 e + 05
	PCM	2	1.86979	8.4912 e + 04	-8.0601 e + 04
		3	3.82852	1.0724 e + 05	-1.21182 e + 05
		4	7.28608	1.3083 e + 05	-1.6171e+05
	CFCM	2	3.733267	8.03e+04	-5.71e+04-
		3	3.772235	6.40e+04	-9.13e+04
		4	6.05966	5.54e+04	-1.18e+04
	IFCM	2	4.029621	1.0133e +05	-6.7873 e + 04
		3	8.135913	7.8841 e +04	-1.1373 e + 05
		4	10.926989	6.6688	-1.4593
HESTAIN	FCM	2	2.267298	5.3906 e+ 04	-2.4286 e+ 04
		3	1.928546	4.9789 e+ 04	-3.4080 e+ 04
		4	4.332554	4.5713 e+ 04	-4.3928 e+ 04
	PCM	2	0.1317	5.0280 e+ 04	-3.6214 e+ 04
		3	0.28401	5.3461 e+ 04	-5.6029 e+ 04
		4	0.42549	5.9751 e+ 04	-7.4691 e+ 04
	CFCM	2	1.046882	3.33e+04	-2.43e+04-
		3	3.435347	2.85e+04	-3.40e+04
		4	5.637113	2.37e+04	-4.40e+04
	IFCM	2	2.604906	4.5779 e+ 04	-3.4807 e+ 04
		3	3.984573	4.1051 e+ 04	-4.8399 e+ 04
		4	5.187209	3.2734 e+ 04	-6.6425 e+ 04

References

[1] R. Krishnapuram and J Keller, " A possibilistic approach to clustering", IEEE Trans, Fuzzy Systems ,vol 1 ,no. 2 , pp 98-110, April 1993.
[2] Fu, S.K.—Mui, J.K.: A Survey on Image Segmentation. Pattern Recognition, Vol. 13, 1981, pp. 3–16.
[3] Haralick, R.M.—Shapiro, L.G.: Image Segmentation Techniques. Comput. Vision Graphics Image Process, Vol. 29, 1985, pp. 100–132.
[4] Pal, N.—Pal, S.: A Review on Image Segmentation Techniques. Pattern Recognition, Vol. 26, 1993, pp. 1277–1294.
[5] Zadeh, L.A.: Fuzzy Sets. Inform. and Control, Vol. 8, 1965, pp. 338–353.
[6] Bezdek, J.C.: Pattern Recognition with Fuzzy Objective Function Algorithms. New York: Plenum Press, 1981.
[7] Chintalapudi K. K. and M. kam, ―A noise resistant fuzzy c-means algorithm for clustering,‖ IEEE conference on Fuzzy Systems Proceedings, vol. 2, May 1998, pp. 1458-1463.
[8] Kaur, P., Gosain, A. (2011), ―A Density Oriented Fuzzy C-Means Clustering Algorithm for Recognizing Original Cluster Shapes from Noisy Data‖ International Journal of Innovative Computing and Applications (IJICA), INDERSCIENCE ENTERPRISES, Vol. 3, No. 2, pp.77–87.
[9] Bezdek, J.C.—Hall, L.O.—Clarke, L.P.: Review of MR Image Segmentation Techniques Using Pattern Recognition. Med. Phys., Vol. 20, 1993, pp. 1033–1048.
[10] J.C Dunn, "A fuzzy relative of the ISODATA process and its use in detecting compact well separated clusters", J Cybern,pp-32-57, 1973
[11] J.C Bezdek, "Pattern recognition with fuzzy objective function", New York,Plenum Press, 1981.
[12] T. Chaira, "A novel intuitionistic fuzzy c means clustering algorithm and its application to medical images", Applied Soft computing 11(2011) 1711-1717
[13] "Novel Intuitionistic Fuzzy C-Means Clustering for Linearly andNonlinearly Separable Data" by Prabhjot Kaur, A. K. Soni, AnjanaGosain, WSEAS TRANSACTIONS on COMPUTERS, Issue 3, Volume 11, March 2012E-ISSN: 2224-2872
[14] http://in.mathworks.com/help/images/register-an-aerial-photograph-to-a-digital-orthophoto.html
[15] http://in.mathworks.com/help/images/examples/color-based-segmentation-using-k-means-clustering.html
[16] Fukuyama Y, Sugeno M. (1989), "A new method of choosing the number of clusters for the fuzzy c- means

method", In: proceedings of fifth fuzzy system symposium; 1989, p. 247–50.
[17]]Xie XL, Beni GA. (1991), "Validity measure for fuzzy clustering", IEEE Trans Pattern Anal Mach Intell 1991; 3:841–6.

I.J. Image, Graphics and Signal Processing, **2015, 8, 28-34**
Published Online July 2015 in MECS (http://www.mecs-press.org/)
DOI: 10.5815/ijigsp.2015.08.03

Design and Implementation of Novel Multiplier using Barrel Shifters

Neeta Pandey and Saurabh Gupta
Name of Institution/Department, City, Zip Code, Country
Dept. of Electronics and Communication Engg, Delhi Technological University, Bawana Road, Delhi, 110042, India
Email: n66pandey@rediffmail.com, saurabhguptadtu@gmail.com

Abstract—The paper presents a design scheme to provide a faster implementation of multiplication of two signed or unsigned numbers. The proposed scheme uses modified booth's algorithm in conjunction with barrel shifters. It provides a uniform architecture which makes upgrading to a bigger multiplier much easier than other schemes. The verification of the proposed scheme is illustrated through implementation of 16x16 multiplier using ISIM simulator of Xilinx Design Suite ISE 14.2. The scheme is also mapped onto hardware using Xilinx Zynq 702 System on Chip. The performance is compared with existing schemes and it is found that the proposed scheme outperform in terms of delay.

Index Terms—Barrel shifter, modified Booths algorithm, multiplier design.

I. Introduction

Due to the recent advancements in the field of multimedia and communication technologies, real-time processing requirement of image, graphics and signals has become more and more important. Multiplication is one of the most important arithmetic operations. It is used in almost all systems that perform any sort of image processing, analog or digital speech processing or any multimedia related operation. Some of the common examples include convolution, inner product, Discrete Wavelet Transform (DWT), Fast Fourier Transform (FFT) etc. For efficient and fast operation of such systems, high speed multiplier is a must requirement. Its importance can be seen from the fact that most DSPs and high end processing systems use a separate multiplier unit for fast multiplication.

Barrel shifter is instrumental for expeditious processing of data in both general purpose and embedded digital signal processors. It is primarily combinational circuit made up of multiplexers wherein the signal passes through constant number of logic gates, thereby making the delay almost fixed, which is independent of the shift value or shifter size. The design of a barrel shifter is hierarchical in a sense that the layers of the multiplexers are linked with each other such that the output of one multiplexer is connected to the input of the next multiplexer and the connection depends upon the required shift distance. An N bit barrel shifter may be constructed by placing N 2:1 multiplexers in $\log_2 N$ layers. Thus an 8 bit barrel shifter requires three layers each having eight 2:1 MUX as shown in the Fig. 1. Here inp(j), out(j) and shift(k) corresponds to j^{th} bit of input, j^{th} bit of output and k^{th} bit of select input; and values of j and k assume values in the range of 0-7 and 0 – 2 respectively. The selection lines of the MUX in i^{th} (i = 1,2,3) layer are connected to $(i-1)^{th}$ bit of shift input. The layer provides shift by 2^{i-1} bit positions if corresponding $(i-1)^{th}$ bit is high. For shift input of "100" the first two layers pass inputs without any shift and third layer shifts input by four bit positions. It be noted that 8 bit barrel shifter can shift a word by 0-7 bit positions (0 being the trivial case) by combining shifts in all the three layers. An n bit position shift operation in barrel shifter can be performed in single cycle in contrast to 'n' cycles in a shift register due to its combinational logic structure. These type of shifters are already used in the floating point add and subtract operations which require proper alignment of the mantissa of the operands [1, 2]. This paper investigates the possibility of using barrel shifters in multiplication where shifting is required rather frequently.

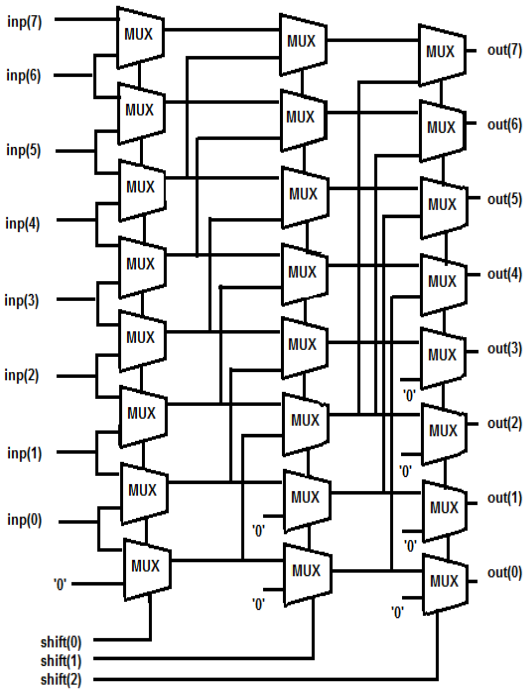

Fig. 1. Barrel Shifter design [1]

The paper is organized as follows: Section 2 briefly describes multiplier architectures followed by proposed design in Section 3. The hardware implementation on Zynq 702 SoC is explained in section 4. Section 5 describes the results as obtained after the implementation and Section 6 constitutes the conclusion and future prospective of the proposed algorithm.

II. Related Work

Numerous designs of multipliers have been proposed in [3-8] and references cited therein. The designs have a tradeoff between the number of parallel units used for implementation and the maximum clock period with which the circuit can operate. The conventional shift-add algorithm is the most basic multiplier that makes use of repetitive shifting and accumulation of multiplicand in accordance with the multiplier. It multiplies two 'n' bit numbers in 'n' clock cycles and thus becomes very lengthy as the number of multiplier bits increase. Although the method requires basic arithmetic operations but demands multiple clock cycles to execute. To overcome this, a combinational design consisting of logic gates and adders is presented and named as array multiplier. In this, the partial products are generated by multiplying each multiplier bit one by one with the multiplicand. The partial products terms are then shifted according to their bit order as defined by shift and add algorithm and then are added up to give final output. This type of multiplier is well suited when the operand size is small, but the design complexity increases manifolds for larger size operands. Other multiplication methods are: Braun multiplier, Baugh-Wooley multiplier, Booth multiplier, Wallace tree multiplier. The Braun multiplier has highly regular structure and is useful in applications where area is of prime concern and speed can be traded off. It uses carry save adders foor adding the intermediate partial product terms and then produces the final result in binary form using ripple carry adder. It can deal with only unsigned numbers which becomes motivation for the Baugh-Wooley multiplier. This multiplier takes advantage of the fact that direct multiplication using 2's complement method can produce the final result directly without requiring complement stages in between, thereby speeding up the process. Further, as the multiplication is done in 2's complement form, signed numbers are automatically taken into account. Both Braun and Baugh-Wooley multipliers are efficient and have uniform structure but are suitable for handling operand sizes less than 16 bits. Booth multiplier provided a significant advancement in this field. The algorithm takes into account that in all other multiplication algorithms one partial product term is generated for each multiplier bit. This algorithm reduces the number of partial products by representing the original multiplier in a higher radix format. As a significant time is used up in the addition process, the reduction in intermediate terms saves a lot of time and hardware cost. The modifications on this method show improvements in overall speed and implementation area. The Wallace tree multiplier is popular in high speed applications and is characterized by complex and irregular routing. It incorporates a special tree structure, wherein the product terms are first grouped together and then added. Because of grouping, less number of additions are required at each stage. Thus the addition complexity is reduced down from O(n) to O(log n). Many compression techniques have been proposed for Wallace tree which further reduces the effective number of additions at each layer of the multiplication process and thus providing better timing results. But due to irregular structure and complex routing, power consumption becomes an important problem for this. Wallace tree is commonly used in conjunction with the booth encoder thereby having the advantage of both the methods and has timing results superior to that of others.

In this work, we have proposed a multiplier design that uses barrel shifters in conjunction with modified booth's algorithm to develop a high speed multiplier circuit. The proposed design can perform both signed and unsigned multiplication. It is then implemented over hardware using Zynq 702 SoC.

III. Proposed Design

This section describes a novel multiplier design based on barrel shifters which takes into account the single clock shifting capabilities of barrel shifters which are utilized to produce the partial products in a parallel fashion. Here the partial products are the shifted version of the multiplicand (Y) accounted on basis of the multiplier (X) bits. The design first uses barrel shifters to produce partial products which are then added up using adder tree. The utility of the proposed multiplier is further enhanced as it can multiply both signed and unsigned numbers by incorporating sign extension of the partial product terms. In addition to the proposed parallel architecture, the design also integrates Booth's encoder which uses modified Booth's algorithm. Due to this the number of partial products reduces from 'n' to 'n/2', 'n' being the number of bits in multiplier which in effect reduces the number of additive layers by one thereby improving the delay by great extent. The following section describes the proposed design step by step.

Table 1. Radix-4 booth encoding

Block	Partial product (operation)
000	0
001	+1*multiplicand
010	+1*multiplicand
011	+2*multiplicand
100	-2*multiplicand
101	-1*multiplicand
110	-1*multiplicand
111	0

A. Booth's Encoder

The modified booth's algorithm [6] i.e. radix-4 booth's encoding is briefly explained in this section. Here the multiplier bits (n) are considered as blocks of 3 bit each where two consecutive blocks have one bit in common as shown (1).

$$X = \sum_{i=0}^{\frac{n}{2}-1} D_i 4^i \qquad \overbrace{X\,X\,X}^{D_2}\;\overbrace{X\,X\,X}^{D_1}\;\overbrace{X\,X\,0}^{D_0} \tag{1}$$

The grouping in multiplier starts from least significant bit (LSB) with a zero bit appended to it. The overlap between the block signifies what happened in last block as the MSB of each block acts like its sign bit. As an example if a 16 bit multiplier is "0010110010010011", then the pairs are as formed as in (2).

$$\overbrace{0\,0}^{D_7}\;\overbrace{1\,0}^{D_5}\;\overbrace{1\,1}^{D_3}\;\overbrace{0\,0}^{D_1}\;\overbrace{1\,0}^{D_6}\;\overbrace{0\,1}^{D_4}\;\overbrace{0\,0}^{D_2}\;\overbrace{1\,1}^{D_0} \tag{2}$$

The multiplicand is either evaluated to zero, multiplied by ±1 or ±2 according to the 3 bit pairs. The exact operation is summarized in Table 1.The MSB of each pair gives the sign with which the corresponding partial product is to be sign extended. As the modified booth's algorithm reduces the number of partial product terms to half as compared to the conventional multiplier, the former requires lesser number of total resources and also has significant speed improvement.

B. Proposed Scheme

The data flow in the proposed design can be described by the flowchart of Fig. 2. The proposed design uses three steps- booth encoding, partial product generation by barrel shifters followed by the addition. Here the x [n-1] and y [n-1] signifies the multiplier and multiplicand respectively, each 'n' bit wide. The steps for partial product generation are:

- Firstly the multiplier is fed into the booth encoder circuit which in turn generates a control signal to control the input to the barrel shifter.
- According to the control generated, the barrel shifters are fed in with either multiplicand in its true form or in 2's complement form.
- The barrel shifters are placed so as to provide a fixed number of bit shifting according to the index they are operated upon.
- To keep signed multiplication into consideration too, the true or the complemented form is extended with the sign bit to '2n' bits i.e. double the number of bits in the multiplicand.

After the barrel shifters are fed with legal inputs then the data word is shifted by the required amount as set by the index of the pair that was formed by the booth encoder. In general, each barrel shifter has shift equivalent of 2(k-1) bits where 'k' signifies the 'k^{th}' encoded multiplier bit group from the booth's encoder.

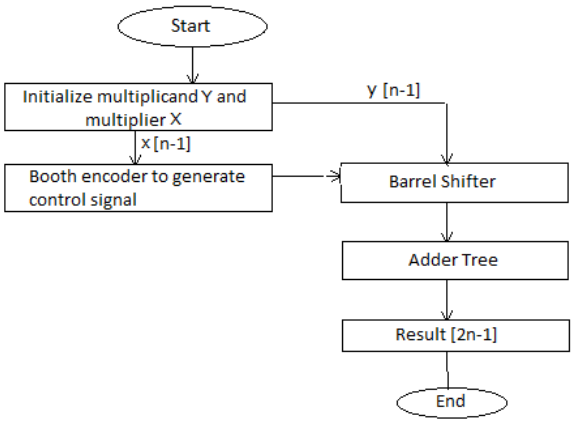

Fig. 2. Data Flow in proposed design

The barrel shifters output reduced partial terms which are to be added to form the final result. For unsigned numbers 'n' bit adders are sufficient for the purpose as the partial product terms are '2n' bits in size but 'n' bits out of these are just zeros, so effectively we need to add only 'n' bit numbers for each partial product term. For signed numbers though we have to use '2n' bit adders, as the partial product terms contain the extended sign bits which have to be taken into account while performing the addition. For efficient adding an adder tree is prepared depending on the number of partial products to be added, as this reduces the number of levels in which addition takes place. For this purpose different types of adders may be incorporated into the design like Ripple Carry Adders, carry skip adders, carry select adders, carry increment adders, carry look ahead adder, tree adders [3-7]. Parallel-prefix adder tree structures such as Kogge-Stone [9], Sklansky [10], Brent-Kung [11], Han-Carlson [12], and Kogge-Stone using Ling adders [13] etc. have one or other advantage over other. The performance of the ripple carry adder is linearly proportional to the number of bits whereas carry bypass, carry select and carry look ahead show square root and logarithm dependence on number of bits. Though the carry look ahead adder provides a significant improvement in delay but becomes inefficient for wide adders as the total delay is dominated by the delay in passing the carry through

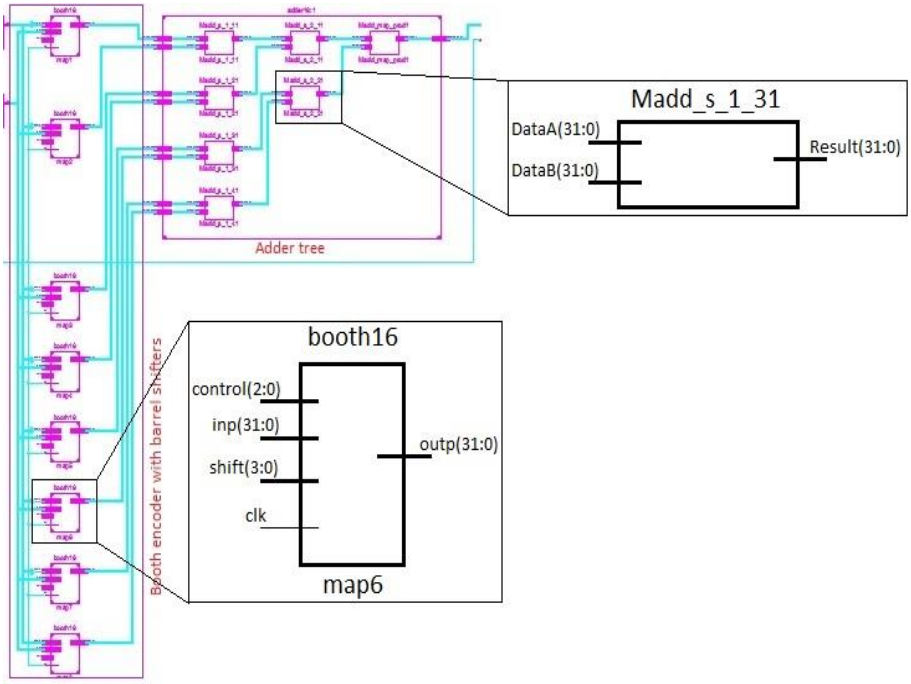

Fig. 3. RTL schematic view of 16x16 multiplier

look ahead stages which can be handled by arranging the look ahead stages in a multilevel tree. Such adders are known as tree adders and some of the examples are Kogge-Stone [8], Sklansky [9], Brent-Kung [10], Han-Carlson [11], and Kogge-Stone using Ling adders [12]. The choice of a particular adder depends on the number of stages of logic, the number of logic gates, maximum fan out on each gate and amount of wiring between the stages. After the addition, the output is stored in a '2n' bit wide output register. The focus in the present work is to establish the concept of barrel shifter in multiplier implementation, therefore default adder available in FPGA in hardware implementation.

IV. Harware Implementation

The proposed multiplication scheme is verified by simulating a 16x16 multiplier in Xilinx Design Suite ISE 14.2. The simulations have been performed using Integrated Software Environment (ISE) included in the Design suite. The scheme is mapped onto hardware using The RTL schematic view of the design showing the various blocks for a 16x16 multiplier is as shown in the Fig. 3.

From left to right the schematic may be viewed in 3 blocks namely the booth encoder, barrel shifter and adder. The 16 bit wide multiplier and multiplicand inputs are stored in registers, an input clock signal to drive the registers and then the final output fed to a 32 bit register. The number of parallel units in the structure depends upon the number of bits which are to be multiplied. Here for 16x16 multiplication, the booth encoder generates 'n/2' i.e. 8 partial product terms thus in total we require 8 barrel shifters which shift the product terms as required in the multiplication algorithm. From the enlarged section comprising booth encoder with barrel shifter has namely 4 input ports control(2:0), inp(31:0), shift(3:0) and clk which correspond to 3 bits of multiplier which will be encoded by booth encoder, the multiplicand, 4 bits to specify required shift value and the clock signal. The output is shifted 32 bit version of the multiplicand. Further then the shifted vector go through an adder tree, each adder having two 32 bit vectors as inputs and giving back an 32 bit output.

The barrel shifters facilitate the shifting operation unlike conventional sequential shifters where the data is shifted one bit position per cycle. Thus the partial product generation becomes faster and results in improved speed performance of the multiplication process. The adder circuit is implemented in the form of a binary tree where each adder is 32 bit wide as each of the partial product terms are of 32 bits due to the extension of the sign bit which has to be taken into consideration for the multiplication of signed numbers. The adder circuit can be implemented using various techniques available. The default adder of FPGA is used to test the proposed method.

The graphical design view, obtained in the Xilinx Platform Studio (XPS) is shown in the Fig. 4 for the target FPGA (Zynq 702 Soc) device where the design is finally ported.

Xilinx Zynq 702 System on Chip is a general purpose board having advantage of parallel units (configurable logic blocks (CLB's)) as well as sequential unit (ARM Cortex A9 Duel core processor). Embedded Design Kit (EDK) is used to model the multiplier in VHDL language.

Further, to communicate with the on-chip processor Software development kit (SDK) is used which serves as a medium to give input to the multiplier and collect the final output. Finally the design is mapped on the FPGA

using the bit stream generated in PlanAhead tool.

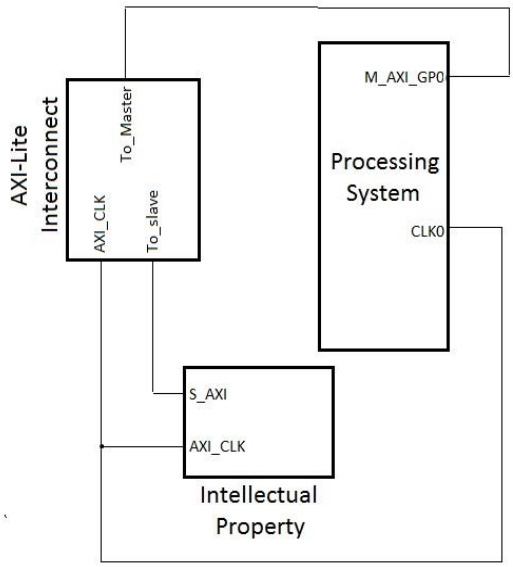

Fig. 4. Block diagram of implemented design over Zc702 evaluation board

The logic of the hardware is implemented as an intellectual property (IP) in the programmable logic (PL) section of the device. The hardware block is driven by the processing system (PS) through an AXI4-Lite bus based on AMBA protocol which is light weight, single transaction memory mapped interface running at 50MHz. The board provides a serial interface (USB) for feeding the data to the hardware. The transaction of operands between the processor and IP is byte oriented i.e. the data is transferred one byte per clock cycle. As shown in figure the processing system is connected to our IP through a AXI interconnect which acts as a interface between the processor running at 800MHz and IP running at 50MHz.The inputs and output are provided by memory read and write operations respectively by specifying the 32 bit address in memory where the hardware block is physically present. The IP is customized to have 3 registers in its wrapper module which by default are 32 bit in size. The input operands are provided in the lower half of two input registers and the final result is collected in a 32 bit output register. The final output can be viewed in the console as provided by Xilinx in Software development kit (SDK).

Further for the purpose of comparison a 4x4 multiplier prototype is also designed and compared with other schemes. The synthesized timing values specifying the delay and maximum operational frequency is shown in the next section.

V. Simulation Results

The ISIM simulation results for the 4x4 and the 16x16 multiplier are shown respectively in Figs. 5 and 6 respectively which verify the functionality of the proposed approach. For both cases, the result is available in the output register at the rising edge of input clock after one clock period of application of input operands.

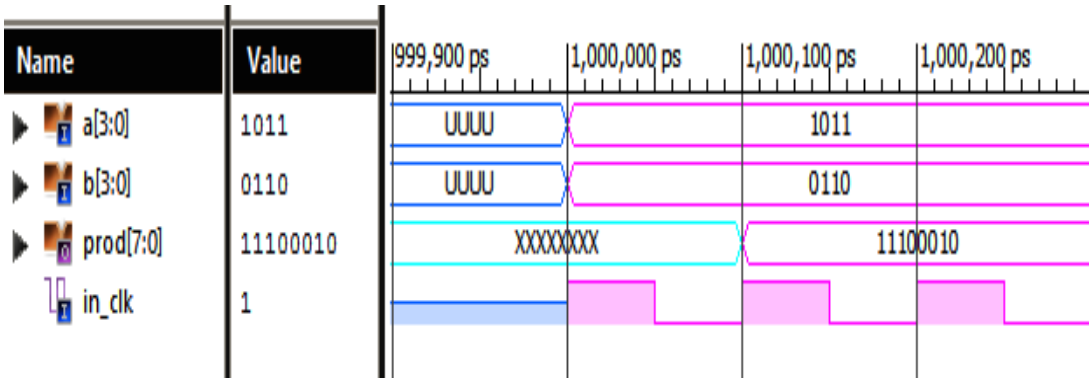

Fig. 5. Simulation results of 4x4 multiplier

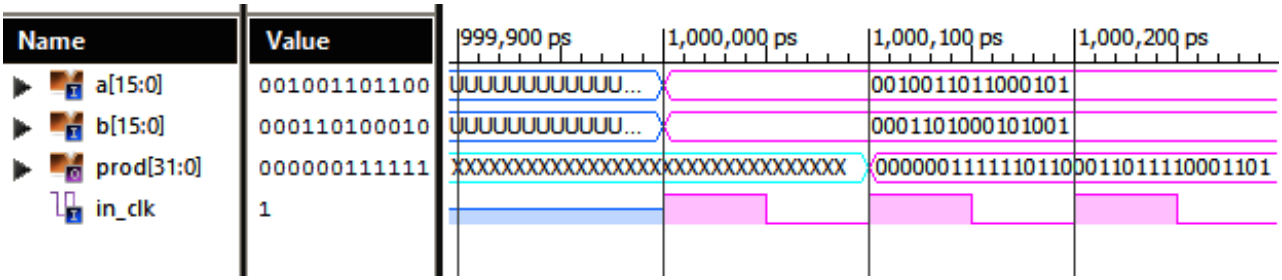

Fig. 6. Simulation results of 16x16 multiplier

A comparison of the proposed multiplier is carried out in reference to Shift Add multiplier, Array, Wallace tree, Booth, Booth encoded Wallace tree and the results are summarized in Table 2. The proposed design has the lowest delay time when compared to that of other's and hence can operate at a clock frequency as high as 788 MHz. Further, a comparison listing the resource utilization is provided which shows the efficient nature of proposed design. Fig 7 gives a graphical representation of the same from which it is clear that the proposed design is much better that the others in both delay and area except for booth encoded Wallace where the area requirements are more by 7% but gives around 16% improvement in timing parameter.

Table 2 Comparison of proposed design's results

Type of Multiplier	Delay (ns)	Maximum operational frequency (MHz)	No. of Slice LUT's utilized
Shift Add multiplier	3.930	254.453	63
Array	2.448	408.497	46
Wallace tree	2.295	435.730	47
Booth	1.864	536.481	49
Booth encoded Wallace tree	1.471	679.809	39
Proposed design	1.269	788.022	42

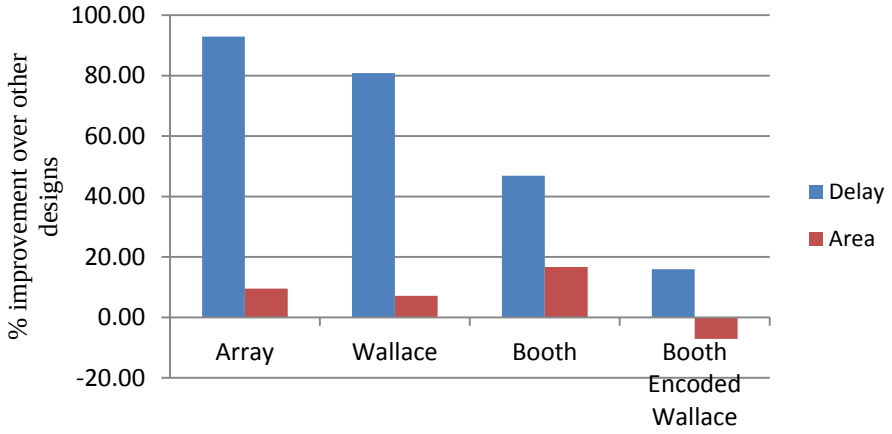

Fig. 7. Comparison of proposed design with other's for delay and area

VI. Conclusion

A multiplier design based on barrel shifter is presented in this paper. The proposed scheme makes use of modified booth's algorithm in conjunction with barrel shifters for improving the delay. The functionality of the design is verified through simulations and performance is compared with existing multipliers. The proposed design shows 16% improvement in delay therefore it can operate at much higher operating speed. Further the proposed multiplier accounts for signed multiplication as well without adding any more complexity. Thus the simplicity and hierarchical design makes it very easy for designing and debugging. Due to these advantages, the multiplier can be used in high speed processing devices such as DSP's etc. The work can further be extended for optimization of proposed multiplier in terms of area and power.

References

[1] J. H. Cline, "Barrel shifter using bit reversers and having automatic normalization", US 4782457 A, 1988.
[2] M. J. S. Smith, *Application Specific Integrated circuits*, Pearson, 2006.
[3] M. Ercegovac, and T. Lang, *Digital Arithmetic*, San Francisco, Morgan Kaufmann, 2004.
[4] B. Pahrami, *Computer Aithmatic and Hardware Design*, New York, Oxford University Press, 2000.
[5] N. H. E. Weste, D. Harris, and A. Banerjee, *CMOS VLSI Design: A Circuit and System perspective*, Pearson, 2006.
[6] M. Rabaey, A. Chandrakasan, and B. Nikolic, *Digital Integrated Circuits A Design Perspective*, PHI, 2003.
[7] K. S. Yeo, and K. Roy, *Low Voltage Low Power VLSI Subsystems*, Tata Mc-Graw Hill, 2009.
[8] V. Kunchigik, L. Kulkarni, and S. Kulkarni, "Pipelined Vedic-Array Multiplier Architecture", International Journal of Image, Graphics and Signal Processing (IJIGSP)", vol. 6, No. 6, pp. 58-64, 2014
[9] P. M. Kogge, and H. S. Stone, "A parallel algorithm for the efficient solution of a general class of recurrence equations", *IEEE Transactions on Computers*, vol. C-22, pp. 786–793, 1973.
[10] J. Sklansky, "Conditional-sum addition logic", *IRE Transactions on Electronic Computers*, vol. 9, pp. 226–231, 1960.
[11] R. P. Brent, and H. T. Kung, "A Regular Layout for Parallel Adders", *IEEE Transactions on Computers*, vol. C-31, (1982), 260–264,.
[12] T. Han, and D. Carlson, "Fast area-efficient VLSI adders", in Proceedings of IEEE Symposium on Computer Arithmetic, pp. 49–56, 1987.
[13] H. Ling, "High-speed binary adder", *IBM Journal of Research and Development*, vol. 25, pp. 156–166, 1981.

Authors' Profiles

Neeta Pandey did her M. E. in Microelectronics from Birla Institute of Technology and Sciences, Pilani and Ph. D. from Guru Gobind Singh Indraprastha University Delhi. She has served in Central Electronics Engineering Research Institute, Pilani, Indian Institute of Technology, Delhi, Priyadarshini College of Computer Science, Noida and Bharati Vidyapeeth's College of Engineering, Delhi in Various capacities. At present, she is Assistant Professor in ECE department, Delhi Technological University. A life member of ISTE, and member of IEEE, USA, she has published papers in International, National Journals of repute and conferences. Her research interests are in Analog and Digital VLSI Design

Saurabh Gupta is a student in 4th year at Delhi Technological University pursuing Bachelors in Electronics & Communication Engineering. His research interests include parallel computing and computer architecture.

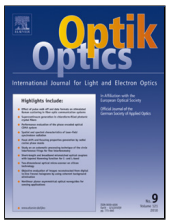

Title: Enhancement of low Exposure Images via Recursive Histogram Equalization Algorithms

Author: Kuldeep Singh Rajiv Kapoor Sanjeev Kr. Sinha

PII: S0030-4026(15)00532-X
DOI: http://dx.doi.org/doi:10.1016/j.ijleo.2015.06.060
Reference: IJLEO 55695

To appear in:

Received date: 6-5-2014
Accepted date: 15-6-2015

Please cite this article as: K. Singh, R. Kapoor, S.Kr. Sinha, Enhancement of low Exposure Images via Recursive Histogram Equalization Algorithms, *Optik - International Journal for Light and Electron Optics* (2015), http://dx.doi.org/10.1016/j.ijleo.2015.06.060

Enhancement of low Exposure Images via Recursive Histogram Equalization Algorithms

Kuldeep Singh [a], *Rajiv Kapoor* [b], *Sanjeev Kr. Sinha* [c]

[a] *Central Research Lab, Bharat Electronics Ltd, Ghaziabad, 201010, India. Phone No: +91-9910101592, email: kuldeep.er@gmail.com*

[b] *Department of Electronics & Communication, Delhi Technological University, Delhi, 110042, India. email: rajivkapoor@dce.ac.in*

[c] *Department of Computer Science, Indian School of Mines, Dhanbad, 826004,India.*

Abstract:

This paper proposes two exposure based recursive Histogram equalization methods for image enhancement. The proposed methods are very effective for images acquired in low light condition like underwater sequences or night vision images. The first method is Recursive Exposure based sub-image histogram equalization (R-ESIHE) that recursively performs ESIHE[20] method till the exposure residue among successive iteration is less than a predefined threshold. The second method is named as Recursively separated Exposure based sub image histogram equalization (RS-ESIHE) that performs the separation of image histogram recursively ; separate each new histogram further based on their respective exposure thresholds and equalize each sub histogram individually. The experimental results show that low exposure image enhancement problem was not addressed by earlier HE based methods , has been efficiently handled by these new methods. The performance evaluation of new methods is done in terms of Image information content as well as visual quality inspection. The proposed methods outperforms earlier HE based contrast enhancement algorithms specifically for low light images.

Keywords:

Recursive Histogram equalization, Image Information content, Image Exposure, Low exposure Imaging

1. Introduction

Although there is a tremendous advancement in image capturing devices, still natural images are often subject to low-exposure problems under low light or underwater conditions. Digital cameras have a limited dynamic range as a result photographs acquired in high dynamic range scenes often exhibit underexposure artifacts in shadow regions [1]. An image captured in a dim light environment encounters low-exposure problem caused by non-ideal camera settings of aperture and shutter speed. Exposure in an image determines the brightness or darkness of each element in the image [2]. In the low illumination scenario, post-processing using image enhancement tools is needed to improve the quality of the acquired image. Many Histogram equalization based image enhancement methods were proposed to cope with contrast related issues. Histogram equalization (HE) is most extensively utilized contrast enhancement technique due to its simplicity and ease of implementation [3]. Histogram Equalization flattens the probability distribution and stretches the dynamic range of gray levels, which in result improves the overall contrast of the image [4]. Applying HE straight away on natural images is not suitable for most consumer electronics applications such as TV, Cameras etc., as it tends to change the mean brightness of the image to the middle level of the gray level range, which in turn produces annoying artifacts and intensity saturation effects. Kim [4] was the first one to propose an algorithm named brightness preserving bi histogram equalization (BBHE) which preserves the mean brightness of the image and improves the contrast. BBHE bisects the histogram based on the input mean brightness and equalizes the two sub histograms independently. Wan et al. [5] proposed an algorithm named dualistic sub image histogram equalization (DSIHE) and claimed that it is better than BBHE in terms of preservation of brightness and information content (entropy) of the image. DSIHE separates the histogram based on median value instead of mean, which implies that each histogram

contains almost equal number of pixels. Chen and Ramli introduced minimum mean brightness error bi-histogram equalization (MMBEBHE) for preserving the mean brightness "optimally" [6]. MMBEBHE is an extension of BBHE, which iteratively calculates the absolute mean brightness error (AMBE) for gray levels 0 to L-1 and bisects the histogram based on the intensity value $\mathbf{X_m}$, which yields minimum AMBE. Chen and Ramli [7] proposed another approach named recursive mean-separate histogram equalization (RMSHE). This technique iteratively performs the BBHE in which the histogram is divided into two parts based on the average input brightness and BBHE is performed to each sub histogram independently. Sim et al. [8] proposed a similar technique to RMSHE known as recursive sub-image histogram equalization (RSIHE). This technique performs the division of histogram based on the median value of brightness instead of mean brightness. Kim and Chung [9] presented a method named Recursively Separated and Weighted Histogram Equalization (RSWHE) similar to RSIHE and RMSHE methods. In addition, RSWHE modify the histogram by weighting process using normalized power law function. These techniques do not provide a mechanism for adjusting the level of enhancement. Clipped histogram based techniques [10-12] were proposed as a solution for controlling the enhancement rate as well as preserving the original brightness. These methods control maximum value of the histogram by clipping histograms higher than the pre specified threshold. Different approaches are proposed for the determination of clipping threshold or plateau limit. Wadud et. al. [13] proposed a new class of histogram partitioning named as dynamic histogram equalization (DHE). The DHE partitions the original histogram based on local minima and then, assigns a new dynamic range to each sub-histogram. The major drawback of this method is that it remaps the histogram peaks by allocating new dynamic range, which significantly changes the mean brightness. Ibrahim and Kong [14], proposed a method brightness preserving dynamic histogram equalization (BPDHE) similar to DHE, which is extension of the DHE. BPDHE applies Gaussian-smoothing filter before the histogram partitioning process is carried out. The

BPDHE uses the local maxima as the separating point rather than the local minima used in DHE. Ibrahim and Kang claimed that the local maxima are better for mean sbrightness preservation. Sheet et. al. [15] proposed a modification of the BPDHE technique named as Brightness Preserving Dynamic Fuzzy Histogram Equalization (BPFDHE). This method uses Fuzzy histogram computation for smoothing operation of histogram before partitioning of image into sub histograms. The authors of BPDFHE method proved the superiority of the algorithm in terms of less computational time and brightness preservation. These dynamic methods are suitable only for the images having significant peaks in the histograms. Quadrants Dynamic Histogram Equalization (QDHE) method was proposed by Ooi and Isa [16] for better contrast enhancement. QDHE partitions the histogram into four sub histograms using the median value of intensity and then clips the histogram according to the mean of intensity occurrence of the input image and finally a new dynamic range is assigned to each sub-histogram before each sub histogram is equalized. Ooi and Isa [17] also proposed Adaptive Contrast Enhancement Methods with Brightness Preserving which comprised of two methods named as dynamic quadrants histogram equalization plateau limit (DQHEPL) and bi-histogram equalization median plateau limit (BHEPL-D). DQHEPL is extension of RSIHE, divides the histogram into four sub histograms, and then assigns a new dynamic range and finally implements clipping process. BHEPL-D is the extension of the BHEPL except that it clips the histogram using the median of the occupied intensity. Chang and Chang [18] presented a simple approach for contrast enhancement named as Simple Histogram Modification Scheme (SHMS). This method modifies the histogram by changing the values of two boundary values of the support of histogram. A new method named as background brightness preserving histogram equalization (BBPHE) proposed by Tan et.al. [19]. The partition method used by BBPHE is based on background levels and non-background levels range. After partition, each sub-image is equalized independently, and then combined into the final output image. It is claimed that the background levels are only stretched within the

original range, hence, the over enhancement can be avoided by BBPHE. Singh and Kapoor [20] proposed Exposure based Sub Image Histogram Equalization (ESIHE) method for enhancement of low exposure images where the image exposure threshold is used for sub dividing image. Low exposure images possess limited dynamic range resulting in poor contrast.. Images having histogram bins concentrated towards the lower part or the darker gray levels possess low intensity exposure whereas images having histogram bins concentrated towards the higher part or the brighter part possess high intensity exposure and both category of images exhibit poor contrast. Although various techniques are available to cater specific problem of contrast enhancement, but enhancement of low exposure images is still less explored area. In this work, two extensions of the ESIHE are proposed. First, a recursive method is proposed as the extension of the ESIHE, called Recursive Exposure based sub image histogram equalization (R-ESIHE). The proposed method iteratively performs ESIHE on the image until the difference of exposure values between subsequent iterations is less than a threshold value. The second method is Recursively separated Exposure based sub image histogram equalization (RS-ESIHE). Unlike the R-ESIHE, the second algorithm first splits the histogram into two or more sub histograms based on the individual exposure thresholds and then performs histogram equalization of all the sub histograms. Clipping of histogram is added in both the proposed methods to avoid excessive enhancement.

This paper is organized as follows: Section 2 describes the proposed algorithms. Section 3 gives experimental results, and section 4 concludes the paper.

2. Recursive Histogram Equalization for Low exposure Images

Both the proposed methods undergo two fundamental steps: Exposure thresholds calculation and Histogram Clipping. The description of each step is presented in the following subsections.

2.1 Exposure Threshold calculation

The categorization of an image into low or high exposure is done based on exposure threshold (Singh et al, 2013). The normalized range of exposure value is [0-1]. The images containing majority of low exposure regions possess exposure values lesser than 0.5 tending towards zero however, the overexposed images have exposure values greater than 0.5 tending towards one. Image intensity exposure value can be calculated as eq. (1).

$$exposure = \frac{\sum_{k=0}^{L-1} h(k)k}{L\sum_{k=0}^{L-1} h(k)} \quad (1)$$

Where h(k) is histogram of image and L is total number of gray levels. Parameter $\boldsymbol{X_a}$ (as calculated in eq. 2) is the gray level boundary value that divides the image into under exposed and over exposed sub images.

$$X_a = L(1 - exposure) \quad (2)$$

2.2 Histogram Clipping

The idea behind histogram clipping is to prevent over enhancement leading to the natural appearance of the image. For limiting the enhancement rate, we need to limit the first derivative of histogram or the histogram itself (Ooi et. al., 2009).The histogram bins having the value greater than the clipping threshold are limited to the threshold (Fig.1).

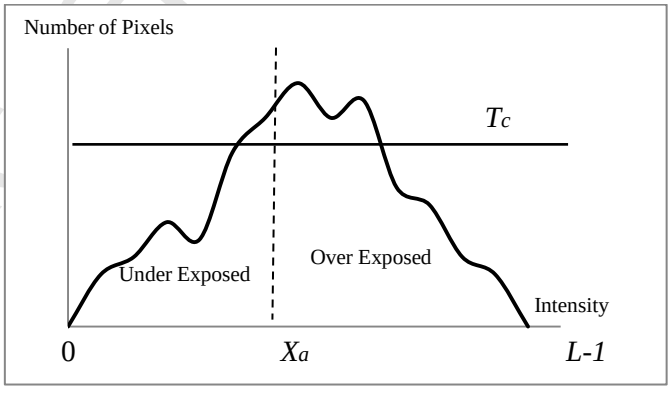

Fig.1. Process of Histogram Sub Division and Clipping

The clipping threshold is calculated as an average number of gray level occurrences. The formula for clipping threshold $\mathbf{T_c}$ is presented in (3) and (4) calculates the clipped histogram

$$T_c = \frac{1}{L}\sum_{k=0}^{L-1} h(k) \quad (3)$$

$$h_c(k) = \begin{cases} h(k), & h(k) < T_c \\ T_c, & h(k) \geq T_c \end{cases} \quad (4)$$

Where *h(k)* and *hc(k)* are the original and clipped histogram respectively. This method of histogram clipping is computationally efficient and consumes lesser time.

2.3 Recursive Exposure based sub-image histogram equalization (R-ESIHE)

The proposed RESIHE method is a recursive variant of ESIHE, which performs ESIHE recursively on the given histogram. The number of recursions is dependent on the exposure difference between successive iteration. The fundamental step of the algorithm is histogram subdivision and equalization.

2.3.1 Histogram Sub Division and Equalization

The original histogram is first bisected in two sub images *WL* and *WU* ranging from gray level 0 to $\mathbf{X_a - 1}$ and $\mathbf{X_a}$ to L-1 based on exposure threshold value Xa as calculated in (2). $\boldsymbol{P_L(k)}$ and $\boldsymbol{P_U(k)}$are corresponding PDF of these sub images as defined in eq. (5-6)

$$P_L(k) = {h_c(k)}/{N_L} \quad for\ 0 \leq k \leq X_a - 1 \quad (5)$$

$$P_U(k) = {h_c(k)}/{N_U} \quad for\ X_a \leq k \leq L - 1 \quad (6)$$

Where $\boldsymbol{N_L}$ and $\boldsymbol{N_U}$ are total number of pixels in sub images *WL* and *WU* respectively. $\boldsymbol{C_L(k)}$ and $\boldsymbol{C_U(k)}$ are corresponding CDF of individual sub images and CDFs can be defined as eq. (7-8)

$$\boldsymbol{C_L(k)} = \sum_{\boldsymbol{k=0}}^{\boldsymbol{X_a - 1}} \boldsymbol{P_L(k)} \quad (7)$$

$$C_U(k) = \sum_{k=X_a}^{L-1} P_U(k) \quad (8)$$

The next step is to equalize all the four sub histograms individually. The transfer functions for Histogram Equalization based on eq. (7-8) can be defined as eq. (9-10)

$$F_L = X_a C_L \quad (9)$$

$$F_U = (X_a + 1) + (L - X_a + 1) C_U \quad (10)$$

$\boldsymbol{F_L}$ and $\boldsymbol{F_U}$ are the transfer functions used for equalizing the sub histograms individually. The final step involves the integration of both sub images into one complete image. The number of iterations is decided based on a threshold £ whose value is normally taken very less (here 0.01).

2.3.2 Algorithm of RESIHE

Step 1: Compute the histogram $\boldsymbol{h(k)}$ *of the image.*

Step 2: Compute the value of exposure and threshold parameter $\boldsymbol{X_a}$.

Step 3: Compute the clipping threshold $\boldsymbol{T_c}$ *and clip the histogram* $\boldsymbol{h_c(k)}$.

Step 4: Divide the clipped histogram into two sub histograms using the threshold parameter $\boldsymbol{X_a}$.

Step 5: Apply the histogram equalization on individual sub histograms.

Step 6: Combine the sub images into one image.

Step 7: Repeat step 1-6 until the exposure difference between successive iterations is less than threshold £.

2.4 Recursively Separated Exposure based sub-image histogram equalization (RS-ESIHE)

Conceptually, RS-ESIHE is a recursive version of ESIHE, which performs recursive decomposition of the histogram. ESIHE decomposes the input histogram only once based on the exposure threshold while RS-ESIHE decomposes it recursively based on exposure thresholds of individual sub histograms up to a recursion level r, generating $\mathbf{2^r}$ sub-histograms. The decomposed sub histograms are then equalized individually. For simplicity

recursion level, r is taken as two. The RS-ESIHE method comprises of Exposure Threshold calculations , Histogram Clipping and Histogram Sub Division and Equalization.

2.4.1 Exposure Threshold Calculations

The Exposure Threshold $\boldsymbol{X_a}$of complete histogram is calculated as per equation (1). Two more exposure thresholds ($\boldsymbol{X_{al}}$ and $\boldsymbol{X_{au}}$) are calculated for two individual sub histogram divided based on $\boldsymbol{X_a}$.

$$X_{al} = L\left[\frac{X_a}{L} - \frac{\sum_0^{Xa-1} h(k)k}{L\sum_0^{Xa-1} h(k)}\right] \quad (11)$$

$$X_{au} = L\left[1 + \frac{X_a}{L} - \frac{\sum_{Xa}^{L-1} h(k)k}{L\sum_{Xa}^{L-1} h(k)}\right] \quad (12)$$

2.4.2 Histogram Sub Division and Equalization

The original histogram is first bisected based on exposure threshold value $X_a$as calculated in (2). These individual sub Histograms are further decomposed into two smaller sub histograms where the individual exposure threshold X_{al} and X_{au} as calculated in (6) and (7) acts as separating point of sub histograms. The Histogram Sub Division process results in four sub imagesW_{Ll}, W_{Lu} , W_{Ul} and W_{Uu} ranging from gray level 0 to $X_{al}-1$, X_{al} to X_a-1, X_a to $X_{au}-1$, X_{au} to L-1. $P_{Ll}(k)$,$P_{Lu}(k)$,$P_{Ul}(k)$ and $P_{Uu}(k)$ are corresponding PDF of these sub images as defined in equations (13-16)

$$P_{Ll}(k) = {h_c(k)}/{N_{Ll}} \; for\; 0 \le k \le X_{al}-1 \quad (13)$$

$$P_{Lu}(k) = {h_c(k)}/{N_{Lu}} \; for\; X_{al} \le k \le X_a-1 \quad (14)$$

$$P_{Ul}(k) = {h_c(k)}/{N_{Ul}} \; for\; X_a \le k \le X_{au}-1 \quad (15)$$

$$P_{Uu}(k) = {h_c(k)}/{N_{Uu}} \; for\; X_{au} \le k \le L-1 \quad (16)$$

$\boldsymbol{N_{Ll}, N_{Lu}, N_{Ul}}$ and $\boldsymbol{N_{Uu}}$ are total number of pixels in sub images $\boldsymbol{W_{Ll}}$, $\boldsymbol{W_{Lu}}$, $\boldsymbol{W_{Ul}}$ and $\boldsymbol{W_{Uu}}$ respectively. $\boldsymbol{C_{Ll}(k)}$,$\boldsymbol{C_{Lu}(k)}$,$\boldsymbol{C_{Ul}(k)}$ and $\boldsymbol{C_{Uu}(k)}$ are corresponding CDF of individual sub images and CDFs can be defined as equations (17-20)

$$C_{Ll} = \sum_{k=0}^{X_{al}-1} P_{Ll}(k) \quad (17)$$

$$C_{Lu} = \sum_{k=X_{al}}^{X_a-1} P_{Lu}(k) \quad (18)$$

$$C_{Ul} = \sum_{k=X_a}^{X_{au}-1} P_{Ul}(k) \quad (19)$$

$$C_{Uu} = \sum_{k=X_{au}}^{L-1} P_{Uu}(k) \quad (20)$$

The next step of RS-ESIHE is to equalize all the four sub histograms individually. The transfer functions for Histogram Equalization based on equations (13-20) can be defined as equations (21-24)

$$F_{Ll} = X_{al} C_{Ll} \quad (21)$$

$$F_{Lu} = (X_{al} + 1) + (X_a - X_{al} + 1) C_{Lu} \quad (22)$$

$$F_{Ul} = (X_a + 1) + (X_{au} - X_a + 1) C_{Ul} \quad (23)$$

$$F_{Uu} = (X_{au} + 1) + (L - X_{au} + 1) C_{Uu} \quad (24)$$

$\boldsymbol{F_{Ll}, F_{Lu}, F_{Ul}}$ and $\boldsymbol{F_{Uu}}$are the transfer functions used for equalizing the sub histograms individually. The RS-ESIHE output image is produced by the combination of all four transfer functions.

2.4.3 Algorithm of RS-ESIHE for Recursion level r=2

Step 1: Compute the histogram $\boldsymbol{h(k)}$ *of the image.*

Step 2: Compute the value of exposure and threshold parameter $\boldsymbol{X_a}$.

Step 3: Compute the clipping threshold $\boldsymbol{T_c}$ *and clip the histogram* $\boldsymbol{h_c(k)}$.

Step 4: Divide the clipped histogram into two sub histograms using the threshold parameter $\boldsymbol{X_a}$

Step 5: Compute exposure thresholds $\boldsymbol{X_{al}}$ *and* $\boldsymbol{X_{au}}$ *for lower and upper sub histograms respectively and divide the sub histograms into further sub histograms using* $\boldsymbol{X_{al}}$ *and* $\boldsymbol{X_{au}}$ *as decomposing threshold, resulting in total four sub histograms.*

Step 6: Apply the histogram equalization on individual sub histograms and combine the sub images into one image for analysis.

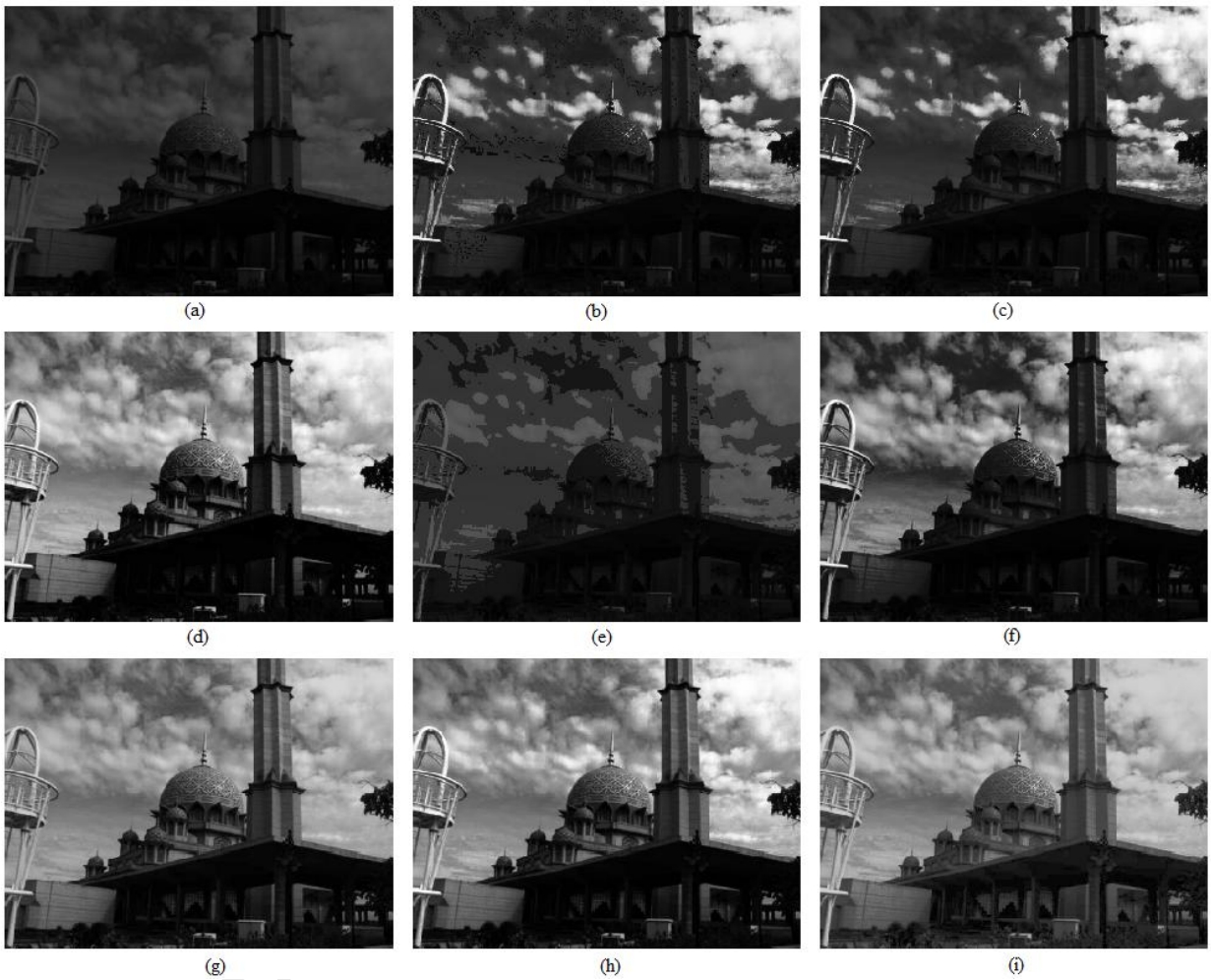

Fig.2. Results of Mosque image (a) Original, (b) RSIHE, (c) RMSHE, (d) QDHE, (e) RSWHE, (f) BHEP-L, (g) ESIHE , (h) RESIHE and (i) RS-ESIHE

3. Experimental Results

In this section, the simulation results of proposed methods are compared with existing histogram equalization based methods i.e. RMSHE, RSIHE, QDHE, RSWHE, BHEPL and ESIHE. In order to analyze and compare the existing methods four low exposure test images:

Fish1, Fish2 Mosque and Couple are taken. Both fish images are underwater sequence while other two images are captured in low light conditions.

Fig.3. Results of Fish2 image (a) Original, (b) RSIHE, (c) RMSHE, (d) QDHE, (e) RSWHE, (f) BHEP-L, (g) ESIHE , (h) RESIHE and (i) RS-ESIHE

3.1 Performance Assessment based on Visual Quality

Images acquired in low light conditions including under water sequences are taken to test the robustness of the proposed method for low exposure imaging.

The analysis of visual results from Figure 2-5 shows the effectiveness of recursive methods especially on low light conditions. The concrete results in terms of contrast enhancement can be clearly observed in Fig. 2 of Mosque image. RSIHE, RMSHE , RSWHE and BHEP-L methods are not able to increase the exposure , however both RESIHE and RS-ESIHE has improved the contrast and the objects are clearly visible. In both the underwater images i.e.

Fish1 and Fish2 in Fig. 3 and Fig. 5 respectively the original images are acquired in very dim light condition and the object is not clearly visible.

Fig.4. Results of *Couple* image (a) Original, (b) RSIHE, (c) RMSHE, (d) QDHE, (e) RSWHE, (f) BHEP-L, (g) ESIHE , (h) RESIHE and (i) RS-ESIHE

The resultant Fish images of proposed methods have the objects clearly distinguishable. The proposed algorithms enhance the overall image quality of couple image in Fig. 4. Low-intensity regions in the background are properly exposed resulting clear vision.

3.2 Performance Assessment based on Average Information Content

To evaluate the performance of the proposed methods , Average information content is being used as an image quality measure [21]. Average information content (entropy) is a measure of richness of the details of the image and usually measured in units as bits. Eq. (25) defines Entropy

$$E(p) = -\sum_{i=0}^{L-1} P(i) log P(i) \qquad (25)$$

Where $P(i)$ is probability density function of a given image at intensity level l and L is total number of gray levels in the image. An image with higher entropy value have richness in details and perceived to have better quality.

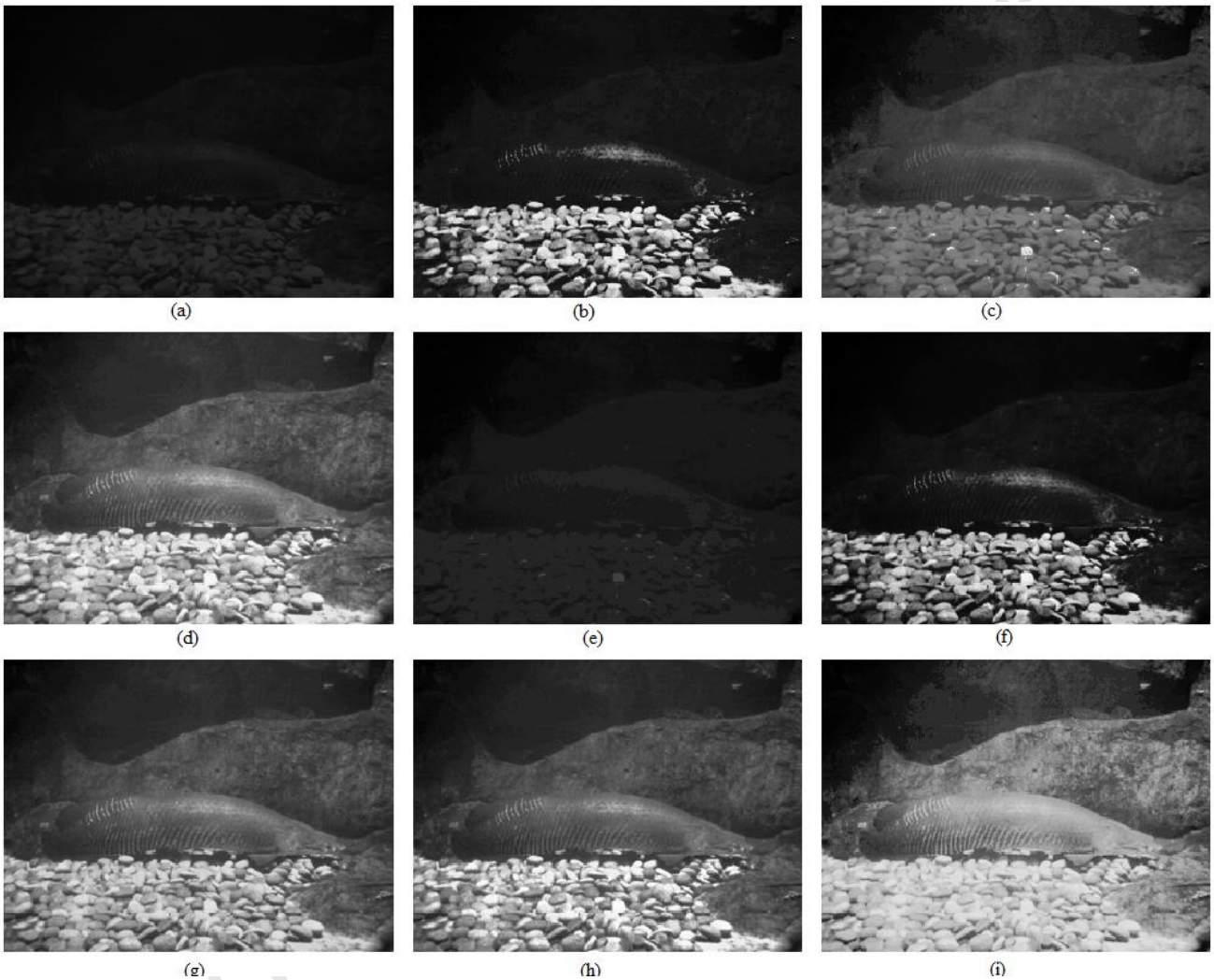

Fig.5. Results of *Fish1* image (a) Original, (b) RSIHE, (c) RMSHE, (d) QDHE, (e) RSWHE, (f) BHEP-L, (g) ESIHE , (h) RESIHE and (i) RS-ESIHE

The entropy results of various methods for all the four images taken for experimentation tabulated in Table 1. For optimum performance the entropy should be as close as possible to the original image. The proposed new methods produces images with entropy very close to the original one thus becomes well suited for bringing out information contents of the image.

Table 1 Average Information Content Results

Images	Original	QDHE	BHEP-L	RSWHE	RESIHE	RS-ESIHE
Fish1	5.050	5.049	5.042	3.323	5.048	5.037
Fish2	4.490	4.487	4.489	3.127	4.487	4.483
Couple	6.398	6.279	6.321	4.559	6.338	6.174
Mosque	6.263	6.101	6.217	4.599	6.259	6.232
Average	5.550	5.479	5.517	3.902	5.533	5.482

4. Conclusion

Effective recursive histogram equalization techniques are proposed here for enhancement of low exposure images. Decomposition of histogram based on exposure based thresholds and individual sub histogram equalization provide very efficient results for low exposure imaging. The methods can be very effective for contrast enhancement of images acquired in dim light conditions i.e. under water or night vision images. Better results in terms of average information contents make these methods more suitable for bringing out information contents of the images. The histogram clipping technique is also combined with histogram equalization to provide control on over enhancement that leads to natural enhancement. The Visual quality of resultant images of recursive methods shows the robustness of the method on low light images.

References

[1] C. H. Lee, L.H. Chen, W. K. Wang , Image contrast enhancement using classified virtual exposure image fusion, IEEE Trans. Consumer Electronics 58(2012),1253-1261.

[2] Y. Wang, S. Zhuo, D. Tao, J. Bu, N. Li , Automatic local exposure correction using bright channel prior for under-exposed images, Signal Processing 93(2013), 3227-3238.

[3] R. C. Gonzalez and R. E. Woods, Digital Image Processing, Prentice Hall, 2002.

[4] Y.T. Kim, Contrast Enhancement Using Brightness Preserving Bi-Histogram Equalization, IEEE Trans. Consumer Electronics 43 (1997) 1-8.

[5] Y. Wan, Q. Chen and B. M. Zhang, Image Enhancement Based on Equal Area Dualistic Sub-Image Histogram Equalization Method, IEEE Trans. Consumer Electronics 45 (1999) 68-75.

[6] S. D. Chen and A. R. Ramli, Contrast Enhancement Using Recursive Mean-Separate Histogram Equalization for Scalable Brightness Preservation, IEEE Trans. Consumer Electronics 49 (2003) 1301-1309.

[7] S. D. Chen and A. R Ramli, Minimum Mean Brightness Error Bi-Histogram Equalization in Contrast Enhancement, IEEE Trans. Consumer Electronics 49 (2003) 1310-1319.

[8] K. S. Sim, C. P. Tso and Y. Y. Tan, Recursive Sub-Image Histogram Equalization Applied to Gray Scale Images, Pattern Recognition Letters 28 (2007) 1209-1221.

[9] M. Kim and M. G. Chung, Recursively Separated and Weighted Histogram Equalization for Brightness Preservation and Contrast Enhancement, IEEE Trans. Consumer Electronics 54 (2008) 1389 - 1397.

[10] Q. Wang, and R. K. Ward, Fast Image/Video Contrast Enhancement Based on Weighted Thresholded Histogram Equalization, IEEE Trans. Consumer Electronics 53 (2007) 757-764.

[11] T. Kim and J. Paik, Adaptive Contrast Enhancement Using Gain-Controllable Clipped Histogram Equalization", IEEE Trans. on Consumer Electronics 54 (2008) 1803-1810.

[12] C.H. Ooi, N.S.P. Kong, H. Ibrahim," Bi-histogram with a plateau limit for digital image enhancement", IEEE Trans. Consumer Electronics 55 (2009) 2072–2080.

[13] M. Abdullah-Al-Wadud, et al, A Dynamic Histogram Equalization for Image Contrast Enhancement, IEEE Trans., Consumer Electronics 53 (2007) 593–600.

[14] H. Ibrahim, and N. S. P. Kong, "Brightness Preserving Dynamic Histogram Equalization for Image Contrast Enhancement", IEEE Trans., Consumer Electronics 53 (2007) 1752–1758.

[15] D. Sheet , H. Garud , A. Suveer , M. Mahadevappa , and J. Chatterjee, Brightness Preserving Dynamic Fuzzy Histogram Equalization, IEEE Trans. Consumer Electronics, 56 (2010) 2475 - 2480.

[16] C.H. Ooi and N. A. M. Isa, Quadrants Dynamic Histogram Equalization for Contrast Enhancement, IEEE Trans. Consumer Electronics 56 (2010) 2552 - 2559.

[17] C.H. Ooi and N. A. M. Isa, Adaptive Contrast Enhancement Methods with Brightness Preserving, IEEE Trans. on Consumer Electronics 56 (2010) 2543 - 2551.

[18] Y. C. Chang and C. M. Chang, A Simple Histogram Modification Scheme for Contrast Enhancement, IEEE Trans. Consumer Electronics 56 (2010) 737 - 742.

[19] T. L. Tan, K.S. Sim and C.P. Tso, Image enhancement using background brightness preserving histogram equalization, Electronic Letters 48 (2012) 155 - 157.

[20] K. Singh, R. Kapoor, Image enhancement using Exposure based Sub Image Histogram Equalization, Pattern Recognition Letters 36 (2014) 10 – 14

[21] S. D. Chen, A New Image Quality Measure for Assessment of Histogram Equalization-Based Contrast Enhancement, Digital Signal Processing 22 (2012) 640–647.

Available online at www.sciencedirect.com

ScienceDirect

Electronic Notes in DISCRETE MATHEMATICS

Electronic Notes in Discrete Mathematics 48 (2015) 255–258 www.elsevier.com/locate/endm

Finite Abelian Group Labeling

Pranjali* [1]

Department of Mathematics,
University of Delhi,
Chhatra Marg, Delhi-110007, India.

Mukti Acharya [2]

Department of Applied Mathematics,
Delhi Technological University,
Delhi - 110042, India.

Purnima Gupta [3]

Department of Mathematics,
Sri Venkateswara College,
University of Delhi-110021, India.

(Dedicated to the memories of Dr. B.D. Acharya)

Abstract

In this paper, we introduce an abelian group labeling (shortly, AGL) over finite abelian groups. We have shown that every finite graph admits an abelian group labeling. In the course of investigation, we found that representation labeling can be obtained from *abelian group* labeling for certain graphs. Several new directions for further research are also indicated through problems.

Keywords: Abelian group labeling, abelian group labeling index.

http://dx.doi.org/10.1016/j.endm.2015.05.038

Let $G = (V, E)$ be a graph and let Γ be a finite abelian group on integers with binary operation $*$. An injective function $f : V(G) \to \Gamma$ is called a *finite abelian group labeling* of G by Γ or abelian group labeling of G by Γ if $\gcd(f(u) * f(v), |\Gamma|) = 1$ for every edge $(u, v) \in E(G)$. A graph which admits such a labeling is called an abelian group labeled graph. For all terminology and notation in graph theory and abstract algebra, we refer to the text-books by Harary [5] and Gallian [4] respectively.

All the existing vertex labelings in the literature fix the set of labels as well as the operation between vertex labels. In this paper, we have introduced a different kind of labeling called abelian group labeling, for which there is no restriction. In the finite abelian group labeling, operation on vertex labels vary according to nature of the group. Motivation to initiate the study on abelian group labeling mainly stems from representation labeling [2]. Another motivation to introduce the new notion is to label the vertices of graph, from the group $\mathbb{Z}_n$, which are not unitary addition Cayley graphs. Viewed in this way, the standard unitary addition Cayley graph turns out to be maximal with respect to abelian group labeling. For more study on unitary addition Cayley graph we refer to [6].

Now we study an abelian group labeling (in short, AGL) for an arbitrary graph with respect to the abelian groups, $\mathbb{Z}_n$ (the group of integers modulo n) and $U(n)$ (the group of units of $\mathbb{Z}_n$ under multiplication modulo n). In the course of investigation, we found that every finite graph admits an abelian group labeling. Moreover, we also found that representation labeling can be obtained from *abelian group labeling* for certain graphs. For literature in graph labeling the reader is referred to [1,3].

We also initiate a study of *'optimal'* index for abelian group labeling as follows: Let G be a finite graph of order n, the *abelian group labeling index* (*AGL-index*) of G with respect to group $\mathbb{Z}_r$ denoted as $\Upsilon_Z =: \Upsilon_{\mathbb{Z}_r}(G)$, is the least positive integer r such that G admits an abelian group labeling by $\mathbb{Z}_r$.

The *AGL-index* of G with respect to the group $U(m)$, denoted as $\Upsilon_U =: \Upsilon_{U(m)}(G)$, is the least positive integer s such that there exists a group of units $U(m)$ under multiplication modulo m of order s with respect to which G admits an abelian group labeling by $U(m)$.

The optimal *AGL-index* of G, denoted by $\Upsilon(G)$, is defined as

$$\Upsilon(G) =: \min\{\Upsilon_Z, \Upsilon_U\}.$$

[1] Email: pranjali48@gmail.com (*Corresponding author)
[2] Email: mukti1948@gmail.com
[3] Email: purnimachandni@rediffmail.com

In general the above definition can be written as:

Let G be an arbitrary graph of order n and $\Gamma_1, \Gamma_2, \Gamma_3, \cdots \Gamma_m$ be finite abelian groups on integers with binary operations $*_1, *_2, *_3, \cdots, *_m$ respectively. If $\Upsilon_{\Gamma_1}, \Upsilon_{\Gamma_2}, \Upsilon_{\Gamma_3}, \cdots, \Upsilon_{\Gamma_m}$ are *abelian group labeling index* (*AGL-index*) of G with respect to Γ_i, $1 \leq i \leq m$, then the optimal AGL-index is denoted by $\Upsilon(G)$ and defined as $\Upsilon(G) = \min\{\Upsilon_{\Gamma_1}, \Upsilon_{\Gamma_2}, \Upsilon_{\Gamma_3}, \cdots, \Upsilon_{\Gamma_m}\}$.

Due to the result that every finite graph admits an abelian group labeling, we have the following inequalities,

$$n \leq \Upsilon_Z(G) \leq p, \tag{1}$$

where p is the least prime not less than $2n + 1$, and

$$n \leq \Upsilon_U(G) \leq 2^k, \tag{2}$$

where n is the order of graph G and k is the ceiling of $\log_2 n$.

The bounds in (1) and (2) indicate the following problem of fundamental importance. *Characterize graphs for which the bounds in (1) as well as in (2) are attained. Also, determine all the abelian groups which provide an optimal abelian group labeling for these graphs.*

In this paper, we solve above problem partially for C_n (cycle of length n) and Q_n (n-dimensional hypercube) and establish a sufficient condition for optimal AGL-index $\Upsilon(G)$. Some of the results reported in the paper are as follows:

Let G be a graph of order 2^k, where $k > 1$. Then G admits an abelian group labeling with $\Upsilon(G) = 2^k$.

For a cycle C_n, abelian group labeling with respect to group $\mathbb{Z}_n$ is same as representation labeling where $n = 2^k$ or an odd prime.

For every hypercube Q_m abelian group labeling with respect to group $\mathbb{Z}_{2^m}$ is same as representation labeling

Acknowledgement

The first author is thankful to Department of Atomic Energy (DAE) for providing the research grant vide sanctioned letter number: **2/39**(26)/2012 - R&D-II/4114.

References

[1] M. Acharya, Pranjali and P. Gupta, Zero-Divisor Labeling of Hypercubes, *Nat. Acad. Sci. Lett.*, **37**(5) (2014), 467–471.

[2] Evans, B. Anthony, Fricke H. Gerd, Maneri C. Carl, Mckee A. Terry and M. Perkel, Representations of Graphs Modulo n, *J. Graph Theory*, **18**(8) (1994), 801–815.

[3] J.A. Gallian, A Dynamic Survey of Graph Labeling, *Electron. J. Combin.*, **17** (2014), #DS6.

[4] J.A. Gallian, *Contemporary Abstract Algebra*, Richard Stratton publisher, 7th ed. Brooks/Cole, Belmont, CA, USA (2009).

[5] F. Harary, *Graph Theory*, Addison-Wesley Publ. Comp., Reading, MA. (1969).

[6] D. Sinha, P. Garg and A. Singh, Some properties of unitary addition Cayley graphs, *NNTDM.*, **17**(3) (2011), 49–59.

Implementation of Electromagnetic & RFID Technology In Ambedkar Institute of Technology, Delhi : A Study

CONFERENCE PAPER · NOVEMBER 2011

1 AUTHOR:

Rama kant Shukla
Delhi Technological University
9 PUBLICATIONS **0** CITATIONS

SEE PROFILE

Implementation of Electromagnetic & RFID Technology In Ambedkar Institute of Technology, Delhi : A Study

R.K. Shukla[1] , P.P.S.Sengar[2] & S. A. Raza Naqvi [3]

Librarian, Delhi Technological University, Delhi
Assistant Librarian: Inmantec Institutions, Ghaziabad
Assistant Librarian: Inmantec Institutions, Ghaziabad

Abstract:

The paper describes application of Electromagnetic & RFID Technology in the Library. The paper also highlights different components of EM and RFID Technology like RFID tags, Antenna, Coupler or reader etc. This paper discusses the need for book checking and managing of library through Electromagnetic & RFID library management system (Hybrid System) in Ambedkar Institute of Technology (AIT), Library Delhi. How can be activated by using a new technology i.e. EM & RFID.

Keywords: AIT, RFID, EM, Security System, LMS.

---

1. Preamble

Radio Frequency Identifications (RFID) is an emerging technology and one of the most rapidly growing segments of today's automatic identification data collection (AIDC) industry. However, this emerging technology is not new, in fact, it is currently being used in numerous applications throughout the world. It was originally implemented during World War II to identity and authenticate allied planes, in an identification system known as Identification, Friend or Foe, and is still being used today for the same purposes. Main objectives of EM and RFID technology is to reduced the theft of books and any type of document in library and reduced the manpower and self check-out and check-in facility.

2. AIT and Its Library

Ambedkar Institute of Technology (AIT) was established in 2001 by the government of NCT of Delhi. It is developing as a centre of excellence imparting technical education and generating competent professionals with a high degree of credibility, integrity and ethical standards. It is the one of the leading engineering college under the umbrella of Guru Gobind Singh Indraprashtha University, Delhi.

The mission of the AIT is to contribute significantly in teaching and research for the

focused application of computers and electronics in an integrated manner. Conducive to the human well being and national welfare evolving new ideas to enable students to learn new technologies, acquire appropriate skills and deliver meaningful services to society by inculcating them with strength of character, self-leadership & self-attainment.

About AIT Library

AIT Library was established in 2001, almost simultaneously with the institute with the mission to serve the education and information needs to its faculty members, students, staffs and to provide quality of services, focusing on student success, teaching and learning excellence. The library is well equipped with modern facilities and resources in the form of books, printed journals, e-journals, project reports, online databases, l magazines, audi-visual materials etc. AIT Library has a collection of approximate 22000 volumes including books and other reading materials . Library has subscribe to national and international full text e- journals of various international publishers like Science Direct, Springer Science, John Wiley, IEEE, ACM Digital Library etc. AIT library is a member of INDEST-AICTE Consortium. AIT library is automated with the help of Libsys software and using EM and RFID technology for fast circulation of library materials.

3. EM & RFID and Its Components

Electromagnetic and Radio Frequency Identification is the latest technology used in library theft detection systems. Unlike EM (Electro-Mechanical) and RF (Radio Frequency) systems, which have been used in libraries for decades, RFID-based systems move beyond security to become tracking systems that combine security with more efficient tracking of materials through out the library, including easier and faster charge and discharge, inventorying, and materials handling.The application of this technology not only able to reduced the theft of books but also reduce the manpower due to its self-check out and check-in facility (Ghosh,2009)

RFID is a combination of radio -frequency-based technology and microchip technology. The information contained on microchips in the tags affixed to library materials is read using radio frequency technology regardless of item orientation or alignment (i.e., the technology does not require line-of-sight or a fixed plane to read tags as do traditional theft detection systems) and distance from the item is not a critical factor except in the case of extra-wide exit gates. The corridors at the building exit(s) can be as wide as four feet because the tags can be read at a distance of up to two feet by each of two parallel exit sensors. [The devices used for circulation and inventorying are usually called "readers" while the ones used at building exits are usually called "sensors."]

EM & RFID based Library Management System is the modern technology used in library theft detection systems . This is a Hybrid Solutions. EM is an additional security layer on the periphery of EM & RFID based Security. RFID allows items to be

tracked and communicated with by Radio waves. RFID is a broad term for technologies that use radio waves to automatically identify people or objects. There are several methods of identification, but the most common is to store a serial number that identify a person or objects and perhaps other information , on a microchip that is attached to an antenna (the chip and the antenna together are called an RFID transponder or an RFID Tag) . The enables the chip to transmit the identification information to a reader. EM and RFID based system beyond security to become tracking systems that combine security, easier and faster charge and discharge, inventory and material handling.

3.1 Main Components of EM & RFID Technology

3.1.1 EM Security Strips

This security strip is a one-piece, flexible, thin, non rusting metallic alloy coated with an adhesive film. The size of the security strips is a 160mm X 3mm (Approximate size). An EM Security Strip is a magnetic, iron-containing strips with an adhesive layer which is attached to the library materials like Books, Journals, CDs, DVDs, Video Cassettes etc, . On check-out, it is desensitized by a desensitizer unit that uses a specific highly intense magnetic field. When a sensitized item is taken across the EAS gates of the library, the magnetic field of the strip within the item interacts with the magnetic field of EAS system and raises a theft alarm. Thereby, ensuring that only desensitized (check-out) item is carried out of the library.

The EM Security Strips are manufactured in two format- permanent (always active) and deactivatable. Deactivatable tags can be deactivated an untimed number of times.

Electromagnetic Security strips

3.2.2 RFID Tags

The RFID tags Flexible, paper thin smart labels that are applied directly to library items (i.e.; Books, Journals, CDs, DVDs, Video Cassettes). It can be fixed inside books, cover or directly on to CD's and video's) . RFID tag (or transponder), made of an IC chip attached to a tiny radio antenna, contains information (serial number and other

data) related to the item it is affixed to or embedded into. In proximity to an RFID-enabled scanner (or reader), the tag information is read automatically and managed into a user database. The chip is both readable and writable and a store information to identify items in the library collections.

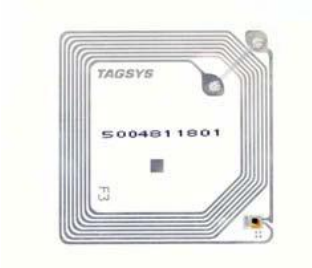

Tags for Books

Tags for CD

Sensitizer /Desensitizer Unit

3.1.3 Sensitizer /Desensitizer Unit

A Sensitizer /Desensitizer Unit is meant for desensitizing and sensitizing the EM tag at the time of check-out/check-in in library. Controlled by the library management software, it detects tag status, performs easy lending & return and simultaneously changes the magnetic status of the tag to sensitized (activated) or desensitized (deactivated). The sensitizer/desensitizer unit is prepared for and upgradeable to RFID based identification.

3.1.4 Antenna

An antenna is a medium between RFID tags and the coupler/reader. The antenna produces Radio Signals to active the tag and read and write data to it. Antennas are the channels between the tag and the reader. Which controls are system's data acquisitions and communications.

3.1.5 Coupler or Reader

The link between EM strips, RFID Tags and PC. First the coupler can send information in two directions. It can read information From a tag and send it to the PC (read modes)or it can read information From the PC and send it to an RFID tag (write mode). Second the reader has been desensitize and resensitize EM strip and audible/visible signal to contain item was processed successfully.

3.1.6 PC/Server

The link between the coupler/ Reader and library automation system, In other words, it is the communication gateway among the various component (Boss 2004). It

receives the information From one or more of the readers and exchange information with the circulation database.

4. Implementation of EM & RFID Technology in AIT Library

In 2010, Ambedkar Institute of Technology (AIT) has adopted EM & RFID based library management system for their library. The quotations were received from various vendors/firms for implementation of RFID in AIT library. Then, sample RFID tags & Electro-magnetic strips were received from the firms/vendors. After the finalizing the firm, the following units have been installed in the library.

4.1 Tagging & Programming Stations (Staff Pad Workstation):

The EM & RFID workstation pad is used to programming of EM strips & RFID tags. Affixed to library materials (eg. Books, CDs, Videos, Project Reports etc.) Firstly, after the accessioning the Books the self adhesive EM security strips is pasted on the book and EM security strip activate security bit for the theft detection system. There is a read / write reader at this location. Secondly, After the pasting of EM strips, the RFID tags are pasted on the books and books ready to the programming of RFID tag. Programming Station attach to the Server and accession Number/ Location is entered through keyboard and the book data is programmed in the tag.

4.2 EM & RFID Circulation Stations (Hybrid System):

The library circulation counter consists of a EM&RFID Reader (LCS Pro) is a attached to the PC and printer (thermal printer). It can identify 4 to 6 books within a second, and the system used anti-collision algorithm that does not limit the number of tags which can be simultaneously identified and read up to3-5 inches high with a book tag.. Each item must be equipped with an EM security Strips and RFID tags.

The LCS Pro hybrid is designed for EM security (reactivating and deactivating EM strips), RFID security (EAS-bit, setting and resetting) and item-ID identification

The photograph is as it is in the AIT library

(LCS-Pro (EM&RFID) **Circulation Station)**

4.3. Self Service Units: These units are operated by patron themselves without the intervention of any library staff-

4.3.1 Self Check –Out Unit (In Kiosk):

This is a self-service station where the books are checked out of the library independently by the borrower without any intervention of library staff, Complete with touch screen monitor and a thermal receipt printer, the patron Self- checkout station helps reduce staff workload and improve user service. The book(s) are placed on EM & RFID Reader (LCS Pro) and Smart card, Patron simply follow the prompts on the screen and make appropriate response s using the touch screen . If the transaction is approved, the Electromegnetic Strips is deactivated. A receipt is printed using the Thermal printer and issued to the patron confirming the borrowing transction details. It consists of one EM & RFID Reader (LCS Pro), one Antenna with multiple Read/Write facility ISO compliant. LCD 15" touch screen monitor with P4 CPU (256 MB RAM, HDD and WinXP operating system), Epson auto cutter thermal printer. The AIT Library is presently using alternate borrowers ID No. through keyboard. In second phase, there is a provision for Smart Card (to be implemented very soon).

. The photograph is as it is in the AIT library

4.3.2 Self Return Book Drop Unit:

These are the units where returned books are placed through suitable slits by patron themselves. As books are returned through Book Drop facility located suitably in library the RFID tags are automatically read and LSmart software will immediately update both patron record and LSEase (Libsys) database. The Book Drop allow patrons to return 24 hours a day.

The photograph is as it is in the AIT library

(RFID Reader/Antenna For Book Drop Unit)

4.3.4 EM Security Gates (Antitheft Detection):

The security gates are two or more Theft Detection Pedestals. EM Security Gates positioned at AIT library exits, they read the security setting that is stored in EM Security Strips and determine whether or not items should be permitted to leave the

library. If items have not been properly checked out, an alarm sounds with red light to alert library staff. The Theft Detection Pedestals will works even when LSmart is down as a single technology is used for item management and theft prevention. At the time a book is checked out through either regular circulation methods or through Self Check –Out Unit (In Kiosk), the EM security strip's theft system is deactivated.

The photograph is as it is in the AIT library

(EM Detection Systems)

4.3.5 Inventory Control System:

This is a shelf management system, normally shelf management and stock checking is a time consuming process but using the inventory control system is made easy and quick. Inventory control on shelves can be performed rapidly and accurately using handheld terminal. Smart Labels secured in books can be read in seconds . Million No. of Books ID numbers can be stored in the system, which is then downloaded to central database through LSmart interface for stock verification. It has an audible signal to indicate successful item identification. The Reader indetify books/items not placed in proper order of class number on the shelves. It is using Handheld WiFi RFID Inventory Reader with mini laptop for stored the inventory report. The RFID Inventory Control System consists of two parts:

- A handheld RFID Reader (Handheld WiFi RFID Inventory Reader) that is used to scan items on shelves .
- System to generate inventory reports about the collected data.

The shelf management system consists of the following components viz. RFID Reader(Handheld WiFi RFID Inventory Reader), Portable battery, Wand Antenna connected to RFID Reader, Mini Laptop (Pocket PC),

(Handheld WiFi RFID Inventory Reader)

5. Advantages due to implementation of EM & RFID Technology in AIT Library:

- It is faster and highly reliable system.
- It is easier and user friendly.
- Self Check-in and Check-out Facilities.
- Book Drop Units for book return.
- Save the time of user and library staff.
- Easy to Stack Checking.
- Easy search fir misshelved books.
- It is highly Security Systems.

6. Conclusion:

EM & RFID Technology is a most accurate but expensive way to identify items/documents and get data into the computer. Its application increase productivity, and eliminates human error, improve speed of operation and services. Its application is also step forward towards to satisfy the Fourth law of Library science (save the time of users). AIT library has implemented EM & RFID technology for managing library operations.

Reference :

Ghosh, T.B. (2009), “Emerging Trends and Technologies in Libraries and information Services” ,KBD Publications, New Delhi.

http://eprints.rclis.org/bitstream/10760/11357/1/RFID_paper_Alahabad%5B1%5D.pdf

Singh, Vevek and Singh, Manisha (2009), "Emerging Trends and Technologies in Libraries and information Services" ,KBD Publications, New Delhi.

Boss, Richard (2004), "RFID Technology in Libraries", ALA Technical Notes prepared on 14 May, 2004 located at
http://www.ala.org/ala/mgrps/divs/pla/plapublications/platechnotes/rfid2009.pdf (access date 08/06/2011)

http://www.dialocid.nl/

R.S.Enterpricses (A unit of RS Barcoders Pvt. Ltd.), New Delhi

http://www.orizin.net/

www.delhi.gov.in/wps/wcm/connect/doit_ait/AIT/Home/About (access date -08/06/2011)

Analog Integr Circ Sig Process (2015) 84:333–340
DOI 10.1007/s10470-015-0587-y

MIXED SIGNAL LETTER

Improved tri-state buffer in MOS current mode logic and its application

Neeta Pandey[1] · **Bharat Choudhary**[1]

Received: 28 May 2015 / Accepted: 15 June 2015 / Published online: 29 June 2015

Abstract This paper presents a new topology to implement MOS current mode logic (MCML) tri-state buffer. The current source section of the available MCML tri-state buffer is modified in the proposed topology which improves output enable time and maintains the low power feature. The functionality of the proposed topology is verified through SPICE simulations by using 0.18 µm TSMC CMOS technology parameters. Its performance is compared with the available one for different values of bias current ranging from 50 to 200 µA. The delay decreases with increase in current and improvement in output enable time is visible throughout the current range. The impact of parameter variations at different design corners and width mismatch on the performance of both the proposed and the available tri-state buffers is also studied and similar variations are found. The significance of the improvement is demonstrated through the implementation of a tri-state buffer based edge triggered register, a key element in digital systems design.

Keywords MOS current mode logic · Tri-state buffer · Low power

✉ Neeta Pandey
n66pandey@rediffmail.com; neetapandey06@gmail.com

Bharat Choudhary
bharatruhela@gmail.com

[1] Department of Electronics and Communication Engineering, Delhi Technological University, Bawana Road, Delhi 110042, India

1 Introduction

Tri-state circuits are preferred in digital systems for their ability to allow connection of multiple devices on a single/same bus or shared bundle of wires without the loss of data. High performance processors, clock/data recovery systems, asynchronous transfer mode (ATM) crossbar switches, and programmable logic devices [1–5] are some examples of the system employing them. In mixed-signal systems, the implementation of the tri-state circuits using MOS current mode logic (MCML) is often employed for its favorable features such as low noise, high speed and frequency independent power consumption. A literature survey reveals that three circuit implementations for MCML tri-state buffer are available [6, 7]. The first circuit place switches at the output of a conventional MCML buffer while a cascade of a source follower and a flipped voltage follower is used in the second one to attain the high impedance state. Both the buffers consume power in the high-impedance state as their current sources are never turned OFF. Further, the third tri-state buffer topology [7] offers power saving by turning OFF some of the current sources in the high impedance state. However, it is observed that this topology has increased output enable time due to the circuitry involved for enabling the current source.

In this paper, an improved low power MCML tri-state buffer is presented to address this issue. The paper briefly discusses the operation of the available low power tri-state buffer [7] in Sect. 2. Thereafter, the structure and the operation of the new topology are presented in Sect. 3. The simulation Sect. 4 verifies the functionality of the proposed tri-state buffer topology, compares its performance with the available low power topology and illustrates the application wherein the use of the proposed topology can be advantageous. Conclusions are drawn in Sect. 5.

2 Available low power MCML tri-state buffer

The available low power MCML tri-state buffer [7] with the differential inputs A and Enable is shown in Fig. 1(a). It consists of a differential to single-ended converter (M8–M12) and a modified MCML buffer (M1–M7). The differential Enable signal is converted to a full swing signal (V_E) through the converter which drives the load and the current source sections of the modified MCML buffer. Depending on the value of the V_E signal, the buffer works as a regular gate or attains a high impedance state. The operation of the buffer for high and low Enable signal is illustrated in Fig. 1(b, c) respectively. The transistors connected to V_E signal are marked with dotted and bold lines respectively to indicate the state of the transistor as OFF and ON. For a low value of V_E signal the transistors M4 and M5 are turned ON and act as loads of a MCML buffer. At the same time, the transistor M6 is ON, and charges node X to V_{BIAS1} as the transistor M7 is OFF. Thus, the transistor M1 operates as current source and provides the required bias current I_{SS1} to the MCML buffer. Therefore in this condition it behaves as a regular buffer. Conversely, for high value of the V_E signal, the transistors M4, M5 and M6 are turned OFF and the transistor M7 is ON which pulls down the potential at node X to the ground potential. Thus, the output node is disconnected from the power supply V_{DD} as well as ground and a high-impedance state is achieved.

On closer examination of the circuit, it may be noted that the time required by the circuit to move from the high impedance state to the enabled state i.e. the output enable time is essentially the sum of the time taken by the transistor M6 to charge node X to the bias potential V_{BIAS1} and the time required to maintain a constant current through the current source (transistor M1). In this paper, an alternate circuit that reduces the output enable time (T_{OET}) by maintaining the low power feature of the available topology is proposed.

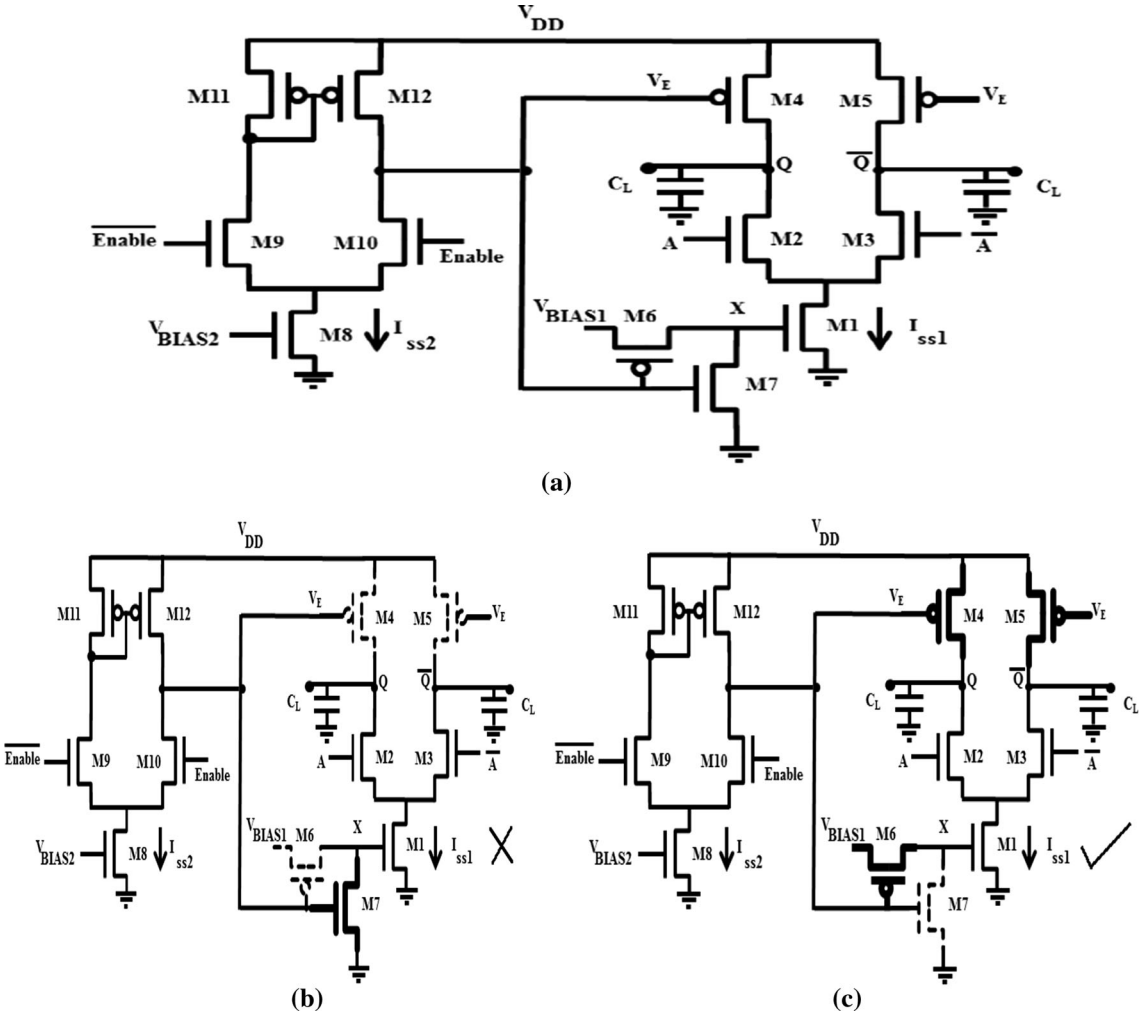

Fig. 1 **a** Available low power MCML tri-state buffer, **b** for high value of V_E, **c** for low value of V_E

3 Proposed MCML tri-state buffer

The schematic of the proposed MCML tri-state buffer is depicted in Fig. 2. It comprises of a differential to single ended converter (M8–M12) and a modified MCML buffer (M1–M6). The circuit and the function of the differential to single ended converter are same as in the available topology. The basic structure of the proposed topology is similar to the available low power tri-state buffer except for the current source section. A PMOS transistor M6 is added between the common source terminal of the transistor pair (M2–M3) and the current source M1 that provides the desired bias current (I_{SS1}). The operation of the tri-state buffer for high and low value of V_E signal value is illustrated in Fig. 2(b, c) respectively. The transistors connected to V_E signal are marked with dotted and bold lines respectively to indicate the state of the transistor as OFF and ON. For high value of the V_E signal, the transistors M4, M5 and M6 are OFF such that the output node is disconnected from the power supply V_{DD} and ground and the high impedance state is attained. Conversely, the transistors M4, M5 and M6 are ON for low value of the V_E signal and the circuit behaves as a regular buffer.

It can be observed that the proposed MCML tri-state buffer topology ensures low power feature by turning OFF the current source M1 as in available low power tri-state buffer. Also, it has reduced output enable time due to the fact that the current source is driven directly by a constant voltage source V_{BIAS1} and avoids the charging mechanism as exhibited in the available low power one.

4 Simulation results

This section first verifies the functionality of the proposed MCML tri-state buffer and then compares the performance with the available one for different values of the bias current. The impact of parameter variations is also studied

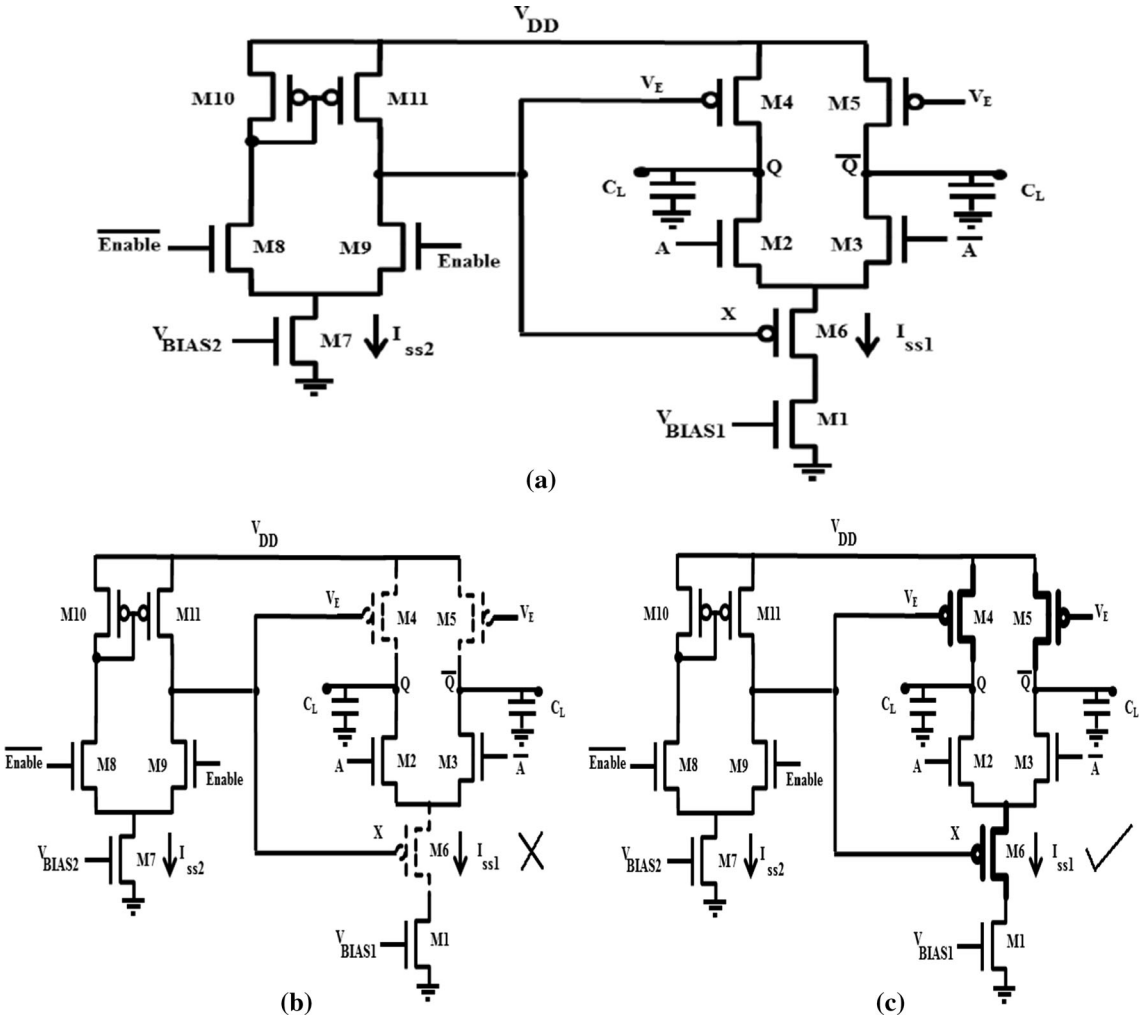

Fig. 2 **a** Proposed low power MCML tri-state buffer, **b** for high value of V_E, **c** for low value of V_E

in the proposed topology. Thereafter, its benefit in the practical situations is illustrated through the implementation of an edge triggered register, an essential element in digital system design. The operating conditions in all the simulations runs use 0.18 μm TSMC CMOS technology parameters, power supply and voltage swing of 1.8 V and 400 mV respectively.

5 Functional verification

The functionality of the proposed MCML tri-state buffer is verified by implementing a bus wherein two tri-state buffers are connected to a node such that at a given instant of time only one gate is able to transfer the data while the other remain in the high impedance state. The complete test bench is shown in Fig. 3. The available and the proposed tri-state buffers are considered and the simulation waveforms at the input nodes and the output node are shown in Fig. 4. It is found that the proposed buffer conforms to the functionality.

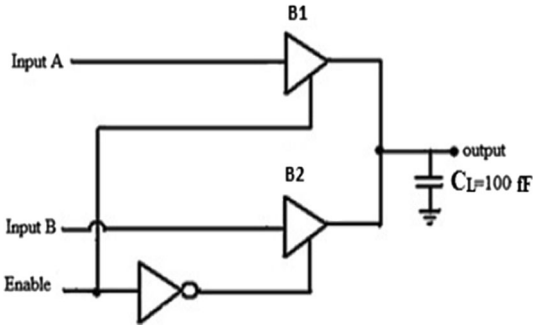

Fig. 3 Two tri-state buffers driving a common node

6 Performance comparison

The proposed and the available tri-state buffers are simulated with load capacitance and bias current (I_{SS1}) of 50, 100, 150, and 200 μA. The performance parameters such as the power consumption, the propagation delay, the power delay product and the output enable time for a bias current of 100 μA are summarized in Table 1. It is found that the proposed tri-state buffer consumes the same power as the available one since there is a mechanism to turn OFF the current sources in the high impedance state. Also, both the tri-state buffers show equal propagation delay due to the fact that they posses similar loads and maintains the same bias current in the enabled state. Hence both the topology has equal power delay product value. However, a remarkable improvement is observed in the output enable time of the proposed tri-state buffer. This can be explained by plotting the waveforms at different nodes in the two buffers in Fig. 5. As both the tri-state buffers use converter therefore, the time required to convert the differential

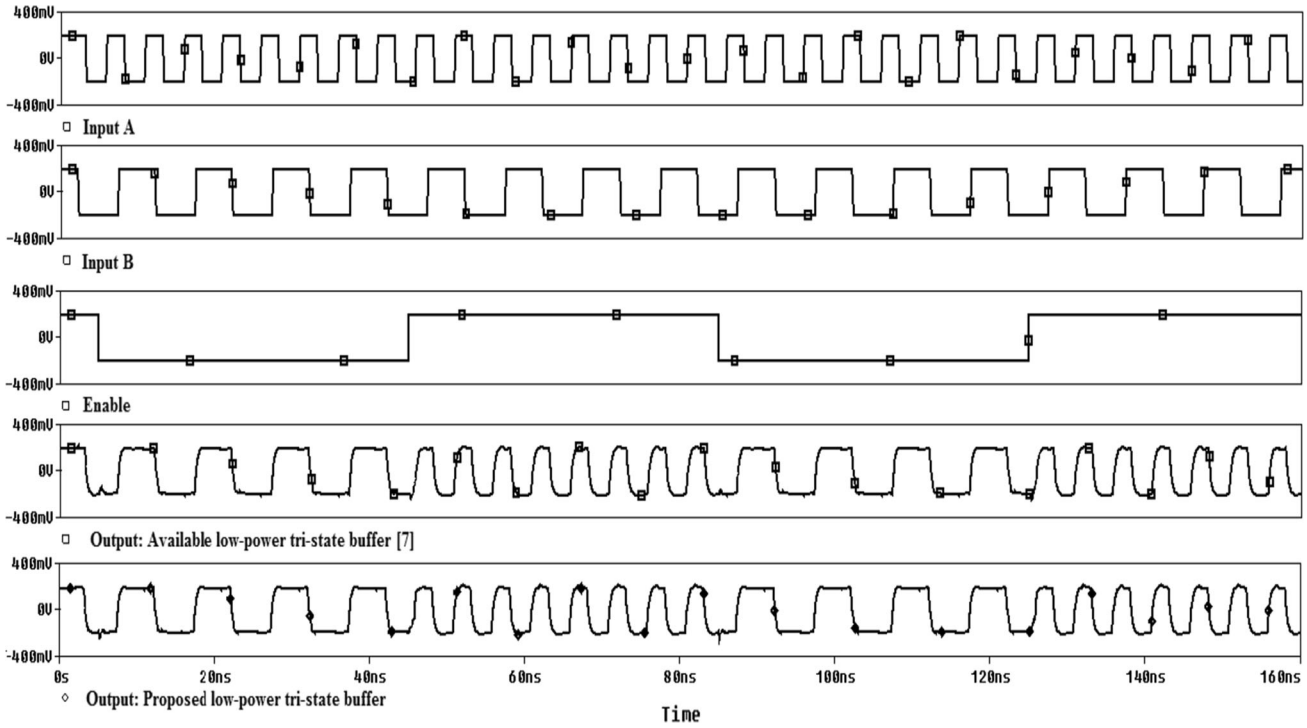

Fig. 4 Simulation waveform of the available and proposed tri-state buffer

Enable signal to single-ended V_E signal (marked as T_{DE} to T_{SE}) is common. In the available tri-state buffer, the low value of the V_E signal, causes the charging of node X after which the bias current is established through the current source transistor M1 and the buffer responds to the input. Therefore, the output enable time for the available tri-state buffer (T_{OET_A}) is defined as the sum of the time required by converter ($T_{SE} - T_{DE}$), the node X to attain desired bias voltage V_{BIAS1} ($T_{AX} - T_{SE}$) and the time taken by the tri-state buffer to maintain a constant bias current in the circuit ($T_A - T_{AX}$) i.e. ($T_{OET\_A} = (T_A - T_{AX}) + (T_{AX} - T_{SE}) + (T_{SE} - T_{DE})$). In contrast to this, a constant voltage source is connected to node X in the proposed tri-state buffer such that there is no requirement to charge node X. Thus the output enable time (T_{OET_P}) is defined as the time it takes to establish a constant current in the circuit for low value of the V_E signal ($T_{OET\_P} = (T_P - T_{SE}) + (T_{SE} - T_{DE})$). Similar results are obtained for other bias current

Table 1 Summary of simulation results of the MCML tri-state buffers

Performance parameters	Available [7]	Proposed
Power (μW)	306	304
Propagation delay (ps)	189	186
Power delay product (fJ)	57.834	56.544
Output enable time (ps)	1047	600

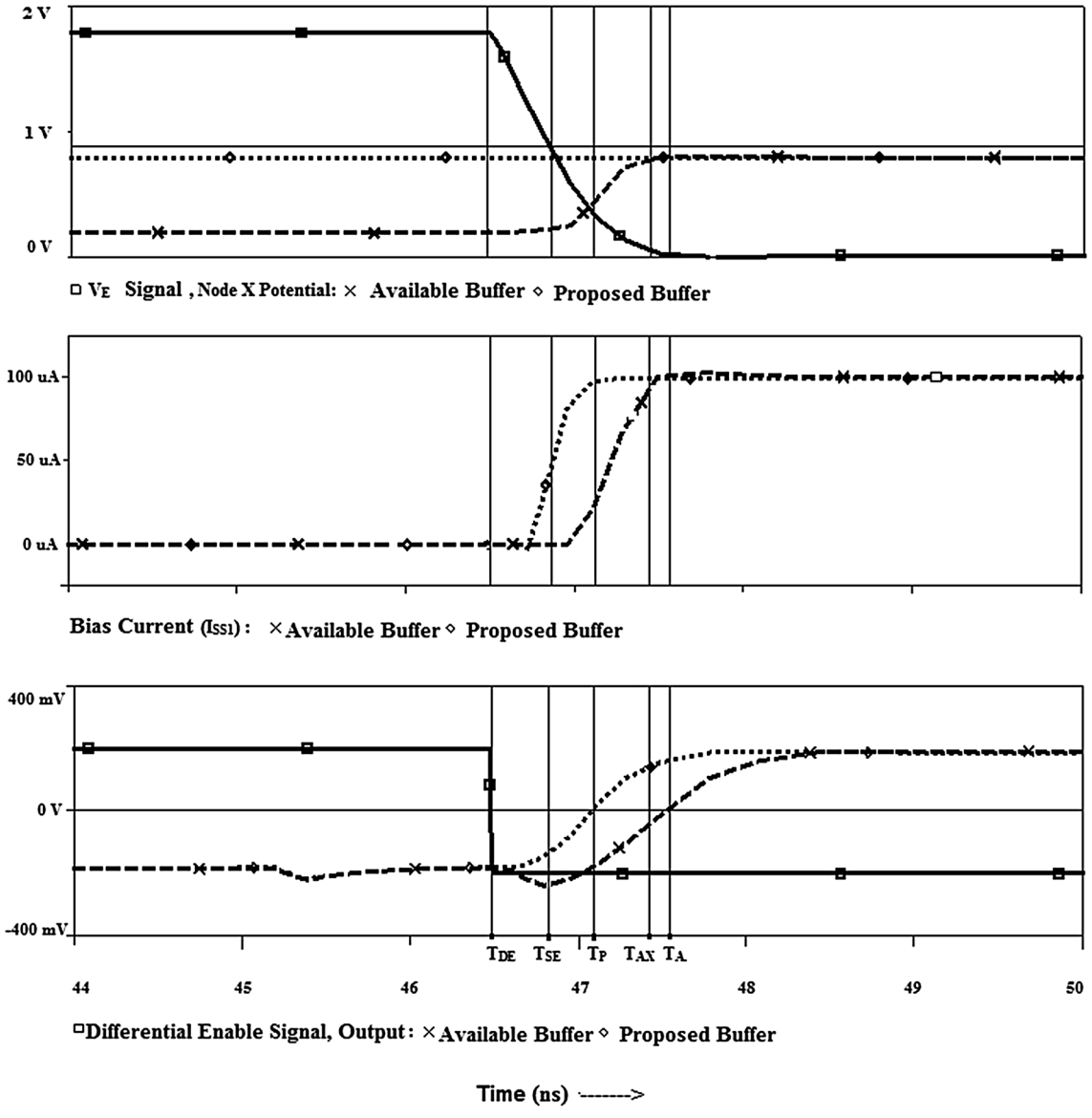

Fig. 5 Simulation waveform of the tri-state buffers for a high to low transition on signal V_E

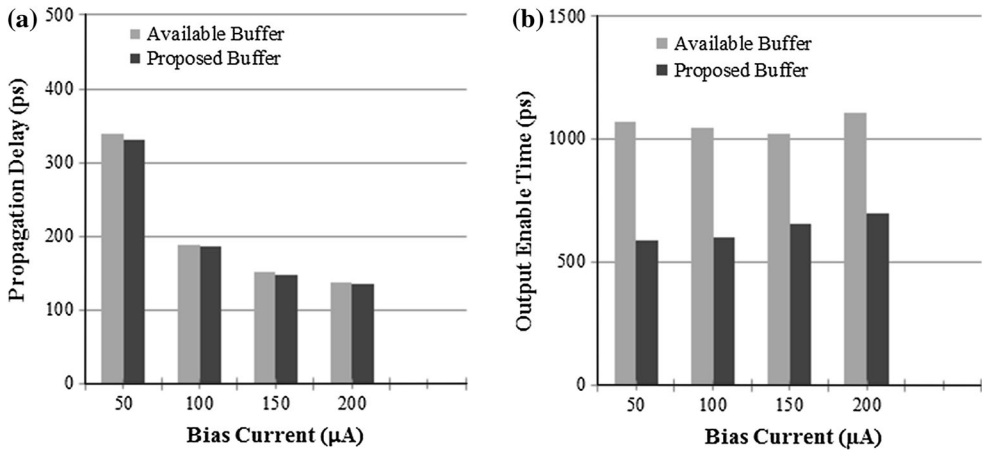

Fig. 6 Variation of propagation delay and output enable time with bias currents

Table 2 Effect of process variation on the performance parameters of the tri-state buffers

Parameter	NMOS PMOS	T T	F F	S S	F S	S F
Power (μW)	Available	306	536	162	462	190
	Proposed	304	535	160	460	189
Propagation delay (ps)	Available	189	168	225	206	180
	Proposed	186	162	223	202	179
Power delay product (fJ)	Available	57.834	90.048	36.450	95.172	34.200
	Proposed	56.544	86.690	35.680	92.920	33.831
Output enable time (ps)	Available	1047	674	2007	814	1561
	Proposed	600	365	1172	476	955

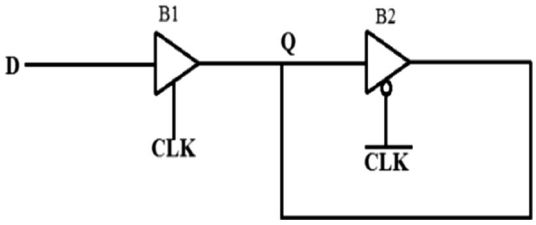

Fig. 7 D latch design using two MCML low power tri-state buffers

values which have not been tabulated for the sake of brevity. A graph illustrating the variation of propagation delay and output enable time with bias current is shown in Fig. 6. It may be noted that the delay decreases with increase in current and improvement in output enable time is visible throughout the current range for both proposed and available buffer.

The impact of parameter variations [8] at different design corners and effect of mismatch are also examined for the above bias current values. The findings for the bias current of 100 μA are summarized in Table 2. It is observed that the proposed tri-state buffer show variation in the power consumption, the propagation delay, the output enable time and the power delay product by a factor of 3.34, 1.38, 3.21 and 2.6 between the best and the worst cases respectively. Similarly, the available buffer shows 3.31, 1.34, 2.98 and 2.61 variations. The effect of width mismatch [9] is also studied on the tri-state buffers. The widths of the transistors are varied by 10 % corresponding to which a change of 2 % is observed in output enable time and 8 % in propagation delay.

7 Positive edge triggered register implementation

To illustrate the usefulness of the proposed tri-state buffer, an edge triggered register [10] may be constructed by using master slave configuration wherein a negative latch (master stage) is cascaded with positive latch (slave stage). A tri-state buffer based latch [11] of Fig. 7 is employed for this particular implementation. The complete gate level schematic of positive edge-triggered register is depicted in Fig. 8. A low on clock signal (CLK) enables the buffers B_1 and puts B_2 in high impedance state. Therefore, the input on D is sampled to the node Q_M. As buffers B_3 and B_4 are respectively in high impedance and enabled state, the slave stage holds the state. A low to high transition on CLK signal, the buffer B_1 enters in high impedance state and stops sampling the input and enters in hold mode as buffer B_2 is enabled. At this time, the buffer B_3 is enabled and copies Q_M to the output Q.

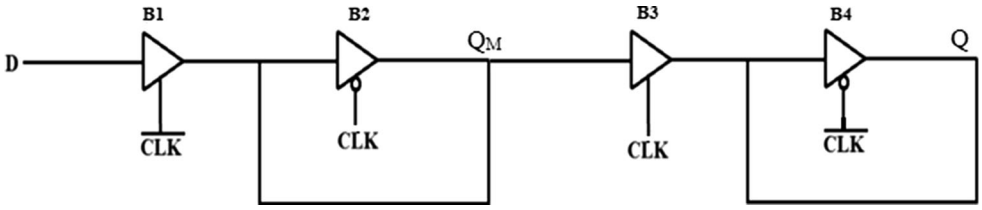

Fig. 8 Master slave based edge triggered register

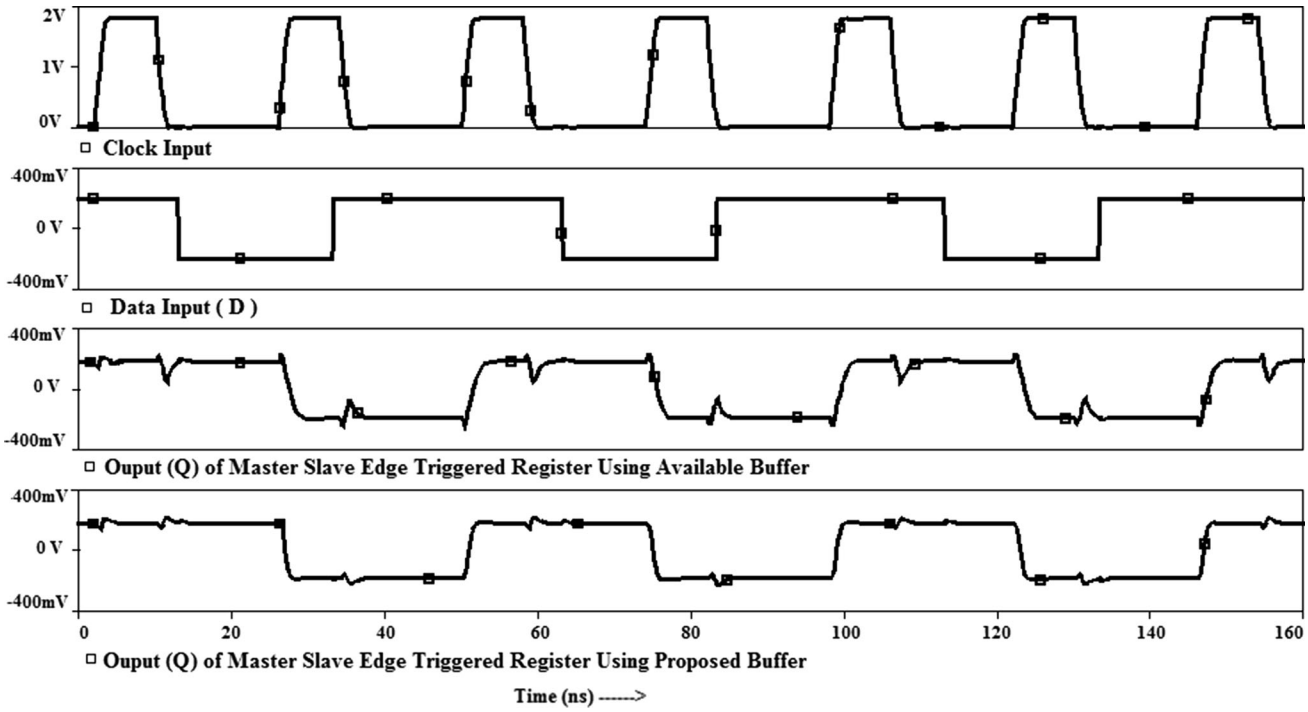

Fig. 9 Simulated waveforms of a edge triggered register based on available and proposed tri-state buffer

Table 3 Timing parameters of master slave edge triggered register

Buffer topology	Parameters			
	Propagation delay $T_{Clk \rightarrow Q}$ (ps)		Set up time T_{set_up} (ps)	Hold time T_{hold} (ps)
	L → H	H → L		
Available	860	855	310	0
Proposed	209	249	345	0

The available and the proposed tri-state buffers are used to construct positive edge triggered register. The timing waveforms for the CLK and D inputs and output Q are shown in Fig. 9 which confirms functionality of the circuit. The simulations are also carried out to compute performance parameters such as set up time (T_{set_up}), hold time (T_{hold}), and the delay ($T_{Clk \rightarrow Q}$). The results are summarized in Table 3. It may be noted that the timing parameters such as T_{set_up} and T_{hold} closely match for both realizations. However, there is significant improvement in $T_{Clk \rightarrow Q}$ which can be attributed to lower output enable time of the proposed buffer. The operating frequency of the register constructed with proposed buffer can work at higher frequency ($f = 1/T = (1/(T_{set\_up} + T_{Clk \rightarrow Q}))$.

8 Conclusions

A new topology to implement MCML tri-state buffer is presented. The current source section is modified in the proposed tri-state buffer which results in considerable reduction in output enable time in comparison to the available MCML tri-state buffer. The functionality is verified through SPICE simulations and impact of parameter

variations at different design corners and width mismatch on performance of both proposed and available buffer is also studied. A tri-state buffer based edge triggered register is included as an example to demonstrate the practical use of the proposed topology.

References

1. Rennie, D., & Sachdev, M. (2007). Comparative robustness of CML phase detectors for clock and data recovery circuits. In *Proceedings of international symposium on quality electronic design* (pp. 305–310).
2. Jonathan, H. C., et al. (1989). A packet video/audio system using the asynchronous transfer mode technique. *IEEE Transaction on Consumer Electronics, 35*, 97–105.
3. Golshan, R., & Haroun, B. (1994). A novel reduced swing CMOS bus interface circuit for high-speed low-power VLSI systems. In *Proceedings of the International Symposium on Circuits and System* (pp. 351–354).
4. Akata, M., et al. (1990). A 250 Mb/s 32 × 32 CMOS cross point LSI for ATM switching systems. In *Proceedings of IEEE international solid-state circuits conference* (pp. 30–31).
5. Louis, L., et al. (1999). A self-sensing tri-state pad driver for control signals of multiple bus controller. In *Proceedings of the IEEE international symposium on circuits and systems* (pp. 447–450).
6. Badel, S., & Leblebici, Y. (2007). Tri-state buffer/bus driver circuits in MOS current- mode logic. In *Proceedings of research in microelectronics and electronics conference* (pp. 237–240).
7. Gupta, K., Pandey, N., & Gupta, M. (2013). Low-power tri-state buffer in MOS current mode logic. In *Analog integrated circuits and signal processing* (vol. 75, pp. 157–160).
8. Bruma, S. (2003). Impact of on-chip process variations on MCML performance. In *IEEE Int. SoC conference*.
9. Hassan, H., Anis, M., & Elmasry, M. (2004). Analysis and design of low-power multi-threshold MCML. In *Proceedings of the IEEE international conference on system-on-chip* (pp. 25–29).
10. Rabaey, J. (2003). *Digital integrated circuits (a design perspective)* (2nd ed.). Englewood Cliffs, NJ: Prentice Hall.
11. Kang, S. M., & Leblebici, Y. (2003). *CMOS digital integrated circuits*. New Delhi: Tata McGraw-Hill Education.

Neeta Pandey received her M. E. in Microelectronics from Birla Institute of Technology and Sciences, Pilani and Ph.D. from Guru Gobind Singh Indraprastha University Delhi. She has served in Central Electronics Engineering Research Institute, Pilani, Indian Institute of Technology, Delhi, Priyadarshini College of Computer Science, Noida and BharatiVidyapeeth's College of Engineering, Delhi in various capacities. At present, she is Assistant Professor in ECE Department, Delhi Technological University. A life member of ISTE, and member of IEEE, USA. She has published papers in international, national journals of repute and conferences. Her research interests are in analog and digital VLSI Design.

Bharat Choudhary received his B.Tech degree in Electronics & Communication Engineering from Rajasthan Technical University, Kota, in 2010. He received his M.Tech degree in Nano Science and Technology, in 2013, from Delhi Technological University, Delhi, where he is currently working as Research Scholar in ECE Department, from 2013. Hisresearch interests include digital VLSI Design and Nanoelectronics.

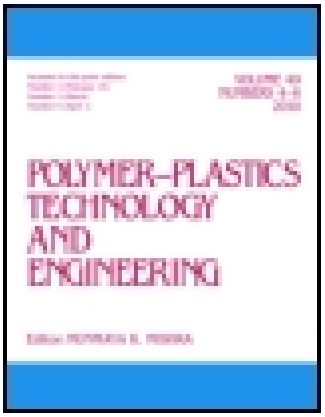

Polymer-Plastics Technology and Engineering
Publication details, including instructions for authors and subscription information:
http://www.tandfonline.com/loi/lpte20

Influence of Dopant Ions on the Properties of Conducting Polyacrylamide/Polyaniline Hydrogels

Reetu Prabhakar[a] & D. Kumar[a]
[a] Department of Applied Chemistry & Polymer Technology, Delhi Technological University, Shahbad Daulatpur, Delhi, India
Accepted author version posted online: 19 Jul 2015.

Influence of Dopant Ions on the Properties of Conducting Polyacrylamide/Polyaniline Hydrogels

Reetu Prabhakar[1], D. Kumar[1]

[1]Department of Applied Chemistry & Polymer Technology, Delhi Technological University, Shahbad Daulatpur, Delhi, India

To whom correspondence should be addressed: Reetu Prabhakar, E-mail: prabhakar6reetu@gmail.com

Abstract

Polyaniline (PANI) impregnated polyacrylamide (PAM) conducting hydrogels have been synthesized chemically via interfacial polymerization route using different acidic doping agents like sulphuric acid (H_2SO_4), hydrochloric acid (HCl), and perchloric acid ($HClO_4$). The best properties were found in case of H_2SO_4 doped PAM/PANI sample when compared with other doping agents. The resulting hydrogel exhibits superior properties including compact structure, high crystallinity, good mechanical strength and electrical conductivity. The maximum electrical conductivity of the order of 9.4×10^{-5} S/cm was found in case of doped H_2SO_4 PAM/PANI.

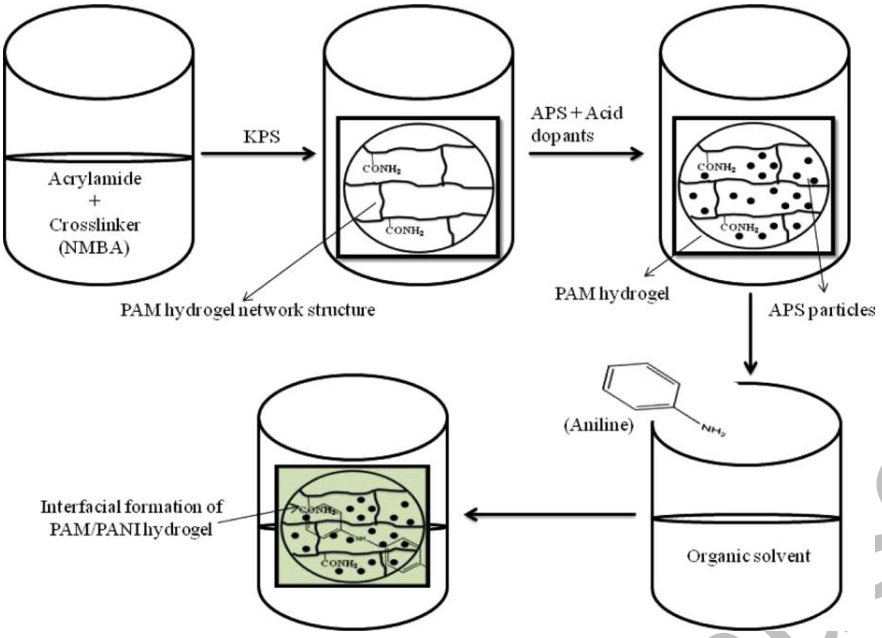

KEYWORDS: Polyacrylamide, Interfacial polymerization, Surface morphology, Electrical conductivity

INTRODUCTION

Conducting polymer hydrogels have emerged as an important area of research interest because of the special and significant advantages it offers[1-3], making their prospect for technological applications[4,5]. Hydrogels are three dimensionally cross-linked hydrophilic network systems which can absorb large amount of water[6]. Conducting polymers have the ability to conduct electricity and also show changes in chemical and physical properties in response to an electrical stimulus. Both hydrogel and conducting polymers have emerged as most promising materials being used for development of newer materials, on account of the conducting property offered by conducting polymers and solid and liquid stability of hydrogel that endure volume changes in response to varying environmental conditions such as temperature, pH, solvent composition, and

electrical stimuli[7-11]. These materials are also called as “smart polymers” or “smart gels”.

There have been a number of studies on the synthesis, characterization, and applications of conducting polymers such as polyaniline, polypyrrole, and polythiophene[12,13]. Amongst conducting polymers, polyaniline (PANI) have gained a great deal of attention because of its easy preparation methods, good conductivity, environmental and thermal stability and its unusual redox property[14-16]. It has been reported in the literature that the electrical conductivity of PANI depends mainly on the nature and concentration of the dopant ions[17,18]. Introduction of different acid dopants for the formation of conducting polymer PANI inside the hydrogel matrix is likely to improve its properties and enhance its application in the field of electrosensors, capacitors, and actuators[19,20]. Inorganic and organic acid dopants can affect the electrical conductivity of conducting polymer in different manner. Bulky size and delocalized charge density of organic dopants restrict their incorporation in to polymer matrix resulting in a conducting polymer with limited electrical conductivity. While, inorganic dopants with smaller sizes and localized charge density can provide required charge neutralisation of the polymer backbone, ensuing in the enhanced conductivities.

Several efforts have been made to synthesize electrically conducting hydrogel. Bajpai et al synthesized electrically conducting composite materials consisting of polyaniline (PANI) nanoparticles dispersed in a polyvinyl alcohol (PVA)-*g*-polyacrylic acid (PAA) hydrogel medium. They studied electrical conductivity and electroactive performance of

swelled hydrogels in an electrolyte solution using effective bending angle (EBA) measurements [21]. Kim et al synthesized PVA/PAA interpenetrating polymer network (IPN) hydrogel and investigated the influence of electrolyte concentration on their bending behaviour under an applied electric field[22].

The three step sequential interpenetrating polymer network route (IPN) was the most commonly adopted method for the synthesis of conducting polymer in the hydrogel[23,24] but main drawback of this method is that the conducting polymer is polymerized in the aqueous solution and not formed properly inside the matrix, causing waste of chemicals and moreover environmental pollution. Further, a unique method of interfacial polymerization[25] has been adopted recently to polymerize conducting polymer at the aqueous/organic interface which directly diffuse into the hydrogel matrix[26,27]. In this method, preformed polyacrylamide (PAM) hydrogel is first immersed in oxidant/dopant aqueous solution and then dipped in an organic solvent containing monomer forming conducting polymer in its doped state at the aqueous/organic interface and its homogeneous diffusion into the hydrogel. This method is considerably more economical and effective than the IPN method to synthesize highly conducting polymer hydrogel. Dai et al. synthesized a high-grade PAM/PANI composite hydrogel by interfacial polymerization route. They discussed in their report that PANI polymerized at the water/organic-solvent interface accumulates impulsively and solely into the preformed PAM hydrogel and exhibited superior properties such as formation of homogeneous structure, improved mechanical strength, high electrical conductivity, and reversible interconversion between the doped and dedoped states. Borauh et al. also discussed the

formation of polyacrylic acid-co-acrylamide/PANI composite hydrogel via interfacial polymerization method using different concentration of crosslinker. This composite hydrogel exhibited significant conducting stability and mechanical strength.

In view of the above reported work, we intend to synthesize conducting PAM/PANI hydrogel using interfacial polymerization method with different acid dopants such as, hydrochloric acid (HCl), sulphuric acid (H_2SO_4), and perchloric acid ($HClO_4$). Aniline is polymerized at the aqueous/organic interface and formed PANI is being doped with different acidic dopants. The main objective of this work is to study the effect of dopant ions on the chemical and mechanical properties, as well as on conductivity and morphology of the PAM/PANI hydrogel using various techniques.

EXPERIMENTAL

Materials Used

All the chemicals including solvents were used as supplied except the monomer aniline which was distilled prior to its use. Acrylamide monomer was purchased from Spectro. Chem. Pvt. Ltd. Aniline monomer and crosslinker N,N'-methylene Bisacrylamide (NMBA) were purchased from SRL, Pvt. Ltd., India. All the solutions used during the study were prepared by using double distilled Milli-Q water.

Synthesis of PAM Hydrogel

Scheme 1 shows the synthesis steps of PAM hydrogel and PANI formation inside PAM matrix. Polyacrylamide (PAM) hydrogel was synthesized via free radical crosslinking

polymerization at room temperature in an aqueous solution consisting of N,N'-methylene Bisacrylamide (NMBA) as crosslinker and potassium persulphate (KPS) as an initiator. A predetermined quantity of acrylamide with a small amount of NMBA (0.1 mol%) was added to a measured quantity of distilled water at ambient temperature. The mixed solution was then degassed by purging nitrogen for 15 min to remove dissolved oxygen that may possibly inhibit the reaction. Then, radical initiator KPS (0.2 mol%) was rapidly added to the above solution under stirring to dissolve KPS. The solution was kept at 60°C for 1h resulting in PAM hydrogel and further at room temperature for one day to ensure the complete polymerization. Thereafter, hydrogel sample was washed repeatedly with distilled water in order to extract unreacted chemicals and impurities and lastly, dried under vacuum up to a constant weight.

Interfacial Polymerization of Aniline within PAM Hydrogel Matrix

In a typical set of synthesis, the incorporation and formation of PANI inside the PAM hydrogel matrix has been carried out through the interfacial polymerization route. The preformed PAM hydrogel samples were separately immersed in 1M different acid solutions (HCl, H_2SO_4 and $HClO_4$ which act as dopant) containing pre-dissolved ammonium persulphate (APS) oxidant until equilibrium swelling is reached.

The pre-swelled PAM hydrogel samples were immersed in the organic solvent, i.e., dichloromethane containing freshly distilled aniline (0.15M) monomer, where the aniline polymerization reaction was allowed to proceed at room temperature until the formation of PANI. The green colour precipitate of PANI was formed at water/organic solvent

interface which diffuses into the hydrogel. This PANI incorporated PAM hydrogels were washed repeatedly with enough amount of distilled water to remove the unexploited reactants and other impurities like oligomers.

Characterization

Fourier Transform Infrared spectroscopy (FTIR) analysis has been carried out in the wavelength range 4000-500 cm^{-1} on Thermo Nicolet (Model-380) infrared spectrophotometer using KBr pressed pellets. UV–Visible (UV-Vis) absorption spectra of the samples were recorded in dimethyl sulfoxide (DMSO) in the range of 200–800 nm on Cary Series UV–Vis spectrophotometer (Agilent Technologies). Morphological study of the samples was carried out using the scanning electron microscope (SEM, Hitachi). Powder X-ray diffraction (XRD) was recorded on an X-ray diffractometer (D8 ADVANCE of Germany BRUKER Co.) using Cu Kα radiation. The electrical conductivity of PAM/PANI hydrogel samples (5mm x 5mm x 1mm) was measured using four probe method by Keithley 4200 instrument. The electrical conductivity of the hydrogel composite was calculated using the following equation:

$$\rho = R(l / A)$$

where, ρ is the resistivity (Ω.cm), R is the resistance (Ω), l is the length of the film (cm), and A is the area of the film (cm^2). The electrical conductivity (σ) of the film expressed in terms of S/cm was obtained by using the following relation:

$$\sigma = 1/\rho$$

Mechanical properties of wet hydrogel samples of 10mm x 10mm x 5mm dimension have been studied by the compressive stress-strain measurements using universal testing

machine (UTM, Instron 33693 model, UK) at a strain rate of 10% min^{-1} till the samples were broken against the stainless steel platform.

The percentage of PANI impregnation within the hydrogel was calculated using the following relation:

$$\text{PANI impregnation} \quad \% \quad = \left[\; W_{PANI} - W_{Dry} \; / W_{Dry} \right. \quad \text{x } 100$$

where, W_{PANI} is the weight of dry PANI incorporated gel and W_{Dry} is the dry weight of the native PAM polymer gel.

Swelling Behaviour Study

The swelling behaviour of the hydrogels was studied in water at room temperature. The weight change was examined till the hydrogels showed constant weight change. The percentage swelling was measured using the following relation:

$$\text{Swelling} \quad \% \quad = \left[\; W_f - W_i \; / W_i \right. \quad \text{x } 100$$

where, W_f is the final weight of fully swelled PAM/PANI hydrogel sample and W_i is the initial weight of PAM/PANI hydrogel before swelling in distilled water.

RESULTS AND DISCUSSION

Analysis of FT-IR Spectra

FTIR spectra of PANI impregnated PAM hydrogel doped with H_2SO_4, HCl and $HClO_4$ acids are shown in Figure 1. In case of H_2SO_4 doped (Fig.1a), spectra show the characteristic peaks at 1615 and 1452 cm^{-1} due to the C=N and C=C stretching mode for the quinoid and benzenoid ring of PANI, respectively[28]. While a characteristic peak

around 1307 cm^{-1} is assigned to C-N stretching of a secondary aromatic amine. Moreover, the characteristic peaks at 3423, 2927, and 1660 cm^{-1} are assigned to N-H bending, -CH_2 stretching and N-H in plane bending in -$CONH_2$ of PAM hydrogel, respectively[6]. The band at around 1253 cm^{-1} can be ascribed as C-N-C stretching vibration in the polaron structure and peak at 1131 cm^{-1} is due to the vibration mode of the NH^+ structure, which is attributed due to the protonation of amine group in aniline and expected in the polymerization progress of PANI. This result supports successful formation of PANI within the PAM hydrogel matrix. When these results were in turn compared with HCl and $HClO_4$ doped PANI gel (Fig. 1b & 1c), it showed the similar characteristic peaks in the same region but of comparatively weaker intensity. This indicates a poor doping of PANI inside the PAM hydrogel matrix.

UV-Visible Analysis

UV-Vis absorption spectra were used to investigate the doping state of the conducting polymer in the hydrogel matrix. The UV-Vis spectra of H_2SO_4 doped PAM/PANI hydrogel (Fig. 2a) exhibited two absorption bands at around 295 and 601 nm. The band at 295 nm is observed due to the π-π* transition of the benzenoid rings while the strong broad band at around 601 nm is associated with the exciton absorption of quinoid rings[29]. Similarly, HCl doped hydrogel (Fig. 2b) showed UV-Vis absorption peak at 280 and 598 nm, which is again due to the benzenoid and quinoid rings, respectively. These results indicate the incorporation of emeraldine PANI within the PAM hydrogel matrix.

On the other hand, absorption spectra of $HClO_4$ doped PANI incorporated PAM hydrogel (Fig. 2c) showed two absorption bands at around 277 and 341 nm while the exciton band at around 600 nm almost disappears. This disappearance of band in $HClO_4$ doped PANI incorporated PAM hydrogel indicates the insufficient doping of PANI inside the PAM matrix.

Morphological Studies

Figure 3 shows the SEM micrographs of PANI impregnated PAM hydrogel doped with different dopant ions. All the images were taken from the cross section of the hydrogel sample. Dopant ions have known to significantly influence the morphological behaviour and electrical property of the synthesized hydrogels. It can be seen that the $HClO_4$ doped PANI impregnated hydrogel formed open pores structure (Fig. 3c). On the other hand, HCl doped PANI (Fig. 3b) containing hydrogel showed irregular surface with less pores while H_2SO_4 doped (Fig. 3a) showed more compact and homogeneous structure. The difference in structure may be related to the formation and incorporation of PANI inside the PAM hydrogel matrix. The open voids observed in $HClO_4$ doped hydrogel may be due to the insufficient incorporation of PANI within the PAM matrix. This inadequate distribution of PANI inside the gel may results in lowering of conductivity of porous hydrogel structure unlike the HCl and H_2SO_4 acid doped PANI gel which in turn presented a compact structure. Thus, the surface morphology and conductivity of the resulting hydrogel can be altered by varying the type of dopant ions.

X-ray Diffraction Study

The XRD pattern of PANI impregnated PAM matrix samples are shown in Figure 4. The XRD diffraction patterns are labelled as a, b, and c of the H_2SO_4, HCl, and $HClO_4$ doped PANI impregnated hydrogels, respectively. The $HClO_4$ and HCl doped PANI hydrogels exhibit broad peak at about 23º which confirms the amorphous nature of doped PANI inside the gel while the H_2SO_4 doped PANI hydrogel shows some diffraction peaks at 2θ = 20º and 23º, respectively. This improvement in crystallinity with H_2SO_4 doping may be ascribed to the more connection of PANI chains to the PAM network structure[30]. These results impart the variations in the surface morphology shown by SEM images. Thus XRD result provides an additional evidence of connection and formation of PANI chains within the PAM network structure in support to the other results.

Electrical Conductivity Behaviour

In the present study, the electrical conductivity value varies with the nature of dopant ion used for the PANI, inside the PAM hydrogel. The electrical conductivity of PAM/PANI hydrogel mainly depends on the existence of conducting polymer PANI inside the hydrogel matrix, as PAM itself is insulating in nature. The electrical conductivity values and percentage of PANI impregnated of PAM/PANI hydrogel samples are summarized in Table 1 and follow the conductivity trend as H_2SO_4 > HCl > $HClO_4$. There is a slight difference which could be due to some chemical changes involved in the polymer chains with different dopant ions. The electrical conductivity value of conducting polymers depends upon the presence of dopant ion attached to the polymer matrix. The lowest conductivity value was observed in $HClO_4$ doped PAM/PANI hydrogel, reason being the

presence of open porous air structure leading to drop in the value of its electrical conductivity as also discussed in SEM results[31].

Swelling Behaviour

The swelling behaviour of the samples is presented in Table 1. The swelling behaviour was found to be higher in case of $HClO_4$ doped PANI impregnated PAM hydrogel. As seen in SEM images, an open porous structure was obtained in $HClO_4$ doped PANI, this open spaces permits higher water uptake ability within the matrix. In contrast, swelling is lower in case of H_2SO_4 doped PANI gel, as formed compact structure and the hydrophobic nature of PANI, leads to the decreasing of swelling behaviour.

Mechanical Strength

To investigate the effect of different dopant ions on the mechanical behaviour of the PAM/PANI hydrogel samples, compression test was performed on swelled hydrogel samples. Figure 5 shows that the mechanical strength increases in case of H_2SO_4 doped PANI impregnated hydrogel when compared to HCl and $HClO_4$ doped PANI. The composite hydrogel doped with H_2SO_4 breaks at a strain rate of 66% and a stress of 0.07MPa, while HCl doped hydrogel breaks at a strain rate of 58% and a stress of 0.05MPa whereas $HClO_4$ doped hydrogel breaks at a strain of 51% and a stress of 0.04MPa. The refinement in the mechanical strength of H_2SO_4 doped PANI embedded hydrogel could be due to the formation of more compact and homogeneous structure as seen in SEM micrographs, thus enhancing the mechanical strength.

CONCLUSIONS

PANI incorporated PAM hydrogel doped with inorganic acids (H_2SO_4, HCl, and $HClO_4$) were successfully synthesized via interfacial polymerization method. The FTIR results show that PANI is synthesized well inside the PAM hydrogel matrix and the characteristic peaks are present in the FTIR spectra. The UV-Vis spectra show the shift in absorption peaks of $HClO_4$ doped sample due to the incomplete formation of PANI inside the hydrogel matrix. The morphological studies show the uniform compact morphology of H_2SO_4 doped PAM/PANI hydrogel. Electrical conductivity was found to be highest in case of H_2SO_4 doped sample. The swelling % was found to be increased in case of $HClO_4$ doped PANI and it reveals that the swelling behavior depends upon the formation of hydrogel network. The mechanical toughness was found to be highest in case of H_2SO_4 doped hydrogel. These differences could be due to characteristics of the dopant acids including amount of acids added; oxidizablility of the acids and incorporation of PANI to PAM matrix. All these factors affect the formation of conducting polymer PANI inside the matrix and lead to the differences in their properties.

ACKNOWLEDGEMENT

The financial assistance from Delhi Technological University (DTU), Delhi to Reetu Prabhakar is acknowledged gratefully.

REFERENCES

1. Chen, Li.; Kim, B.; Nishino, M.; Gong, J.P.; Osada Y. Environmental response of polythiophene hydrogels. Macromol. **2000**, *33*, 1232-1236.

2. Donat, B.P.; Viallat, A.; Blachot, J.F.; Lombart, C. Electromechanical polymer gels combining rubber elasticity with electronic conduction. Adv. Mater. **2006**, *18*, 1401-1405.

3. Justin, G.; Guiseppi-Elie, A. Characterization of electroconductive blends of p(HEMA-*co*-PEGMA-*co*-HMMA-*co*-SPMA) hydrogels and p(Py-*co*-PyBA). Biomacromol. **2009**, *10*, 2539-2549.

4. Karbarz, M.; Gniadek, M.; Donten, M.; Stojek, Z. Intra-channel modification of environmentally sensitive poly(N-isopropylacrylamide) hydrogel with polyaniline using interphase synthesis. Electro. Comm. **2011**, *13*, 714–718.

5. Small, C.J.; Too, C.O.; Wallace, G.G. Responsive conducting polymer-hydrogel composites. Polym. Gels & Netw. **1997**, *5*, 251-265.

6. Golikand, A.N.; Didehban, K.; Rahimi, R. Investigation of the properties of conductive hydrogel composite containing Zn particles. J. App. Polym. Sci. **2012**, *126*, 436–441.

7. Sasase, H.; Aoki, T.; Katono, H.; Sanui K.; Ogata, N. Regulation of temperature-response swelling behaviour of interpenetrating polymer networks constructed with poly(acrylic acid) and poly(N,N dimethyl acrylamide). Macromol. Chem. Rapid Commun. **1992**, *13*, 577-581.

8. Hu, Y.; Horie, K.; Tori, T.; Ushiki, H.; Tang, X. Change in micro-environments in poly(acrylamide) gel with pyrenyl probe due to its volume phase transition induced by pH change. Polym. J. **1993**, *25*, 123-130.

9. Hirokawa, Y.; Tanaka, T. Volume phase transition in nonionic gel. J. Chem. Phys. **1984**, *81*, 6379-6380.

10. Tanaka, T.; Nishio I.; Sung S.T.; Ueno-Nishio. Collapse of gels in electric field. Science. **1982**, *218*, 467-469.

11. Ghosh, S.; Rasmusson, J.; Inganas, O. Superamolecular selfassembly for enhanced conductivity in conjugated polymer blends: ionic crosslinking in blends of poly(3,4-ethylenedioxythiophene)-poly(styrenesulfonate) and poly(vinylpyrrolidone). Adv. Mater. **1998**, *10*, 1097-1099.

12. Shirakawa, H.; Louis, E.J.; MacDiarmid, A.G.; Chiang, C.H.; Heeger, A.J. Synthesis of electrical conducting organic polymers: halogen derivatives of polyacetylene. J. Chem. Soc. Chem. Commun. **1977**, 578–580.

13. MacDiarmid, A.G. A novel role for organic polymers. Synth. Met. (Rev). **2002**, *125*, 11–22.

14. Jaymand, M. Recent progress in chemical modification of polyaniline. Prog. Polym. Sci. **2013**, *38*, 1287– 1306.

15. Asberg, D.P.; Inganas, O. PEDOT/PSS hydrogel networks as 3D- enzyme electrodes. Synth. Met. **2003**, *137*, 1403-1404.

16. Moschou, E.A.; Peteu, S.F.; Bachas, L.G.; Madou, M.J.; Daunert, S. Artificial muscle material with fast electroactuation under neutral pH conditions. Chem. Mater. **2004**, *16*, 2499-2502.

17. Cao, Y.; Smith, P.; Heeger, A.J. Counter-ion induced processibility of con-ducting polyaniline and of conducting polyblends of polyaniline in bulk polymers. Synth. Met. **1992**, *48*, 91–97.

18. MacDiarmid, A.G.; Epstein, A.J. The concept of secondary doping as applied to polyaniline. Synth. Met. **1994,** *65*, 103–116.

19. Tang, Q.; Wu, J.; Sun, H.; Lin, J.; Fan, S.; De, Hu. Polyaniline/polyacrylamide conducting composite hydrogel with porous structure. Carbohyd. Polym. **2008**, *74*, 215–219.

20. Adhikari, S.; Banerji, P. Polyaniline composite by in situ polymerization on a swollen PVA gel. Synth. Met. **2009**, *159*, 2519–2524.

21. Bajpai, A.K.; Bajpai, J.; Soni, S.N. Preparation and characterization of electrically conductive composites of poly(vinyl alcohol)-g-poly(acrylic acid) hydrogels impregnated with polyaniline (PANI). eXPRESS Polym. Lett. **2008**, *2*, 26–39.

22. Kim, S.J.; Park, S.J.; Lee, S.M.; Lee, Y.M.; Kim, H.C.; Kim, S.I. Electroactive characteristics of interpenetrating polymer network hydrogels composed of poly(vinyl alcohol) and poly(N-isopropylacrylamide). J. Appl. Polym. Sci. **2003**, *89*, 890−894.

23. Kim, H.; Park, S.J.; Kim S.J. Volume behavior of interpenetrating polymer network hydrogels composed of polyacrylic acid-*co*-poly(vinyl sulfonic acid)/polyaniline as an actuator. Smart Mater. Struct. **2006**, *15*, 1882–1886.

24. Siddhanta, S.K.; Gangopadhyay, R. Conducting polymer gel: formation of a novel semi-IPN from polyaniline and crosslinked poly(2-acrylamido-2-methyl propanesulphonicacid). Polym. J. **2005**, *46*, 2993-3000.

25. Huang, J.X.; Kaner, R.B. A general chemical route to polyaniline nanofibers. J. Am. Chem. Soc. **2004**, *126*, 851-855.

26. Dai, T.; Qing, X.; Wang, J.; Shen, C.; Lu, Y. Interfacial polymerization to high quality polyacrylmide/polyaniline composite hydrogels. Compos. Sci. & Tech. **2010**, *70*, 498–503.

27. Boruah, M.; Kalita, A.; Pokhrel, B.; Dolui, S.K.; Boruah, R. Synthesis and characterization of pH responsive conductive composites of poly(acrylic acid-co-acrylamide) impregnated with polynilineby interfacial polymerization. Adv. Polym. Tech. **2013**, *32*, 20-30.

28. Kang, E.T.; Neoh, K.G.; Tan, K.L. Polyaniline: A polymer with many interesting intrinsic redox states. Prog. Polym. Sci. **1998**, *23*, 277–324.

29. Kuwabata, S.; Okamoto, K.; Yoneyama, H. Conductivity of polypyrrole films doped with aromatic sulphonate derivatives. J. Chem. Soc. Faraday Trans. **1988**, *184*, 2317–2326.

30. Malik, H.; Gupta, N.; Sarkar A. Anisotropic electrical conduction in gum Arabia-A biopolymer. Mat. Sci. Eng. C. **2002**, *20*, 215–218.

31. Kulkarni, M.V.; Viswanath, A.K.; Marimuthu, R.; Seth, T. Spectroscopic, transport, and morphological studies of polyaniline doped with inorganic acids. Polym. Eng. Sci. **2004**, *44*, 1676–1681.

Table 1. Electrical conductivity, PANI impregnation and swelling % of PAM/PANI hydrogel doped with different acid dopants

Sample	Dopants	Electrical Conductivity (S/cm)	PANI content (wt %)	Swelling (%)
1.	**H_2SO_4**	9.4×10^{-5}	18.6	61
2.	**HCl**	2.1×10^{-5}	12.84	71
3.	**$HClO_4$**	8.4×10^{-6}	12.4	91

Scheme 1. Schematic of polyacrylamide and polyacrylamide/polyaniline hydrogel synthesis

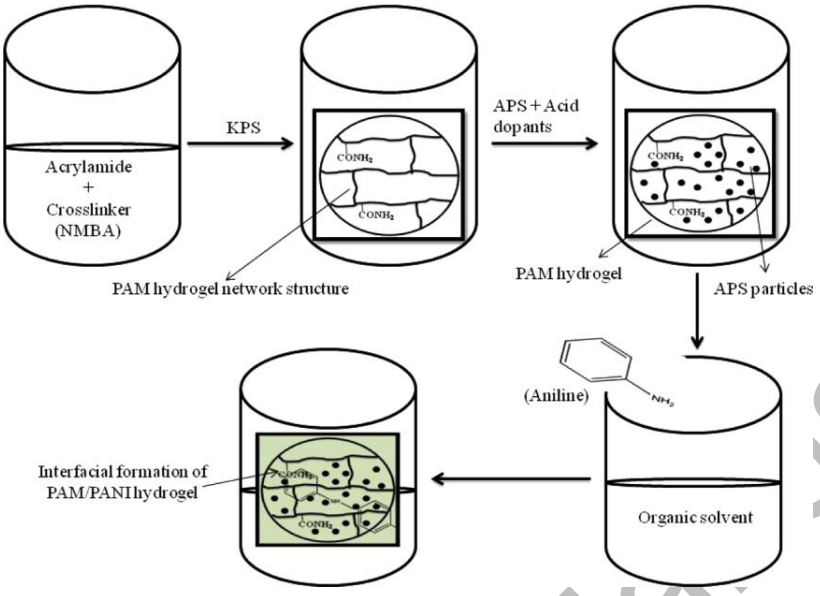

Figure 1. FTIR spectra of PAM/PANI hydrogel doped with different acid dopants (a) H_2SO_4, (b) HCl, and (c) $HClO_4$

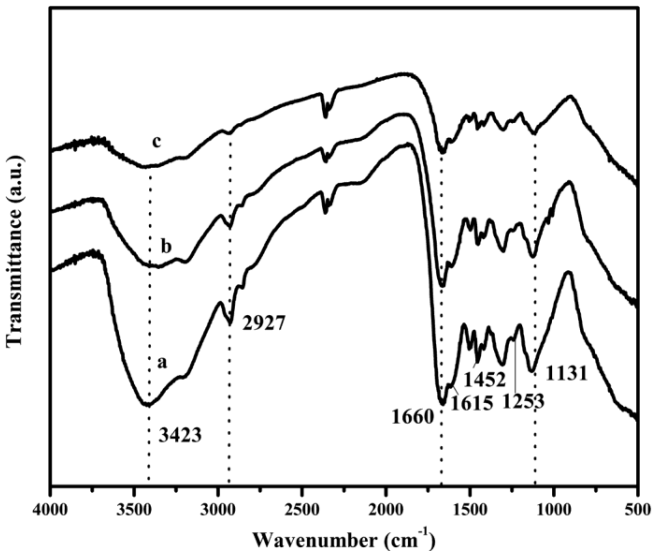

Figure 2. UV-Vis spectra of PANI impregnated PAM hydrogel samples doped with different dopants (a) H_2SO_4, (b) HCl, and (c) $HClO_4$

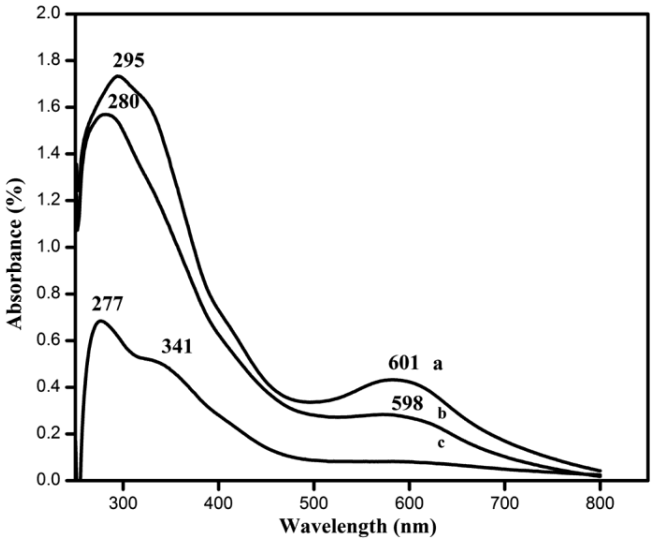

Figure 3. SEM micrographs of PAM/PANI hydrogels doped with (a) H_2SO_4, (b) HCl, and (c) $HClO_4$

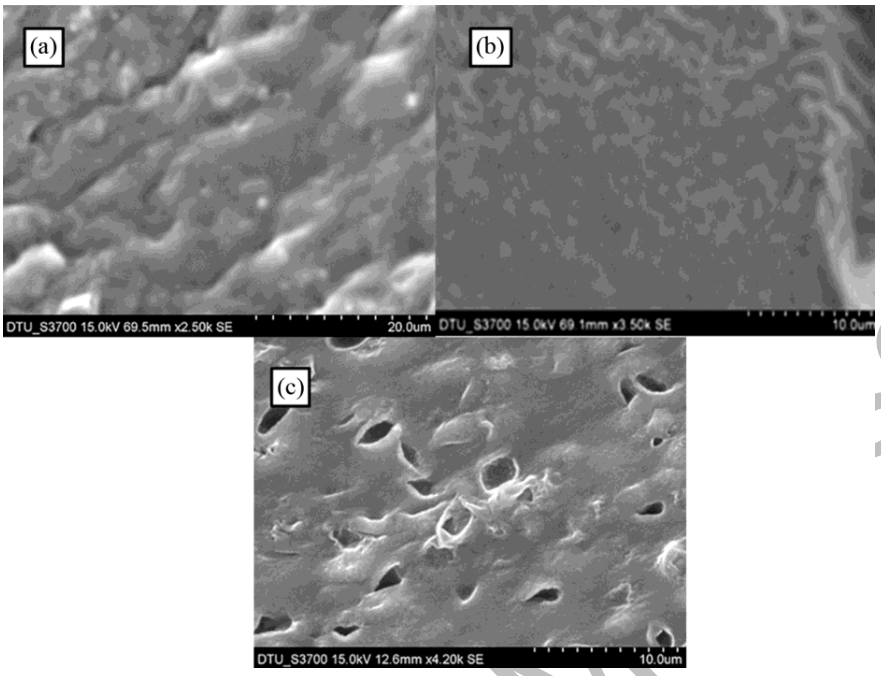

Figure 4. XRD pattern of PAM/PANI hydrogel doped with (a) H_2SO_4, (b) HCl, and (c) $HClO_4$

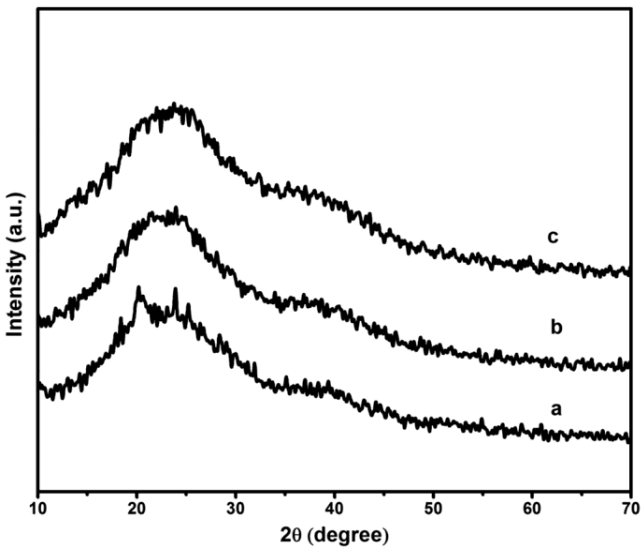

Figure 5. Compressive Stress-Strain graph of PAM/PANI hydrogel samples doped with (a) H_2SO_4, (b) HCl, and (c) $HClO_4$

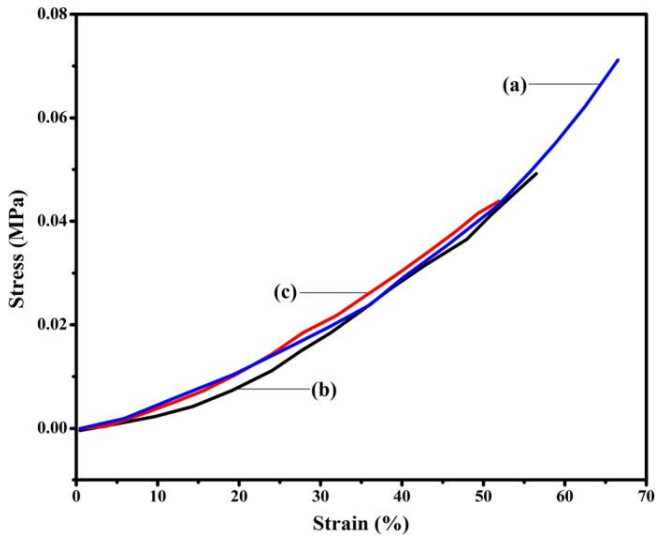

Volume 3, Issue 2 (2015) 321-327 ISSN 2347 - 3258
International Journal of Advance Research and Innovation

Irreversibility Reduction in Vapour Compression Refrigeration Systems Using Al_2O_3 Nano Material Mixed in R718 as Secondary Fluid

R. S. Mishra
Department of Mechanical Engineering, Delhi Technological University, New Delhi, India

Article Info

Article history:
Received 02 April 2015
Received in revised form
20 May 2015
Accepted 28 May 2015
Available online 15 June 2015

Keywords

Performance Improvement,
Reduction in System Irreversibility,
Energy-Exergy Analysis,
Vapour Compression Refrigeration System,
Ecofriendly Refrigerants,
Second Lawefficiency Improvement

Abstract

The several methods are available in the literature for improving first law efficiency in terms of coefficient of performance. The second law efficiency is helped for finding the irreversibilities the systems. The uses of nano refrigerants in the vapour compression refrigeration play a very important role for reducing irreversibility in the system and improving its thermodynamic performances. This paper describes thermal modelling of vapour compression refrigeration system using energy - exergy analysis. In this system, the utility of ecofriendly twelve refrigerants in primary circuit is highlighted and Al_2O_3-Water based nanofluids in secondary circuit. This model takes care the nanoparticles mixed in the fluids as input conditions in the secondary evaporator circuit as geometric characteristics of the system such as size of nanoparticles and the compressor speed to predict the secondary fluids output temperatures, the operating pressures, the compressor power consumption and the system overall energy performance. Such design analysis is conveniently useful to compare the thermal performance of different nano-particles of Al_2O_3 based nano-fluid as a secondary fluid in a vapour compression refrigeration system. The influence of input variables on the irreversibilities in terms of exergy destruction ratio of the system is presented. Such a model can also be used to design various components viz. evaporator, compressor, condenser and throttle valve for vapour compression refrigeration systems for any desired cooling capacity. This model takes care of use of nanofluids as a secondary fluid in vapour compression refrigeration systems and simulate the non linear equations of the system. The use of R407c as ecofriendly refrigerants is quite adequate while first law performance improvement is around 13.491% by using nano particles. The % improvement in first law efficiency is found to be 11.04% by using nano particles as compared to without nano particles. While by using R134a 12.60% improvement. Similarly It was also observed that second law performance improvement is ranging between 15% to 39.13%. The better second law efficiency is 39.13% improvement due to, by using R1234yf as compared to 16.52% improvement by using R1234ze in the primary evaporator circuit. The reduction in the irreversibility in terms of exergy destruction ratio in the system and maximum exergy destruction ratio around 25.294% was observed by using R152a and exergy destruction ratio is 22.79% by using R290 hydrocarbon and 23.403% by using R407c as ecofriendly refrigerant. The Reduction in EDR is 20.09% by using R404a, and 21.37% by using R134a. The R1234ze and R1234yf have slightly less reduction in EDR as compared by using R134a.

1. Introduction

Global warming potential and ozone layer depletion are one of the important issues in front of the researcher. As R22 and R12 is the most widely used as refrigerants in industrial and household applications .Lately it was found that these have high value of ozone depletion potential. Most of researches are going on searching better refrigerant and replacement of old refrigerants have high global warming potential and ozone depletion potential with modern one have low both GWP and ODP values . First law analysis (energy analysis) is restricted to calculate only coefficient of performance of system but exergy analysis is the one of the most useful analyses to evaluate the plant losses, the actual amount of energy flow through process exergetic efficiency and exergetic destruction ratio. Comparative analysis of three refrigerants (R134a, R1234yf and R1234ze) working in a multi-evaporators VCR system with subcooling and superheating and using of both energy and exergy analysis on multi-evaporators vapor compression refrigeration system emphasized on replacement of R134a with R1234ze and R1234yf is also a important Because R134a having high global warming potential (GWP=1426), on the other hand R1234ze has zero ODP & 6 GWP) and R1234yf (GWP =4 and zero ODP) respectively.

Corresponding Author,
E-mail address: professor_rsmishra@yahoo.co.in

2. Use of Nano Refrigerants in Vapour Compression Refrigeration System

Vapour compression is used to transfer heat from low temperature zone higher temperature zone. It has four thermodynamics process as below. Isobaric Evaporation, Isentropic Compression, Isobaric Condensation, Throttling (Expansion), Vapour compression cycle can be used in temperature range 50°C to -40°C easily. Nowadays, there is a high energy consumption associated with refrigeration and air conditioning systems. Most of these facilities are based on the vapour compression cycle. In order to reduce their consumption, it is necessary both to have efficient systems and to operate them properly. To achieve these objectives, it is convenient to use complete models, which take under consideration a large amount of factors and facilitate the design of efficient systems. The heat transfer from the refrigerant at the compressor discharge line to the condenser inlet has been modeled, due to the considerable length of the line in the experimental chiller facility, using expression. The condenser behavior is modeled by dividing the heat exchanger into two zones: the superheated vapor zone and the condensing zone, assuming no sub-cooling at the condenser outlet, as it has been stated in the assumptions.

The overall heat exchanger is then For the computation of the convection heat transfer coefficient associated to the refrigerant one can distinguish between the convection heat transfer coefficient in the superheated vapor zone modeled with two energy balances, one using the secondary fluid heat flow rate. By using nanofluid in secondary circuit we can increase the performance of VCS by 15-18 %. Comparison was made using other eco friendly refrigerant it may reached upto 22 %. Also by using nanoparticles, one can reduce the evaporator size as well as condenser size for the fixed cooling capacity which helps for reducing the minimum cost of manufacturing. Nanofluid is a fluid containing nanometer-sized particles, called nano-particles. These fluids are engineered colloidal suspensions of nano-particles in a base fluid. The nanoparticles used in nanofluids are typically made of metals, oxides, carbides, or carbon nanotubes. Common base fluids include water, ethylene glycol and oil. Nanofluids have novel properties that make them potentially useful in many applications in heat transfer, including microelectronics, fuel cells, pharmaceutical processes, and hybrid-powered engines, engine cooling/vehicle thermal management, domestic refrigerator, chiller, heat exchanger, in grinding, machining and in boiler flue gas temperature reduction. They exhibit enhanced thermal conductivity and the convective heat transfer coefficient compared to the base fluid. Knowledge of the rheological behaviour of nanofluids is found to be very critical in deciding their suitability for convective heat transfer applications.

In analysis such as computational fluid dynamics (CFD), nanofluids can be assumed to be single phase fluids. However, almost all of new research papers, uses two-phase assumption. Classical theory of single phase fluids can be applied, where physical properties of nanofluid are taken as a function of properties of both constituents and their concentrations. An alternative approach simulates nanofluids using a two-component model.

Synthesis of nanofluids:

Nanofluids are supplied by two methods called the one-step and two-step methods. Several liquids including water, ethylene glycol, and oils have been used as base fluids. Nanomaterials used so far in nanofluid synthesis include metallic particles, oxide particles, carbon nanotubes, grapheme nano-flakes and ceramic particles.

3. Literature Review

Few studies have been illustrated as a part of literature review related to theoretical study and experimental investigation of refrigeration systems based on first law and second law analysis with different ecofriendly refrigerants. M.Ghanbarpour (2014) investigated thermal properties and rheological behavior of water based Al_2O_3 nanofluid as a heat transfer fluid and found that Thermal conductivity and convective heat transfer of nanofluid increases due to increase in mass concentration of nanofluids. Mishra[12]. presented the Effect of different nano-particle shapes on shell and tube heat exchanger using different baffle angles and operated with nanofluid, By analyzing the effect of nanoparticle in terms of volume fraction on overall heat transfer coefficient, entropy generation & heat transfer rate and found that by increasing the volume fraction of nanoparticle the overall heat transfer coefficient & heat transfer rate increases and entropy generation decreases. Mishra [13] had experimentally investigated increase in heat transfer coefficient by using Fe_2O_3/water nanofluid in an air finned heat exchanger concluded that the nanofluid have greater heat transfer coefficient compared with water and also found that the increasing the inlet liquid temperature decreases the overall heat transfer coefficient and increasing liquid and air Reynold number also increases the overall heat transfer coefficient

Mishra[7] presented an experimental analysis of the influence of an internal heat exchanger on the performance of a vapour compression system using R1234yf as a drop-in replacement for R134a and compared the energy performance of a monitored vapour compression system using both refrigerants,R134a and R1234yf, with and without the presence of an internal heat exchanger under a wide range of working conditions. He has carried out experimental tests by varying the condensing temperature, the evaporating temperature and the use of internal heat exchanger. And observed the reductions in cooling capacity and COP between 6% to 13%, when R134a is replaced by the drop-in fluid R1234yf, although the presence of an heat exchanger can help to lessen these reductions between 2 and 6%. Mishra [16] studied Heat transfer and flow characteristics of AL_2O_3–water nanofluid in a double tube heat exchanger and evaluated viscosity, relative viscosity of nanofluid at different mass fraction and sizes of nanoparticles and found that viscosity, Nusselt number increases due to mass fraction and size of nanoparticles. For a given refrigerating mass faction of nanoparticles, viscosity, Nusselt number. Reynolds number increases of base fluid. Chopra [1] explained the nature of the effect of fouling on performance parameters (such as compressor power consumption and COP) as well as properties (such as condenser pressure and superheat temperature at the compressor exit) using a simple vapour compression cycle in order to augment theoretical studies found in the open literature. The results of the experiments indicate that the above-mentioned quantities demonstrate a logarithmic behavioural change when the ambient and room

temperatures are kept constant. Chopra[5] presented a comparable evaluation of R600a (isobutane), R290 (propane), R134a, R22, for R410a, and R32 and optimized finned-tube evaporator by analyzing the evaporator effect on the system coefficient of performance (COP) without accounting for evaporator effects, the COP spread for the studied refrigerants was as high as 11.7% by including evaporator effects, the COP of R290 was better than that of R22 around 3.5%, while the remaining refrigerants performed approximately within a 2% COP band of the R22 baseline for the two condensing temperatures considered. Mishra[15] had evaluated the performance parameters of a vapour compression refrigeration system with different lubricants including nanolubricants and derived conclusions that the R134a refrigerant and mineral oil mixture with nanoparticles worked normally and Freezing capacity of the refrigeration system is higher with SUNISO 3GS + alumina nanoparticles oil mixture compared the system with POE oil. The power consumption of the compressor reduces by 25% when the nanolubricant is used instead of conventional POE oil and the coefficient of performance of the refrigeration system also increases by 33% when the conventional POE oil is replaced with nano refrigerant (v) the energy enhancement factor in the evaporator is 1.53.

Mishra[13] had investigated the use of nanofluids as secondary coolants in vapor compression refrigeration systems and developed simulation model for a liquid-to-water heat pump, with reciprocating compressor and double-tube condenser and evaporator and conducted studied of different nanoparticles (Cu, Al_2O_3, CuO and TiO_2) in terms of different volume fraction and particle diametersand observed that that, for a given refrigerating capacity, evaporator area and refrigerant-side pressure drop are reduced when: (i) the volume fraction of nanoparticles increase; (ii) the diameter of nanoparticles decrease. Similarly the nanofluid side pressure drop and, consequently, pumping power, increase with nanoparticle volume fraction and decrease with nanoparticle size. Mishra [17] had proposed a lumped model for vapour compression refrigeration system to find out the effect of variable compressor speed, mass flow rate of brine, mass flow rate of water, inlet water temperature, inlet brine temperature on the C.O.P of lumped model. Simulation program have been prepared and result are plotted for the same. Mishra [2, 4, 9] studied the performance degradation due to fouling in a vapour compression cycle has investigated for various applications. Considering the first set of refrigerants i.e. R134a, R410a and R407a, and found that from a first law stand point, the COP indicates that R134a always performs better unless only the evaporator is being fouled and also a second-law standpoint, the second-law efficiency indicates that R134a performs the best in all cases. For second set of refrigerants (i.e. R717, R404a and R290) from a first law standpoint, the COP of R717 is better unless only the evaporator is being fouled. In contrast to this, from a second-law standpoint, the second-law efficiency of R717 is best in all cases.

Volumetric efficiency of R410a and R717 remained the highest under the respective conditions and performance degradation of the evaporator has a larger effect on compressor power requirement while that of the condenser has an overall larger effect on the COP. A.S. Dalkilic et al (2010) also presented a theoretical performance studies on a traditional vapour compression refrigeration system with refrigerant mixtures based on HFC134a, HFC152a, HFC32, HC290, HC1270, HC600, and HC600a for various ratios and their results are compared with CFC12, CFC22, and HFC134a as possible alternative replacements.

In spite of the HC refrigerants' highly flammable characteristics, they are used in many applications, with attention being paid to the safety of the leakage from the system, as other refrigerants in recent years are not related with any effect on the depletion of the ozone layer and increase in global warming. Lot of theoretical results showed that all of the alternate refrigerants investigated in the analysis have a slightly lower performance coefficient (COP) than CFC12, CFC22, and HFC134a for the condensation temperature of 50 °C and evaporating temperatures ranging between −30 °C and 10 °C. Refrigerant blends of HC290/HC600a (40/ 60 by wt.%) instead of CFC12 and HC290/HC1270 (20/80 by wt.%) instead of CFC22 are found to be replacement refrigerants among other alternatives. The following conclusions were drawn from literature review

1. Performance analysis of VCS has been done for different type of refrigerant its combination/mixture.
2. Performance parameter of nanofluid for different concentration of nano particles.
3. Many of the literatures present also show heat transfer enhancement property using nanofluid.
4. But almost none of the literature represents the use of nanofluid (containing nanoparticle) as a secondary fluid in VCS (chiller system) for different types of eco friendly refrigerants and also the effect of this secondary fluid on the energetic efficiency of VCS and the effect of nanoparticle plated material used in condenser and evaporator on the performance of VCS.

4. Research Gaps Identified

Lots of researches have been done and going on based on the performance evaluation of various combinations of different types of refrigerant and also nanoparticle behavior on the nanofluid. On the other hand the performance of VCS using nanofluid (with different nanoparticle) for different types of eco friendly refrigerant is yet to be analyzed. Th use nano fluid in VCS (chiller system) is presented in this paper and, the performance evaluation of vapour compression refrigeration system is explored by using new and alternative ecofriendly refrigerants HFO1234yf, HFO1234ze backed by the fact that they are more environments friendly can replaced. R134a, R407c, R404a and R125 in the coming future. This paper presents following research objectives.Thermodynamic analysis of simple vapour compression system using twelve ecofriendly alternative refrigerants.Thermodynamic analysis in terms of % improvement in first law efficiency and second law efficiency by using exergetic analysis of simple vapour compression system using Al_2O_3 as nanofluid and comparison of results of performance evaluation in terms of reduction in irreversibility without nanofluid and with nanofluids.

5. Results and Discussions

The performance **of** HFO1234yf, HFO1234ze backed by the fact that they are more environments friendly can

replaced. R134a, without nano fluid are presented in the Fig-1-8 and with nano mixed with water is also presented in Table-1-4 respectively. From Fig-(1), it was observed that first law efficiency in terms of COP increases with increasing evaporator temperature and decreases with increasing condenser temperature. Similarly from fig -2, the second law efficiency id decreases with increasing evaporator. The system defect in terms of exergy destruction ratio is increases as shown in Fig-3. The increases in superheating in evaporator at condenser inlet, the first law efficiency (i.e. COP) and second law efficiency is increases as shown in Fig (4-5) respectively. Similarly by increasing condenser temperature the first law efficiency (COP) and exergetic efficiency of system is decreases as shown in Fig-(6)& (7) respectively.

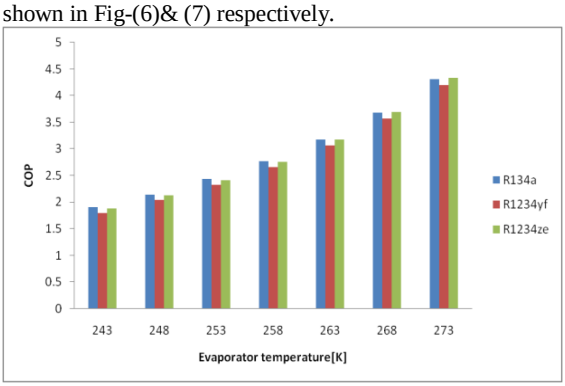

Fig: 1. Variation of COP with evaporators' Temperatures

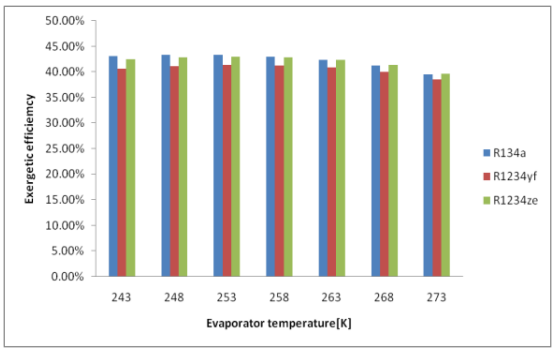

Fig: 2. Variation of exergetic efficiency with evaporators' temperatures

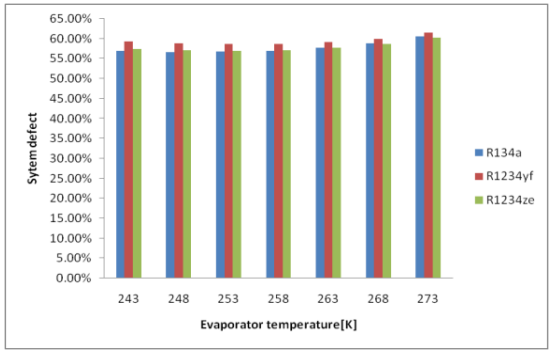

Fig: 3. Variation of system defect with evaporator temperatures

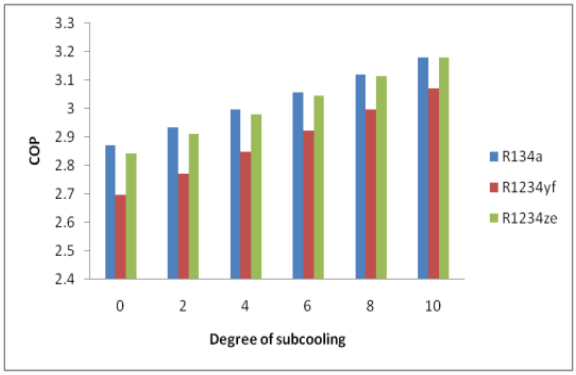

Fig: 4. Variation of COP with degree of subcooling at condenser outlet

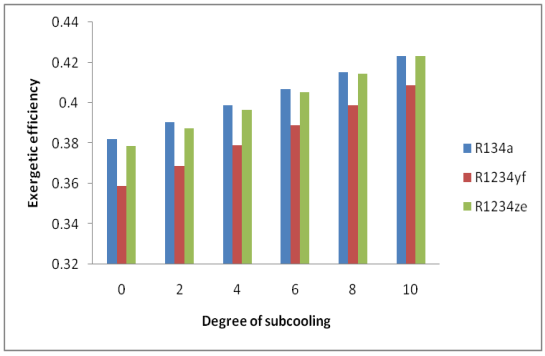

Fig: 5. Variation of exergetic efficiency with degree of subcooling at condenser outlet

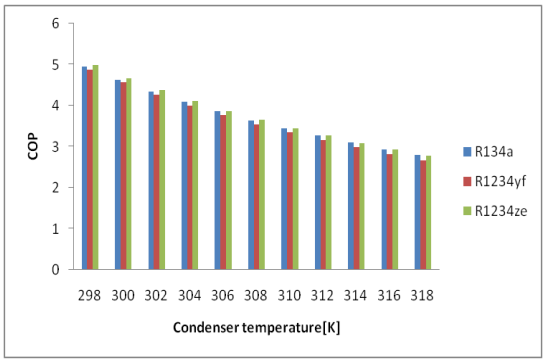

Fig: 6. Variation of COP with condenser temperature

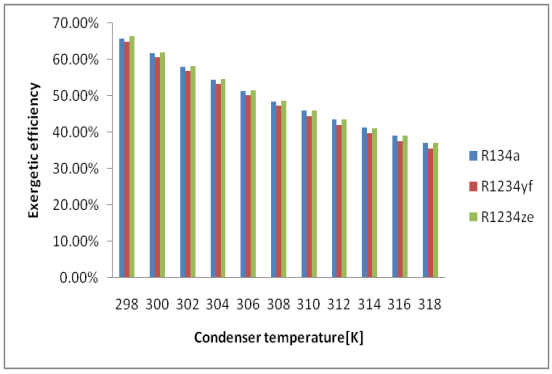

Fig: 7. Variation of exergetic efficiency with condenser temperature

Table-1 shows the % improvement in first law efficiency in terms of cop improvement by using nano particles mixed with R718 in the secondary evaporator circuit it was observed that first law efficiency without nano particles using R152a is maximum while by using R410a is minimum however second highest is found to be by using R290 as hydrocarbon in the primary evaporator circuit. The use of R407c as ecofriendly refrigerants is quite adequate while first law performance improvement is around 13.491% by using nano particles. The % improvement in first law efficiency is found to be 11.04% by using nano particles as compared to without nano particles. While by using R134a 12.60% improvement was observed. The use of hydrocarbons (R290, R600a and R600) and R152a is prohibited due to flammable nature, therefore other ecofriendly R134a, R404a, R407c, R507a and R125 refrigerants are used due to reduction in global warming and ozone depletion. Due to1300 global warming potential of R134a, the next alternate refrigerant R1234yf (GWP=4, and ODP=0) is suitable which can replace R134a in the coming future. It was also observed that without using nano particles, the first law performance by using R1234ze is better than R1234yf.

Table: 1. Performance evaluation (% Improvements in first law efficiency) of vapour compression refrigeration system using ecofriendly refrigerant in the primary circuit and water flowing in the condenser in secondary circuit and brine flow in the secondary circuit in the evaporator using Al_2O_3 as nano material of 10 micron size

Refrigerant	COP with Al_2O_3 nano	COP without nano	% Improvement in first law efficiency
R1234yf	4.002	3.604	11.0432
R1234ze	3.836	3.434	11.7064
R134a	4.36	3.872	12.6033
R404a	4.316	3.862	11.7555
R407c	4.736	4.173	13.4914
R152a	5.169	4.531	14.0807
R507a	4.328	3.868	11.8924
R125	4.044	3.646	10.916
R600a	4.009	3.617	10.8377
R600	3.605	3.217	12.0609
R290	4.826	4.274	12.9153

Table-2: shows the second law efficiency in terms of exergetic efficiency for twelve ecofriendly refrigerant and second law performance improvement while by using nano particles, in terms of exergetic efficiencyand maximum exergetic efficiency is found by using R152a as ecofriendly refrigerant and second highest is also found by using R290 hydrocarbon as ecofriendly refrigerant in the primary evaporator circuit. The second law performance by using R134a, R404a, R507a and R125 as nearly similar with small variations. while R152a and hydrocarbon is prohibited due to flammable nature, and also R134a, R404a , R507a and R125 are having higher global warming potential , therefore R1234yf and R1234ze can replace these refrigerants in the future. It was also observed that second law performance is better due to 39.13% improvement by using R1234yf as compared to 16.52% improvement by using R1234ze in the primary evaporator circuit.

Table: 2a. Performance evaluation (% Improvements in second law efficiency) of vapour compression refrigeration system using ecofriendly refrigerant in the primary circuit and water flowing in the condenser in secondary circuit and brine flow in the secondary circuit in the evaporator using Al_2O_3 as nano material of 10 micron size

Eco friendly Refri-gerants	Exergetic efficiency with Al2O3 nano particles	Exergetic efficiency without nano	% improve-ment in second law efficiency
R1234yf	0.3360	0.2415	39.1304
R1234ze	0.3174	0.2724	16.5198
R134a	0.3761	0.3215	16.9828
R404a	0.3712	0.3204	15.8551
R407c	0.4162	0.3552	17.1734
R152a	0.4666	0.3952	18.0668
R507a	0.3725	0.3211	16.0074
R125	0.3407	0.2962	15.0236
R600a	0.3368	0.2930	14.9488
R600	0.2916	0.2481	17.5332
R290	0.4282	0.3665	16.8349

Table: 2b. Performance evaluation (% Improvements) of vapour compression refrigeration system using ecofriendly refrigerant in the primary circuit and water flowing in the condenser in secondary circuit and brine flow in the secondary circuit in the evaporator using Al_2O_3 as nano material of 10 micron size

Refrige Eco Friendly refri-gerants	Exergetic efficiency with nano	Exergetic efficiency without nano	% improve Ment in second law effectiveness
R1234yf	0.4479	0.4035	11.0037
R1234ze	0.4294	0.3844	11.7065
R134a	0.4880	0.4334	12.59806
R404a	0.4831	0.4323	11.7511
R407c	0.5301	0.4671	13.487476
R152a	0.5786	0.5072	14.077287
R507a	0.4844	0.4330	11.87067
R125	0.4527	0.4087	10.765843
R600a	0.4486	0.4049	10.79279
R600	0.4036	0.3601	12.07998
R290	0.5402	0.4784	12.91806

Table: 3. Reduction in irreversibility in terms of exergy destruction ratio of vapour compression refrigeration system using ecofriendly refrigerant in the primary circuit and water flowing in the condenser in secondary circuit and brine flow in the secondary circuit in the evaporator using Al_2O_3 as nano material of 10 micron size

Refrigerant	EDR with nano	EDR without nano	% reduction In EDR
R1234yf	1.976	2.43	18.6831
R1234ze	2.15	2.67	19.4756
R134a	1.659	2.11	21.3744
R404a	1.694	2.12	20.0943
R407c	1.391	1.816	23.403

R152a	1.143	1.53	25.2941
R507a	1.685	2.114	20.2932
R125	1.935	2.377	18.5948
R600a	1.969	2.413	18.4003
R600	2.429	3.03	19.8349
R290	1.335	1.729	22.7877

Table: 3. represents the reduction in the irreversibility in terms of exergy destruction ratio in the system and maximum exergy destruction ratio around 25.294% was observed by using R152a and exergy destruction ratio is 22.79% by using R290 hydrocarbon and 23.403% by using R407c as ecofriendly refrigerant. The Reduction in EDR is 20.09% by using R404a and 21.37% by using R134a. The R1234ze and R1234yf have slightly less reduction in EDR as compaired by using R134a

6. Conclusions

In this paper, first law and second law analysis of vapour compression refrigeration system with and without nano particles using ecofriendly refrigerants (R134a, R1234yf, and R1234ze) have been presented. And following conclusions have been drawan:

(i) First law and second law efficiency for vapour compression refrigeration system without Al_2O_3 nano particles mixed in R718 in the secondary evaporator circuit and ecofriendly refrigerants in the primary circuit (i.e. R134a and R1234ze) are matching the same values, both are better than that for R123yf which has low GWP (i.e. GWP =4) is showing 2–6% higher value of first law efficiency (i.e.COP) and second law efficiency (i.e. exergetic efficiency) in comparison to R123yf.

(ii) Both energetic and exergetic increase with increase in degree of subcoolingIt was found that energetic and exergetic efficiency greatly affected by changes in evaporator and condenser temperature. R1234ze is the best among considered refrigerant since it has 218 times lower GWP values than R134a and R1234ze is ecofriendly has both ODP and GWP are lowest.

(iii) The R1234yf and R1234ze can replace R-134a after 2030 due to low global warming potential.

References

[1] K. Chopra, V. Sahni, R. S. Mishra, Energetic and Exergetic Based Comparison Multiple Evaporators with Compound Compression and Flash Intercooler with Individual or Multiple Throttle Valves International Journal of Advance Research & Innovations, 1, 2013, 73-81

[2] R.S. Mishra Irriversibility Analysis of Multi-Evaporators Vapour Compression Refrigeration Systems Using New and Refrigerants: R134a, R290, R600, R600a, R1234yf, R502, R404a and R152a and R12, R502" International Journal of Advance Research & Innovations International Journal of Advance Research & Innovations, 1, 2013, 180-193

[3] K. Chopra, V. Sahni, R. S. Mishra, Energetic and Exergetic Based Comparison Multiple Evaporators with Compound Compression and Flash Intercooler with Individual or Multiple Throttle Valves International Journal of Advance Research & Innovations, 1, 2013, 73-81

[4] R. S. Mishra, Irriversibility Analysis of Multi-Evaporators Vapour Compression Refrigeration Systems Using New and Refrigerants: R134a, R290, R600, R600a, R1234yf,R502, R404a and R152a and R12, R502" International Journal Advance Research & Innovations International Journal of Advance Research & Innovations, 1, 2013, 180-193

[5] K. Chopra, V. Sahni, R. S. Mishra, Thermodynamic Analysis of Multiple evaporators vapour compression Refrigeration Systems with R-410a, R290, R1234yf, R502, R404a, R152a and R134a, International Journal of Air conditioning and Refrigeration, 22(1), 2014, 14

[6] K. Chopra, V. Sahni, R. S. Mishra, Methods for improving first and second law efficiencies of vapour compression refrigeration systems using flash-intercooler with ecofriendly refrigerants, 1, 2014, 50-64

[7] R. S. Mishra, Thermodynamic performance evaluation of multiple evaporators, single compressor ,single expansion valve and liquid vapour heat exchanger in vapour compression refrigeration systems using thirteen ecofriendly refrigerants for reducing global warming and ozone depletion, International Journal of Advance Research & Innovations, 1, 2014, 163-171

[8] R. S. Mishra, Thermal Performance of Low Cost Rocked Bed Thermal Energy Storage Systems for Space Heating and Crop Drying Applications in the Rural Areas, International Journal of Advance Research & Innovations, 1, 2013, 172-177

[9] R. S. Mishra, Thermodynamic performance evaluation of multiple evaporators, single compressor ,single expansion valve and liquid vapour heat exchanger in vapour compression refrigeration systems using thirteen ecofriendly refrigerants for reducing global warming and ozone depletion, International Research Journal of Sustainable Science & Engineering, 2(3), 2014, 1-10

[10] R. S. Mishra, Methods for improving thermal performance of six vapour compression refrigeration System using Multiple evaporators compressor systems, Journal of Multi Disciplinary Engineering Technologies, 7(2), 2013, 1-11

[11] R. S. Mishra, Methods for improving thermal performance of seven vapour compression refrigeration Systems of multiple evaporators –compressors and expansion valves in series and parallel combinations with eleven ecofriendly refrigerants for reducing ozone depletion, Journal of Rasayan, 2014, 15-30

[12] R. S. Mishra, Methods for improving thermodynamic performance of vapour compression refrigeration systems using thirteen ecofriendly refrigerant refrigerants in primary circuit and TiO2 nano particles mixed with R-718 used in secondary evaporator circuit for reducing global warming and ozone depletion, International Journal of Advance Research & Innovations, 2(4), 732-735

[13] R. S. Mishra, Methods for Improving Thermodynamic Performance of Vapour Compression Refrigeration Systems Using R134a Ecofriendly Refrigerant in Primary Circuit and Three Nano Particles Mixed with R718 used in Secondary Evaporator Circuit for

Reducing Global Warming and Ozone Depletion, 2(4), 784-789

[14] R. S. Mishra, Appropriate Vapour Compression Refrigeration Technologies for Sustainable Development International Journal of Advance Research & Innovations, 2014, 551-556

[15] R. S. Mishra, V. Jain, S. S. Kachhwaha, Comparative Performance Study of Vapour Compression Refrigeration System With R22/R134a/R410a/R407c/ M20, International Journal of Energy and Environment, 2, 2011, 297-310

[16] R S. Mishra, Methods for Improving Thermodynamic Performance of Vapour Compression Refrigeration System Using Twelve Ecofriendly Refrigerants in Primary Circuit And Nanofluid (Water-Nano Particle Based) in Secondary Circuit, International Journal of Engineering Technology and Advanced Research, 4, 2014, 878-890

[17] R. S. Mishra, Methods for improving thermodynamic performance of vapour compression refrigeration systems using thirteen ecofriendly refrigerants in primary circuit and TiO2 nano particles mixed with R718 used in secondary evaporator circuit for reducing global warming and ozone depletion, International Journal of Advance Research & Innovations, 3, 2015

[18] R.S. Mishra, Methods for improving thermodynamic performance of vapour compression refrigeration systems using thirteen ecofriendly refrigerants in primary circuit and TiO2 nano particles mixed with R718 used in secondary evaporator circuit for reducing global warming and ozone depletion, International Journal of Advance Research & Innovations, 2015

Operational Transresistance Amplifier Based PID Controller

Rajeshwari PANDEY[1], *Neeta PANDEY*[1], *Saurabh CHITRANSHI*[1], *Sajal K. PAUL*[2]

[1]Department of Electronics and Communication Engineering, Shahbad Daulatpur, Delhi Technological University, Bawana Road, DL - 42, Delhi, India
[2]Department of Electronics Engineering, Indian School of Mines, Dhanbad – 826004, Jharkhand, India

rpandey@dce.ac.in, neetapandey@dce.ac.in, chitransi.dtu@gmail.com, sajalkpaul@rediffmail.com

DOI: 10.15598/aeee.v13i2.1164

Abstract. *This paper presents Operational transresistance amplifier (OTRA) based proportional-integral-derivative (PID) controller with independent electronic tuning of proportional, integral, and derivative constants. The configuration can be made fully integrated by implementing the resistors using matched transistors operating in the linear region. Theoretical propositions are verified through SPICE simulations using 0.18 μm process parameters from MOSIS (AGILENT). In order to demonstrate the workability of the proposed controller, its effect on step response of an OTRA based second order system is analyzed and presented.*

Keywords

OTRA, PD, PI, PID, second order system.

1. Introduction

A controller monitors and modifies the operational conditions of a given dynamical system. These operational conditions are referred to as measured output variables and can be modified by adjusting certain input variables. The controller calculates the difference between a measured output variable and a desired set point as an error value and attempts to minimize the error by adjusting the process control inputs. In general controllers can be classified as (i) conventional and (ii) non-conventional controllers. For conventional controllers, such as PID controller, a prior knowledge of the mathematical model of the process to be controlled is required in order to design a controller whereas for unconventional controllers this information is generally not needed. P, PI, PD, and PID are few typical examples of conventional controllers, and neuro-fuzzy controllers are representatives of the unconventional class. The controllers based on proportional-integral-derivative (PID) algorithm are most popularly used in the process industries. These are used to control various processes satisfactorily with proper tuning of controller parameters. Generally operational amplifiers (OPAMPs) are used to design classical analog controllers [1], [2]. However the OPAMPs, being voltage mode circuit, have their limitations of constant gain bandwidth product (f_T) and low slew rate. This inaccurately limits the speed of the OPAMP-based controllers and might influence the dynamics of the system [3]. It is well known that inherent wide bandwidth almost independent of closed loop gain; greater linearity and large dynamic range are the key performance features of current mode technique [4]. Therefore, the current mode building blocks would be a good alternative of OPAMP for designing the analog controllers. Literature survey reveals that number of current mode circuits have been reported relating to PID controllers [3], [5], [6], [7], [8]. Operational transconductance amplifier (OTA) based controllers are proposed in [5] and are electronically tunable. However, these provide voltage output at high impedance making a buffer necessary to drive the voltage input circuits. The current difference buffered amplifier (CDBA) based PID controller presented in [6] uses an excessively large number of active and passive components. References [3], [7], [8] present current conveyor II (CCII) based PID controllers. Two different structures are proposed for voltage and current outputs respectively in [7], [8] whereas [3] presents only voltage output configuration. All the CCII based voltage mode designs deliver output voltage at high impedance and are thus not suitable for driving voltage input circuits. The OTRA is yet another, relatively recently proposed current mode build-

Tab. 1: Comparison of proposed work with existing literature.

Reference	Active block used	No. of Active block used	Passive elements	Outputs	Output Impedance	Electronic Tunability
[1]	Opamp	4	8R, 2C	Voltage	Low	No
[3]	Opamp	1	3R, 3C	Voltage	Low	No
[5]	OTA	8	2C	Voltage	High	Yes
[6]	CDBA	4	8R, 2C	Voltage	Low	No
[7]	CCII	3	4R, 2C	Fig. 2: Current Fig. 3: Voltage	High High	No No
[8]	CCII	3	4R, 2C	Fig. 2: Current Fig. 3: Voltage	High High	No No
Proposed work	OTRA	2	4R, 3C	Voltage	Low	Yes

ing block which is a high gain current input, voltage output amplifier [9].

Being a current processing analog building block, it inherits the advantages of the current mode technique. Additionally it is also free from the effects of parasitic capacitances at the input due to virtually internally grounded input terminals [10] and hence the non-ideality problem is less in circuits implemented using OTRA. Therefore, this paper aims at presenting OTRA based PID controller with orthogonally tunable proportional, integral and derivative constants. The proposed circuit can be made fully integrated by implementing the resistors using MOS transistors operating in the non-saturation region. This also facilitates electronic tuning of the controller parameters. A detailed comparison of the PID controllers available in the literature is given in Tab. 1 which suggests that OTRA based structure is the most suitable choice for voltage mode operation.

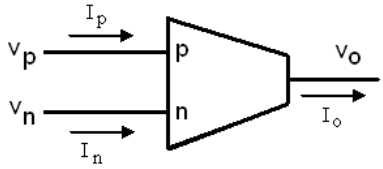

Fig. 1: The OTRA circuit symbol.

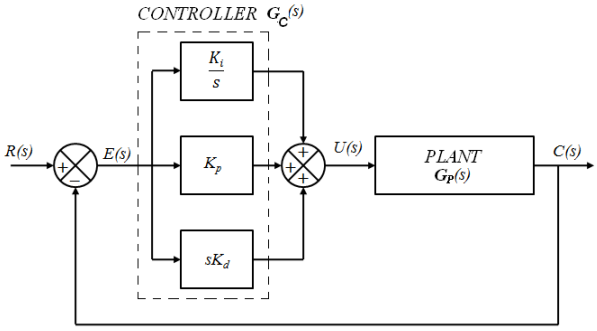

Fig. 2: Block diagram of a closed loop system with PID controller.

2. Proposed Circuits

The OTRA is a three terminal device shown symbolically in Fig. 1 and its port relations can be characterized by the matrix as follows:

$$\begin{bmatrix} V_p \\ V_n \\ V_0 \end{bmatrix} = \begin{bmatrix} 0 & 0 & 0 \\ 0 & 0 & 0 \\ R_m & -R_m & 0 \end{bmatrix} \begin{bmatrix} I_p \\ I_n \\ I_0 \end{bmatrix}, \qquad (1)$$

where R_m is the transresistance gain of the OTRA. For ideal operations, R_m approaches infinity and forces the input currents to be equal. Thus, OTRA must be used in a negative feedback configuration [9], [10].

2.1. PID Controller

In a given system the proportional action improves the rise time of the system, the integral action improves the steady-state error whereas the derivative action improves the degree of stability. So, none alone is capable of achieving the complete improvement in system performance [11]. This leads to the motivation of using a PID controller so that the best features of each of the PI and PD controllers are utilized. In a PID controller as shown in Fig. 2 the proportional, integral and the derivative of the error signal $E(s)$ are summed up to calculate the output actuating signal $U(s)$ of the controller which controls the plant's $(G_P(s))$ function. Thus, the transfer function $G_C(s)$ of the PID controller can be written as:

$$G_C(s) = K_p + \frac{K_i}{s} + sK_d, \qquad (2)$$

where K_p, K_i, and K_d are the proportional, integral and derivative constants respectively.

In the following subsection first an OTRA based PI controller is introduced followed by a PD controller. By combining these two controllers, the proposed PID controller is designed.

1) Proposed PI Controller

The PI controller comprises of proportional and integral actions and can be derived from the controller block of Fig. 2 if the derivative block is excluded. The transfer function $G_{PI}(s)$, of the PI controller so obtained is given by:

$$G_{PI}(s) = K_p + \frac{K_i}{s}. \tag{3}$$

The OTRA based proposed PI controller is shown in Fig. 3.

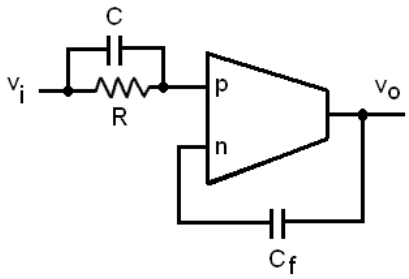

Fig. 3: Proposed PI controller.

Using routine analysis the voltage transfer function of the proposed controller can be as expressed as:

$$G_{PI}(s) = \frac{V_o}{V_i} = \frac{C}{C_f} + \frac{1}{s \cdot C_f \cdot R}. \tag{4}$$

From Eq. (4) the controller parameters can be computed as:

$$K_p = \frac{C}{C_f},\ K_i = \frac{1}{R \cdot C_f}. \tag{5}$$

It is clear from Eq. (5) that K_p value can be adjusted independently of K_i by varying C, and K_i can be independently controlled by varying R.

2) Proposed PD Controller

A PD controller can be obtained if proportional and derivative actions only are taken into consideration in Fig. 2. Transfer function of a PD Controller $G_{PD}(s)$, can be represented as:

$$G_{PD}(s) = K_p + s \cdot K_d. \tag{6}$$

Figure 4 shows the proposed PD controller circuit and the transfer function of this controller is obtained as:

$$G_{PD}(s) = \frac{V_o}{V_i} = \frac{R_f}{R} + s \cdot C \cdot R. \tag{7}$$

The controller parameters can be expressed as:

$$K_p = \frac{R_f}{R},\ K_d = s \cdot C \cdot R. \tag{8}$$

From Eq. (8) it is clear that by varying R, K_p value can be adjusted independently of K_d and by simultaneous variation of R_f and R such that R_f/R remains constant, K_d can be independently controlled.

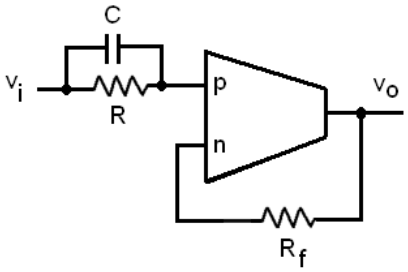

Fig. 4: Proposed PD controller.

3) Proposed PID Controller

The proposed OTRA based PID Controller can be derived by combining the proposed PI and PD controllers and is shown in Fig. 5. The routine analysis of this circuit gives the transfer function of the controller as:

$$G_{PID}(s) = \frac{V_o}{V_i} == \left(\frac{R_4}{R_2} + \frac{R_4 \cdot C_1}{R_3 \cdot C_1}\right) + \frac{R_4}{s \cdot C_3 \cdot R_1 \cdot R_3} + s \cdot C_2 \cdot R_4, \tag{9}$$

from Eq. (9) the controller parameters can be identified as:

$$K_p = \frac{R_4 \cdot C_1}{R_3 \cdot C_3} + \frac{R_4}{R_2},\quad K_i = \frac{R_4}{C_3 \cdot R_1 \cdot R_3},\quad K_d = C_2 \cdot R_4. \tag{10}$$

It is observed from Eq. (10) that the K_p value can be adjusted independently by varying R_2, independent tuning of K_i is possible through R_1 variation whereas K_d can be controlled independently by simultaneous variation of R_2, R_3 and R_4, such that R_4/R_2 and R_4/R_3 remain constant.

2.2. MOS-C Implementation and Electronic Tuning of the Proposed Controllers

It is well known that the linear passive resistor consumes a large chip area as compared to the linear resistor implementation using transistors operating in the non-saturation region. The differential input of OTRA

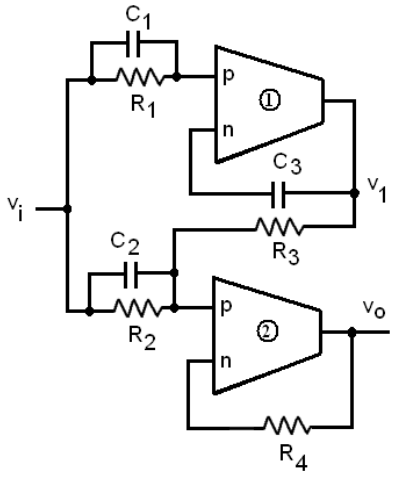

Fig. 5: Proposed PID controller.

allows the resistors connected to the input terminals of OTRA to be implemented using MOS transistors with complete non-linearity cancelation [10]. Figure 6(a) shows a typical MOS implementation of resistance connected between negative input and output terminals of OTRA. The resistance value may be adjusted by appropriate choice of gate voltages thereby making controller parameters electronically tunable. The value of resistance so obtained is given by:

$$R = \frac{1}{\mu_n \cdot C_{ox} \cdot \left(\frac{W}{L}\right) \cdot (V_a - V_b)}, \tag{11}$$

where V_a and V_b are control gate voltages; the parameters μ_n, C_{ox}, W, and L represent electron mobility, oxide capacitance per unit gate area, effective channel width, and effective channel length respectively and their value are expressed as:

$$\mu_n = \frac{\mu_0}{\theta\,(V_{GS} - V_T)}, \tag{12}$$

$$C_{ox} = \frac{\varepsilon_{ox}}{t_{ox}}, \tag{13}$$

$$W = W_{Drawn} - 2W_D, \tag{14}$$

$$L = L_{Drawn} - 2L_D, \tag{15}$$

where the symbols have their usual meaning.

The MOS transistors based implementation of linear resistors not only reduces the chip area but also makes controller parameters electronically tunable. The MOS-C implementation of the circuit of Fig. 5 is shown in Fig. 6(b).

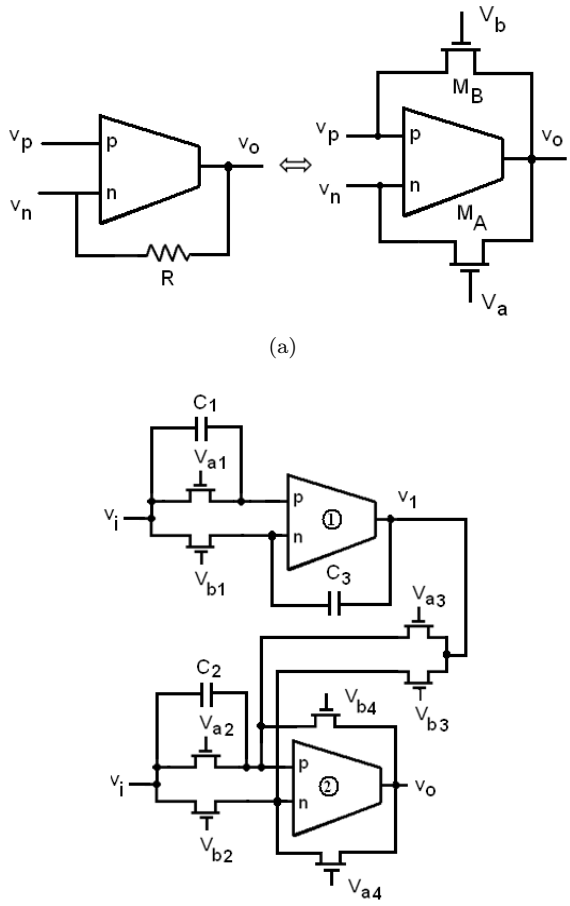

Fig. 6: MOS implementation of (a) linear resistance, (b) proposed PID controller.

3. Nonideality Analysis of PID Controller

The non-idealities associated with OTRA based circuits may be divided into two groups. The first group results due to finite trans-resistance gain whereas the second one concerns with the nonzero impedances of p and n terminals of OTRA.

3.1. Nonideality due to Finite Transresistance Gain

Here the effect of finite transresistance gain (R_m) on PID controller is considered, and passive compensation is employed for high-frequency applications. Ideally the R_m is assumed to approach infinity. However, practically R_m is a frequency dependent finite value. Considering a single pole model for the trans-resistance gain, it can be expressed in Eq. (16):

$$R_{\mathrm{m}} = \frac{R_0}{1 + \frac{s}{\omega_0}}, \tag{16}$$

$$R_m(s) \approx \frac{1}{s \cdot C_p}. \tag{17}$$

$$\begin{aligned} G_{PID}(s)_{NI} = \frac{V_o}{V_i} = &\left(\frac{R_4}{R_2 \cdot (1 + s \cdot C_{p2} \cdot R_4)} + \frac{R_4 \cdot C_1}{R_3 \cdot (C_3 + C_{p1}) \cdot (1 + s \cdot C_{p2} \cdot R_4)} \right) \\ &+ \frac{R_4}{s \cdot R_1 \cdot R_3 \cdot (C_3 + C_{p1}) \cdot (1 + s \cdot C_{p2} \cdot R_4)} + \frac{s \cdot C_2 \cdot R_4}{(1 + s \cdot C_{p2} \cdot R_4)}, \end{aligned} \tag{18}$$

$$\begin{aligned} \frac{V_o}{V_i} = &\frac{R_4}{R_2 \cdot (1 + s \cdot (C_{p2} - Y) \cdot R_4)} + \frac{R_4 \cdot C_1}{R_3 \cdot (C_3 + C_{p1}) \cdot (1 + s \cdot (C_{p2} - Y) \cdot R_4)} \\ &+ \frac{R_4}{s \cdot R_1 \cdot R_3 \cdot (C_3 + C_{p1}) \cdot (1 + s \cdot (C_{p2} - Y) \cdot R_4)} + \frac{s \cdot C_2 \cdot R_4}{(1 + s \cdot (C_{p2} - Y) \cdot R_4)}. \end{aligned} \tag{19}$$

where R_0 is dc transresistance gain. For high-frequency applications the transresistance gain reduces to Eq. (17).

The term C_p represents parasitic capacitance associated with OTRA and is given by $C_p = R_0\omega_0$. Taking this effect into account Eq. (9) modifies to Eq. (18), where C_{p1} and C_{p2} are the parasitic capacitances of OTRA1 and OTRA2 respectively.

For high-frequency applications, compensation methods must be employed to account for the error introduced in Eq. (9). The effect of C_{p1} can be eliminated by pre-adjusting the value of capacitors C_3 and thus achieving self-compensation. The sC_{p2} term appearing in parallel to R_4 will result in the introduction of a parasitic pole having radian frequency as $\omega = 1/R_4C_{p2}$. The effect of C_{p2} can be eliminated by connecting an admittance Y between the non-inverting terminal and the output as shown in Fig. 7. Considering the circuit of Fig. 7, Eq. (18) modifies to Eq. (19).

By taking $Y = sC_{p2}$, Eq. (19) reduces to Eq. (9) thus eliminating the effect of C_{p2} and hence achieving the passive compensation.

3.2. Effect of Nonzero Impedances of p and n Terminals

Ideally the input as well as output resistances of an OTRA are assumed to be zero. Considering the input (R_n and R_p) and output (R_o) resistances of the OTRA to be finite, the equivalent model of proposed PID controller can be drawn as shown in Fig. 8.

Routine analysis of circuit of Fig. 8 results in terminal currentsIp1 and I_{n1} as:

$$I_{p1} = \frac{V_i \cdot (1 + s \cdot C_1 \cdot R_1)}{R_1 + R_{p1} + s \cdot C_1 \cdot R_1 \cdot R_{p1}}, \tag{20}$$

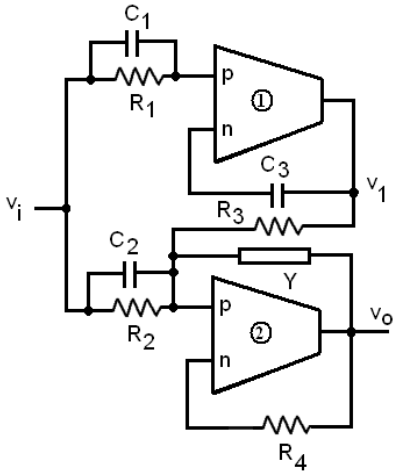

Fig. 7: Compensated PID controller.

$$I_{p1} = \frac{V_i \cdot s \cdot C_3}{1 + s \cdot C_3 \cdot R_{n1}}, \tag{21}$$

where I_{p1} and I_{n1} are the currents and R_{p1} and R_{n1} are the input resistances of p and n terminals respectively of OTRA 1. Considering R_{m1} to be the transresistance gain and R_{o1} is the output resistance of OTRA1, the output voltage of OTRA1, can be computed as:

$$V_1{}' = R_{m1}(I_{p1} - I_{n1}) - R_0 \cdot I_{n1}, \tag{22}$$

$$V_1{}' = R_{m1} \cdot I_{p1} - (R_{m1} + R_0) \cdot I_{n1}, \tag{23}$$

as $R_{m1} >> R_{o1}$, so $R_{m1} + R_{o1} \approx R_{m1}$ and hence:

$$V_1{}' = R_{m1} \cdot (I_{p1} - I_{n1}), \tag{24}$$

$$\begin{aligned} \frac{V_1'}{V_i} = &\frac{R_{m1} \cdot (1 + s \cdot C_1 \cdot R_1)}{R_1 + R_{p1} + s \cdot C_1 \cdot R_1 \cdot R_{p1}} \\ &\cdot \frac{1 + s \cdot C_3 \cdot R_{m1}}{1 + s \cdot C_3 (R_{m1} + R_{n1})}, \end{aligned} \tag{25}$$

$$\frac{V_1'}{V_i} = \frac{(1+s\cdot C_1\cdot R_1)\cdot(1+s\cdot C_3\cdot R_{m1})}{R_1\cdot(1+s\cdot C_1\cdot R_{p1})\cdot\left(\frac{1}{R_{m1}}+s\cdot C_3\right)}, \tag{26}$$

$$V_i' = \frac{(1+s\cdot C_1\cdot R_1)\cdot(1+s\cdot C_3\cdot R_{m1})\cdot V_i}{R_1\cdot(1+s\cdot C_1\cdot R_{p1})\cdot(s\cdot C_3)}, \tag{27}$$

$$I_{p2} = \frac{V_1'R_2 + V_iR_3\,(1+sC_2R_2)}{R_2R_{p2}+R_2R_3+R_{p2}R_3\,(1+sC_2R_2)} = \frac{V_1'R_2 + V_iR_3\,(1+sC_2R_2)}{R_2\,(R_{p2}+R_3)+R_{p2}R_3\,(1+sC_2R_2)}$$

$$\approx \frac{V_1'R_2 + V_iR_3\,(1+sC_2R_2)}{R_2R_3+R_{p2}R_3\,(1+sC_2R_2)} = \frac{V_1'R_2 + V_iR_3\,(1+sC_2R_2)}{R_3\,(R_2+R_{p2})+sC_2R_2R_3R_{p2}} \tag{28}$$

$$\approx \frac{V_1'}{R_3\,(1+sC_2R_{p2})} + \frac{V_i\,(1+sC_2R_2)}{R_2\,(1+sC_2R_{p2})},$$

$$I_{p2} = \frac{(1+sC_1R_1)(1+sC_3R_{m1})V_i}{R_1R_3(1+sC_2R_{p2})(1+sC_1R_{p1})(sC_3)} + \frac{V_i(1+sC_2R_2)}{R_2(1+sC_2R_{p2})}. \tag{29}$$

Substituting I_{p1} and I_{n1}, Eq. (24) results in Eq. (25). As $R_1 >> R_{p1}$ and $R_{m1} >> R_{n1}$, Eq. (25) yields to Eq. (26). It can be further simplified to Eq. (27) since $1/R_{m1} << 1$.

From Fig. 8 I_{p2}, the p terminal current of OTRA2, can be written as Eq. (28), where R_{p2} is the p terminal resistance of OTRA2. Substituting for from Eq. (27) I_{p2} can be expressed as Eq. (29)

Similarly considering R_{n2} to be the n terminal resistance of OTRA2 the I_{n2} can be represented as Eq. (30) shown bellow:

$$I_{n2} = \frac{V_o}{R_4+R_{n2}}, \tag{30}$$

and the output voltage of OTRA2, can be computed as:

$$V_o = R_{m2}(I_{p2}-I_{n2}) - R_{o2}I_{n2}, \tag{31}$$

where R_{m2} and R_{o2} are transresistance gain and output resistance of OTRA2 respectively. Since $R_{m2} >> R_2$, so $R_{m2}+R_{o2} \approx R_{m2}$ and hence

$$V_o \approx R_{m2}\,(I_{p2}-I_{n2}), \tag{32}$$

$$V_o = \frac{R_4(1+sC_1R_1)(1+sC_3R_{n1})V_i}{R_1R_3sC_3(1+sC_1R_{p1})(1+sC_2R_{p2})} + \frac{R_4(1+sC_2R_2)V_i}{R_2(1+sC_2R_{p2})}, \tag{33}$$

and the transfer function V_o/V_i modifies to:

$$\frac{V_o}{V_i} = \frac{1}{(1+sC_2R_{p2})}\left(\frac{R_4C_1\,(1+sC_3R_{n1})}{R_3C_3\,(1+sC_1R_{p1})} + \frac{R_4}{R_2}\right) + \frac{R_4\,(1+sC_3R_{n1})}{R_1R_3sC_3\,(1+sC_1R_{p1})\,(1+sC_2R_{p2})} + \frac{sC_2R_4}{(1+C_2R_{p2})}. \tag{34}$$

It is observed from Eq. (34) that the nonzero values of input resistances at n and p terminal of OTRAs result in introduction of parasitic pole and zero in proportional and integral terms and the derivative term consists of a parasitic pole. The numerical values of poles and zeros are very high as parasitic resistances of OTRA are very small. Thus, the parasitic zero and pole frequencies would not practically influence the system performance.

4. Simulation Results

The theoretical propositions are verified through SPICE simulations using 0.18 µm CMOS process parameters provided by MOSIS. The CMOS implementation of the OTRA, proposed in [13] with supply voltages ± 1.5 V was used for simulation. For performance evaluation of the proposed controllers, their time domain responses are obtained. The ideal and simulated time domain responses of the proposed PI controller of Fig. 3, for a 50 mV step input voltage with 20 ns rise time, are shown in Fig. 9(a). The passive component values of the PI controller are chosen as R = 50 kΩ, C = 4 pF and C_f = 2 pF and the corresponding controller parameters are computed to be K_p = 2, $K_i = 10^7$ s^{-1}. For transient analysis of PD controller of Fig. 4, a 50 mV peak triangular input voltage is applied. The ideal and simulated transient responses are depicted in Fig. 9(b). The component values for the PD controller are chosen as R = 10 kΩ, R_f = 20 kΩ and C = 20 pF and the controller parameters are computed to be K_p = 2, K_d = 0.4 µs. For the PID controller of Fig. 5, values of the capacitors are taken as $C_1 = C_3$ = 10 pF and C_2 = 0.05 pF. The resistive component values are chosen as $R_1 = R_2 = R_3 = R_4$ = 50 kΩ. Using these passive component values various controller parame-

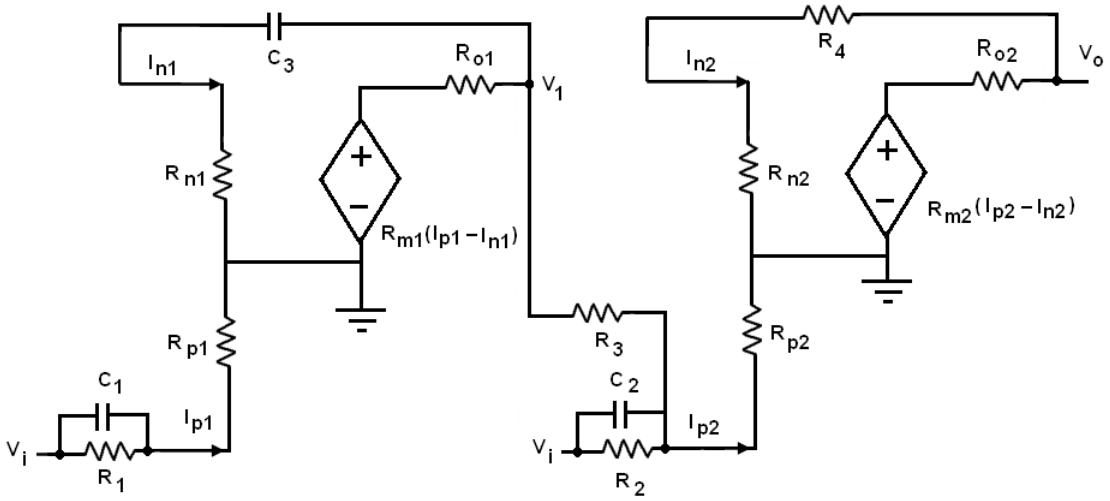

Fig. 8: Equivalent model of proposed PID controller.

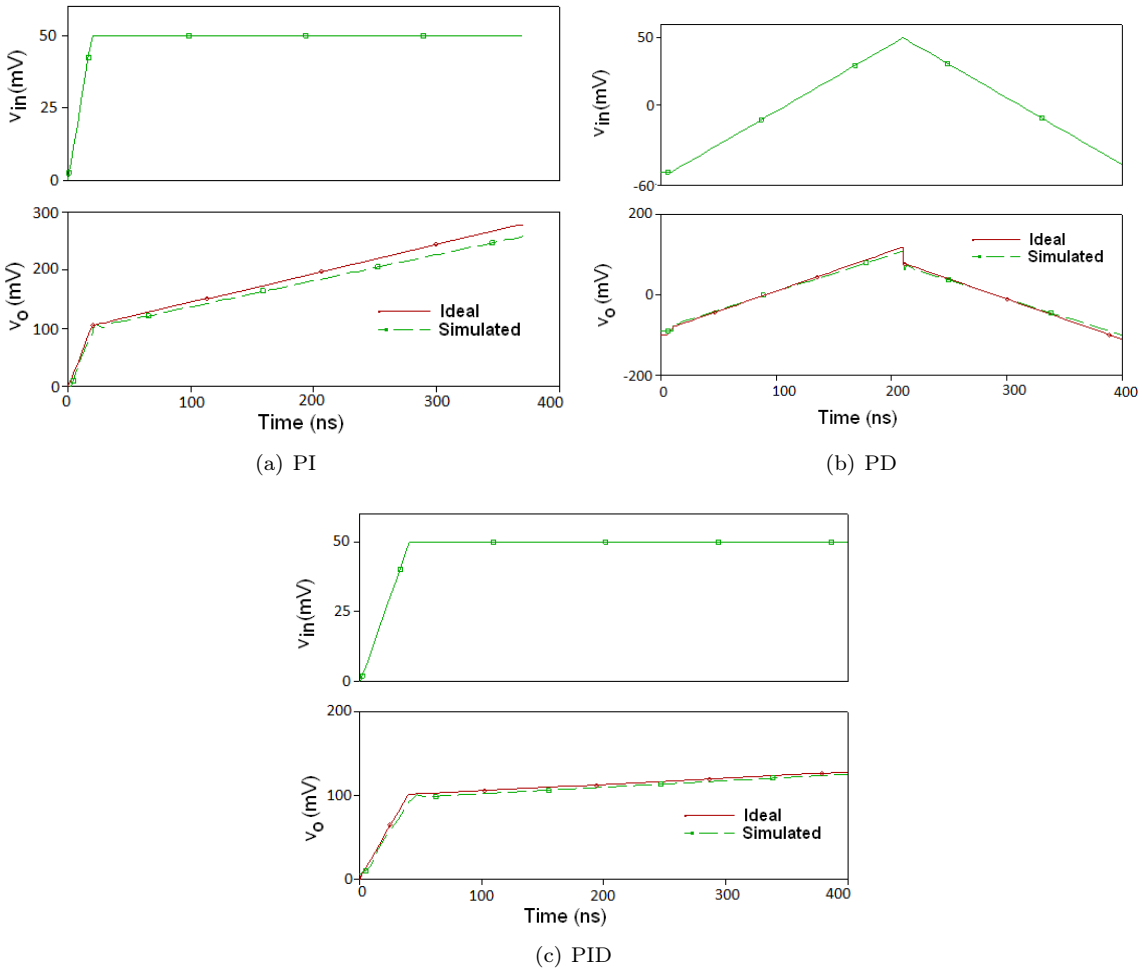

Fig. 9: Time domain response of the proposed controllers.

ters are computed as $K_p = 2$, $K_i = 2 \cdot 10^6$ s^{-1} and $K_d = 2.5$ ns. For time domain analysis, a 50 mV step signal with 10 ns rise time is applied. The transient response of proposed PID controller is shown in Fig. 9(c). It is observed that for all the controllers the simulated and ideal responses are in close agreement.

5. Performance Evaluation of the Proposed Controllers

To evaluate the effect of various controllers, the performance of a second order plant is analyzed by forming a closed loop system as shown in Fig. 10(a) where $G_P(s)$ represents the open loop transfer function of a unity feedback system. For OTRA based realization of the closed loop system the low-pass filter (LPF) presented in [14] is used and is modified as shown in Fig. 10(b). The OTRA1, resistors R_1, R_2, along with capacitors C_1 and C_2 form the second order plant whereas OTRA2 along with resistors R_a and R_b is used as subtractor thereby forming the error signal. The circuit of Fig. 10 can also be made electronically tunable by implementing all the related resistors using MOS transistors operating in the linear region.

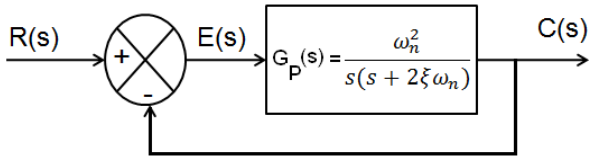

(a) Block diagram.

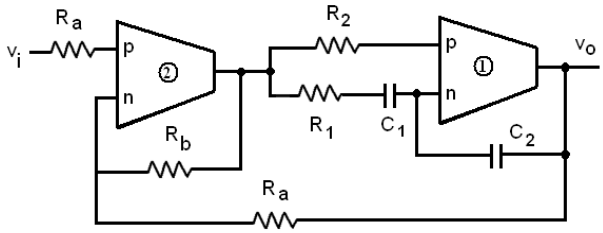

(b) OTRA based realization.

Fig. 10: Second order closed loop system.

The transfer function of the circuit of Fig. 10(b) using equal component design with $R_1 = R_2 = R$ and $C_1 = C_2 = C$ can be derived as:

$$\frac{V_o(s)}{V_i(s)} = \frac{\frac{K}{R^2C^2}}{\left(s^2 + \frac{s}{CR} + \frac{K}{R^2C^2}\right)}, \tag{35}$$

where

$$K = \frac{R_b}{R_a}. \tag{36}$$

The standard characteristic polynomial, $D(s)$, of second order system [12] is given by:

$$D(s) = s^2 + 2\xi\omega_n s + \omega^2{}_n, \tag{37}$$

where ω_n is the natural frequency of oscillations and ξ represents the damping factor. Comparing the denominator of Eq. (35) with Eq. (37) the ω_n and ξ for the LPF can be computed as:

$$\omega_n = \frac{\sqrt{K}}{RC} \; and \; \xi = \frac{1}{2\sqrt{K}}. \tag{38}$$

In the study that follows, the step response of the open loop second order system (LPF) is analysed first and then the effect of various proposed controllers on this second order system is observed by forming closed loop with controllers.

For the second order system shown in Fig. 10(b), the passive component values are chosen as $R_a = R_b = 20$ kΩ, $R_1 = R_2 = R_3 = 2$ kΩ, and $C_1 = C_2 = 20$ pF. The f_n and ξ for the LPF can be computed as 3.98 MHz and 0.5 respectively.

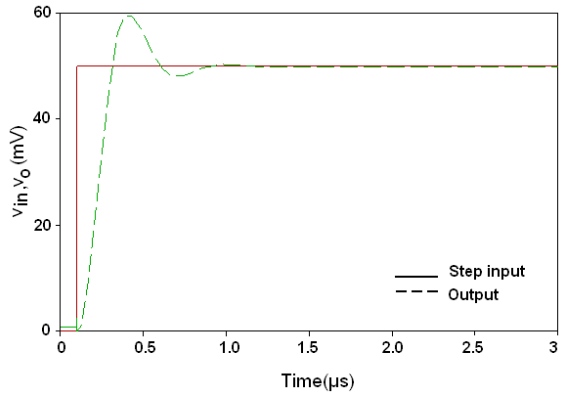

(a) with fixed ξ

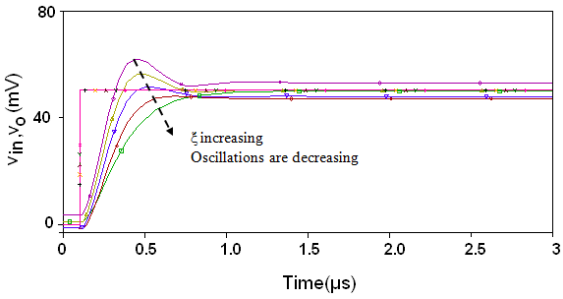

(b) with varying ξ

Fig. 11: Step Response of LPF.

To observe the step response of the LPF a step input of 50 mV is applied, and the simulated response is shown in Fig. 11(a). The effect of damping ratio, ξ on the step response of the second order LPF is shown in Fig. 11(b). To change ξ, R_b is kept constant while R_a

Tab. 2: Performance Comparison of second order system.

Parameter	Unity feedback closed loop system	Closed loop with PD controller ($K_p = 2$, $K_i = 10^7$ s^{-1})	Closed loop with PI controller ($K_p = 2$, $K_d = 0.4$ µs)	Closed loop with PID controller ($K_p = 2$, $K_i = 2 \cdot 10^6$s^{-1}, $K_d = 2.5$ ns)
Overshoot	19.56 %	12.47 %	18.76 %	8.16 %
Peak output	58.26 mV	56.52 mV	57.83 mV	52.59 mV
Rise time	140.43 ns	119.89 ns	112.28 ns	99.75 ns
Settling time	303.12 ns	274.35 ns	266.11 ns	252.27 ns

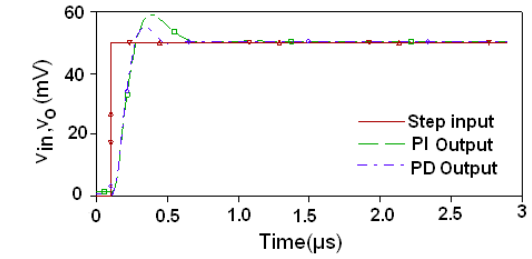

(a) with PI and PD controllers.

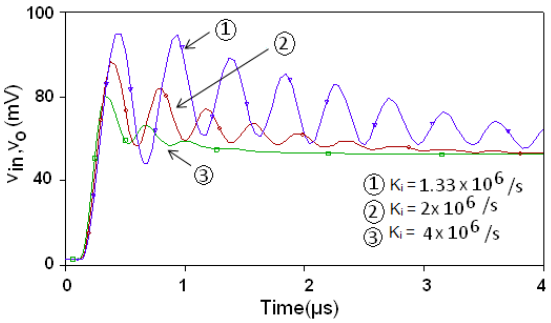

(b) with variable K_i for PI controller.

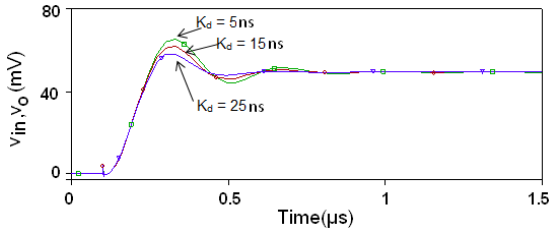

(c) with variable K_d for PD controller.

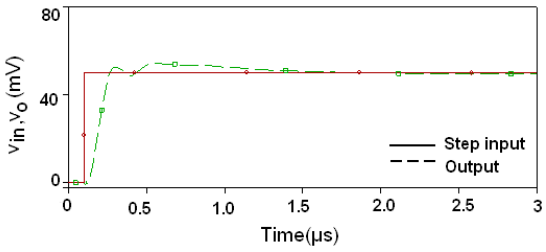

(d) PID controller.

Fig. 12: Response of a second order system.

is varied electronically by changing gate voltages of the transistors used for implementing it. It is observed that with the increase in ξ, oscillations are decreasing and is perfectly in tune with the theoretical concept. The performance of PI, PD, and PID controllers is evaluated by comparing step responses of closed loop systems based on these controllers. Figure 12(a) depicts the effects of proposed PI ($K_p = 2$, $K_i = 10^7$ s^{-1}) and PD ($K_p = 2$, $K_d = 0.4$ µs) controllers on step response of the closed loop system. Step response for varying values of K_i, while keeping $K_p = 2$ constant, is depicted in Fig. 12(b). The effect of variable K_d on the step response of the system, keeping $K_p = 2$ constant, is shown in Fig. 12(c). System step response with PID controller is represented by Fig. 12(d). Performance parameters such as overshoot, peak output, rise time and settling time of the closed-loop system with different controllers are measured and tabulated in Tab. 2. The study of the table clearly suggests that with the help of controllers the system performance is improved in a desired manner. The PD controller prominently improves the overshoot whereas PI controller influences mainly the settling time as compared to all other parameters. The PID includes best features of all individual controllers and results in improvement of all the performance measure parameters.

6. Conclusion

Operational transresistance amplifier based PI, PD and PID controllers have been presented which possess the feature of independent tuning of proportional (K_p), derivative (K_d) and integral (K_i) constants. By implementing the resistors using MOS transistors operating in linear region MOS-C equivalent of the controllers can be obtained which are suitable for full integration. This also results in reduced chip area and power consumption as compared to passive resistors. To verify the functionality of the proposed controllers their effect on a second order closed loop system was analyzed through simulations. The simulated results are in line with the proposed theory. The performance analysis reveals that PD controller improves percentage overshoot, PI controller refines settling time while PID as a combination of the two, enhances transient as well as the steady-state response of the system.

References

[1] FRANCO, S. *Design with operational amplifiers and analog integrated circuits.* 3rd ed. Boston: McGraw-Hill, 2002. ISBN 00-723-2084-2.

[2] KARA, M. T. and M. E. RIZKALLA. Single op-amp proportional-integral compensator with antiwindup. In: *1993 IEEE International Symposium on Circuits and Systems.* Chicago: IEEE, 1993, pp. 2260–2263. ISBN 0-7803-1281-3. DOI: 10.1109/ISCAS.1993.394212.

[3] MICHAL, V., C. PREMONT, G. PILLONET and N. ABOUCHI. Single active element PID controllers. In: *20th International Conference Radioelektronika 2010.* Brno: IEEE, 2010, pp. 1–4. ISBN 978-1-4244-6318-3. DOI: 10.1109/RADIOELEK.2010.5478563.

[4] TOUMAZOU, C., F. J. LIDGEY and D. G. HAIGH. *Analogue IC Design the Current Mode Approach.* 1st ed. London: Peter Peregrinus on behalf of the Institution of Electrical Engineers, 1990. ISBN 08-634-1297-1.

[5] EDRAL, C., A. TOKER and C. ACAR. OTA-C Based Proportional- Integral-Derivative (PID) Controller and Calculating Optimum Parameter Tolerances. *Turkish Journal of Electrical Engineering and Computer Sciences.* 2001, vol. 9, no. 2, pp. 189–198. ISSN 1303-6203.

[6] KESKIN, A. U. Design of a PID Controller Circuit Employing CDBAs. *International Journal of Electrical Engineering Education.* 2006, vol. 43, no. 1, pp. 48–56. ISSN 0020-7209. DOI: 10.7227/IJEEE.43.1.5

[7] MINAEI, S., E. YUCE, S. TOKAT and O. CICEKOGLU. Simple Realizations of Current-Mode and Voltage-Mode PID, PI and PD Controllers. In: *Proceedings of the IEEE International Symposium on Industrial Electronics.* Dubrovnik: IEEE, 2005, pp. 195–198. ISBN 0-7803-8738-4. DOI: 10.1109/ISIE.2005.1528911

[8] YUCE, E., S. TOKAT, S. MINAEI and O. CICEKOGLU. Low-Component-Count Insensitive Current-Mode and Voltage-Mode PID, PI and PD Controllers. *Frequenz.* 2006, vol. 60, no. 3–4, pp. 65–70. ISSN 2191-6349. DOI: 10.1515/FREQ.2006.60.3-4.65.

[9] CHEN, J. J., H. W. TSAO and C. C. CHEN. Operational transresistance amplifier using CMOS technology. *Electronics Letters.* 1992, vol. 28, no. 22, pp. 2087–2088. ISSN 0013-5194. DOI: 10.1049/el:19921338.

[10] SALAMA, K. N., A. M. SOLIMAN and C. C. CHEN. CMOS operational transresistance amplifier for analog signal processing. *Microelectronics Journal.* 1999, vol. 30, no. 3, pp. 235–245. ISSN 0026-2692. DOI: 10.1016/S0026-2692(98)00112-8.

[11] ASTROM, K. J., T. HAGGLUND and C. C. CHEN. The future of PID control. *Control Engineering Practice.* 2001, vol. 9, no. 11, pp. 1163–1175. ISSN 0967-0661. DOI: 10.1016/S0967-0661(01)00062-4.

[12] GOLNARAGHI, M. and B. C. KUO. *Automatic control systems.* 9th ed. Hoboken, NJ: Wiley, 2010. ISBN 978-047-0048-962.

[13] KAFRAWY, A. K. and A. M. SOLIMAN. A modified CMOS differential operational transresistance amplifier (OTRA). *AEU - International Journal of Electronics and Communications.* 2009, vol. 63, no. 12, pp. 1067–1071. ISSN 1434-8411. DOI: 10.1016/j.aeue.2008.08.003.

[14] GOKCEN, A., S. KILINC and U. CAM. Second Order Analog Filter Design Using a Single OTRA Suitable for Integration. In: *15th Signal Processing and Communications Applications.* Eskisehir: IEEE, 2007, pp. 1–4. ISBN 1-4244-0719-2. DOI: 10.1109/SIU.2007.4298816.

About Authors

Rajeshwari PANDEY did B.Tech. (Electronics and Telecommunication) from University of Allahabad, India, M.E. (Electronics and Control) from Birla Institute of Technology and Sciences, Pilani, Rajasthan, and Ph.D. from Delhi University, India.Currently, she is Associate Professor in Department of Electronics and Communication Engineering, Delhi Technological University, Delhi. Her research interests include Analog Integrated Circuits, and Microelectronics.

Neeta PANDEY did M.E. in Microelectronics from Birla Institute of Technology and Sciences, Pilani, Rajasthan, India and Ph.D. from Guru Gobind Singh Indraprastha University Delhi, India. At present she is Associate Professor in Department of Electronics and Communication Engineering, Delhi Technological University, Delhi. A life member of ISTE, and member of IEEE, USA, she has published papers in International, National Journals of repute and conferences. Her research interests are in Analog and Digital VLSI Design.

Saurabh CHITRANSI did B.Tech. (Electronics and Communication) from Uttar Pradesh Technical

University of Lucknow, India and M.Tech. (VLSI Design and Embedded System) from Delhi Technological University, Delhi, India. Currently, he is Executive Engineer in Diffusion and CVD Department, SITAR, DRDO, Bangalore, India. His research interests include Analog Integrated Circuits, MEMS and Silicon process integration.

Sajal K. PAUL did B.Tech., M.Tech., and Ph.D. in Radio Physics and Electronics from the Institute of Radio Physics and Electronics, University of Calcutta. He has served Webel Telecommunication Industries, Kolkata; Indira Gandhi National Open University (IGNOU), Kolkata; Advanced Training Institute for Electronics and Process Instrumentation(ATI-EPI), Hyderabad; North Eastern Regional Institute of Science Technology(NERIST), Nirjuli and Delhi College of Engineering(DCE), Delhi in various capacities. He has served the Department of Electronics Engineering, Indian School of Mines, Dhanbad as Head of the Department and at present Professor of the same department. His research interest includes Microelectoncic Devices, Electronic Properties of Semiconductor and Bipolar and MOS Analog Integrated Circuits. He has more than 60 research publications in International and National journals of repute and conferences.

International Journal of Science and Research (IJSR)
ISSN (Online): 2319-7064
Index Copernicus Value (2013): 6.14 | Impact Factor (2013): 4.438

Space Time Block Codes for MIMO systems: History to Recent Developments

Himanshu Khanna

Maharaja Agrasen Institute of Technology, Sector 22, Rohini, Delhi-110086, India

Abstract: ***Multi Input Multi Output (MIMO) communication is a proven technique to increase the throughput, diversity gain and increase the energy gain by reducing the energy consumption of the wireless network. Space time diversity used in MIMO systems is a technique to mitigate multipath fading. The same information is transmitted over multiple channels that fade independently. So, space time diversity is achieved. Transmit space time diversity is achieved if the transmitter has knowledge of the channel. But, if the transmitter does not know the channel then it is necessary to code across both space and time to achieve diversity which is termed as space time coding. In this article, we discuss the developments in MIMO systems and Space Time Block Coding Techniques for MIMO systems, over the years.***

Keywords: Space time block codes, diversity, fading, relay channel, user cooperation

1. Introduction

Wireless networks are designed to provide high voice quality and services at very high data bit rate. At the same time, they should be deployable in any environment and must be bandwidth efficient. Further, they should provide mobility, portability, minimum interference from other users, privacy and security. The major challenge to meet all these expectations is posed by time varying multipath fading [1], [2]. So, it is necessary to understand the behavior of wireless channel. In wireless channels, there are many different paths through which a signal is propagated between transmitter and receiver. The interference between two or more versions of the transmitted signal which arrive at the receiver at slightly different times causes fading. The resulting signal generally varies widely in amplitude and phase. Time varying multipath fading can be slow or fast; frequency selective or frequency flat [3]-[5]. Due the destructive addition of multipaths, the fading channel suffers from sudden decline in power. This can lead to deep fades and reliable recovery of the signal at the receiver becomes immensely difficult. In other words, if the ratio of signal power to noise power (SNR) at the receiver falls below a certain threshold, it leads to outage. The most effective technique to mitigate fading is through power control. But, the requirement of the transmitter dynamic range and knowledge of the channel which results in throughput degradation and complexity made this approach unpopular [3].The technique of diversity is used to mitigate the effects of multipath fading. It provides different replicas of transmitted signal to receiver. If these replicas fade independently, the possibility of all experiencing deep fading simultaneously is very low.

Diversity can be implemented in space (spatial), time (temporal), frequency, using different directional antennas (angular) and using different polarizations to transmit the same signal (polarization) diversity[6]-[10]. In many situations, however, the channel is both significantly frequency selective and time varying i.e. the wireless channel can be assumed to be quasi static and frequency flat. The system engineers can deploy multiple antennas at both transmitter and receiver to achieve spatial diversity.

Relay networks have the capability of providing spatial diversity to mitigate the effects of fading, thereby providing robustness gain [11]-[13]. It is practically not feasible to place multiple antennas on a small size terminal. A single antenna receiver can therefore use relay nodes as virtual antennas. Besides providing spatial diversity in Multiple Input Multiple Output (MIMO) systems [14] and [15] the capacity of wireless channel also grows manifold with the number of transmit and receive antennas and offers multiplexing gain [3], [5].

In a two-way cooperative MIMO system, relays can be passive i.e. they do not transmit their own data but rather choose to cooperatively listen. In another case, a user can act as relay and can transmit other users' data when idle [16]-[20]. Cooperative MIMO which is also referred to as distributed, virtual or networked MIMO, uses cooperating nodes with multiple antennas to emulate a virtual antenna array. In a large set of single antenna relay nodes, only a small set of relay nodes are active at any given time. Such type of MIMO systems are studied in [21], [22], and find applications in ad- hoc and sensor networks employing decode and forward relaying. A new class of Distributed space time block codes (DSTBC) is suggested in [23] which enable efficient node cooperation in networks with large number of relay nodes. In practice, such code design is often very difficult to realize due to the distributed and ad-hoc nature of cooperative links as compared to codes designed for co-located MIMO systems [24]-[26]. Single selection opportunistic relaying with decode-and-forward (DaF) and amplify-and-forward (AaF) strategies, is presented in [27]. Here distributed relay selection algorithms are used for outage optimal opportunistic relaying and outage probability is analyzed under an aggregate power constraint. But, such schemes often require large cooperation overhead.

One of the key problems in cooperative system is the requirement of a global channel state information (CSI) [28], [29]. When CSI is known, pair of neighboring nodes can cooperatively beamform [30] towards final destination to increase capacity and enhance performance of multi antenna system [16]. Optimal channel estimation and training design for two way AaF relay networks is proposed in [31]. Novel

channel estimation for two hop MIMO relay systems using parallel factor analysis is discussed in [32]. The proposed algorithm provides destination node full knowledge of all channel matrices and at the same time requires lesser number of training blocks, yields less estimation error, and is applicable to both one way and two way MIMO relay systems with single and multiple relay nodes. Other recent works on channel estimation problem for multi relay MIMO systems using tensor approach can be found in [33]-[37]. Comparison of different channel estimation schemes for MIMO two way relaying system is done in [38]. A rate efficient two phase training protocol for cascaded channel estimation, required for maximum likelihood (ML) detection [3], [4], [5], [42], [45] has been recently proposed in [39]. But, it requires a complex maximum likelihood detector.

2. An Overview

2.1 Space Time Block Codes & Space Time Trellis Codes

The goal of the space time coding is to achieve maximum diversity which is the product of transmitting antennas and receiving antennas in an MIMO system. When the channel is unknown, space time block codes (STBC) can provide maximum diversity, coding gain, high throughput and lower encoding and decoding complexity [40]. The decoding complexity should be low as the mobile transceiver has a limited available battery power. Space time trellis coding (STTC) proposed in [41] combines signal processing at the receiver with coding techniques used for multiple transmit antennas. Alamouti suggested a rate one orthogonal space time block coding (OSTBC) scheme for two transmit and one receive antennas in [42]. The codes provided full diversity and simple decoding using only linear processing. But, there is a loss in performance compared to STTC. Alamouti scheme is still more appealing due to its simplicity in implementation, albeit, with some performance penalty. STBC introduced in [43], [44] generalized the transmission scheme suggested by Alamouti to arbitrary number of antennas and is able to achieve full diversity. The performance of STBC is evaluated further in [45] and details of encoding and decoding procedures have been provided. Real and complex orthogonal designs for STBC based on Radon and Hurwitz theories, and theory of amicable designs [46], are suggested in [43]. Damen et al. suggested construction of space time codes based on number theory in [47]. It is a class of STBCs that provides full diversity with no mutual information penalty. Design of STBCs based on groups and their representation theory have been reported in [48]-[51]. STBCs constructed using Division Algebras and Field Extensions can also be found in literature [52]-[55].

Although, OSTBC can provide full diversity at low computational cost, it suffers loss in capacity for multiple receive antennas and when code rate is less than one. Moreover, complex orthogonal designs that provide full rate and full diversity are impossible to be designed for more than two transmit antennas [43]. To design full rate codes for complex constellations, quasi orthogonal space time block codes (QOSTBC) were proposed in [56], [57]. Here, the separate decoding property is relaxed. It is possible to construct rate one full diversity QOSTBC by using rotated versions of the symbols. Such codes are called rotated QOSTBCs [58]-[64]. STBCs provide full diversity and low decoding complexity but do not provide large coding gains. On the other hand STTCs are designed to provide full diversity and high coding gain at the expense of higher decoding complexity [65], [66]. High coding gains can also be achieved if STBC is concatenated with outer trellis code designed for AWGN channel. Such codes are called Super orthogonal space time trellis codes (SOSTTC) [67], [68]. SOSTTC considers STBC as modulation schemes for multiple transmit antennas. The outer trellis code for slow fading channel are usually based on the set partitioning concepts of Ungerboeck codes [69] for the additive white Gaussian noise (AWGN) channel [70]. The codes discussed so far, use different channel estimation techniques for detection. The transmitter sends the pilot signals during training phase and receiver uses them to estimate the channel [71]. In all these, quasi static fading is assumed. But, the problem becomes worse for fast fading channels.

2.2 Differential Space Time Modulation

Differential space time modulation employs differential modulation schemes for MIMO channels that neither requires channel knowledge nor pilot symbols, for detection of symbols [72]-[75].

However, if there is a career offset due to the mismatch between transmit and receive clock or relative motion of the receiver and transmitter, the channel does not remain stationary over two consecutive time periods. In such cases, the performance of differential detection scheme degrades significantly. To overcome this problem, Bhatnagar et al. proposed a double differential modulation scheme in [76] for cooperative wireless communication over fast fading Nakagami-m channels.

2.3 Spatial Multiplexing

To achieve highest possible throughput, Spatial Multiplexing (SM) is used. Foschini introduced multilayered space-time architecture in [77]. Since then, different space time architectures have been proposed such as the Bell Labs Layered Space Time architectures (BLAST) [78], [79]. In the SM scheme, the input is demultiplexed into N separate streams and each stream is transmitted from an independent antenna. As a result, the throughput increases N-fold as N symbols per channel are transmitted from N transmit antennas. But, the diversity gain suffers and hence, SM is better suited for high data rate systems operating at relatively high SNRs. On the other hand, STBC is more appropriate for transmitting at low rates and low SNRs. Sphere Decoding (SD) [80] instead of ML decoding, is used in SM. In ML detection, a search for closest integer lattice point to the given vector is performed. So, ML detection reduces to solving an integer least squares problem. In some applications like SM, the complexity in decoding grows exponentially making ML detection computationally intractable. SD limits the number of possible codewords by considering only those codewords (lattice points) that are within a sphere centered at received signal vector. The closest lattice point inside the sphere would also be the closest lattice point for the whole lattice. The problem of finding the closest lattice point to the point of interest is discussed in [81]-[83]. Another approach to design receivers with low decoding

complexity than ML decoding is to use equalization techniques to separate different symbols [3], [84]. Combination or hybrid of SM and STBC is generally used to achieve maximum possible diversity and higher throughput [85], [86].

2.4 MIMO-OFDM

MIMO-Orthogonal Frequency Division Multiplexed (MIMO-OFDM) systems [3], [5], [87], [88] are designed for frequency selective fading channels. A frequency selective channel provides an additional degree of diversity called frequency diversity i.e. the code could operate over space, time and frequency. Thus, maximum diversity can be achieved by transmitting symbols through different antennas and different frequencies. MIMO-OFDM systems still does not provide maximum possible diversity gain because frequency diversity and correlation among subcarriers are ignored in such systems. Space time coded OFDM (STC-OFDM) system designed in [89]-[92] is another approach for transmission over MIMO channels using OFDM. A STC-OFDM also known as space frequency code replaces time with OFDM frequencies in the structure of space time codes.

3. Recent Developments

STBC designs based on quadratic field extensions for two transmitting antennas are reported in [93]. The average codeword error rate of the proposed optimal quadratic STBC is lower than the optimal cyclotomic [94] and golden STBCs [95]. Full diversity non coherent Alamouti based Toeplitz STBCs are proposed in [96]. The proposed codes use the Alamouti coding scheme and the Toeplitz matrix structure to construct a non coherent non unitary STBC. These codes outperform differential codes. Natarajan et al. proposed full diversity multi group decodable STBCs with rate greater than one in [97]. For group g greater than or equal to 3, these are the first instances of multi group decodable codes having rate greater than one reported in the literature. S. Zhao et al. proposed a concatenated scheme with Polar codes [98]-[100] and STBC named Polar-STBC scheme in [101]. The proposed scheme inherits the advantages of Polar codes that can achieve high capacity and low encoding and decoding complexity; at the same time, sufficient diversity gain is also achieved due to concatenation with STBCs.

STBCs that provide full rate and achieve high spectral efficiency, transmit linear combinations of information symbols through every transmit antenna. But, inappropriate choice of coefficients for linear combination may lead to increased processing bits and peak to average power ratio (PAPR) values. Integer Space Time Codes of [102] utilizes integer coefficients in the code structure to reduce the number of processing bits and PAPR values.

STBCs find applications in multi-static/MIMO radar systems also as they allow the use of non-orthogonal waveforms while providing waveform diversity with full signal separation. But, use of STBCs necessitates the assumption of a stationary or immobile target. A modified adaptive block coding scheme suggested in [103] alleviates the issue of target Doppler shifts. The proposed scheme attempts to reduce the ambiguity in detection at lower antenna transmit power too. Le et al. recently proposed a spatially modulated OSTBC (SM-OSTBC) scheme in [104] that is based on the concept of spatial constellation codewords (SC) [107]. The proposed scheme generates transmit codeword matrices by multiplying SC matrices with OSTBC codeword matrices. The proposed SM-OSTBC scheme is able to achieve high spectral efficiency; low decoding complexity and second order transmit diversity by satisfying the non vanishing determinant property [95], [105], [106]. STBCs for MIMO channels have been constructed by Salomon et al. in [108], by concatenating orthogonal designs with diversity transforms (DT) [109]. DT spreads the channel alphabets without sacrificing information rate, bandwidth or Euclidean distance. The distribution of the obtained code alphabet becomes Gaussian like leading to high diversity gain. It has low implementation complexity and high transmission rate. Recently, an efficient MIMO scheme with signal space diversity for future mobile communications is proposed in [110]. It uses rotated modulation and space time component interleaver, and attempts to jointly optimize channel coding and modulation. At the same time, it maximizes achievable rate for MIMO systems and improves link reliability and energy efficiency.

4. Conclusion

Use of STBCs for MIMO systems have generated lot of interest for increasing spectral efficiency and improved performance in wireless communication systems. Although, lot of work has been carried out in the area of STBC-MIMO systems and literature is now extensively available but orthogonal designs suggested by Alamouti [42], Tarokh et al. [44], [45], [71] remain popular and are still relevant in the present context; as orthogonal designs lead to simple, optimal receiver structure due to the possibility of decoupled detection along orthogonal dimensions of space and time.

References

[1] W. C. Jakes, Ed., Microwave Mobile Communications, New York: Wiley, 1974.
[2] M.K.Simon, M.S.Alouini, Digital communication over fading channels,2nd edition, John Wiley and sons, 2005.
[3] Hamid Jafarkhani, Space Time Coding, Theory and Practice, Cambridge University Press, 2005.
[4] E.G. Larsson, P.Stoica and J.Li, "Space-Time Block Codes: ML Detection for Unknown Channels and Unstructured Interference", IEEE Asilomar conf. on Signals, Systems and Computers, vol. 2, pp. 916-920, Nov. 2001.
[5] E. Larsson, P. Stoica, Space time block coding for wireless communications, Cambridge University Press, 2003.
[6] A. Hiroike, F. Adachi, and N. Nakajima, "Combined effects of phase sweeping transmitter diversity and channel coding", IEEE Trans. Vehicular Technology., vol. 41, pp. 170–176, May 1992.
[7] G.J.Pottie,"System design issues in personal communications", IEEE Personal Commun. Mag., vol. 2, no. 5, pp. 50–67, Oct. 1995.
[8] G. Raleigh and J. M. Cioffi, "Spatio-temporal coding for wireless communications," in Proc. IEEE GLOBECOM, pp. 1809–1814, Nov. 1996.

[9] V.Weerackody, "Diversity for direct-sequence spread spectrum system using multiple transmit antennas", in Proc. IEEE ICC, pp. 1775–1779, May 1993.
[10] J. Winters, J. Salz, and R. D. Gitlin, "The impact of antenna diversity on the capacity of wireless communication systems," IEEE Trans. Commun., vol. 42, no. 234, pp. 1740–1751, 1994.
[11] R. U. Nabar, H. Bolcskei, and F. W. Kneubuhler, "Fading relay channels: Performance limits and space-time signal design," IEEE J. Selected Areas Commun., vol. 22, no.6, pp. 1099-1109, Aug. 2004.
[12] G. Kramer, M. Gastpar, and P. Gupta," Cooperative strategies and capacity theorems for relay networks", IEEE Trans. Inf. Theory, vol. 51, no. 9, pp. 3037-3063, Sp. 2005.
[13] M. Gastpar, and M. Vetterli," On the capacity of large Gaussian relay networks", IEEE Trans. Inf. Theory, vol. 51, no. 3, pp. 765-779, March 2005.
[14] A.J.Paulraj, R.U.Nabar and D.A.Gore, "Introduction to space-time wireless communications",Cambridge, UK, Cambridge Univ. Press, 2003.
[15] G.B.Giannakis, Z.Liu, X.Ma and S.Zhou, "Space time coding for broadband wireless communications", Wiley, 2004.
[16] A. Sendonaris, E. Erkip, and B. Aazhang, "User cooperation diversity—Part I: System description", IEEE Trans. Commun., vol. 51, no.11, pp. 1927–1938, Nov. 2003.
[17] ——, "User cooperation diversity—Part II: Implementation aspects and performance analysis", IEEE Trans. Commun., vol. 51, no. 11, pp.1938–1948, Nov. 2003.
[18] J. N. Laneman, D. N. C. Tse and G. W. Wornell, "Cooperative diversity in wireless networks: efficient protocols and outage behavior", IEEE Trans. Inform. Theory, vol. 50, no. 12, pp. 3062–3080, 2004.
[19] L. Cao, J. Zhang, N. Kanno, "Multi-user cooperative communications with relay-coding for uplink IMT-advanced 4G systems", IEEE GLOBECOM Proc. Honolulu, vol. 1, no. 1, pp. 1–6 , Nov. 2009.
[20] M. Janani, A. Hedayat, T. E. Hunter, and A. Nosratinia, "Coded cooperation in wireless communications: Space-time transmission and iterative decoding," IEEE Trans. Signal Process., vol. 52, no. 2, pp. 362–371, Feb. 2004.
[21] J. N. Laneman and G. W.Wornell, "Distributed space-time block coded protocols for exploiting cooperative diversity in wireless networks," IEEE Trans. Inf. Theory, vol. 49, no. 10, pp. 2415–2425, Oct. 2003.
[22] H. El Gamal and D. Aktas, "Distributed space-time filtering for cooperative wireless networks," in Proc. Global Telecommunicatons Conf., San Francisco, CA, Dec. 2003, pp. 1826–1830.
[23] S.Yiu, R. Schober, "Distributed Space time block Coding", IEEE Trans. Commun., vol. 54, no. 7, pp. 1195–1206, July 2006.
[24] X.B. Liang and X.G. Xia, "Unitary signal constellations for differential space–time modulation with two transmit antennas: Parametric codes, optimal designs, and bounds", IEEE Trans. Inform. Theory, vol. 48, no. 8, pp. 2291–2322, Aug. 2002.
[25] H. Wang and X.G. Xia, "Upper bounds of rates of complex orthogonal space–time block codes", IEEE Trans. Inform. Theory, vol. 49, no. 10, pp. 2788–2796, Oct. 2003.
[26] K. Lu, S. Fu, and X.G. Xia, "Closed form designs of complex orthogonal space–time block codes of rates (k + 1)/(2k) for 2k − 1or 2k transmit antennas", IEEE Trans. Inform. Theory, vol. 51, no. 12, pp. 4340–4347, Dec. 2005.
[27] A. Bletsas, H. Shin, M. Z. Win, "Cooperative Communications with Outage Optimal Opportunistic Relaying", IEEE Trans. Wireless Commun., vol. 6, no. 9, September 2007.
[28] P. Larsson and H. Rong, "Large-scale cooperative relay network with optimal coherent combining under aggregate relay power constraints," in Proc. Working Group 4, World Wireless Research Forum WWRF8 Meeting, Feb. 2004.
[29] Y. Jing and B. Hassibi, "Distributed space–time coding in wireless relay networks", IEEE Trans. Wireless Commun., vol. 5, no. 12, pp. 3524–3536, Dec. 2006.
[30] J. Litva and T.K.Y.Lo, "Digital Beamforming in Wireless Communications", Artech House Publishers, 1996.
[31] F. Gao, R. Zhang, and Y.-C. Liang, "Optimal channel estimation and training design for two-way relay networks," IEEE Trans. Commun., vol. 57, no. 10, pp. 3024-3033, Oct. 2009.
[32] Y. Rong, M.R.A. Khandaker, Y.Xiang, "Channel estimation of dual-hop MIMO relay system via parallel factor analysis", IEEE Trans. Wireless Commun., vol. 11, no. 6 , pp. 2224–2233, 2012.
[33] F. Roemer, M. Haardt, "Tensor-based channel estimation and iterative refinements for two-way relaying with multiple antennas and spatial reuse", IEEE Trans. Signal Process., vol. 58, no. 11, pp. 5720–5735, 2010.
[34] C.A.R. Fernandes, A.L.F. de Almeida, D.B. Costa, "Unified tensor modeling for blind receivers in multiuser uplink cooperative systems", IEEE Signal Process. Lett., vol. 19, no. 5, pp. 247–250, 2012.
[35] A.L.F. de Almeida, C.A.R. Fernandes, D. Benevides da Costa, "Multiuser detection for uplink ds-cdma amplify-and-forward relaying systems", IEEE Signal Process. Lett., vol.20, no.7, pp. 697–700, 2013.
[36] L.R. Ximenes, G. Favier, A.L.F. Almeida, Y.C.B. Silva, "PARAFAC-PARATUCK semi-blind receivers for two-hop cooperative MIMO relay systems", IEEE Trans. Signal Process., vol. 62, no. 14, pp. 3604–3615, 2014.
[37] Xi Han, A.L.F. de Almeida and Z.Yang, "Cannel estimation for MIMO multi relay systems using a tensor approach", EURASIP J. Advances in signal processing, 2014.
[38] Z. Fang and H. Shan "Comparison of channel estimation schemes for MIMO two-way relaying systems," in Proc. Cross Strait Quad-Regional Radio Science and Wireless Technology Conference (CSQRWC), Ningbo, China, July 26-30, 2011, pp. 719 - 722.
[39] Arti M.K., M.R.Bhatnagar, "Performance analysis of two way AF MIMO relaying of OSTBCs with imperfect channel gains", IEEE Trans. Vehicular Techn., vol. 63, no. 8, pp. 4118-4124, 2014.
[40] A. Y. Panah and R. W. Heath, "MIMO two-way amplify-and-forward relaying with imperfect receiver CSI", IEEE Trans. Vehicular Techn., vol. 59, no. 9, pp. 4377-4387, Nov. 2010.

[41] V. Tarokh, N. Seshadri, and A. R. Calderbank, "Space–time codes for high data rate wireless communication: Performance analysis and code construction", IEEE Trans. Inform. Theory, vol. 44, no. 2, pp. 744–765, Mar. 1998.
[42] S. M. Alamouti, "A simple transmitter diversity scheme for wireless communications", IEEE J. Select. Areas Commun., vol. 16, pp. 1451–1458, Oct. 1998.
[43] V. Tarokh, H. Jafarkhani, and A. R. Calderbank, "Space-time block codes from orthogonal designs", IEEE Trans. Inf. Theory, vol. 45, pp. 1456-1467, July 1999.
[44] ——, "The application of orthogonal designs to wireless communication," in Proc. IEEE Information Theory Workshop, Killarney, Ireland, June 1998, pp. 46–47.
[45] V. Tarokh, H. Jafarkhani, and A. R. Calderbank, "Space-time block coding for wireless communications: Performance results", IEEE J. Select. Areas Commun., vol. 17, no. 3, pp. 451-460, March 1999.
[46] A. V. Geramita and J. Seberry, Orthogonal Designs, Quadratic Forms and Hadamard Matrices, Lecture Notes in Pure and Applied Mathematics, vol. 43. New York and Basel: Marcel Dekker, 1979.
[47] M.O.Damen, A.Tewfik and J.C.Belfiore, "A construction of a space-time code based on number theory", IEEE Trans. on Inform. Theory, vol. 48, no. 3, pp. 753–60, Mar. 2002.
[48] A.Shokrollahi, B.Hassibi, B.M.Hochwald, and W.Sweldens, "Representation Theory for High-Rate Multiple-Antenna Code Design", IEEE Trans. on Inf. Theory, vol. 47, no. 6, pp. 2335-67, Sep. 2001.
[49] B.Hasssibi and M.Khorrami, "Fully Diverse Multiple Antenna Signal Constellations and Fixed Point Free Lie Groups", in proc. IEEE International Symp. on Inf. Theory, 2001.
[50] B.L.Hughes,"Optimal Space Time constellations from groups", IEEE Trans. Inf. Theory, vol. 49, no. 2, pp. 401-10, Feb. 2003.
[51] A. Shokrollahi, "Design of Unitary Space-Time Codes from Representations of SU(2)", in proc. IEEE International Symp on Inf. Theory, June 2001.
[52] S. Galliou and J.-C. Belfiore, "A new family of full rate, fully diverse space time codes based on Galois theory", in Proc. IEEE International Symp. Inform.Theory, p. 419, IEEE, June 30-July 5,2002.
[53] B.A.Sethuraman, B.S.Rajan,and V. Shahsidhar "Full diversity high rate Space Time Block Codes from Division Algebras", IEEE Trans.on Inf. Theory, vol. 49, no. 10, pp. 2596-2616, Oct. 2003.
[54] V. Shashidhar, K. Subrahmanyam, R. Chandrasekharan, B. Sundar Rajan, and B. A. Sethuraman, "High-rate, full-diversity STBC's from field extensions", in Proc. IEEE Int. Symp. Information Theory, Yokohama, Japan, pp. 126, June 29–July 4.
[55] V. Shashidhar, B. Sundar Rajan, and B. A. Sethuraman, "STBC's using capacity achieving designs from cyclic division algebras", in Proc. CommunicationTheory Symop., GLOBECOM, San Francisco, CA, 2003.
[56] H. Jafarkhani, "A quasi-orthogonal space-time block code", IEEE Trans. Commun., vol. 49, no. 1, Jan. 2001.
[57] O. Tirkkonen, A. Boariu, and A. Hottinen, "Minimal non-orthogonality rate 1 space-time block code for 3+ Tx antennas", in Proc. International Symp. on Spread Spectrum Techniques and Applications, vol. 2, pp. 429-432, Sept. 2000.
[58] O. Tirkkonen, "Optimizing space-time block codes by constellation rotations", in Proc. Finnish Wireless Commun. Workshop, vol. 1, pp. 1-6, 2000.
[59] W. Su and X. Xia, "Quasi-orthogonal space-time block codes with full diversity," in Proc. Global Telecom. Conf., vol. 2, pp. 1098-1102, Nov. 2002.
[60] H. Jafarkhani and N. Hassanpour, "Super-quasi-orthogonal space-time trellis codes for four transmit antennas," IEEE Trans. Wireless Commun., vol. 4, pp. 215-227, Jan. 2005.
[61] D. Wang and X. Xia, "Optimal diversity product rotations for quasi orthogonal STBC with MPSK symbols", IEEE Commun. Lett., vol. 9, no. 5, pp. 420-422, May 2005.
[62] N. Sharma and C. B. Papadias, "Improved quasi-orthogonal codes through constellation rotation", IEEE Trans. Commun., Oct. 2001.
[63] D. Rainish, "Diversity transform for fading channels", IEEE Trans. Commun., vol. 44, pp. 1653-1661, Dec. 1996.
[64] Y. Xin, Z. Wang, and G. B. Giannakis, "Space-time diversity systems based on linear constellation precoding", IEEE Trans. Wireless Commun., vol. 2, no. 2, Mar. 2003.
[65] S. Sandhu, R. W. Heath Jr., A. Paulraj, "Space time block codes versus space time trellis codes", IEEE International conference on commun., vol.4, pp. 1132-1136, June 2001.
[66] J. Cheng, H. Wang, M. Chen, S. Cheng, "Performance comparison and analysis between STTC and STBC", IEEE Vehicular Tech. Conf., vol. 4, pp. 2487-2491.
[67] S. Siwamogsatham and M. P. Fitz, "Improved high rate space time codes via orthogonality and set partitioning", IEEE wireless commun. and networking conf., vol.1, pp. 264-70, March 2002.
[68] H. Jafarkhani, N. Seshadri, "Super orthogonal space time trellis codes", IEEE Trans. Inform. Theory, vol. 49, no. 4, pp. 937-50, April 2003.
[69] G. Ungerboeck, "Trellis coded modulation with redundant signal sets, part I: Introduction", IEEE commun. Magazine, vol. 25, no. 2, Feb. 1987.
[70] S. Alamouti, V. Tarokh and P. Poon, "Trellis-coded modulation and transmit diversity: design criteria and performance evaluation", IEEE International Conference on Universal Personal Communication, vol.1, pp. 703-707, 1998.
[71] V.Tarokh, A. Naguib, N. Seshadri, and A. R. Calderbank, "Space-time codes for high data rates wireless communications: performance criteria in the presence of channel estimation errors, mobility and multiple paths", IEEE Trans. on Commun., vol. 47, no. 2, pp. 199–207, Feb. 1999.
[72] T. Himsoon, W. Su, and K. J. R. Liu, "Differential Transmission for Amplify-and-Forward Cooperative Communications", IEEE Signal Proc. lett., vol. 12, no. 9, pp. 597–600, Sep. 2006.
[73] K. L. Clarkson, W. Sweldens, and A. Zheng, "Fast multiple antenna differential decoding", IEEE Transactions on Commun., vol. 49, no. 2, pp. 253-261, Feb. 2001.

[74] G. Ganesan and P. Stoica, "Space-time block codes: a maximum SNR approach", IEEE Trans. on Inform. Theory, vol. 47, no. 4, pp. 1650-1656, 2001.
[75] B. L. Hughes, "Differential space-time modulation", IEEE Trans. on Inform. Theory, pp. 2567-2578, Nov. 2000.
[76] M. R. Bhatnagar, A. Hjørungnes, L. Song, R. Bose, "Double-Differential decode and forward cooperative communications over Nakagami-m channels with carrier offsets", IEEE Sarnoff Symposium, pp. 1-5, April 2008.
[77] G.J.Foschini, Jr., "Layered space-time architecture for wireless communication in a fading environment when using multi-element antennas", Bell Labs Technical Journal, pp. 41–59, Autumn 1996.
[78] G.J.Foschini, Jr., D.Chizhik, M.J.Gans, C.Papadias, and R.A. Valenzuela, "Analysis and performance of some basic space-time architectures", IEEE Journal on Selected Areas in Commun., vol. 21, no. 3, pp. 303–20, Apr. 2003.
[79] P. W. Wolniansky, G. J. Foschini, G. D. Golden, and R. A. ValenZuela, "V-Blast: An architecture for realizing very high data rates over the rich-scattering channel", in Proc. Int. Symp. Signals, Systems and Electronics, pp. 295–300, 1998.
[80] E.Viterbo and J.Boutros, "A universal lattice code decoder for fading channels", IEEE Trans. on Information Theory, vol.45, no.5, pp. 1639–42, July 1999.
[81] M.Pohst, "On the computation of lattice vectors of minimal length, successive minima and reduced bases with applications", ACM SIGSAM Bull., vol. 15, pp. 37–44, Feb. 1981.
[82] U.Fincke and M.Pohst, "Improved methods for calculating vectors of short length in a lattice, including a complexity analysis", Math. Comput., vol. 44, pp. 463–471, Apr. 1985
[83] B.Hassibi and H.Vikalo, "On the Sphere-Decoding Algorithm I,Expected Complexity", IEEE Trans.on Signal Process., vol. 53, no. 8, Aug. 2005.
[84] J.G.Proakis, Digital Communications, McGraw-Hill Inc., 1989.
[85] L. Zheng and D. Tse, "Diversity and multiplexing: a fundamental tradeoff in multiple antenna channels", IEEE Trans. Inform. Theory, vol. 49, pp. 1073-1096, May 2003.
[86] R. W. Heath and A. Paulraj, "Diversity versus multiplexing in narrow-band MIMO channels: a tradeoff based on euclidean distance", IEEE Trans. Commun., submitted 2002.
[87] G.L. Stuber, J.R. Barry, S. W. Mclaughlin, M.A.Ingram, T.G. Pratt, "Broadband MIMO-OFDM wireless communications", in Proc. of IEEE, vol. 92, no. 2, Feb. 2004.
[88] A. F. Molisch, M. Z. Win, and J. H. Winters, "Space-time-frequency (STF) coding for MIMO-OFDM systems", IEEE Commun. Lett., vol. 5, pp. 2465-2476, Oct. 2002.
[89] D.Agrawal, V.Tarokh, A.Naguib and N. Seshadri, "Space-time coded OFDM for high data-rate wireless communication over wideband channels", IEEE Vehicular Tech. Conf., pp. 2232–6, May 1998.
[90] H. Bolcskei and A. J. Paulraj, "Space-frequency coded broadband OFDM systems," in Proc. IEEE Wireless Commun. & Networking Conf., vol. 1, pp. 1-6, 2000.
[91] W. Su, Z. Safar, M. Olfat, and K. J. R. Liu, "Obtaining full-diversity space-frequency codes from space-time codes via mapping", IEEE Trans. Signal Process., vol. 51, pp. 1451-1458, Nov. 2003.
[92] W. Su, Z. Safar and K. J. R Liu, "Full-rate full-diversity space-frequency codes with optimum coding advantage", IEEE Trans. Inf. Theory, Jan. 2005.
[93] W.Genyuan, Zhang, M.Amin, "Space-Time Block Code Designs Based on Quadratic Field Extension for Two-Transmitter Antennas", IEEE Trans. Information Theory, vol. 8, no.6, pp. 4005-13, Jan. 2012.
[94] B.A.Sethuraman and B.Sundar Rajan, "Optimal STBC over PSK Signal Sets from Cyclotomic Field Extensions", in proc. IEEE International conf. on Commun., vol. 3, pp. 1783-87, 2002.
[95] J.-C. Belfiore, G. Rekaya and E. Viterbo, "The Golden Code: A 2×2 Full-Rate Space-Time Code with Non-Vanishing Determinants", in proc. IEEE International Symp. Inform. Theory, p. 310, 2004.
[96] X. Dong, J.K. Zhang, S. Dumitrescu, and F.K.Gong, "Full diversity non coherent Alamouti based Toeplitz Space Time Block Codes", IEEE Trans. Signal process., vol. 0, no. 10, pp. 5241-53, July 2012.
[97] L.P.Natarajan and B.S.Rajan, "Asymptotically-Good, Multigroup Decodable Space-Time Block Codes", IEEE Trans. Wireless Commun., vol. 12, no. 10, pp. 5035-47, Sep. 2013.
[98] E. Arikan, "Channel Polarization: A Method for Constructing Capacity-Achieving Codes for Symmetric Binary-Input Memoryless Channels", IEEE Trans. Inf. Theory, vol. 55, no. 7, pp. 3051–3073, Jul. 2009.
[99] S. B. Korada, "Polar Codes for Channel and Source Coding", Ph.D. dissertation, EPFL, Lausanne, Switzerland, Jul. 2009.
[100] I. Tal and A. Vardy, "How to Construct Polar Codes", IEEE Trans. Inf. Theory, vol. 59, no. 10, pp. 6562-82, July 2013.
[101] Z.Shengmei, S.Qian, F.Ming-Kun and Z.Baoyu, "A concatenation scheme of Polar codes and space-time block codes in multiple-input multiple-output channels", 6th International Congress on Image and signal processing, vol. 3, pp. 1216-20, Dec. 2013.
[102] J.Harshan and E.Viterbo, "Integer Space-Time Block Codes for Practical MIMO Systems", IEEE Wireless Commun. Lett., vol. 2, no. 4, pp. 455-58, June 2013.
[103] J.Akhtar, "Doppler compensated space time block coding for multistatic radar systems", in proc. IEEE Conf. on Radar, pp. 1-5, 2013.
[104] Minh-Tuan Le, Vu-Duc Ngo, Hong-Anh Mai, Xuan-NamTran and M.D.Renzo, "Spatially Modulated Orthogonal Space-Time Block Codes with Non-Vanishing Determinants", IEEE Trans. Commun., vol. 62, no. 1, pp. 85-99, Jan. 2014.
[105] T. Kiran and B. S. Rajan, "STBC-scheme with non vanishing determinant for certain number of transmit antennas", IEEE Trans. Info.Theory, vol. 51, no. 8, pp. 2984–2992, Aug. 2005.
[106] G. Rekaya, J.-C. Belfiore, and E. Viterbo, "Algebraic 3×3, 4×4, 6×6 space-time codes with non-

vanishing determinants", in Proc. IEEE Int.Symp.Information Theory and its Applications, Parma, Italy, pp. 325–329 Oct. 10-13, 2004.

[107] Minh-Tuan Le, Vu-Duc Ngo, Hong-Anh Mai, and Xuan-Nam Tran, "High rate space time block coded spatial modulation,"in Proc. International Conf. Advanced Tech. for Commun., ATCIREV 2012, Hanoi, Vietnam, pp. 278-282, Oct. 2012.

[108] A. J. Salomon and O. Amrani, "Increased diversity space time coding using the diversity transform", EURASIP J. on wireless communication and networking, Jan. 2014.

[109] D. Rainish, "Diversity Transform for fading channels", IEEE Trans. Commun., vol. 44, no. 12, pp. 1653-61, 1996.

[110] W.Zhanji and G.Xiang, "An efficient MIMO scheme with signal space diversity for future mobile communications", EURASIP J. on wireless communication and networking, 2015.

Author Profile

Himanshu Khanna received M.E. degree in Electronics and Communication Engineering form Delhi College of Engineering, Delhi University in 2007. Presently, he is working as an Assistant Professor, ECE Department, Maharaja Agrasen Institute of Technology, Rohini, Delhi. He has keen interests in the area of signals and systems, applications of signal processing in communication systems, MIMO systems and application of coding techniques to MIMO systems for performance enhancement.

Volume 3, Issue 2 (2015) 440-445 ISSN 2347 - 3258
International Journal of Advance Research and Innovation

Thermal Evaporation and microstructure study of CdTe

Shailendra Kumar Gaur, R. S. Mishra
Department of Mechanical, Production & Industrial and Automobiles Engineering Delhi Technological University Delhi, India

Article Info
Article history:
Received 10 April 2015
Received in revised form
30 April 2015
Accepted 20 May 2015
Available online 15 June 2015

Keywords
Physical Vapor Deposition,
Film Thickness,
CdTe Evaporation,
Thin Film Deposition

Abstract
Thin films of CdTe deposited by thermal evaporation at evaporation rate of 1000Å thickness on Si substrate.Deposited thin filmthickness is optimized with vacuum deposition conditions by comparing film thickness value from in-process quartz crystal(piezoelectric transducer) with stylus operated dektek surface profiler.CdTe film of thickness 1000 Åhasbeen deposited on silicon substrate by vacuum evaporation method. The thin films are characterized and properties of deposited film depend upon the deposition rate, geometrical position of substrate from the source and surface condition of the silicon substrate. X-ray diffraction (XRD) studyshows that CdTe films are polycrystalline with preferential orientation of (111) plane in cubic phase for 1, 5 & 10 Å/sec deposition rates.Energy dispersive X-ray analysis of CdTe films at 1, 5 & 10 Å/sec deposition rates after quantification gives Te/Cd ratio of 0.98, 1.14 and 1.18 respectively. Scanning electron microscopy (SEM)micrographs of CdTeat different magnifications show grain size in the range of 19-25, 21-28 & 17-20 nm for deposition rates of 1, 5 & 10 Å/sec respectively along the grain boundaries. SEM micrograph at deposition rate of 10 Å/sec has smaller size, smooth, void-free and uniformly distributed over the surface of substrate than the other deposition rates.

1. Introduction

CdTe and ZnS are II-VI group semiconductor with a large band gap in the near UV region. A.A. Ibrahim et. al. [1] discussed that ZnTe a member of II-VI semiconductor having large band gap studied with structural and electrical properties for evaporation film. E.E. Khawaja et al.[2] discussed that ZnTe chemical in homogeneity has been examined by varying deposition rate for thermal evaporation process. S. Larramendi et.al.[3] discussed that ZnTe and CdTe can be grown in form of epitaxial and polycrystalline film by isothermal closed sublimation(vacuum deposition). R. R. Singh et.al. [4] Discussed that CdS has also been identified as a passivant layer for HgCdTe (MCT) IR detector & studied its various physical, electrical and optical properties as an alternative to CdTe and ZnS. Thus combination of CdTe & ZnS provides a very large band gap has been proved to be excellent passivant of MCT based IR applications. R. Pal et.al. [5] Stated that CdTe as a passivant studied and analyzed for interface composition for HgCdTe photodector. CdTe & ZnSthin films have been usually deposited by many techniques such as chemical vapor deposition, electrode position, vacuum deposition, molecular beam epitaxial. K. Nagamani et.al [6] stated that ZnSis used in copper indium gallium diselenide (CuInGaSe2)-based solar cells by lowering its resistivity by Al doped chemical bath process. But vacuum deposition is best since it controls the deposition parameter effectively and it is very conventionally stablized process. F. Gode et. al.[7] discussed that ZnS deposited by chemical bath process at 80°C shows hexagonal structure with polycrytalinity with grain size 40-80nm. Physical methods produce the atoms that deposit on the substrate by evaporation and sputtering. Sometimes called vacuum deposition because the process is usually done in an evacuated chamber.PVD is used for metals while dielectrics can be deposited using specialized equipments. It rely on thermal energy supplied to the crucible or boat to evaporate atoms. Evaporated atoms travel through the evacuated space between the source and the sample and stick to the sample. Few, if any, chemical reactions occur due to low pressure can force a reaction by flowing a gas near the crucible. Surface reactions usually occur very rapidly and there is very little rearrangement of the surface atoms after sticking. Thickness uniformity and shadowing by surface topography, and step coverage are issues. Ali Moarrefzadeh et al. [8] discussed that Physical vapor deposition (PVD) includes a wide range of vacuum coating processes in which material is physically taken out from a source by evaporation or sputtering, transported through a vacuum or partial vacuum by the energy of the vapor particles, and condensed as a film on the surfaces of appropriately placed parts or substrates. The dependent parameters are starting composition, oxidation state, and crystalline structure and packing density.PVD techniques used generally are basically two in nature: thermal evaporation by resistively heating or by using an electron- beam heating, and sputtering, a no thermal process. Deposited films are typically evaluated for visual defects, thickness, and adhesion. Visual defects such as bare spots, small voids, incorporated flakes, or debris can be observed with a stereo microscope having a magnification of 10 to 100 times. Film thickness is generally measured by with dektek surface profilometer with diamond size of 12.5µm radius stylus. In thermal evaporation process, load the source material-to-be-deposited (evaporant) into the container (crucible). Then resistively heat the container (tungsten or molybdenum boat) containing source to high temperature i.e. evaporation temperature depending upon the material to be deposited. The source material evaporates and evaporant vapor

Corresponding Author,
E-mail address: professor_rsmishra@yahoo.co.in

transports to and impinges on the surface of the substrate. Evaporant condenses on and is absorbed by the surface.

Thermal evaporation is very old, easy, reliable and good method of deposition while E-beam evaporation requires elaborate and complex system. Moreover high velocity electron creates surface defects and stress on the deposited surface**.**

2. Literature Review

Vivienne Denise Falcão et.al. [9] discussed that CdTe deposition used in photovoltaic applications by closed space sublimation process depends upon the influence of deposition parameters on the properties of CdTe film. E. R. Shabban et.al. [10] discussed that film thickness influence the microstructure and optical properties . He found that crystallite size increases while microstrain decreases with increasing film thickness. Laxman Gouda et.al. [11} discussed that the properties of CdTe film deposited on glass and ITO coated glass by chemical bath method depends upon the chemical composition of the chemicals used. The atomic ratio in the film is a function of the Cd/Te concentration ratio in the solution used in deposition. A. Romeo et.al. [12] stated that crystallization and morphology of the CdTe is strongly affected not only by the CdCl2 treatment but also by the deposition method and the structure of the CdS windows on the TCO substrates, they also affect the influence of post-deposition treatment on CdTe.M. Estela Calixto et.al. [13] stated that CdTe can be deposited for Cu (In, Ga) Se2 thin film solar cells by close spaced vapor transport technique, named as "CSVT", is a variant of the sublimation technique, it uses two graphite blocks, where independent high electrical currents flow and due to the dissipation effect of the electrical energy by Joule's heat makes the temperature in each graphite block to rise. One of the graphite blocks is named the source &other substrate with inert gas atmosphere. The rate of deposition is controlled by gas flow and pressure. Wagner Anacle to Pinheiro et. al. [14] carried out study on different CdTe source like affecting the deposition rate and found that largest deposition rate was achieved when a paste made of CdTe and propylene glycol was used as the source and compacting the powder the deposition rate increases due to the better thermal contact between powder particles. G. Gordillo et.al. [15] discussed that the interest in studying CdTe & ZnS materials is due to their capability in using photovoltaic solar cells applications and by changing their composition structure changes. J. Wang et.al. [16] Near-Infrared (NIR) fluorescence-based bio-sensor and imaging applications used quantum dots of CdTe/CdS by synthesing microwave-assisted. Osvaldo de Melo et.al. [17] stated that alumina membrance used during vacuum evaporation develops pattern applicable in functional nano-strutures, nano-arrays and organic sensors. K.A.M.H. Siddiquee et al. [18] discussed that CdTe/CdS based solar cell can be developed by chemical bath & electrode position optimized process condition through characterization. Condensation and nucleation- Atoms that impinge on a surface in a vacuum environment may be reflected immediately, re-evaporate after a residence time, or condense on the surface. Mean free path is the minimum distance between two successive collisions. Based on this mean free path source to substrate distance is optimized for constant flux and better deposited film quality. Vapor pressure varies depending upon the source temperature and is different for different materials. Re-evaporation is a function of bonding energy between the adatom and the surface, the surface temperature, and the flux of mobile adatoms e.g. the deposition of cadmium on a steel surface having a temperature greater than about 200 ˚C will result in total re-evaporation of the cadmium. The energy of the atom, atom-surface interaction (chemical bonding), and the temperature of the surface influence the capability of an atom on a surface. The mobility on a surface can change because of variations in chemistry or crystallography. The various crystallographic plates of a surface have different surface free energies that influence the surface diffusion. Atoms condense on a surface by losing energy. They lose energy by: -forming and breaking chemical bonds with the substrate atoms. -Finding preferential nucleation sites (lattice defects, atoms steps, and impurities)- interacting with another diffusing surface atoms (same species) - Colliding or reacting with adsorbed surface species.

Atoms form nuclei after condensation. Homogenous nucleation is said to occur if the surface is of same material as the deposition atoms and if they are different materials, the process is called heterogeneous. In semiconductor field, heterogeneous nucleation forms hetero- junctions.

3. Experimental Set-Up

The island films were prepared using a laboratory thermal evaporation setup working at residual vacuum of (2.5 - 4) $\times 10^{-6}$ mbar. The deposition setup was equipped with the two-stage vacuum system based on turbo molecular along with. In case of oil based pumps the ultimate vacuum achieved in the system depends upon the vapor pressure of the oil used in pumps, generally Silicone based oils are used to achieve vacuum of1.0×10^{-6} mbar order in the chamber. The films were deposited on the substrates cleaned in the ultrasound bath in isopropyl alcohol and drained by a compressed air flux. High purity 99.999% CdTe small chunks (pieces) used as source material with open type molybdenum boats. During the deposition, all substrates were kept at room temperature i.e no substrate heating or cooling.

In this case, certain assumptions about the structure of the film, the shape and size of the islands, can be made only on the basis of measurement of electrical and optical

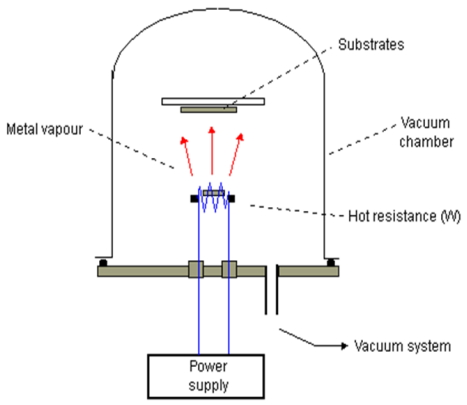

Fig: 1. Mechanism of Thermal evaporation process (ref. [8])

properties of this film and topographic surveillance using SEM or AFM. Optical absorption and transmittance of CdTe films on glass substrates were measured in wavelength range from 200 to 1100 nm using the 640FT IR spectrometer. Flow regimes are categorized quantitatively via the Knudsen number (Kn), which represents the ratio of the molecular mean free path to the flow geometry size for gases. Generally, the ambient temperature is fixed based on the experimental setup or experimental conditions but the evaporation temperature can be varied as per the thickness or mass transfer to be deposited on the substrate. This evaporation temperature can be increased or decreased depending considering the vapour pressure, to make fast the mass transfer keeping the good adhesion with uniformity on the substrate surface.

4. Results and Discussion

In table 1 various input parameters required for computing the depositing film thickness during the thermal evaporation process of different source material like CdTe in our case by a piezoelectric transducer using quartz crystal are given.

Table 1: Input parameters for Digital Thickness Monitor (DTM)

Name of material	Density (g/cm^3)	Acoustic Impedance Value	Tooling factor
CdTe	4.85	9.01	100
ZnS	8.85	11.39	100
Tin	7.30	100.00 Pa	100
Indium	7.31	0.11871kg/mol	100
Gold	7.36 g/cm^3	7.36E3 kg/m³	100

Generally the deposited film thickness value does not match with the value given by DTM. So, we measure the deposited film thickness at different points on the substrate surface from Dektek surface profiler which are shown in figure 2. Generally, the variation in thickness value from DTM is 5-15%. So, we have to keep the DTM thickness value such that the actual value measured from Dektek matches with required thickness value. This can be achieved by doing a no of repetitive experiments and reducing gap between substrate and quartz crystal.

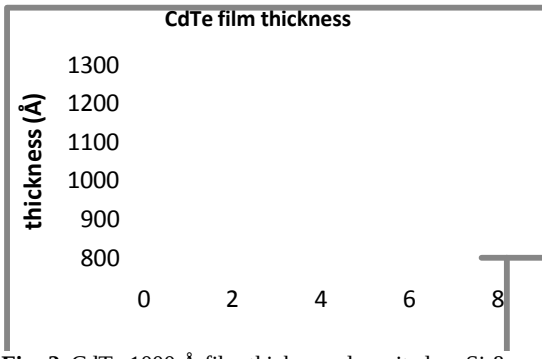

Fig: 2. CdTe 1000 Å film thickness deposited on Si & measured at different points on Si substrate surface

The film thickness may vary by varying the evaporation temperature with time and vapor pressurefrom the centre of substrate to outer surface and it is maximum at the centre as definitely there is loss of source material during thermal evaporation since only a fraction of the material is deposited on the surface while we are evaporating a large quantity of it.

4.1 XRD Results

Figure 3(a), 3(b), 3(c) shows the XRD patternby using Kα (wavelength 1.541874) of CdTe on silicon with deposition rate of 1, 5 & 10 Å/sec. Several well defined peaks are observed in the XRD pattern. The XRD analysis reveals that the films are polycrystalline, and the sharp peaks are identified as (111), (220), and (311) planes of CdTe. The strong peak at 23.76° corresponds to the reflection of cubic (111) plane for all the deposition rates. No diffraction peaks associated with metallic Cd, Te or other compounds were observed. This shows that respective layered structures present a single phase with highly oriented CdTe crystallites with the (111) planes parallel to the substrated. The nature of substrate on which CdTe is deposited influence the grain orientation in the film. The low intensity peaks observed in XRD pattern shows that the films are coarsely fine crystallites or nano-crystalline. The broad hump in the displayed pattern is due to the Si substrate and also possibly due to some amorphous phases present in the CdTe thin films as shown in figure 3(a). The intensity of the peaks of 1A/sec is stronger than other deposition rates indicates the improvement of crystalline quality. The Strong and sharp peak diffraction peaks indicate the formation of well crystalline film. It shows that the major peak (111) is strongly dominating the other peaks as shown in fig 3(a), (b), (c)). Figure 3(d) shows the XRD of polished silicon used as reference for comparing the depositing CdTe film of different thickness at different deposition rate. Thus from these XRD results it shows that fcc structure for fixed thickness of CdTe is independent of deposition rates.

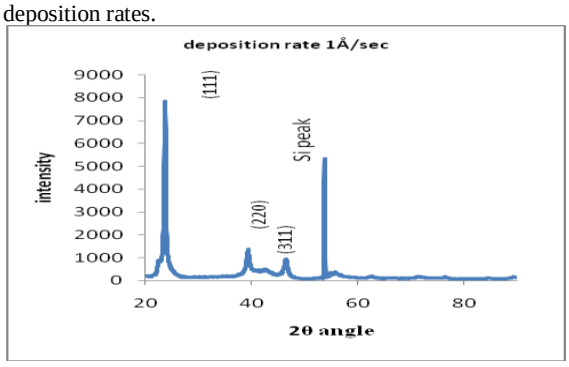

Fig: 3(a) CdTe deposition on Si at deposition rate of 1Å/sec

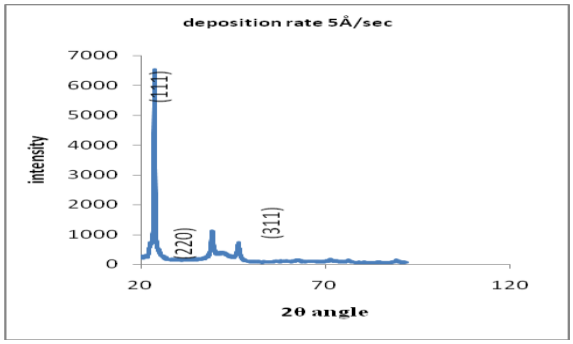

Fig: 3(b) CdTe deposition on Si at deposition rate of 5Å/sec

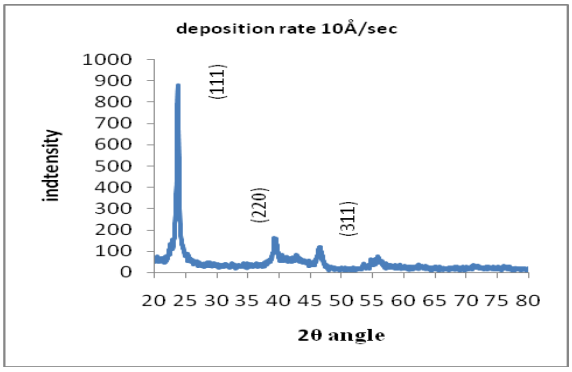

Fig: 3(c). CdTe deposition on Si at deposition rate of 10Å/sec

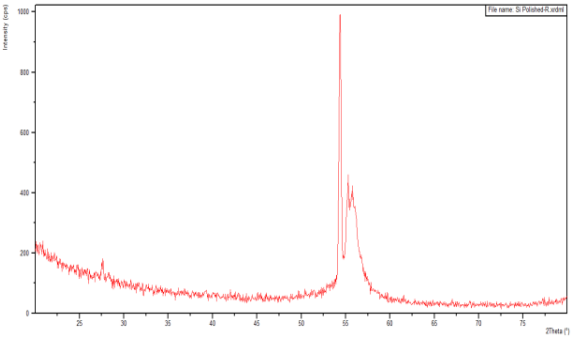

Fig: 3(d). XRD Analysis of Polished Silicon

4.2 EDX Results

Energy dispersive X-ray (EDX) analysis indicated the presence of Cd and Te for all the deposited layers as shown in figure 4. The average atomic ratio of Te/Cd, calculated from the quantification of the peaks, gives the values of 0.98, 1.14 and 1.18 for different deposition rates 1, 5 & 10Å/sec respectively. Also the atomic percentage of Te increases while Cd decreases with increasing deposition rates as shown in table no.2. These results indicate that the average atomic ratio of Te/Cd increases with decreasing deposition rate, ratios of the films are not matching with the stoichiometric ratio (Te/Cd =1) and the surface of the sample is rich in metal. Deviation from the atomic percentages of Te/Cd ratios could be attributed to the presence of higher atomic percentage of oxygen revealed from the EDX of the films.

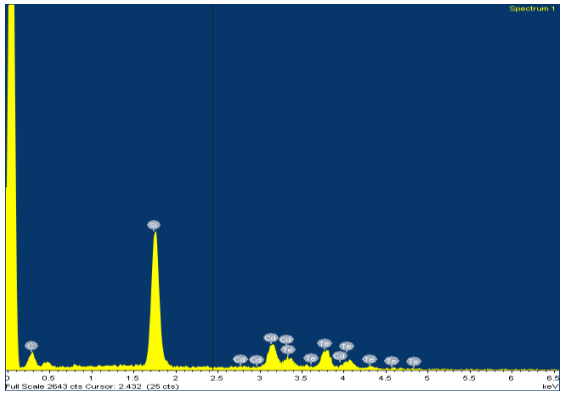

Fig: 4. EDX Scanning Pattern of CdTe on silicon

Oxygen or other impurities may be incorporated in the film either from the atmosphere or from the outgassing from chamber walls etc. Atomic percentage of oxygen or other impurities increases with the increase in deposition rates. EDX analysis of CdTe thin films with different deposition rates are listed in Table 2

Table: 2. EDX Analysis of CdTe with Different Deposition Rates

Deposition rate	Atomic %			Wt.%	
	Te	Cd	Te/Cd ratio	Te	Cd
1Å/sec rate	49.94	50.06	0.98	53.11	46.89
5Å/sec rate	53.47	46.53	1.149	56.61	43.39
10Å/sec rate	54.16	45.84	1.18	57.28	42.72

4.3 SEM Results

Figure 5(a), 5(b), 6(a), 6(b) &7(a), 7(b) shows the SEM micrographs of CdTe 1000 Å thin film with 1, 5 &10 Å/sec deposition rates on silicon substrate respectively at 50KX &100KX magnifications, 5KVEHT, for study the microstructure and grain size.

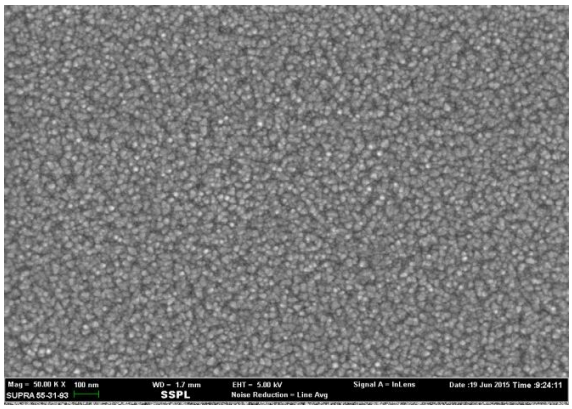

Fig: 5(a). SEM micrographs of CdTe at 50KX magnification with 5KV at deposition rate of 1 Å/sec

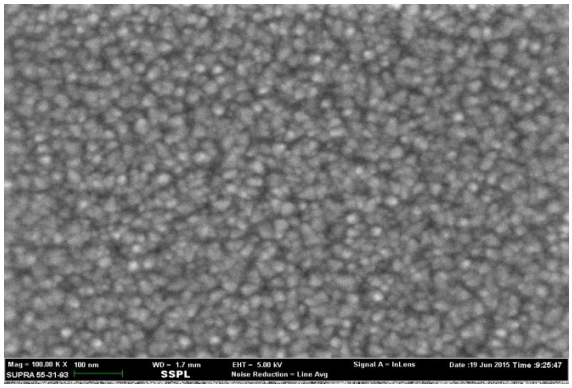

Fig: 5(b). SEM micrographs of CdTe at 100KX magnification with 5KV at deposition rate of 1 Å/sec

The SEM micrographs show that the Si substrate is deposited with CdTe without cracks and pin-holes and is well covered. In case of deposition rate of 10 Å/sec, the grain size is very small and more evenly distributed. The grain size is in the range of 17-20 nm. The 20 nm grain size

grains are very few which means most of them are below 20 nm size as shown in figure 6(a),6(b).The SEM micrographs of.deposition rate of 1 Å/sec as shown in figure 4(a),4(b), also shows the good uniformity with grain size of 19-25 nm but not so good as in case of 10 Å/sec deposition rates i.e. variation in grain sizes is more. But in case of deposition rate of 5 Å/sec as shown in figure 5(a),5(b), the grains are poorly distributed over the Si surface and grain sizes are coarse & uneven in size. The grains are in the sizes of 21-28 nm which can be improved by annealing.

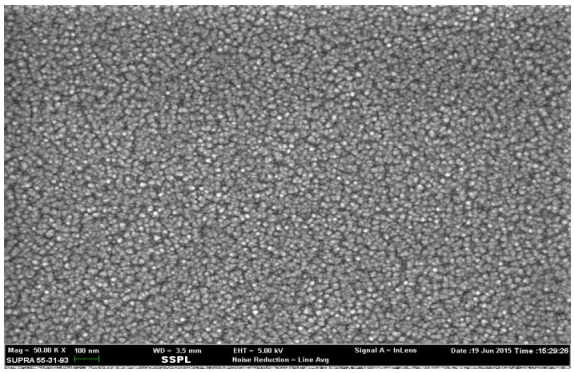

Fig: 6(a). SEM micrographs of CdTe at 50KX magnification with 5KV at deposition rate of 5 Å/sec

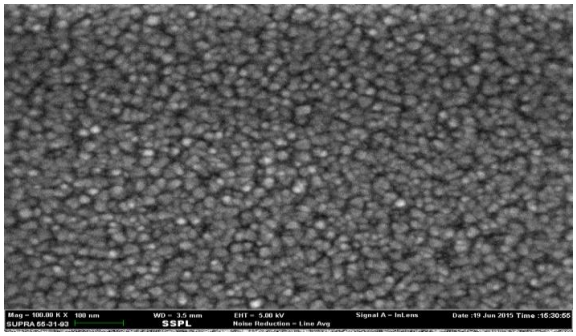

Fig: 6(b). SEM micrographs of CdTe at 100KX magnification with 5KV at deposition rate of 5 Å/sec

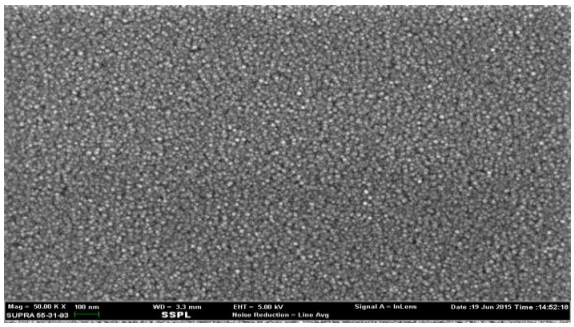

Fig: 7(a). SEM micrographs of CdTe at 50KX magnification with 5KV at deposition rate of 10 Å/sec

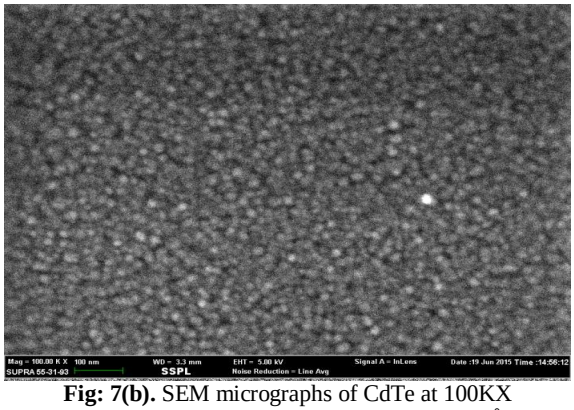

Fig: 7(b). SEM micrographs of CdTe at 100KX magnification with 5KV at deposition rate of 10 Å/sec

5. Conclusion

Thin films of CdTe are prepared by thermal evaporation process on silicon substrates by 1, 5 & 10Å/sec deposition rates. Deposited films thicknesses are measured at different points on Si substrate by dektek surface profiler and compared with the film thickness value shown by Digital Thickness Monitor (DTM) using piezoelectric quartz transducer of having and this variation is found to vary 5-10%. Actually, a comparison is done between film deposited on Si substrate and quartz which are placed close together in the vacuum chamber. This variation can be minimized by reducing the gap between them & regular cleaning of quartz. Also by doing a set of repetitive experiments we can reduce this variation. XRD analysis shows that the CdTe films are polycrystalline with preferential orientation of (111) plane with cubic phase for all the deposition rates of 1, 5 & 10Å/sec.SEM micrographs at 50KX & 100KX magnification shows that film obtained for CdTe at 10 Angstrom/sec is smoother, void free, uniform and regular granular shaped grains than the 5 & 1Å/sec deposition rate. Though comparatively at 1Å/sec deposition rate, microstructure of CdTe is better than 5Å/sec deposition rate. The grain sizes of CdTe at 1, 5 & 10Å/sec is estimated to be in the range of 19-25, 21-28 & 17-20 nm respectively. The EDX analysis shows that the Te/Cd ratio at 1, 5 & 10Å/secis 0.98, 1.14 and 1.18 respectively. Thus we can say CdTe deposition rate of 1 Å/sec is more favorable because of high intensity peaks for preferential (111) plane indicating good crystalline cubic structure, good grain size along with better uniformity on Si substrate and very close to stoichiometric ratio (Te/Cd =1).

Acknowledgement

We are very thankful to Solid State Physics Lab. for giving support in this work.

References

[1] A. A .Ibrahim et. al., Structural and electrical properties of evaporated ZnTe thin film, Journal of Vacuum, 75, 2004 , 189–194

[2] E. E. Khawaja et al., Chemical Inhomogeneity in Zinc Telluride thin films prepared by thermal evaporation, Journal of Thin Solid Films, 485, 2005, 16–21

[3] S. Larramendi et al., Growth of ZeTe and CdTe films using the isothermal close space sublimation technique in vacuum environment, Journal of Crystal Growth, 312, 2010, 892–896

[4] R. R. Singh et.al. Investigation of Passivation Processes for HgCdTe/ CdS structure for Infrared

application, Journal of thin solid films, 510, 2006, 235–240
[5] R. Pal et. al., Engineering Interface Composition for Passivation of HgCdTe Photodiodes, IEEE Transactions on Electron Devices, 53(11), 2006, 2727-2734
[6] K. Nagamani et.al., Properties of Al-doped ZnS Films Grown by Chemical Bath Deposition, Physics Procedia 25, 2012, 137–142
[7] F. Gode et. al., Investigations on the Physical properties of the polycrystalline ZnS thin films deposited by chemical bath deposition method, Journal of Crystal Growth, 299, 2007, 136–141
[8] Ali Moarrefzadeh et.al., Simulation and Modeling of Physical Vapor Deposition (PVD) Process, Wseas Transactions on Applied and Theoretical Mechanics, 7(2), 2012
[9] V. D. Falcão W. A. Pinheiro, C. L. Ferreira, L. R. de O. Cruz, Influence of Deposition Parameters on the Properties of CdTe Films Deposited by Close Spaced Sublimation, Journal of Materials Research, 9(1), 2006, 29-32
[10] E. R. Shabban, N. Afify, A. El. Taher, Effect of film thickness on microstructure parameters and optical constants of CdTe thin film, Journal of Alloys and Compunds, 482, 2009, 400-404
[11] L. Gouda, Y. R. Aniruddha, S. K. Ramasesha, Correlation between the Solution Chemistry to Observed Properties of CdTe Thin Films Prepared by CBD Method, Journal of Modern Physics, 3, 2012, 1870-1877
[12] A. Romeo, G. Khrypunov, S. Galassini, H. Zogg, A. N. Tiwari, N. Romeo, A. Bosio, S. Mazzamuto, Comparison of CSS-CdTe and PVD-CdTe with different activation, 22nd European Photovoltaic Solar Energy Conference, 2007, Milan, Italy
[13] M. Estela Calixto, M. L. Albor-Aguilera, M. Tufiño-Velázquez, G. Contreras-Puente, A. Morales-Acevedo, Chemical Bath Deposited CdS for CdTe and Cu(In,Ga)Se2 Thin Film Solar Cells Processing, www.intechopen.com
[14] W. A. Pinheiro, V. D. Falcão, L. R. de O. Cruz, C. L. Ferreira, Comparative Study of CdTe Sources Used for Deposition of CdTe Thin Films by Close Spaced Sublimation Technique, Journal of Materials Research, 9(1), 2006, 47-49
[15] G. Gordillo, E. Romero et.al., Structural characterization of thin films based on II-VI ternary compounds deposited by evaporation, Journal of Thin Solid Films, 484, 2005, 352–357
[16] J. Wang et al., Microwave-assisted synthesis of high quality CdTe/CdS @ ZnS-SiO2 near-infrared-emitting quantum dots and their applications in Hg2+ sensing and imaging, Journal of Sensors and Actuators, B 207, 2015, 74–82
[17] Osvaldo de Melo et. al., Growth of CdSe and CdTe crystals shaped by thick alumina membranes, Journal of Crystal Growth, 311, 2008, 26–31
[18] K. A. M. H. Siddiquee et al., Investigation of CdS and CdTe thin films and Influence of CdCl2 on CdTe/CdS structure, Journal of Optics, 124, 2013, 4383–4388

*International Research Journal of Environment Sciences*_____ ISSN 2319–1414
Vol. **4(7),** 86-95, July **(2015)** *Int. Res. J. Environment Sci.*

Urban Canyon Modelling: A Need for the Design of Future Indian Cities

Kanakiya R.S.[1], Singh S.K.[1] and Mehta P.M.[2]
Environmental Engineering Department, DTU, formerly Delhi College of Engineering, Delhi, INDIA
Allana College of Architecture, Pune University, Pune, INDIA

Available online at: www.isca.in, www.isca.me
Received 8th May 2015, revised 15th June 2015, accepted 20th July 2015

Abstract

India has experienced a high rate of Urbanization, higher density of population in cities has more of it. The higher population Density with cities like Mumbai having population densities of 20680 person/km^2 has led to crowded space in a urban setting decreased Natural Ventilation of Air Pollutants. Using the advanced Computational and Mathematical models pollutant concentrations are estimated. Street Canyon models, which may include simplified photochemistry and particle deposition-suspension algorithms. These models when used in a knowledgeable way principles that govern the dispersion and transformation of atmospheric pollutants. A study of vehicle exhaust dispersion within different street canyons models in urban ventilated by cross-wind is conducted at this work to investigate how air pollutant dispersion is exaggerated by wind speed, building height to width ratios, street and building geometries and canyon street number.

Keywords: Urban canyon modelling, urban heat island, net radiation flux.

Introduction

The Future planned Indian Cities of Durgapur, West Bengal, Greater Noida, Uttar Pradesh, Lavasa, Maharashtra, Mohali, Punjab, GIFT, Gujarat, New Town, Kolkata, Sri Gangbanger, Rajasthan, Sricity, Andhra Pradesh and so forth are spreading at a fast pace in its width there are to take into consideration the effect of the congregation of the air pollutants due to peculiar geometry of the design of the buildings urban canopy.

The World Bank has given status of Indian Urban Area as it is going to be 50% by 2050 from 2013. So we need to build these future areas in such a way that it mitigates the effect of Urban Heat Island and have natural ventilation in the cities.

The Cities have experienced rapid urbanisation which has brought more clusters of tall buildings, compact urban space and the smaller street geometry in the metro cities; it influences the urban climate in quite large manner. It is very necessary to study the urban canyon at a micro-scale and how it does affect the overall climatic condition on an urban scale also the concept associated with it urban canopy, urban heat island Roughness subsurface and boundary layers.

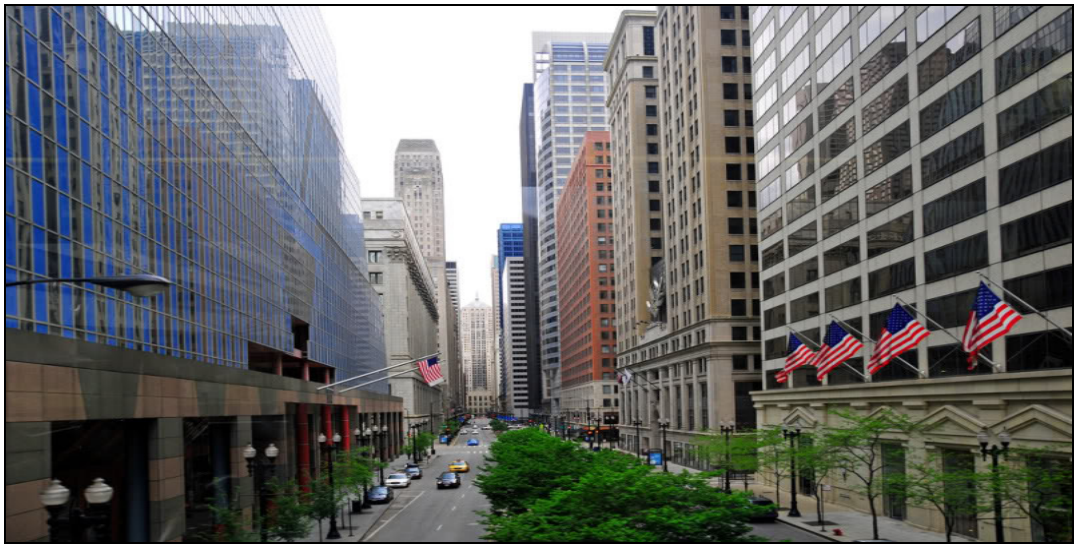

Figure-1
Typical Urban Street Canyon

As the Vehicles Need Fossil Fuel to operate like diesel, petrol, natural gas they contribute to air pollution significantly[1].

Particulate Matter, Hydrocarbon, Carbon Monoxide, Nitrogen Oxide, Ozone which are most important Traffic-related air pollutants in modern urban agglomerations. Air quality limit values, whose objective is to safeguard public health, are frequently exceeded, particularly in busy streets and urban areas. The dilution and removal of vehicular traffic exhausts in urban street canyons is of great importance for the public health and quality of life of people living or working in city centres.

Urban Canyon Modelling Definition

Air dispersion characteristic modelling in a typical urban space where there is a restriction of the vehicular pollution emission dispersion. The modelling can be done in different scales from micro-scale (street level) to Meso-scale (whole city) which is given in the below figure. The nature of our research influences the selection of the size of area which is to be considered.

The buildings change air flow field, influencing pair exchanges and dispersion of pollutants in urban areas where population and traffic density are relatively high human exposure to dangerous substances is significant. Due to this distress, the street canyons are considered as hot spots for air pollution problems.

Irregular shaped buildings increase turbulence and vertical mixing in atmosphere; W/H ratios of urban canyons affect street air dispersion.

Urban Heat Island (UHI): Atmospheric temperature rise experienced due to heat island phenomenon has been commonly linked with cities. These types of surfaces are dark, dry which are characterized by low albinos, high impermeability and favourable thermal properties which are capable of heat energy storage and subsequent heat release. The lesser is the sky view factor the greater is the absorbance and the remittance from their surface in the urban canyon. Due to these factors urban areas have greater temperature in relation to their rural counterparts which have more vegetation, and thus their temperatures are maintained through the evapotranspiration progression, shades of trees and interception of sun's radiation.

Components of urban Canyon Modeling

Emissivity of the material[2]**:** The relative ability of its building surface to its emit energy by radiation, important related to the UHI phenomenon is called as Emissivity. As the Urban Agglomerate is built up usually by Bricks, Concrete and Asphalt there is enormous amount of heat emitted which is 0.93, 0.88, and 0.93. High Emissive Materials emit radiation at night making the temperature of the Surface Urban Heat Island is comparatively higher at nights than the rural counterparts.

Albedos of the Different Material: Commonly used materials like concrete, brickwork and bitumen heats up rapidly in the day time in contrast to water bodies. Due to nature of the surface its albedo is lower. More Heat is enthralled and conducted through the Material. Warmth is added into the atmosphere as the heat is emitted slowly. This phenomenon keeps urban climates relatively high and the contrast between the urban environment and the rural fringe is highest at night.

Sky View Factor (SVF): It is one of the most vital factors in Urban Heat Island required as a parameter in its modelling using Arc View GIS and the possibilities of the 3DSkyView Tool.SVF is the ratio of the radiation received by a planar surface to the radiation by the entire hemispheric environment.

Urban Sub-surface Roughness: The roughness sub layer is usually termed as the region where the flow is influenced by the individual roughness elements as reflected by the spatial in homogeneity of the mean flow, for example[3], in the atmospheric context states that in the Urban Scenario it is affected by the High-rise Buildings thus giving in homogeneity to the mean flow.

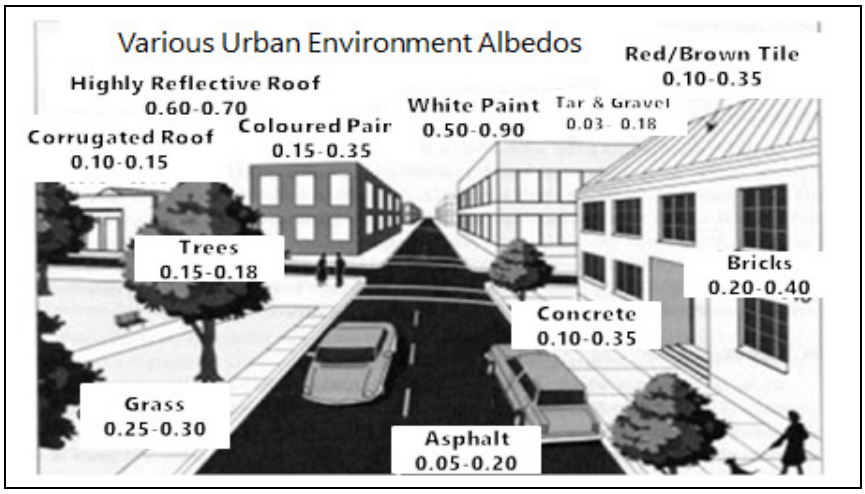

Figure-2
Albedos of different material in Urban City

Net Radiation Flux: Net Radiative Flux of the underlying surface is difference between the absorbed radiant energy and

that emitted by the underlying surface, the atmosphere or by the earth-atmosphere system. Greatest variations of meteorological parameters in urban areas are caused due to short wavelengths. Long-wave radiations are as a result of reemitting from the urban surface downward to where it is retained by the ground. Representation of Heat Flow in Urban setting in figure-3.

Gartland[4] stated that although anthropogenic heat, low wind speeds, and air pollution in urban areas can contribute to UHI creation, there may be two main explanations for formation of UHI

Due to impermeable material used in the new-age construction the moisture is been trapped this does not allow heat to dissipate in the atmosphere; In a canyon set-up dry, dark surfaces can reach upto 88°C and the vegetated surface with moist soil can reach only upto 18°C building and pavements trap more heat of the sun's energy

Faces of the building in a Urban Setting: In the transverse, vertical plane at mid-canyon show that the pollutant concentrations has higher concentrations at leeward face than that at windward faces, and has higher concentrations above downwind buildings than that above upwind buildings, Longitudinal distributions of pollutant concentrations at leeward and windward faces show decreasing of the concentration with increasing building height. While calculating the impacts of the pollutant it's important to specify which direction of walls and if these are unequal in dimension that the whole models changes as the dispersion characteristics will change.

Distinction between Urban Surface Energy Balance and Rural Energy Surface Balance: Sensible heat flux is greater due to the man-made materials like more use bricks, cements, paving and intensification of surface area, Latent heat flux is lower due to a lower fraction of vegetative land-use cover, Urban surfaces have higher thermal inertia due to high heat capacity of the man-made surfaces, leading to a non-negligible storage flux, Complex processes of shadowing and multiple reflections affect short-wave radiation fluxes, and the wide range of materials affect the emissivity and thus long-wave fluxes, resulting (surprisingly) in little difference in net radiation flux, and Anthropogenic heat sources act in addition to the solar-driven energy balance, effectively increasing the sensible heat flux. The urban surface energy balance drives not only the temporal advancement of the urban heat island (UHI), but also the evolution and vertical structure of the UBL.

Roughness elements are large, and exert significant drag on the flow. An urban roughness sub layer (RSL) can be defined of depth between 2–5H, where H is the mean building height. Within this layer, flow is highly spatially dependent (figure-4); turbulence can dominate the mean flow; and turbulence has different characteristics from the flow in the inertial sub-layer (ISL) above, where the turbulence is homogeneous and fluxes vary little with height. The urban canopy layer is defined as the layer up to mean roof height.

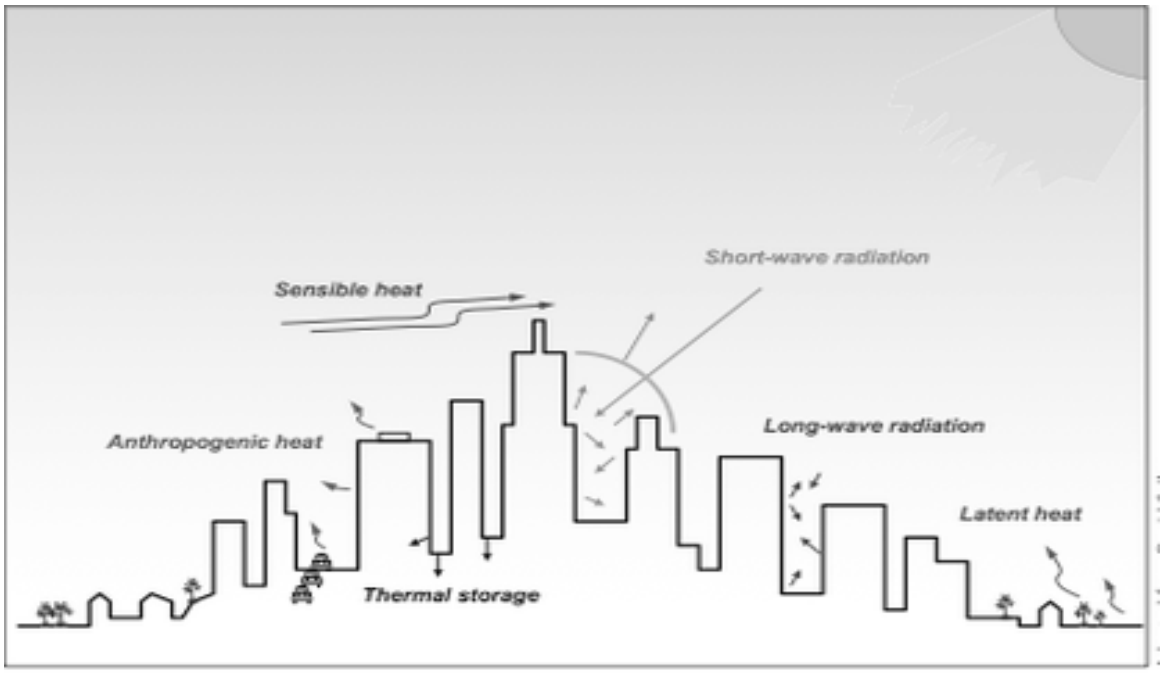

Figure-3
Typical Radiation Energy flow in a Urban Setting

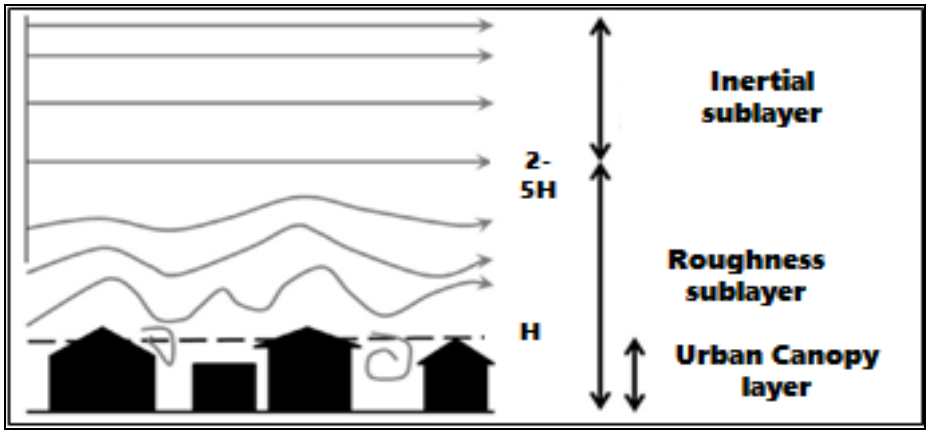

Figure-4
Schematic diagram of roughness and inertial sub-layers, Grey arrows indicate streamlines. Dashed line indicates mean building height H

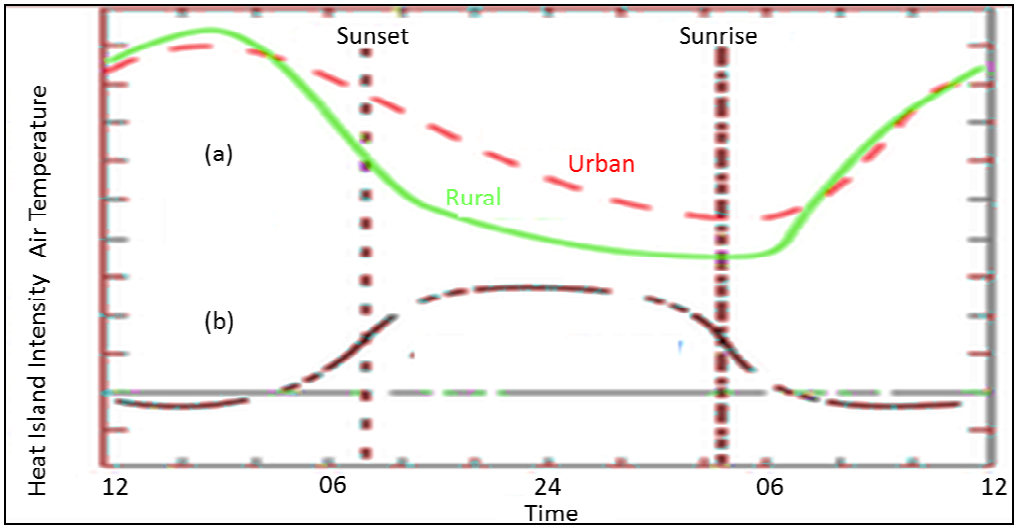

Figure-5
Diurnal Heat Change with Calm Atmospheric Conditions (Runnels and Oke, 2000)

From Figure-5 As shown in Section A During the day the heat is absorbed by the building surface material and during nights it reemits that is why the cooling is far lesser in urban area in the Time 18:30 to 5:30. So in nights temperature is higher in the urban areas as compared to the rural areas.

Urban areas are characterised very high more than 70% impermeable material and experience has lesser evapo transpiration as compared to rural areas. This difference contributes between urban and rural area to higher surface area temperatures[5].

The Pollutants when in atmosphere are either of these fates in their lifespan which are Advection Moving along with air in the atmosphere which is given by expression J=C*U

Where J=Advection, C=concentration, U=Velocity of the flow, Diffusion process through which pollutant molecules move through air which is given by Jd=-D ∂C/ ∂x or Dispersion, When a pollutant moves dissolved in volatilized in air. Change in pollutants concentration= Ma-Sd, Where Ma = Movement due to advection Sd = Spreading due to Diffusion/dispersion.

Street Canyon Modelling

The issue of dispersion of the atmospheric air pollutants is completely different in case of street. The results of this air quality models can be used for air quality management and traffic control, urban design planning, interpretation of monitoring data, time scale pollution forecasting, etc. Although there are no clear-cut distinctions between different categories, models might be classified into groups according to their physical (or mathematical principles and their level of sophistication Dispersion models gives current and impending

air pollution levels air quality by providing forecasting with time-based and three-dimensional variations [5]

Wind flow: In the street canyon we take into consideration the microclimate and the urban geometry rather than the mesoscale forces regulatory the environment of the Boundary Layer A clear discrepancy is made between the synoptic above roof-top wind conditions and the local wind flow within the cavity of the canyon (figure -6).

Depending on the free stream winds having velocity can be having 3 main dispersion circumstances can be identified: i. Condensed winds lower than 1.5m/s, ii. Upright flow for synoptic winds over 1.5 m/s blowing at an angle which is more than 30° to the canyon area, iii. Lateral or just lateral flow for winds over 21.5 m/s. In the case of Upright flow, the Windward side of the canyon is usually called leeward.

Typical regimes of winds might be observed in the case of study of cross section in the mid-canyon region with speed of the winds greater than 2 m/s [5] (figure-7). i. Isolated Roughness Flow, ii. Wake Interference Flow, iii. Skimming Flow.

For wide canyons (H/W<3), the buildings are well spaced and act essentially as isolated roughness elements, since the air movements a sufficient distance downwind of the first building beforehand coming across the next hindrance.

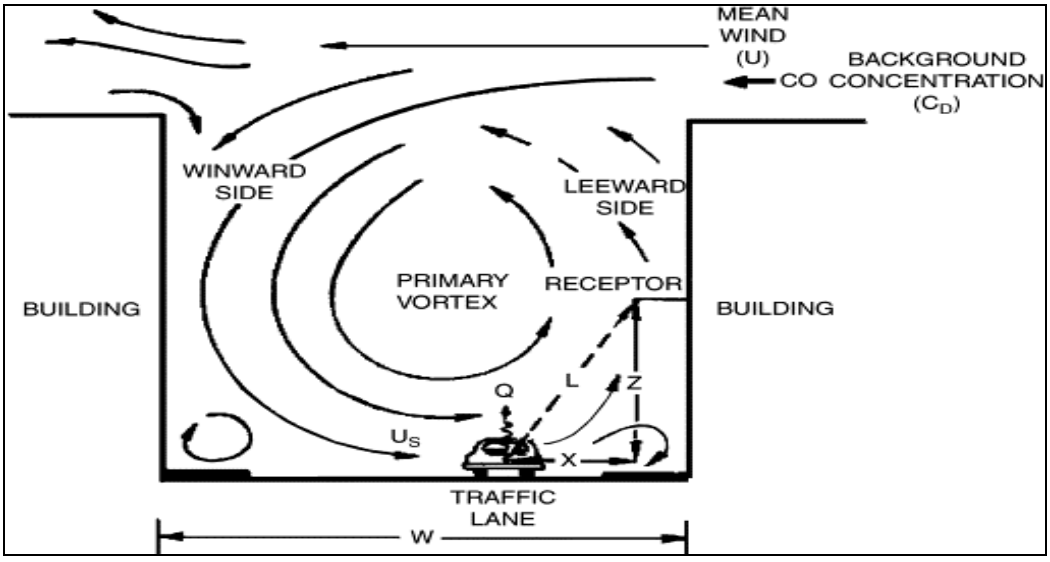

Figure-6
The Flow of the wind in Urban Agglomerate

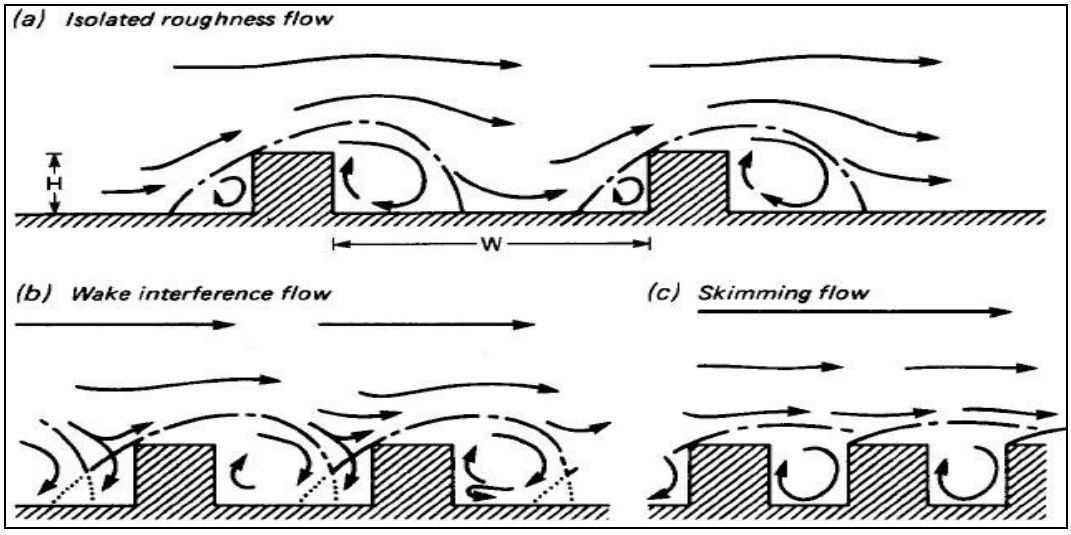

Figure-7
Flow Regimes linked with Air Flow over Building

The stability of the atmosphere and also it has its shape and also heating of walls strength and shape of the wind vortices are affected[7].

A: The robust flow is deflected down the building, B: Calm zone develops amongst buildings, C: Combination of huge buildings with streets forms canyons which yield enhanced wind flow.

Pollutant dispersion: Dispersion of gaseous pollutants in the vertical direction of the atmosphere and in the lateral direction with the associative streets[6] .With greater L/H the maximum street-level concentration occurs when synoptic winds are parallel to the axis of the street. The build-up of emissions on path of line source outweighs the ventilation brought by parallel winds[8].

Due to Low synoptic helps air pollution augmentation in urban zones[9].Whenpthepsynoptic wind speed is below 1.5 m/s, the wind vortex in the canyon vanishes and the air stagnates in the street.[10]declared coarse particles are to be monitored in the street canyon as compared to the finer particles as the later disperses very quickly just like gases into the atmosphere.

Considerations in the Urban Canopy Model: Models are to be designed as according taking into consideration cities urban heat flux, geometry, Atmospheric Stability for that particular geographical location of the city. Urban Canopy Models have three components namely roads, roofs and walls characterized by the width of street canyon and building and is thus possible to taking into version the sink of momentum over the complete structure of the building, along with shadowing energy trapping effects. The Urban Canyon Modelling is essential for the setup of the new industry in Urban so its influence is essential to ensure that the location has its pollutants levels in limits.

Types of Models used in Street Canyon Modelling

Models based on Gaussian Plume Dispersion: These Models are governed on basis of equations the 3 dimensional concentration field made generally by a point source. These Gaussian plume concentrations from a unceasingly releasing source are proportional to the emission rate, inversely proportional to the wind speed, and that the time averaged pollutant concentrations horizontally and vertically are properly defined by Gaussian equation of dispersion.

The Gaussian plume model assumes that there is no chemical or removal processes in process and that pollutant material reaching the ground or the top of the mixing layer as the plume grows is replicated back towards the plume centerline.

Computational Fluid models: In Computational Fluid Dynamics models simulation is done of fluid flow, air flow by means algorithmic based mathematical models.CFD models are widely used in the environmental modelling such as for water pollution and the air pollution.

CFD codes are user friendly consists of three main elements:

The pre-processor, creates a grid of the computational field, is been generated in which all chemical and physical phenomenon to be modelled are displayed.

Figure-8
The figure exhibits the wind flow around different structures such as tall and short buildings

The solver, for computation of flow variables governing atmospheric flow using the mathematical equations.

The post-processor gives the results in plots or graphs vectors like showing wind direction and contours showing varied pollutant concentration can also give the result in graphic animated form.

FLUENT is widely used CFD Software for Modeling Complex Fluid Stream and Heat Transfer in varied geometries. It calculates using finite volume structure on non-orthogonal using a collected variable arrangement

Reduced scale Wind tunnel: Having the similar urban scenario like the Roof Shape Emissivity, Wind Characteristics, Fixed and Moving obstacles in the wind tunnel is performed by the researcher. In this research the tracer also can be used in the study the air dispersion the sulphur hexafluoride (SF_6) analyser is the common tracer generally used and its concentration is measured.

Models based on Box Dispersion: These Models have a restricted set of boundary conditions the pollutants are set to be content within this set of atmospheric air pollutant concentration is termed as the Accumulation is equal to Input to the box – Output from the box (+ or -) rate of transformation of pollutant[11]. used a single box model and calculated initial dispersion and car induced turbulence called STREET BOX Model[9] concluded based on the assumption that concentrations of the pollutant occurring on the roadside consist of both the components, the urban background concentration and the concentration component because of vehicular emissions created in the specific street. Then, it calculates pollutant concentrations, taking in account the mixing height of pollutants, lateral distance of the simulated receptor.

Results and Discussion

A typical urban street of Katraj Box modelling is been done taking into consideration the vehicular traffic flow for the peak traffic hours (9:30 to 9:45),(9:45 to 10:00),(20:00 to 20:15) and (20:15 to 20:30) categorizing the vehicles into different sub-groups as Light Duty Vehicles Two Wheelers , Three Wheelers, Passenger Cars (Petrol), Passenger Cars (Diesel), , Buses,, Heavy Duty Vehicles taking into consideration respective pollution potential as in table-1 the vehicular traffic flow in (vehicles/hour) as in table-2.

Table-1
Vehicular traffic flow converted into vehicles/hour

Timings	9:30-9:45	9:45-10:00	20:00-20:15	20:15-20:30
Two Wheeler	1387	1455	1206	1040
Three Wheelers	255	245	190	164
Passenger Cars (Petrol)	455	551	352	574
Passenger Cars (Diesel)	28	13	18	31
Light Duty Vehicles	74	81	31	25
Heavy Duty Vehicles	147	155	175	125
Bus	70	65	45	36

Table-2
Vehicular their emission potential in µg/km as per ARAI, India

Vehicle Category	CO	NOx	SPM	PM10
Two Wheelers	1	0.19	0.05	0.1
Three Wheelers	1.4	1.28	0.2	0.2
Passenger Cars (Petrol)	1.2	0.2	0.03	0.1
Passenger Cars (Diesel)	0.8	0.5	0.07	1
Light Duty Vehicles	2.5	2	0.56	1.25
Heavy Duty Vehicles	3	6.3	0.28	2
Buses	4.8	12	0.56	1.5

Table-3
Vehicular emissions in µg/km/hour

	9:30-9:45				9:45-10:00			
Vehicle Category	**CO**	**NOx**	**SPM**	**PM10**	**CO**	**NOx**	**SPM**	**PM10**
Two Wheelers	1387	263.53	69.35	138.7	1455	276.45	60.3	13.87
Three Wheelers	357	326.4	51	51	343	313.6	38	10.2
Passenger Cars(Petrol)	546	91	13.65	45.5	661.2	110.2	10.56	4.55
Passenger Cars (Diesel)	22.4	14	1.96	28	10.4	6.5	1.26	28
Light Duty Vehicles	185	148	41.44	92.5	202.5	162	17.36	115.625
Heavy Duty Vehicles	441	926.1	41.16	294	465	976.5	49	588
Buses	336	840	39.2	105	312	780	25.2	157.5

Table-4
Vehicular emissions in µg/km/hour

	20:00-20:15				20:15-20:30			
Vehicle Category	**CO**	**NOx**	**SPM**	**PM10**	**CO**	**NOx**	**SPM**	**PM10**
Two Wheelers	1206	229.14	60.3	120.6	1040	197.6	52	104
Three Wheelers	266	243.2	38	38	229.6	209.92	32.8	32.8
Passenger Cars (Petrol)	422.4	70.4	10.56	35.2	688.8	114.8	17.22	57.4
Passenger Cars (Diesel)	14.4	9	1.26	18	24.8	15.5	2.17	31
Light Duty Vehicles	77.5	62	17.36	38.75	62.5	50	14	31.25
Heavy Duty Vehicles	525	1102.5	49	350	375	787.5	35	250
Buses	216	540	25.2	67.5	172.8	432	20.16	54

Pollutants	**CO**	**NOx**	**SPM**	**PM10**
Average Vehicular Emissions	3011.075	2324.46	208.6175	725.2363
Background Concentration	0.71	12.25	153.25	210

Pollutants	**CO**	**NOx**	**SPM**	**PM10**
Total Calculated concentration (µg/m^3)	4.602294	12.26454	164.4371	248.8908

Calculating Concentrations Using Box Model: Formula used: $C= Q/(U_{ll}*H/L*W+(D+ lU_p))W/H + C_b$

Where: C: Calculated concentration in the street (µg/m^3)C_b: Background Concentration (µg/m^3), Q: Discharge source strength (µg/m^3), H: Avg Building Height (m)= 11m, W : Size of street (m) = 8m, L : Length of the street (m) = 100m, U_{ll} : Parallel Wind speed = 1 m/s, U_p : Perpendicular Wind speed =2.8 m/s, l : Characteristic Mixing Length (m) = 1m, D : Diffusion Coefficient (m^2/s) = 1.5 m^2/s .

After Application of Box Model to the street of Katraj, Result ant pollutant concentrations are NOx are 19.77 µg/m^3. Like-wise we can calculate for other pollutants by this box model.

Conclusion

Indian Environmental agency like CPCB, SPCB's are suggested undertake this project of Urban Canyon Modeling for the future cities of India. Analysing Pollutant dispersion for a particular location through Urban Canyon Dispersion Model essential for the urban city planner as to how to tackle this increasing Urban Heat Island Effects in the city and a health risk to the urban dwellers as the natural dispersion, wind flow, turbulence Innovative solutions are to be found out by a proper designing the Future cities in India such by the for this problem.

Scientists experimented with different street canyon geometry using Urban Canyon Models for analysis it was recommended

by them for the city planners is that trees shall have smaller foliage as it will restrict the dispersion of air pollutants and as far as spacing is concerned it shall have sufficient spaces so as it enables atmospheric overflow and disperses the Polluted Air.

Increasing vehicular traffic growth and emissions and their impact on human health and urban air quality there is an urgent necessity for a new pollution control regulatory framework for the management of vehicular traffic, air quality and emissions at all scales from local to global [13]Air quality models can help to develop air quality management action plans and serves as an effective tool for improving air quality in urban centers.

Air quality models predicts the dispersion and dilution processes of the pollutants in the atmosphere using the releases, prevailing meteorological conditions and street configurations to determine the ambient air concentrations [8].

Recommendations to avoid the Negative Impact of Urban Street Canyon: The primary reason of heat island in cities is due to the absorption of solar radiation by massive building structures, roads and urban surfaces contained within the street canyon. The absorbed heat is subsequently reradiated to the settings and increase in ambient temperatures at night. To reduce the heat island effect it is advisable to use appropriate materials in order to improve the thermal characteristics of the urban environment. For example, light coloured surfaces are environmentally more beneficial as compared to dark coloured surfaces in urban areas. This can be used to increase the alertness among urban planners, designers and decision makers on the importance of construction material choices which may be not only for aesthetic aspect but also for their effect local microclimate and indirectly on energy usage of buildings.

In order to avoid the urban canyon effect, materials of surfaces that affect the environment in the canyon may be wisely chosen. Alternatives for a few examples of certain materials commonly used on building surfaces are mentioned below:

Light coloured concrete may prove to be effective in reflecting up to 50% more light as compared to asphalt which will further reduce heat absorption eventually reducing the heat island effect.

In place of clay bricks wool bricks or mud bricks may be used in buildings because wool and mud bricks are sun-dried unlike clay bricks which are dried in kilns. Being sustainable in production these two types of bricks offer better sound absorption, higher thermal mass and are manufactured from natural resources.

Using coated glass or double glazed glass reduces the heat gain and loss into the building, keeping the surrounding environment of the building sustainable. In extremely hot climates solar control glass can be used which minimizes the solar heat gain and helps control glare. Glass may be a very good substitute instead of other opaque materials used on fenestrations of buildings since it helps control the exterior as well as the interior energy consumption of the building.

Similarly many other building materials may have alternatives that may be used to keep the environment of urban canyons clear of dispersions and enhance the quality within them.

To avoid urban street canyon effect, planting of trees along the street may prove to be beneficial. Trees lined along the street become obstacles in the path of wind flow and dampen the air thus reducing the dispersion and number of pollutants in the canyon. Thus, by providing trees the atmospheric wind is able to intrude avoiding relevant concentration increase in the street canyon.

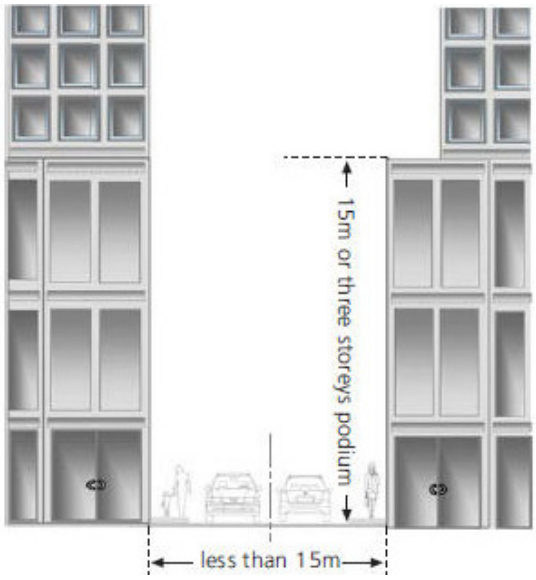

Figure-9
The "Canyon" effect takes place when taller buildings are Adjoining narrower streets that results in poor wind flow, higher temperature and deteriorated air quality

References

1. Gour A.A., Singh S.K., Tyagi S.K. and Mandal A., Variation in Parameters of Ambient Air Quality in National Capital Territory (NCT) of Delhi (India), *Atmospheric and Climate Sciences*, **5,** 13-22 **(2015)**

2. Sobrino J.A., Emissivity mapping over urban areas using a classification-based approach: Application to the Dual-use European Security IR Experiment (DESIREX), *International Journal of Applied Earth Observations and Geo information,* 08 **(2012)**

3. Klein M.P., Metropolitan effects on atmospheric patterns: important scales, Metropolitan sustainability, **(2012)**

4. Gartland on Urban Heat Island " www.hindawi.com" thebritishgeographer.weebly.com, **(2015)**

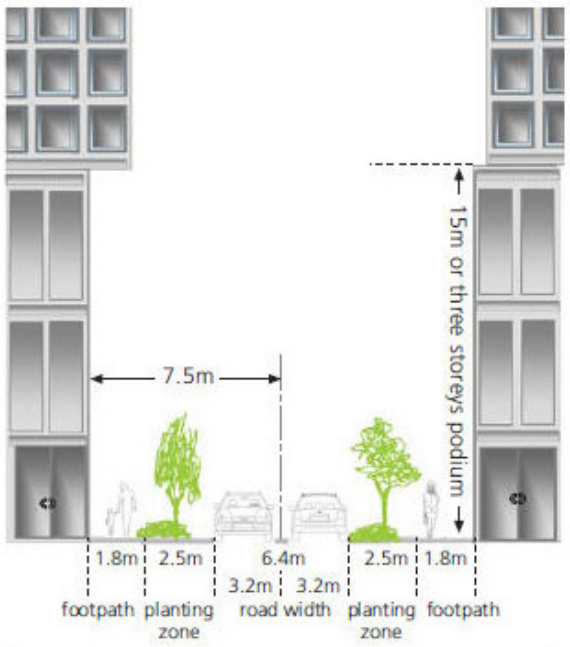

Figure-10
Building setback can improve the wind flow either, through or around the building, enhance air quality, in the neighbourhood and provide a better environment

5. Riain C.M.N., Fisher B., Martin C.J., Littler J.,. Flow field and pollution dispersion in a central London street. Environmental Monitoring and Assessment, **52,** 299-314 **(1998)**

6. Watson I.D. and Johnson G.T., Graphical estimation of sky viewfactors in urban environments, *J. Climatology*, **7,** 193–197 **(1987)**

7. Ganguly R. and Broderick B.M., Estimation of CO concentrations for an urban street canyon in Ireland, *Air Qual Atmos Health,* **3,** 195–202 **(2010)**

8. Sotiris Vardoulakis, Bernard E.A. Fisher, Koulis Pericleous and Norbert Gonzalez-Flesca. Modelling air quality in street canyons: a review, *Atmospheric Environment, Elsevier,* **37(2),** 155-182 **(2003)**

9. A brief definition of the main heat island types February 23, **(2010)**

10. http://www.urbanheatislands.com/home, **(2015)**

11. Oke T.R., Urban environments. The Surface Climates of Canada, Bailey, W.G., T.R. Oke, and W.R. Rouse McGill-Queen's University Press, Montreal, 303-327 **(1997**

Adequacy assessment studies of improved circular clarifier for type-II settling for storm water treatment.

ARTICLE · OCTOBER 2013

Source: PubMed

2 AUTHORS, INCLUDING:

Girish Pophali
National Environmental Engineering Resea…

16 PUBLICATIONS **90** CITATIONS

SEE PROFILE

ISSN 0367-527 X VOLUME 55 NO. 4 OCTOBER 2013

Journal of Environmental Science & Engineering

CSIR-National
Environmental
Engineering
Research
Institute
Nagpur 440 020
INDIA

J Environ. Science & Engg. Vol. 55, No. 4, p. 481-490, October 2013

Adequacy Assessment Studies of Improved Circular Clarifier for Type – II Settling for Storm Water Treatment

NANDITA AHUJA[1] AND GIRISH R. POPHALI[2+]

The adequacy of an improved circular clarifier was assessed for solids-liquid separation of chemically treated storm water. The storm water was treated with alum and polyelectrolyte to enhance settling. The performance of the clarifier was studied under various operating conditions by varying suspended solids concentrations and turbidity, and the hydraulic retention time. It was observed that the clarifier worked at an optimum hydraulic retention time of 1.5 hours for initial suspended solids concentration of less than 500 mg/L. However, for treatment of storm water with suspended solids concentration more than 500 mg/L, the hydraulic retention time needs to be selected taking the required effluent turbidity and effluent usage into consideration, i.e. for high turbidity removal an optimum hydraulic retention time of 2 hours must be used against a hydraulic retention time of 1.5 hours for a relatively low turbidity removal. Thus, the clarifier can be effectively used on field scale for solids-liquid separation of flocculent suspensions.

Key words: *Improved circular clarifier, suspended solids, turbidity, hydraulic retention time*

Introduction

The main objective of a primary clarifier in water and wastewater treatment plants (WTP) is to remove suspended solids from the influent (AWWA 1999)[2]. The efficient functioning of clarifier has direct influence on the subsequent treatment units (Kawamura 2000)[7]. The understanding of the dynamics of primary clarifiers is, indeed, important to the overall effectiveness of the treatment plant (Lindeborg *et al.*1996)[9]. The working principle on which a clarifier is based is referred to as sedimentation or settling (Chris *et al.* 2002)[3].

Sedimentation or settling is the gravity separation of a suspension into a supernatant clear fluid and denser slurry containing a higher concentration of solids (Kirk 2008)[8]. Chief determinants of rate and degree of sedimentation are the suspension characteristics and characteristics of the fluid in which suspension is present (Degremont, 2007)[5]. Sedimentation is divided into four major categories depending upon the type of suspension to be settled (Hendricks 2006)[6]. Type-I Settling is called "Discrete Particle Settling" in dilute suspensions. This type of settling takes place in suspensions in which the particle concentration is low and particles do not flocculate.

[1] Under-graduate Student, Department of Environmental Engineering, Delhi Technological University (formerly Delhi College of Engineering), New Delhi, India-110 042 (e-mail: nandita.ahuja@dce.edu)

[2] Senior Scientist, CSIR - National Environmental Engineering Research Institute (CSIR-NEERI), Nehru Marg, Nagpur– 440 020, India

[+] Corresponding author: e-mail: girishrpophali@yahoo.com, gr_pophali@neeri.res.in; Tel: (O) +91 712 2249885–88, Extn. 411, Fax: (O): + 91 712 2249900

Type-II settling is known as "Flocculent Settling" in dilute suspensions, which occurs when suspension is formed by addition of coagulation chemicals and flocculants that convert slowly flocculating suspensions (diuternal) suspensions into rapidly flocculating suspensions (caducous suspension). Type-III and Type-IV Settling are called "Hindered or Zone" and "Compression settling" respectively and are generally observed in biological suspensions, whereas, Type-I and Type-II settlings are generally observed in water treatment process train (Crittenden *et al.*2005)[4]. The chief constituents of raw surface waters are mineral and organic particles. Mineral particles have densities ranging from 2000-3000 kg/m^3 and settle readily, whereas, organic particles have densities ranging from 1010 to 1100 kg/m^3 and may require longer time for settling (Crittenden *et al.*2005)[4]. In order to reduce the settling time for organic particles, coagulation and flocculation are carried out prior to settling (AWWA 2010)[1]. Addition of coagulants destabilizes the particles and forms large aggregates that settle out easily and thus follows flocculent settling (Kirk 2008)[7].

The process of sedimentation is a low cost and energy efficient method but it often involves complications that render proper sedimentation basin design a challenge for many engineers (Crittenden *et al.*2005)[4]. Since intermittent flow type clarifiers have now become obsolete and continuous flow type clarifiers are invariably used in water treatment, the design of these clarifiers become a challenge because it is difficult to study particle behavior and their settling characteristics in the dynamic condition (Degremont, 2007)[5].

The present study aims at evaluating the performance of a bench scale improved clarifier developed by Pophali et *al.* (2009a, b)[10,11] for flocculent or type-II settling of chemically treated storm water. The performance of the clarifier was evaluated based on the suspended solids and turbidity removal (Quasim, 1999)[12].

Materials and methods

Improved Circular Clarifier

Fig. 1 illustrates a side view of the primary clarifier and a top view of the clarifier is shown in Fig. 2. The clarifier was made of a transparent perspex cylinder with a diameter of 0.3 m and side water depth (SWD) of 0.2 m. The inlet diameter of

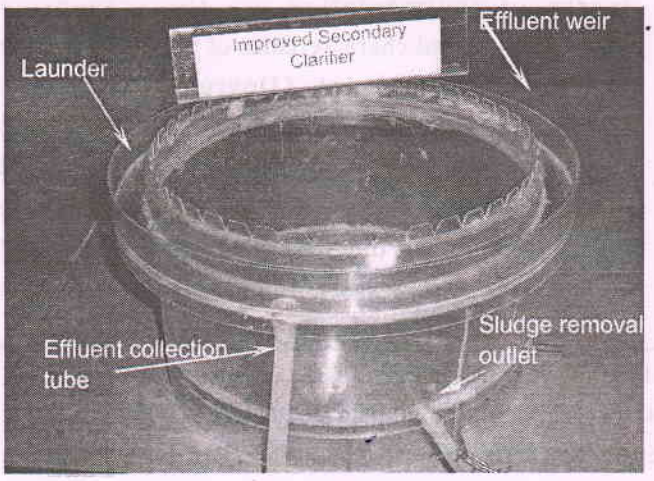

Fig. 1: Side view of the clarifier (Pophali *et al.* 2009 a, b)[10,11]

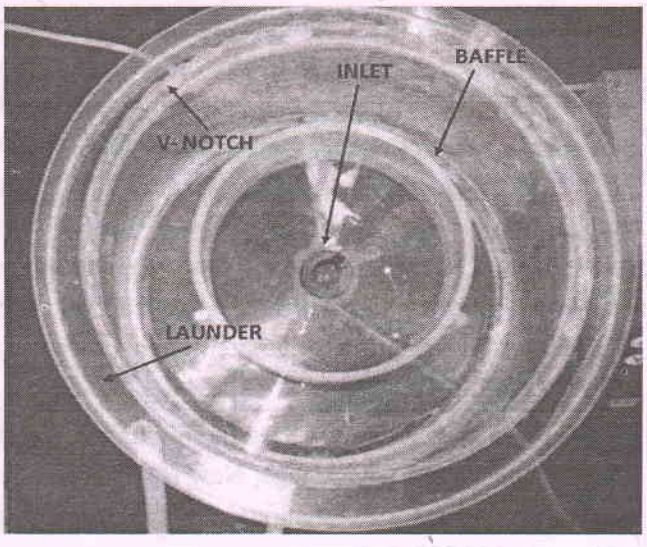

Fig. 2: A top view of the clarifier (Pophali *et al.* 2009 a, b)[10,11]

Type-II settling is known as "Flocculent Settling" in dilute suspensions, which occurs when suspension is formed by addition of coagulation chemicals and flocculants that convert slowly flocculating suspensions (diuternal) suspensions into rapidly flocculating suspensions (caducous suspension). Type-III and Type-IV Settling are called "Hindered or Zone" and "Compression settling" respectively and are generally observed in biological suspensions, whereas, Type-I and Type-II settlings are generally observed in water treatment process train (Crittenden *et al.*2005)[4]. The chief constituents of raw surface waters are mineral and organic particles. Mineral particles have densities ranging from 2000-3000 kg/m^3 and settle readily, whereas, organic particles have densities ranging from 1010 to 1100 kg/m^3 and may require longer time for settling (Crittenden *et al.*2005)[4]. In order to reduce the settling time for organic particles, coagulation and flocculation are carried out prior to settling (AWWA 2010)[1]. Addition of coagulants destabilizes the particles and forms large aggregates that settle out easily and thus follows flocculent settling (Kirk 2008)[5].

The process of sedimentation is a low cost and energy efficient method but it often involves complications that render proper sedimentation basin design a challenge for many engineers (Crittenden *et al.*2005)[4]. Since intermittent flow type clarifiers have now become obsolete and continuous flow type clarifiers are invariably used in water treatment, the design of these clarifiers become a challenge because it is difficult to study particle behavior and their settling characteristics in the dynamic condition (Degremont, 2007)[5].

The present study aims at evaluating the performance of a bench scale improved clarifier developed by Pophali et *al.* (2009a, b)[10,11] for flocculent or type-II settling of chemically treated storm water. The performance of the clarifier was evaluated based on the suspended solids and turbidity removal (Quasim, 1999)[12].

Materials and methods

Improved Circular Clarifier

Fig. 1 illustrates a side view of the primary clarifier and a top view of the clarifier is shown in Fig. 2. The clarifier was made of a transparent perspex cylinder with a diameter of 0.3 m and side water depth (SWD) of 0.2 m. The inlet diameter of

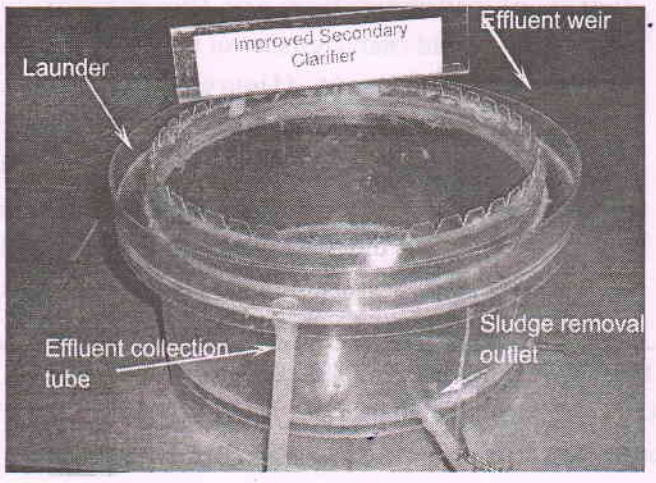

Fig. 1: Side view of the clarifier (Pophali *et al.* 2009 a, b)[10,11]

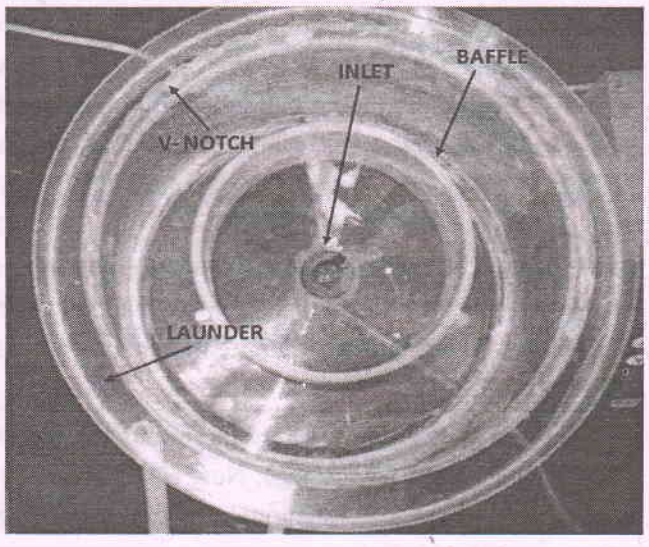

Fig. 2: A top view of the clarifier (Pophali *et al.* 2009 a, b)[10,11]

Table 1: Performance of primary clarifier using alum as a coagulant

Run	Alum Dose (mg/L)	HRT (hr)	Total Suspended Solids(mg/L)			pH		Turbidity(NTU)	
			Raw Water	Influent	Treated Effluent	Raw Water	Treated Effluent	Raw Water	Treated Effluent
1	20	1	74	79	40	8.2	7.7	56.6	21.1
2		1.5			34				18.55
3		2			30				17.79
4		2.5			25				14.90
5	30	1	233	258	106	8.1	7.5	129.11	68.22
6		1.5			82				43.80
7		2			73				40.60
8		2.5			64				33.57
9	50	1	483	506	166	8.6	7.8	268	132.91
10		1.5			129				109.10
11		2			119				99.81
12		2.5			96				71.70

the clarifier is 1.2 cm. The bottom of the clarifier was made of a transparent, flexible 2-mm thick polycarbonate sheet, sloping radially outward rather than sloping toward the center as in conventional circular clarifiers. The bottom slope for full-scale clarifiers is usually 1 in 10 to help the transport of sludge; in this clarifier, however, the bottom slope was 1 in 8. For circular clarifiers, bottom slopes ranging from 1 in 25 to 1 in 10 have also been reported (Quasim, 1999; WPCF 1985)[12,13].

Description and functioning of the clarifier

The "Improved Secondary Clarifier" (Pophali et *al.*2009a, b)[10,11] that was designed for clarification of biological sludge i.e. Type III and Type IV Settling was tested for its efficiency to work as a primary clarifier for treatment of flocculent suspensions (i.e. Type II Settling). The clarifier has a low level inlet with a gradually increasing diameter to reduce the velocity of water and thereby dissipating substantial hydraulic energy of incoming water and prevent jetting. This helps in distributing the water uniformly at the bottom. A plume, forms as a result of hydraulic energy dissipation and resistance to incoming flow offered by the bulk mass of solids (as shown in Fig 3). This in turn, provides natural flocculation at the central lower portion, increases floc size, and ensures absolute quiescent conditions in the clarification zone. The plume settles quickly on the outwardly sloped bottom and forms a sludge blanket all along the clarifier. A baffle wall placed at the center serves as a precautionary measure to prevent escape of solids. The treated effluent rises in the clarifier and is collected uniformly in the launder through effluent V – notch weirs.

Storm water samples (SWS)

The storm water samples were collected from storm water drains of NEERI campus, Nagpur during the months of June and July, 2011.

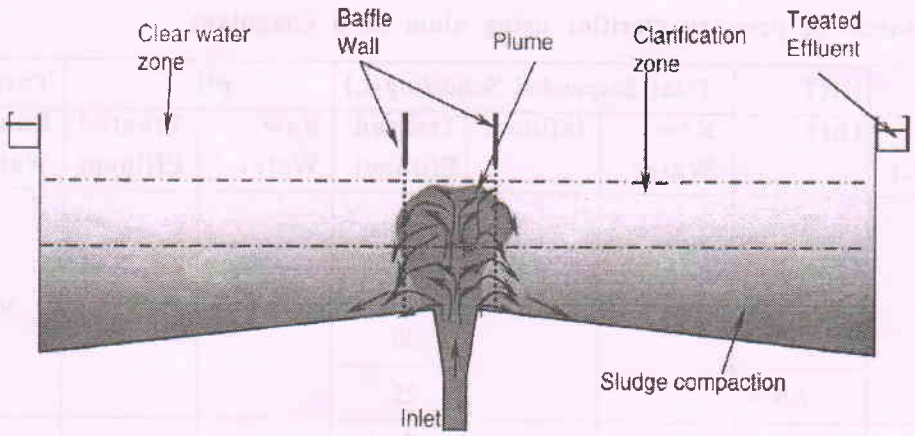

Fig. 3: A schematic diagram of working mechanism of proposed clarifier (Pophali *et al.* 2009a, b)[10,11]

Total suspended solids, turbidity and pH assessment

For the assessment of TSS 100mL sample was passed through 47µm pore size GFC paper using a Millipore Vacuum Pump. The filter paper was dried in the Sigma Hot Air Oven for 24 hrs at 100°C before and after the experiment. The difference in weight of the filter paper indicated the TSS concentration in 100 mL of sample. Turbidity of the raw water and treated water was measured using a Eutech Instruments Turbidity Meter TN-100 and a PTTster-35 pH meter was used for measurement of pH.

Coagulation and flocculation

Alum used for coagulation was of commercial grade and with purity of 45 - 48% and analytical grade polyelectrolyte was used as a flocculent. A 10% solution of alum and 0.5% solution of polyelectrolyte were used. Jar Tests were conducted to optimize the alum and polyelectrolyte dose for the chemical treatment of storm water using a Phipps and Bird Jar Test Apparatus.

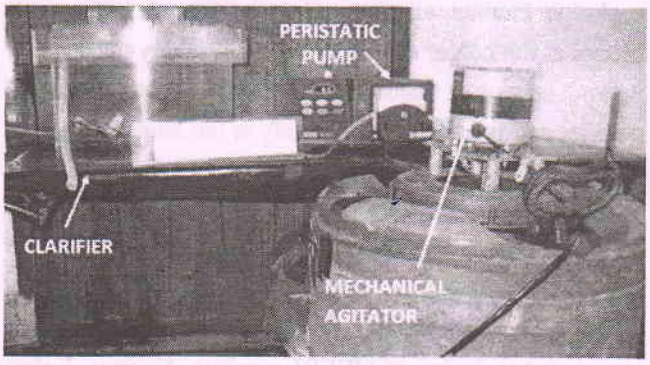

Fig 4: Experimental set-up of the equipment

Influent preparation

The influent solution was prepared in a separate tank by adding various doses of alum and polyelectrolyte into storm water samples to arrive at the optimum coagulant and flocculent doses. The influent was provided with a mechanical agitator (paddle type) and rotated at 90 rpm for rapid mixing of chemicals and at 20 rpm for keeping the flocs in suspension. The performance of clarifier was also tested using a diffused aerator. The influent solution was pumped into the clarifier using a Watson Marlow 505S peristatic pump as shown in Fig 4.

Results and discussion

Total settleable solids

The storm water samples (SWS) collected were initially passed through the primary clarifier (PC) to test the presence of readily settleable solids without coagulation and flocculation aide. It was observed that

Table 2: Comparative analysis of performance of the clarifier using a Diffused Aerator and a Mechanical Agitator

Mixing Device	Run	Alum Dose (mg/L)	Poly-electrolyte (mg/L)	HRT (hr)	Total Suspended Solids(mg/L)			TSS Removal (%)	Turbidity (NTU)		Turbidity Removal (%)
					Raw Water	Influent	Treated Effluent		Raw Water	Treated Effluent	
Diffused Aerator	1	200	3	1	1330	1505	183	87.8	735	227	69.1
	2			1.5			117	92.2		163.2	77.8
	3			2			83	94.5		77.79	89.4
Agitator	1			1	1449	1572	68	95.7	613	73.9	87.9
	2			1.5			47	97		41.8	93.2
	3			2			22	98.6		9.46	98.5

after initial settling of readily settleable solids, suspension had majority of suspended solids that could not be removed by plain sedimentation.

Clarifier performance study using alum as a coagulant

In order to remove the suspended solids and turbidity present in the SWS, coagulation was carried out using alum. Performance of primary clarifier was then evaluated for several storm water samples with varying turbidity and suspended solids concentration. **Table** 1 shows the results of various storm water samples with varying hydraulic retention time (HRT), initial suspended solids concentration and turbidity.

The low suspended solids and turbidity removal from the storm water through the primary clarifier can be attributed to the small size and light weight of flocs formed on addition of alum as a coagulant. This necessitated the use of a flocculent aide along with alum for formation of larger sized and heavier flocs. Therefore, polyelectrolyte was used as a flocculent along with alum.

Comparative analysis between diffused aeration and mechanical stirring

The influent solution was prepared after addition of alum and polyelectrolyte to the SWS in a separate unit. The flocs formed were kept in suspension by using a diffused aerator and an agitator and the performance of both the devices was then compared as shown in **Table 2.**

The results of the above runs clearly indicate high suspended solids and turbidity removal with an agitator as compared to a diffused aeration as a mixing device. From the above results and visual examination of the influent it was concluded that the use of a diffused aerator resulted in improper agglomeration of flocs thereby affecting its settling characteristics and increasing the turbidity of the influent. The performance of the primary clarifier was thus evaluated using storm water samples of varying suspended solids concentration using alum and polyelectrolyte as coagulation and flocculation chemicals and a mechanical agitator for aiding floc formation.

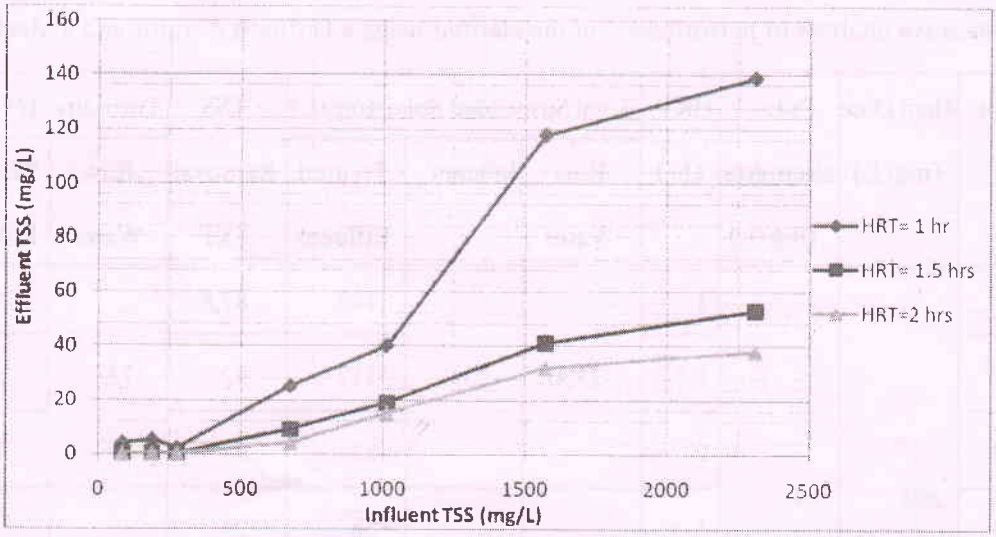

Fig. 5: Graphical representation of TSS removal of the clarifier for varying HRT

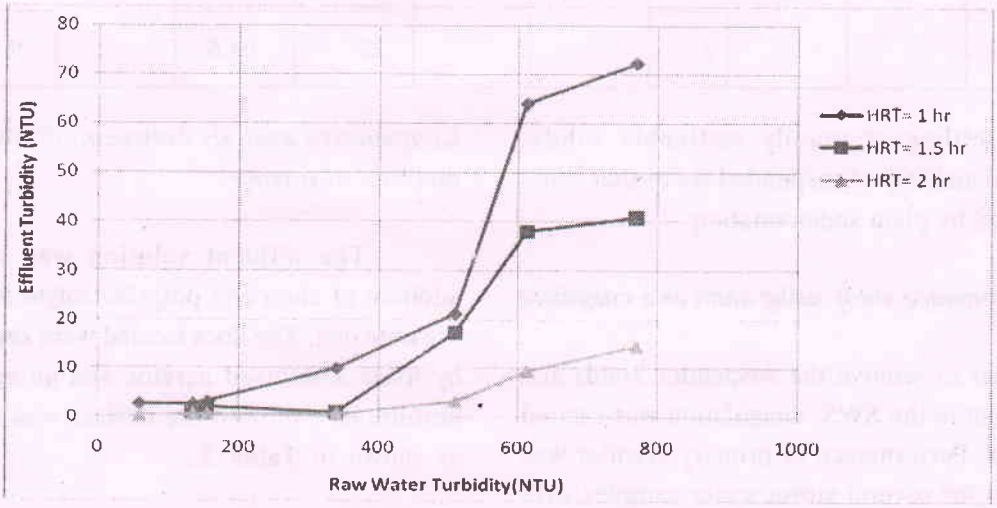

Fig. 6: Graphical representation of turbidity removal of the clarifier at varying HRT

The efficiency of the clarifier was studied on the basis of suspended solids removed from the influents to the clarifier. Turbidity removal from water was also studied as a parameter of clarifier efficiency. It was calculated as the turbidity removed from raw water sample as against the influent turbidity in case of suspended solids removal efficiency. This is so because turbidity of chemically treated influent has no significance and cannot be measured accurately due to its heterogeneous floc size and distribution.

Performance analysis of clarifier for storm water samples A – G

A storm water sample of initial suspended solids concentration of 2200 mg/L was chemically treated with 250 mg/L of Alum and 4 mg/L of polyelectrolyte. The removal of suspended solids and turbidity was observed for three runs 1, 2 and 3 with HRT of 1, 1.5 and 2 hours respectively. For the 1st run it was observed that the plume formation at the inlet

of the tank was indistinct and distorted. Whereas, for the 2nd and 3rd runs, the plume was distinctly formed. The suspended solids removal efficiency was least for the 1st run and was quite high for the 2nd and 3rd runs as is shown in **Table 3**.

Several runs were subsequently conducted on storm water collected during the month of July, 2011. The results of the runs are presented in **Table 4** with decreasing order of suspended solids concentration.

From the results shown in **Table 4** it can be seen that the suspended solids removal efficiency as well as the turbidity removal efficiency of the primary clarifier is higher than 95% in all the runs for a HRT of 1hr. However, the effluent turbidity is much higher at an HRT of 1hr in comparison to the effluent turbidity at an HRT of 1.5 and 2hrs.

For the samples with initial suspended solids concentration range of less than 500mg/L the floc was found to be settling near the inlet due to a decrease in velocity at the inlet. This problem can be overcome by decreasing the inlet diameter and thereby increasing the inlet velocity. This shall increase the height of the plume formed and aide in uniform settling of the flocs across the base of the reactor.

From the graphical representation of the TSS removal data as shown in **Fig 5** it can be inferred that the clarifier performance is very good for TSS removal when influent TSS concentration is less than 500mg/L at an HRT of 1hr and the TSS removal in the clarifier is almost similar at an increased HRT of 1.5 hrs and 2 hrs.

From trend observed in the **Fig 5** it can also be concluded that for the influent with TSS more than 500mg/L the HRT plays a significant role with the increasing influent TSS concentration. However, the TSS removal is almost similar for HRT of 1.5 hrs and 2 hrs indicating that a large percentage of particles

Table 3: Performance evaluation of Primary Clarifier for Sample "A"

Storm Water Sample	Run	Alum Dose (mg/L)	Poly electro -lyte Dose (mg/L)	pH		HRT (hr)	Total Suspended Solids(mg/L)		TSS removal (%)	Turbidity (NTU)		Turbidity Removal (%)	Sludge Volume (mL/L)
				Raw Water	Treated Effluent		Raw Water	Influent	Treated Effluent		Raw Water	Treated Effluent		
A	1	250	4	8.6	7.5	1	2200	2310	41	98.2	770	40.92	94.7	36
	2					1.5			249	89.2		72.1	90.6	37
	3					2			34	98.5		14.7	98.1	34

Table 4: Performance evaluation of primary clarifier for storm water samples for July, 2011 (Samples B – G)

Storm Water Sample	Run	Alum Dose (mg/L)	Poly elect-rolyte Dose (mg/L)	pH		HRT (hr)	Total Suspended Solids(mg/L)			TSS removal (%)	Turbidity (NTU)		Turbidity Removal (%)	Sludge Volume (mL/L)
				Raw Water	Treated Effluent		Raw Water	Influent	Treated Effluent		Raw Water	Treated Effluent		
B	1	200	3	8.1	7.2	1	1449	1572	68	95.7	613	63.9	89.6	13
	2					1.5			47	97		38	93.8	12
	3					2			22	98.6		9.46	98.5	10
C	1	185	0.8	8.4	7.3	1	950	1010	37	96.3	509.7	21.2	95.8	14
	2					1.5			20	98		14.4	97.2	12
	3					2			15	98.5		3.3	99.3	12
D	1	140	0.5	8.6	7.8	1	593	671	16	97.6	339	5.91	98.3	9
	2					1.5			9	98.7		1.23	99.6	8
	3					2			4	99.4		0.61	99.8	8
E	1	50	0.27	8.4	7.6	1	243	274	2	99.3	135	3.04	97.7	3
	2					1.5			<1	=100		1.17	99.1	3
	3					2			<1	=100		0.62	99.5	3
F	1	40	0.22	8.6	8.3	1	161	188	5	97.3	155	2.62	98.3	3
	2					1.5			1	99.5		1.17	99.2	3
	3					2			<1	=100		0.65	99.6	3
G	1	25	0.18	8.3	7.8	1	76	83	4	95.2	58.8	2.56	95.6	2
	2					1.5			<1	=100		0.66	98.9	2
	3					2			<1	=100		0.20	99.7	2

have a settling time more than 1 hr and less than 1.5 hrs and a very small percentage of particles require a settling time of more than 1.5 hrs.

Turbidity removal in SWS A – G as shown in Fig 6 depicts a low effluent turbidity in samples with initial turbidity less than 500mg/L, a trend similar to that of TSS removal. However, as against a similar TSS removal for an HRT of 1.5 hrs and 2hrs, the turbidity removal for 1.5 hr HRT is distinctly less than that for an HRT of 2 hrs.

Conclusions

The performance study on the primary clarifier along with its ability to provide natural flocculation as a result of dissipation of hydraulic energy at the inlet indicates its adequacy to be used as clari-flocculator in water treatment process for settling of flocculent suspension and also for solid liquid separation of chemically (with coagulants and flocculants) treated storm water. The clarifier can be effectively used at an optimum HRT of 1 hr for treatment of water with suspended solids concentration of less than 500 mg/L. However, for treatment of water with TSS more than 500mg/L the HRT should be optimized taking the required effluent turbidity and effluent usage into consideration. For very low effluent turbidity it is recommended to carry out a cost-benefit analysis between the usage of the clarifier at a high HRT and a tertiary treatment following the treatment of water at a low HRT. For treatment of water with low TSS (i.e. <500mg/L) it is recommended to optimize the inlet diameter to ensure sufficient influent velocity, which prevents settling of particles at the inlet and allows proper plume formation. There is a promising scope for further studies on this clarifier such as testing its performance using other coagulants; effect of sludge scrapping mechanism on clarifier performance and effect on plume formation with a reduced inlet diameter for treatment of water with a TSS concentration of less than 500mg/L. These studies are in progress.

Acknowledgement

The authors thank the Director, CSIR-NEERI, Nagpur for granting permission to carry out the R & D studies in the laboratory of Wastewater Technology Division.

References

1. American Water Works Association (AWWA) 2010, *Operational Control of Coagulation and Filtration Processes.*

2. American Water Works Association (AWWA) 1999, Water quality and treatment: a handbook of community water supplies, 5th edition, Mc GrawHill.

3. Chris, B., Martin, K., George, S. 2002, Basic Water Treatment, Royal Society of Chemistry.

4. Crittenden, J. C., Trussell, R. R., Hand, D. W., Howe, K. J. 2005, Tchobanoglous, Water treatment principles and design, 2nd ed.; John Wiley & Sons, MWH.

5. Degremont France 2007, Water Treatment Handbook, 7th edition, vol 2, 825-871.

6. Hendricks, D. W. 2006, Water Treatment Unit Processes: Physical and Chemical, Taylor & Francis, 139-199.

7. Kawamura, S. 2000 Integrated design and operation of water treatment facilities; John Wiley and Sons, 147-149.

8. Kirk-Othmer 2008, Separation Technology; 2nd edition; John Wiley & Sons, 872-892.

9. Lindeborg, C., Wiberg, N. and Seyf, A., Studies of the dynamic behaviour of a primary

sedimentation tank. *Wat. Sci. Tech.* 34 (3–4), 213–222 (1996)

10. Pophali, G. R., Kaul, S. N., Nandy, T. and Devotta, S. 2009a Circular Secondary Clarifier for Wastewater Treatment and an Improved Solids-Liquid Process Thereof, US Patent No. 7637379.

11. Pophali, G. R., Kaul, S. N., Nandy, T. and Devotta, S., Development of a novel circular secondary clarifier for improving solids-liquid separation in wastewater treatment, *J. of Water Environment Research,* 81, 2, 140-149 (2009b)

12. Quasim, S. R. 1999. Wastewater Treatment Plants: Planning, Design and Operation, 2nd ed.; Technomic Publishing: Basel, Switzerland.

13. Water Pollution Control Federation (WPCF) 1985. Clarifier Design, Manual of Practice FD – 8, Facilities Development.

Available online at www.sciencedirect.com

ScienceDirect

Electronic Notes in DISCRETE MATHEMATICS

Electronic Notes in Discrete Mathematics 48 (2015) 65–72

www.elsevier.com/locate/endm

Zero Ring Labeling of Graphs

Mukti Acharya [1]

Department of Applied Mathematics,
Delhi Technological University,
Delhi - 110042, India.

Pranjali* [2]

Department of Mathematics,
University of Delhi,
Chhatra Marg, Delhi-110007, India.

Purnima Gupta [3]

Department of Mathematics,
Sri Venkateswara College,
University of Delhi-110021, India.

Abstract

This paper introduces the notion of zero ring labeling of a graph and its empirical study demonstrates that every graph admits a zero ring labeling with respect to some zero ring. The zero ring graph $\Gamma(R^0)$ turns out to be maximal with respect to an injective zero ring labeling. In particular, we determine the optimal zero ring index for some well-known graphs.

Keywords: labeling, zero ring.

http://dx.doi.org/10.1016/j.endm.2015.05.010

1 Introduction

For all terminology and notation in graph theory and abstract algebra, not specifically defined in this paper, we refer the reader to the text-books by Harary [3] and Jacobson [4] respectively. Unless mentioned otherwise, all graphs considered in this paper are simple, connected and finite.

A ring in which the product of any two elements is 0 is called a *zero ring* and denoted by R^0, where 0 is the additive identity. One of the standard examples of *zero ring* is the set of 2×2 matrices

$$\left\{ \begin{bmatrix} r & -r \\ r & -r \end{bmatrix} \right\},$$

where $r \in R$ and R is a commutative ring. Throughout the paper we shall denote the above set by $M_2^0(R)$. The above example implies the validity of the following remark.

Remark 1.1 [6] For every positive integer n, there exists a zero ring of order n.

Proposition 1.2 [6] *If $n = p_1^{a_1} \cdot p_2^{a_2} \cdot p_3^{a_3} \cdots p_k^{a_k}$, then the number of zero rings of order n are $p(a_1) \cdot p(a_2) \cdots p(a_k)$, where $p(a_i)$ denotes the partition of the natural number a_i.*

In this paper, we focus on vertex labeling of graphs in which vertices are labeled by the elements of finite zero rings.

Definition 1.3 [5] Let $(R^0, +, \cdot)$ be a finite zero ring. The *zero ring graph*, denoted by $\Gamma(R^0)$, is a graph whose vertices are the elements of R^0 in which two distinct vertices x and y are adjacent if and only if $x + y \neq 0$, where 0 is the additive identity of R^0.

We begin with a new notion of labeling and for various types of labelings reader is referred to [1] and [2].

Definition 1.4 Let $G = (V, E)$ be a graph with vertex set $V =: V(G)$ and edge set $E =: E(G)$, and let R^0 be a finite zero ring. An injective function $f : V(G) \to R^0$ is called a *zero ring labeling* of G if $f(u) + f(v) \neq 0$ for every edge $uv \in E$.

[1] Email: mukti1948@gmail.com
[2] Email: pranjali48@gmail.com (*Corresponding author)
[3] Email: purnimachandni@rediffmail.com

Example 1.5 Consider the cycle C_4. Consider the zero ring $M_2^0(\mathbb{Z}_4)$ whose elements are

$$b_0 = \begin{bmatrix} 0 & 0 \\ 0 & 0 \end{bmatrix}; b_1 = \begin{bmatrix} 1 & -1 \\ 1 & -1 \end{bmatrix}; b_2 \begin{bmatrix} 2 & -2 \\ 2 & -2 \end{bmatrix}; b_3 = \begin{bmatrix} 3 & -3 \\ 3 & -3 \end{bmatrix}.$$

Define a function $f : V(C_4) \to M_2^0(\mathbb{Z}_4)$ such that

$$f(v_i) = b_i, \quad 0 \leq i \leq 3.$$

Clearly, f is injective and for every $(v_i, v_{i+1}) \in E(C_4)$ the sum of the labels b_i and b_{i+1} is nonzero. The zero ring labeling of C_4 is shown in Fig. 1.

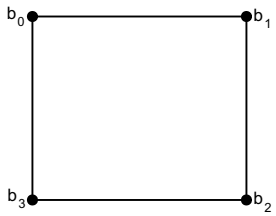

Fig. 1. Zero ring labeling of C_4

One can quickly notice the following facts about zero ring labeling.

Remark 1.6 If f is a zero ring labeling of a graph G, then f is a zero ring labeling of every subgraph of G.

Remark 1.7 If $f : V(G) \to R^0$ is a zero ring labeling of a graph G with respect to R^0, then f is a zero ring labeling of every supergraph G' of G, obtained by adding edges that join pairs of distinct vertices x, y that were not joined in G and having the property that $f(x) + f(y) \neq 0$. Hence, such a supergraph $M_{R^0}^f$ so obtained is a subgraph of the zero ring graph $\Gamma(R^0)$. Further, if f is onto, then $M_{R^0}^f \cong \Gamma(R^0)$.

The following question arises naturally.

Does every graph admit a zero ring labeling with respect to some zero ring?

We answer this question affirmatively.

Theorem 1.8 *Every finite graph admits a zero ring labeling.*

Proof. Let G be a finite graph of order n. Consider the zero ring $M_2^0(\mathbb{Z}_2[x]/\langle x^k \rangle)$ associated with polynomial quotient ring $\mathbb{Z}_2[x]/\langle x^k \rangle$, where k is the ceiling of

$\log_2 n$. The elements of $M_2^0(\mathbb{Z}_2[x]/\langle x^k\rangle)$ are

$$\left\{\begin{bmatrix}0 & 0\\ 0 & 0\end{bmatrix}, \begin{bmatrix}1 & -1\\ 1 & -1\end{bmatrix}, \cdots, \begin{bmatrix}x^{k-1} & -x^{k-1}\\ x^{k-1} & -x^{k-1}\end{bmatrix}, \begin{bmatrix}x^{k-1}+1 & -(x^{k-1}+1)\\ x^{k-1}+1 & -(x^{k-1}+1)\end{bmatrix}\right\}.$$

Any injective function $f : V(G) \to M_2^0(\mathbb{Z}_2[x]/\langle x^k\rangle)$ is a zero ring labeling as the sum of any two distinct elements of $M_2^0(\mathbb{Z}_2[x]/\langle x^k\rangle)$ is nonzero. Thus f is a zero ring labeling of G. □

Theorem 1.8 leads us to define more prospective notion.

Definition 1.9 Let $G = (V, E)$ be a finite graph of order n. The *zero ring index* of G, denoted as $\xi(G)$, is the least positive integer n_0 such that there exists a zero ring R^0 of order n_0 with respect to which G admits a zero ring labeling. Any zero ring labeling f of G is *optimal* if it uses a zero ring having $\xi(G)$ elements.

In view of above definition together with Theorem 1.8, we have

$$n \leq \xi(G) \leq 2^k, \tag{1}$$

where n is the order of the graph and k is the ceiling of $\log_2 n$.

The bounds in (1) indicate the following problem of fundamental importance.

Problem 1.10 *Characterize graphs for which the bounds in (1) are attained. Also, determine all the zero rings which provide an optimal zero ring labeling for these graphs.*

In the following theorem, we give a necessary and sufficient condition for K_n to attain the lower bound as mentioned in (1).

Theorem 1.11 *$\xi(K_n) = n$ if and only if $n = 2^{k_0}$, $k_0 > 1$.*

Proof. Necessity: Let $\xi(K_n) = n$. Suppose $n \neq 2^{k_0}$. Then either n is the product of primes, odd prime, power of an odd prime or the product of powers of primes. We will study each case separately.

Case 1. n is either prime or a product of distinct primes.

In view of Proposition 1.2, there exists only one zero ring of order n, namely, $M_2^0(\mathbb{Z}_n)$. Choose any injective function $f : V(K_n) \to M_2^0(\mathbb{Z}_n)$ in which

$$f(v_i) = \begin{bmatrix}1 & -1\\ 1 & -1\end{bmatrix} \text{ and } f(v_j) = \begin{bmatrix}n-1 & -(n-1)\\ n-1 & -(n-1)\end{bmatrix}$$

for some v_i and v_j and this assignment produces the zero sum which is not possible for a zero ring labeling (as for all distinct $v_i, v_j \in V(K_n)$, $(v_i, v_j) \in E(K_n)$). Therefore, optimal zero ring index cannot be n, which is a contradiction to the assumption.

Case 2. $n = p^{a_1}$, p is an odd prime and $a_1 > 1$.

Again in light of Proposition 1.2 there exist $P(a_1)$ zero rings of order p^{a_1}. Now for different values of a_1, we need to consider the following sub-cases:

Sub-case(i). If $a_1 = 2$, then $n = p^2$.

By Proposition 1.2 there are two zero rings of order p^2; namely $M_2^0(\mathbb{Z}_{p^2})$ and $M_2^0(\mathbb{Z}_p[x]/\langle x^2\rangle)$, where $\mathbb{Z}_p[x]/\langle x^2\rangle$ is a polynomial quotient ring over $\mathbb{Z}_p$.

Firstly, for the zero ring $M_2^0(\mathbb{Z}_{p^2})$, we get a contradiction similar to Case 1. Secondly, for the zero ring $M_2^0(\mathbb{Z}_p[x]/\langle x^2\rangle)$, choose any injective function $f : V(K_{p^2}) \to M_2^0(\mathbb{Z}_p[x]/\langle x^2\rangle)$ in which

$$f(v_i) = \begin{bmatrix} x & -x \\ x & -x \end{bmatrix} \text{ and } f(v_j) = \begin{bmatrix} p-x & -(p-x) \\ p-x & -(p-x) \end{bmatrix}$$

for some v_i and v_j and this assignment produces the zero sum, which is not possible for a zero ring labeling. Therefore, optimal zero ring index can not be n, i.e., $\xi(K_n) \neq n$, which is a contradiction.

Sub-case(ii). If $a_1 = 3$, then $n = p^3$.

In view of Proposition 1.2 there exist three zero rings of order p^3, namely, $M_2^0(\mathbb{Z}_{p^3})$, $M_2^0(\mathbb{Z}_p[x]/\langle x^3\rangle)$ and $M_2^0(\mathbb{Z}_{p^2}[x]/\langle x^2, px\rangle)$, where $\mathbb{Z}_{p^2}[x]/\langle x^2, px\rangle$ is a polynomial quotient ring over $\mathbb{Z}_{p^2}$. To show the non-existence of zero ring labeling the arguments are analogous to those used in sub-case (ii).

From the above analysis, we conclude that if we take $a_1 > 3$, then by a similar argument we arrive at a contradiction to the assumption.

Case 3. $n = p_1^{a_1} \cdot p_2^{a_2}$, $p_1 \neq p_2$ and $a_1, a_2 > 0$.

We consider the following sub-cases:

Sub-case(i). $a_1 = a_2 = 1$.

Then n becomes the product of primes, which is already covered in Case 1.

Sub-case(ii). $a_1 = 2$ and $a_2 = 1$.

Then $n = p_1^2 p_2$. Using Proposition 1.2 there exist two zero rings of order $p_1^2 p_2$, namely, $M_2^0(\mathbb{Z}_{p_1^2 p_2})$ and the subring of $\mathbb{Z}_2[x, y]/\langle x, y\rangle^2 \times \mathbb{Z}_9$. For the zero ring $M_2^0(\mathbb{Z}_{p_1^2 p_2})$, we follow the procedure as used in Case 1 and get $\xi(K_n) > n$, which is a contradiction. Secondly, take the zero ring (subring of $\mathbb{Z}_{p_1}[x, y]/\langle x, y\rangle^2 \times \mathbb{Z}_{p_2^2}$) consisting the elements $\{(0,0), (0,p_2), \cdots, (0, p_2(p_2 -$

$1)), (x,0), (x,p_2), \cdots, (x,p_2(p_2-1)), (y,0), (y,p_2), \cdots, (y,p_2(p_2-1)), (x+y,0), (x+y,p_2), \cdots, (x+y,p_2(p_2-1))\}$. Define any injective function $f : V(K_n) \to$ subring of $\mathbb{Z}_{p_1}[x,y]/\langle x,y\rangle^2 \times \mathbb{Z}_{p_2^2}$ in which we always have the assignment to the vertices such that $f(v_i) = (0,p_2)$ and $f(v_j) = (0,p_2(p_2-1))$, but $f(v_i) + f(v_j) = (0,0) \pmod{p_2^2}$, again a contradiction.

Sub-case(iii). $a_1 = a_2 = 2$.

Then $n = p_1^2p_2^2$. In light of Proposition 1.2 there are four zero rings of order $p_1^2p_2^2$, namely, $M_2^0(\mathbb{Z}_{p_1^2p_2^2})$, subring of $\mathbb{Z}_{p_1}[x,y]/\langle x,y\rangle^2 \times \mathbb{Z}_{p_2^4}$, subring of $\mathbb{Z}_{p_2}[x,y]/\langle x,y\rangle^2 \times \mathbb{Z}_{p_1^4}$ and subring of $\mathbb{Z}_{p_1}[x,y]/\langle x,y\rangle^2 \times \mathbb{Z}_{p_2}[a,b]/\langle a,b\rangle^2$.

For the zero ring $M_2^0(\mathbb{Z}_{p_1^2p_2^2})$, we follow the procedure as used in Case 1 and get $\xi(G) > n$, which is a contradiction.

Further, to show the non-existence of zero ring labeling for the subring of $\mathbb{Z}_{p_1}[x,y]/\langle x,y\rangle^2 \times \mathbb{Z}_{p_2^4}$ and subring of $\mathbb{Z}_{p_2}[x,y]/\langle x,y\rangle^2 \times \mathbb{Z}_{p_1^4}$ the arguments are analogous to those used in sub-case (ii) of Case 3. Finally, consider the subring of $\mathbb{Z}_{p_1}[x,y]/\langle x,y\rangle^2 \times \mathbb{Z}_{p_2}[a,b]/\langle a,b\rangle^2$, which have the elements $\{0,x,y,x+y,\cdots,(p_1-1)x,(p_1-1)y,(p_1-1)(x+y)\} \times \{0,a,b,a+b,\cdots,(p_2-1)a,(p_2-1)b,(p_2-1)(a+b)\}$. Define any injective function $f : V(K_n) \to$ subring of $\mathbb{Z}_{p_1}[x,y]/\langle x,y\rangle^2 \times \mathbb{Z}_{p_2}[a,b]/\langle a,b\rangle^2$ in which we have $f(v_i) = (0,a)$ and $f(v_j) = (0,(p_2-1)a)$. This assignment produces the zero sum which is not possible for a zero ring labeling. Therefore, optimal zero ring index can not be n, a contradiction.

Furthermore, for distinct values of $a_1, a_2 \geq 3$, the problem can be tackled by giving the arguments analogous to those used in the above sub-cases.

Case 4. $n = p_1^{a_1}p_2^{a_2}\cdots p_l^{a_l}$, all p_i are distinct and $a_i > 0,\ 1 \leq i \leq l$.

Again we consider the following sub-cases:

Sub-case(i). If all a_i are 1, then n becomes the product of primes which is already covered in Case 1.

Sub-case(ii). If $a_1 = 2$ and other a_i are 1, then $n = p_1^2.p_2\cdots p_s$ and following the same procedure as in Case 3, we arrive at a contradiction.

Sub-case(iii). If $a_1, a_2 > 1$ and the remaining a_i are 1, then arguments are analogous to those used in Case 3.

For other values of a_i, other sub-cases will come either in above cases or can be tackled in similar manner. Hence, all the cases, we conclude that $n = 2^{k_0}$.

Sufficiency: Let us assume that $n = 2^{k_0},\ k_0 > 1$. In view of Proposition 1.2 there exist $P(k_0)$ (partition of k_0) zero rings of order 2^{k_0} and out of which two are $M_2^0(\mathbb{Z}_{2^{k_0}})$ and $M_2^0(\mathbb{Z}_2[x]/\langle x^{k_0}\rangle)$. Any injective function $f : V(K_n) \to M_2^0(\mathbb{Z}_2[x]/\langle x^{k_0}\rangle$ is a zero ring labeling (from the proof of Theorem 1.8) and it is clear that the sum of any two distinct elements of $M_2^0(\mathbb{Z}_2[x]/\langle x^{k_0}\rangle)$ is

nonzero. Hence $\xi(K_n) = n$. □

Theorem 1.12 *Let G be a graph of order n. If $n = 2^{k_0}$, $k_0 \geq 1$, then $\xi(G) = n$.*

Proof. The result follows directly from the sufficiency part of the Theorem 1.11 together with the fact that every graph is a subgraph of complete graph.□

Remark 1.13 It should be noted that the converse of Theorem 1.12 is not true, i.e., if G is a graph of order n, then $\xi(G) = n$ need not imply that $n = 2^{k_0}$. For example $\xi(C_5) = 5$, but 5 is not of the form of 2^{k_0}, for any k_0.

Theorem 1.14 *The n-dimensional hypercube Q_n admits a zero ring labeling with optimal zero ring index 2^n.*

Proof. The proof of the result can easily be derived using Theorem 1.12 together with the fact that $|V(Q_n)| = 2^n$. □

Theorem 1.15 *Let G be a finite graph of order n and let G is a spanning subgraph of a zero ring graph $\Gamma(R^0)$. Then $\xi(G) = n$.*

Proof. If G is a spanning subgraph of a zero ring graph, then using Remark 1.6, one can easily verify that any injective function yields an optimal zero ring labeling with optimal zero ring index $\xi(G) = n$. □

Now we study the optimal zero ring labeling for a subgraph H of an arbitrary graph G.

Theorem 1.16 *Let G be a finite graph of order n and let H be a subgraph of G, then $\xi(H) \leq \xi(G)$.*

Proof. Let G be a graph of order n and let f be a zero ring labeling of G. In view of Remark 1.6 it is clear that f is a zero ring labeling of H as well. Now, if G is a spanning subgraph of a zero ring graph $\Gamma(R^0)$, then $\xi(G) = n$, consequently $\xi(H) \leq n$. On the other hand, if G is not a spanning subgraph of $\Gamma(R^0)$, then $\xi(G) > n$, however H may or may not be a spanning subgraph of $\Gamma(R^0)$, if it is, then $\xi(H) < \xi(G)$. Otherwise $\xi(H) \leq \xi(G)$. □

Remark 1.17 Note that instead of zero ring $M_2^0(R)$ the other zero rings like subring of $\mathbb{Z}_{p^2}$ and the subring of $\mathbb{Z}_p[x, y]/\langle x, y\rangle^2 \times \mathbb{Z}_{q^2}$, for some prime p and q can be taken for zero ring labeling.

Remark 1.18 For every positive integer n there exists a graph of order n such that $\xi(G) = n$.

Acknowledgement

Authors would like to remember Dr. B.D. Acharya who gave the idea but could not witness its growth. The second author is thankful to Department of Atomic Energy (DAE) for providing the research grant vide sanction letter number: 2/39(26)/2012 -R&D-II/4114. Finally, we would like to thank Professor Thomas Zaslavsky for his thought provoking suggestions.

References

[1] M. Acharya, Pranjali and P. Gupta, Zero-Divisor Labeling of Hypercubes, *Nat. Acad. Sci. Lett.*, **37**(5) (2014), 467–471.

[2] J.A. Gallian, A Dynamic Survey of Graph Labeling, *Electronic J. Combin.*, **17** (2014), #DS6.

[3] F. Harary, *Graph Theory*, Addison-Wesley Publ. Comp., Red., MA. (1969).

[4] N. Jacobson, *Lectures in Abstract Algebra*, East-West Press P. Ltd., New Delhi (1951).

[5] Pranjali and M. Acharya, *Graphs associated with finite zero rings*, submitted.

[6] http://en.wikipedia.org/wiki/Zero_ring#cite_note-10